

**COMPUTATIONAL METHODS FOR DESIGNING NEW PASSIVE FLUID
BORNE NOISE SOURCE REDUCTION STRATEGIES IN HYDRAULIC
SYSTEMS**

by

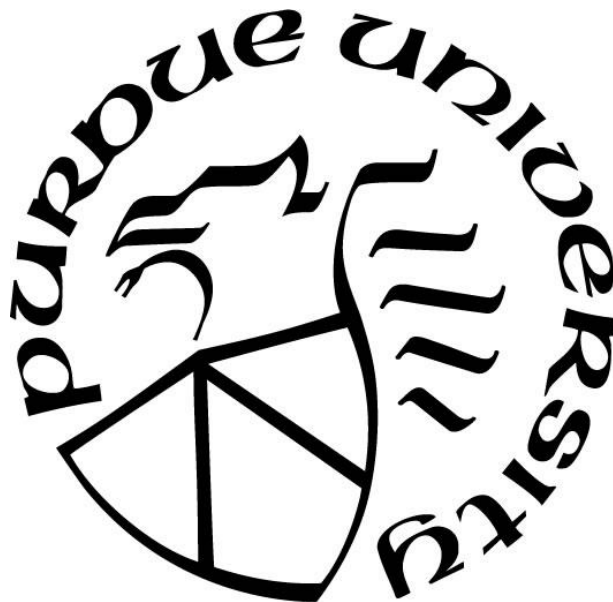
Leandro Henschel Danes

A Dissertation

Submitted to the Faculty of Purdue University

In Partial Fulfillment of the Requirements for the degree of

Doctor of Philosophy



Department of Agricultural & Biological Engineering

West Lafayette, Indiana

December 2020

**THE PURDUE UNIVERSITY GRADUATE SCHOOL
STATEMENT OF COMMITTEE APPROVAL**

Dr. Andrea Vacca, Chair

School of Mechanical Engineering
Department of Agricultural and Biological Engineering

Dr. Stuart J. Bolton

School of Mechanical Engineering

Dr. John Lumkes

Department of Agricultural and Biological Engineering

Dr. José Garcia Bravo

School of Engineering Technology

Approved by:

Dr. Nathan Mosier

I dedicate this work to my family, friends, and those who have all given me encouragement to pursue my doctoral degree and support overcoming the obstacles in the way.

ACKNOWLEDGMENTS

Firstly I would like to acknowledge my sponsor, the Conselho Nacional de Desenvolvimento Científico e Tecnológico(CNPq), for the financial support through all these years. Without their support, the development of this work would not be possible.

I thank both my advisors: My first advisor, Professor Monika Ivantysynova, who unfortunately passed away in August 2018, for giving me the unique opportunity of working at the Maha fluid power research center and for all the consulting and guidance provided during the first three years of my research. My second advisor, Professor Andrea Vacca, supported the continuity of my Ph.D. program and related research. Without his guidance, patience, motivation, and immense knowledge, my work's conclusion would not be possible.

I also acknowledge my Ph.D. advisory committee members: Prof. J. Stuart Bolton, Prof. John Lumkes, and Prof. Jose M. Garcia-Bravo, which contributed significantly to this work with their expertise and availability.

I would also like to acknowledge my colleagues at Maha Fluid Power Center, which helped me develop this work both through work assistance and guidance. I thank my colleagues for the support and assistance when developing my projects in especially Jeremy Beale and Paul Kalbfleisch, which always have me good advice. I also thank the lab technicians, Dave Johnson and Anthony Franklyn, for their primary assist in constructing the experimental benches used for performing the experiments that supported the validation and discoveries of my work.

Finally, I offer this endeavor to God Almighty for giving me strength and wisdom to conclude this work despite all my limitations.

TABLE OF CONTENTS

LIST OF TABLES	8
LIST OF FIGURES	9
NOMENCLATURE	15
LIST OF ABBREVIATIONS.....	18
ABSTRACT.....	19
1. INTRODUCTION.....	21
1.1 Background.....	21
1.2 Motivation.....	23
1.2.1 Noise Generation	23
1.2.2 Noise in Swash-plate Axial Piston Units.....	26
1.2.3 Noise in hydraulic circuits	30
1.3 Research Objectives.....	34
1.4 Thesis Organization and Original Contributions	36
2. STATE OF ART.....	38
2.1 Noise Cancellation Overview	38
2.1.1 Active Noise Cancellation	40
2.1.2 Adaptive-Passive Noise Cancellation.....	44
2.1.3 Passive Noise Cancellation.....	47
2.1.4 Hydraulic Unit Design for Pressure Ripple Mitigation	50
2.2 Line Models Overview	53
2.2.1 Lumped Parameter Models.....	55
2.2.2 Transfer Function Approaches	56
2.2.3 Time-Domain Line Models Derived with the Method of Characteristics	59
3. COUPLED-SYSTEM MODELING	61
3.1 The relevance of a coupled system model	61
3.2 Method of characteristics based line model.....	64
3.3 Discretized Parameter Hydraulic Line Model	70

3.4	Line branches Model.....	73
3.5	Axial piston unit model.....	75
3.5.1	Pressure and flow calculation model	75
3.6	Solver	79
3.7	Validation.....	82
3.7.1	Example of a coupled system simulation	82
3.7.2	Simulation.....	84
3.7.3	Experimental Setup.....	85
3.7.4	Comparative Results	91
4.	A HOLISTIC COMPREHENSIVE METHOD FOR USING THE MOC MODEL AT THE FREQUENCY-DOMAIN.....	98
4.1	Model and methodology	98
4.2	Line length influence	101
4.3	Major influencing parameters	106
4.4	The downstream magnitude and phase influence	110
4.5	Passive fluid-borne noise elements influence	113
4.5.1	Duct Profiles	113
4.5.2	Side branch closed-end silencers	117
4.5.3	Quincke tube.....	121
4.6	Fluid borne noise source reduction summary	124
5.	SOURCE FLOW RIPPLE REDUCTION STRATEGY BASED ON SECONDARY SOURCE.....	127
5.1	A noise reduction method based on alternative component sizing.....	127
5.2	Destructive interference arrangement	128
5.3	Verification through simulation	132
5.4	Results.....	134
5.5	Symmetrical lines results	139
6.	EXPERIMENT DESIGN FOR PROPOSED PASSIVE ELEMENTS EXPERIMENTAL EVALUATION.....	144
6.1	Experimental Setup.....	144
6.2	Sensors and Components	149

6.3	Test rig Assembly	153
6.4	Measured Operation Conditions	155
6.5	Repeatability	158
7.	EXPERIMENTS WITH THE PROPOSED PASSIVE TECHNIQUES.....	160
7.1	Passive Elements Experimental Results	160
7.2	Tandem unit destructive interference index results	175
7.3	Sound Pressure Measurements	180
8.	CONCLUSIONS	183
	APPENDIX A. HYBRID-IN-THE-LOOP HYDRAULIC SCHEMATICS	186
	APPENDIX B. COUPLED UNITS HYDRAULIC SKETCH.....	187
	APPENDIX C. HYBRID-IN-THE-LOOP ELECTRONICS	188
	APPENDIX D. GENERAL TOOL FOR PASSIVE FBNS ATTENUATION	189
	VITA	190
	REFERENCES	191
	PUBLICATIONS.....	199

LIST OF TABLES

Table 3.1 Equivalent Factor for different line discontinuities(Menon, 2004)	72
Table 3.2 Experiment Operating Conditions	85
Table 3.3 HIL Hydraulic Components.....	86
Table 3.4 HIL Test rig Hydraulic sensors.....	90
Table 4.1 Default Simulation bounds	102
Table 4.2 Side branch simulation bounds	118
Table 4.3 Quincke tube simulation bounds.....	122
Table 5.1 Simulated sources	132
Table 5.2 Operation conditions.....	134
Table 6.1 Sensors installed at the tandem unit circuit	150
Table 6.2 Operation condition set 1	156
Table 6.3 Operation condition set 2.....	157
Table 6.4 Measurements sets and configuration summary.....	157
Table 6.5 Comparison Study.....	157
Table 7.1 Sound pressure measurements: Passive elements vs baseline	181
Table 7.2 Sound pressure measurements: 20° Index vs 0° Index	181

LIST OF FIGURES

Figure 1.1 Hydraulic noise areas of study (Edge, 1999).....	24
Figure 1.2 Noise generation, transmission, propagation, radiation, and preception.....	25
Figure 1.3 Cross-section and angle reference for the swash-plate type axial piston unit(Ivantisynin and Ivantysynova, 2001).....	27
Figure 1.4 Valve plate schematic (Klop,2015)	29
Figure 1.5 Simple example of unidirectional hydrostatic hydraulic transmission.....	31
Figure 1.6 A-weights and C-weights regarding human ear perception	33
Figure 1.7 Research guidelines flowchart.....	36
Figure 2.1 Types of Fluid-Borne Noise Cancellation.....	39
Figure 2.2 Two waves shifted by 180° to achieve a destructive interference pattern	40
Figure 2.3 Example of a piezoelectric actuator acting at the fluid in a duct (Wang,2008)	42
Figure 2.4 Two-weight notch LMS filter with delay unit compensation. (Kim,2017).....	44
Figure 2.5 A variable volume Helmholtz resonator by the principle of a movable wall (Bedout et al.,1996)	46
Figure 2.6 Helmholtz resonator schematics and its attenuation frequency response trend (Ortwig,2005).....	49
Figure 2.7 Expansion chamber schematics and its attenuation frequency response trend (Ortwig,2005).....	49
Figure 2.8 Quincke tube example: Segments 2 and 3 have interference patterns among each others frequency content.....	50
Figure 2.9 Passive vibration control system (Masuda and Ohuchi [1996]).....	51
Figure 2.10 Cross-section of the rotating parts of the floating cup machine (Achten [2004])	52
Figure 2.11 Two examples of bending waves propagating into the structure of a duct: a) source vibrations. b) curvatures(Kartha,2000)	54
Figure 2.12 Cross-section of duct	58
Figure 3.1 Necessary blocks for simulating pressure ripple generation and propagation	63
Figure 3.2 Necessary blocks for simulating pressure ripple generation and propagation	64
Figure 3.3 Diagram of a hydraulic line node	67
Figure 3.4 One Dimensional Line Grid Solution.....	67

Figure 3.5 Approximation to variable-property series system.....	71
Figure 3.6 Diagram of a branch approximated to a line node	74
Figure 3.7 Cross-sectional view of a piston in a displacement chamber	76
Figure 3.8 Bulk Modulus HLP 32.....	78
Figure 3.9 Density HLP 32	78
Figure 3.10 Hydraulic system model solver flowchart.....	81
Figure 3.11 Hybrid-in-the-loop hydraulic circuit	83
Figure 3.12 Hybrid-in-the-loop test rig model using the coupled hydraulic system model	84
Figure 3.13 Hybrid-in-the-loop Experimental Bench.....	88
Figure 3.14 Line A ₁ features and sensor placement.....	91
Figure 3.15 Measurement vs four simulation models time-domain results at 100 bar, unit 1 speed equal to 3000 rpm, unit 2 speed equal to 1387 rpm.....	92
Figure 3.16 Measurement vs four simulation models time-domain results at 100 bar, unit 1 speed equal to 2000 rpm, unit 2 equal to 915 rpm.....	92
Figure 3.17 Measurement vs four simulation models time-domain results at 300 bar, unit 1 speed equal to 2000 rpm, unit 2 speed equal to 818 rpm.....	93
Figure 3.18 Measurement vs four simulation models fast Fourier transform at 100 bar unit 1 speed equal to 3000 rpm, unit 2 speed equal to 1387 rpm.....	94
Figure 3.19 Measurement vs four simulation models fast Fourier transform at 300 bar unit 1 speed equal to 2000 rpm, unit 2 speed equal to 818 rpm.....	95
Figure 3.20 Pressure ripple magnitude for four simulated models compared to the measured data	96
Figure 3.21 Pressure ripple RMS for four simulated models compared to the measured data....	97
Figure 4.1 Hydraulic line with upstream and downstream excitation	100
Figure 4.2 Amplitude of the pressure oscillations in each node of the line.....	100
Figure 4.3 Default model used for the study.....	101
Figure 4.4 Targeted amplitudes of the pressure oscillations in a 25 mm diameter line: a) Max pressure ripple; b) Mean pressure ripple; c) Pressure ripple at the Upstream ; d) Pressure ripple at the downstream	102
Figure 4.5 Influence spatial frequency at the a) maximum,b) mean, c) upstream and d) downstream pressure oscillations in a 25.4-millimeter diameter steel pipe.....	104
Figure 4.6 Amplitudes of the pressure oscillations in a 25 mm diameter line neglecting friction effects: (a) Max pressure ripple (b) Pressure ripple at the upstream	105

Figure 4.7 Speed of sound in steel duct of 25.4 mm internal diameter and 31.75 mm external diameter (Klop,2010).....	107
Figure 4.8 Influence of the diameter on the magnitude of the a) maximum,b) mean, c) upstream and d) downstream pressure oscillations in a 1-meter long duct with 50 l/min mean flow and 20 l/min flow ripple	108
Figure 4.9 Influence of fluid oscillation magnitude at mean pressure oscillations in a 1 meter long, 25.4 millimeter diameter steel pipe.....	109
Figure 4.10 Influence of fluid oscillation magnitude at upstream pressure oscillations in a 1 meter long, 25.4-millimeter diameter steel pipe	109
Figure 4.11 Influence of the mean pressure at the maximum pressure ripple in a 1 meter long, 25.4-millimeter diameter steel pipe	110
Figure 4.12 Influence of downstream flow ripple magnitude in proportion to upstream flow ripple magnitude at a) maximum, b) mean, c) upstream and d) downstream pressure oscillations in a 1 meter long, 25.4-millimeter diameter steel pipe	111
Figure 4.13 Influence of downstream flow ripple phase shift in respect to upstream flow ripple at the a)maximum,b)mean, c) upstream and d)downstream pressure oscillations in a 1 meter long, 25.4-millimeter diameter steel pipe	113
Figure 4.14 Pressure variation normalization from a special featured line to a standard line	114
Figure 4.15 Line profile in barrel format and barrel-cornet format.....	115
Figure 4.16 Normalized response of a barrel shape profile to a default profile response in respect to: a) maximum, b) mean, c) upstream and d) downstream pressure oscillations	116
Figure 4.17 Normalized response of a barrel-cornet shape profile to a default profile response in respect to: a) maximum, b) mean, c) upstream and d) downstream pressure oscillations.....	117
Figure 4.18 A closed-end side-branch, with the line length ratio proposed for multiple frequency pressure ripple reduction.....	118
Figure 4.19 Spatial response of a line with a 1/8 length side-branch silencer placed in the center of the line(n=4) normalized to the response of a default profile in respect to the a)maximum,b)upstream, pressure oscillations.....	119
Figure 4.20 Spatial response of a line with a 1/8 length side-branch silencer placed in the center of a line normalized to the response of a default profile in respect to the downstream pressure oscillations	120
Figure 4.21 Downstream pressure ripple spatial response of a line with a 1/8 length side-branch silencer, at n =4, normalized to n=1.....	120
Figure 4.22 Response of a line with a 1/8 length side-branch silencer in place at 1/8 of the line extension profile normalized to the default profile response in respect to the upstream pressure oscillations	121

Figure 4.23 A standard Quincke tube dimension proposed for multiple frequency pressure ripple reduction	122
Figure 4.24 Normalized response of a line with a shorter quincke tube ($L_2=0.7$ meters) versus a larger quincke tube ($L_2=1.0$ meter), both placed at the center of the line, concerning the maximum pressure oscillations	123
Figure 4.25 Normalized response of a line with a default Quincke tube placed at the center ($L_2=1.2$ meters) versus default profile response in respect to the a) maximum,b) upstream.....	123
Figure 4.26 Generic hydraulic system passive solution implementation flowchart for a multiple frequency fluid borne noise source reduction.....	125
Figure 4.27 Generic hydraulic system passive solution implementation flowchart for a single frequency fluid borne noise source reduction.....	126
Figure 5.1 Modeling flow source with two units connected to the same axis.....	127
Figure 5.2 Coherent interference patterns: Constructive interference and destructive interference	128
Figure 5.3 Rotating kit index	129
Figure 5.4 Phase-shift for different harmonics	131
Figure 5.5 Hydraulic diagrams for baseline system and proposed system.....	133
Figure 5.6 Simulation Schematics for baseline and proposed system.....	133
Figure 5.7 Pressure oscillations at the branch & the downstream nodes at 250 bar 2000 rpm .	135
Figure 5.8 Pressure oscillations fast Fourier transform at the branch &downstream nodes at 250 bar 2000 rpm.....	136
Figure 5.9 Pressure oscillations at the downstream nodes at 420 bar 3400 rpm	137
Figure 5.10 Pressure oscillations fast Fourier transform at the branch and at the downstream nodes at 420 bar 3400 rpm	137
Figure 5.11 Pressure ripple root mean square value for the baseline and three coupled units rotating group index angles strategies for the branch and downstream nodes.....	138
Figure 5.12 Hydraulic diagram for the proposed system and similar lines sized baseline.....	139
Figure 5.13 Pressure oscillations at the branch and the downstream nodes at 250 bar 2000 rpm for the similarity-guided design lines.	140
Figure 5.14 Pressure oscillations fast Fourier transform at the branch and & downstream nodes at 250 bar 2000 rpm for the similarity-guided design lines.....	141
Figure 5.15 Pressure oscillations at the downstream nodes at 420 bar 3400 rpm for the similarity-guided design lines.....	142
Figure 5.16 Pressure oscillations fast Fourier transform at the branch & downstream nodes at 420 bar 3400 rpm for the similarity-guided design lines.....	142

Figure 5.17 Pressure ripple rms value for the baseline and three coupled units (Cp) rotating group index angles strategies for the branch and downstream nodes for the similarity-guided design lines	143
Figure 6.1 Single unit hydraulic circuit schematics	145
Figure 6.2 Tandem unit hydraulic circuit schematics	145
Figure 6.3 Segments of the hydraulic load	146
Figure 6.4 Configurations of the hydraulic line; a) Baseline; b) Halfway Silencer; c) Eightway Silencer; d) Quincke tube; e) Tandem unit arrangement	147
Figure 6.5 Halfway silencer normalized to baseline load with a line length of 403 cm and 25 mm diameter; a) Downstream; b) Upstream; c) Maximum;	148
Figure 6.6 Eightway silencer normalized to baseline load with a line length of 403 cm and 25 mm diameter; a) Downstream; b) Upstream; c) Maximum;	149
Figure 6.7 cDAQ-9178 and main modules used for the experiment	151
Figure 6.8 Selected tandem unit display; (a) Closed case; (b) Rotation kit;	152
Figure 6.9 Tandem unit indexation reference	153
Figure 6.10 Candidate passive elements in the hydraulic circuit; (a) Configuration B - Halfway silencer; (b) Configuration D - Quincke tube	154
Figure 6.11 Assembled test rig with Configuration E ; (a) Tandem Unit; (b) Hydraulic circuit	154
Figure 6.12. Accelerometers positioning the hydraulic circuit	155
Figure 6.13 First 20 harmonics for 1200 rpm and 1940 rpm speeds	156
Figure 6.14 Measured pressure ripple Δp_1 at 170 bar (a) 1200 rpm (b) 1920rpm	158
Figure 6.15 Measured pressure ripple Δp_2 at 170 bar (a) 1200 rpm (b) 1920rpm	158
Figure 6.16 Measured Acceleration A_1 at 170 bar (a) 1200 rpm (b) 1920rpm	159
Figure 6.17 Measured Acceleration A_2 at 170 bar (a) 1200 rpm (b) 1920rpm	159
Figure 7.1 Spatial power ratio with unit 1 at 1200 rpm, configuration A; $x = \Delta p_1$ $y = \Delta p_2$	161
Figure 7.2 Spatial power ratio with unit 1 at 1200 rpm, Configuration A; $x = \Delta p_2$ $y = \Delta p_3$	162
Figure 7.3 Normalized Spatial power ratio with unit 1 at 1200 rpm; $x = \Delta p_1$ $y = \Delta p_2$;	164
Figure 7.4. Modification Spectral Power Ratio for p_2 at 1200 rpm	166
Figure 7.5. Modification Spectral Power Ratio for Δp_2 at 1940rpm	167
Figure 7.6. Modification Spectral Power Ratio for A_4 at 1200 rpm	168
Figure 7.7. Modification Spectral Power Ratio for A_4 at 1940rpm	169
Figure 7.8. Modification Spectral Power Ratio for Measured Sound Pressure at 1200 rpm	170

Figure 7.9. Modification Spectral Power Ratio for Measured Sound Pressure at 1940rpm.....	171
Figure 7.10 Measured pressure ripples at 1920 rpm 170 bar (a) Δp_1 (b) Δp_2	172
Figure 7.11. Measured pressure ripples at 1200 rpm 250 bar (a) Δp_1 (b) Δp_2	173
Figure 7.12. Measured pressure ripples at 1920 rpm 250 bar (a) Δp_1 (b) Δp_2	173
Figure 7.13 Measured pressure ripples at 1920 rpm 250 bar (a) Δp_1 (b) Δp_2	174
Figure 7.14. Measured accelerations at 1200 rpm 250 bar (a) A_I (b) A_4	174
Figure 7.15 Measured accelerations at 1920 rpm 250 bar (a) A_I (b) A_4	175
Figure 7.16 MSPR frequency response function: 20° Index normalized over 0° index n=1200 rpm	177
Figure 7.17 MSPR frequency response function: 20° Index normalized over 0° index n=1660 rpm;	178
Figure 7.18 Measured pressure ripples at 1200 rpm 250 bar (a) Δp_1 (b) Δp_2	179
Figure 7.19 Measured pressure ripples at 1660 rpm 250 bar (a) Δp_1 (b) Δp_2	179
Figure 7.20 Measured Acceleration A_I at 170 bar (a) 1200 rpm (b) 1660rpm	179
Figure 7.21 Transfer Function Ratio of pressure ripple vs pipe wall acceleration n=1660 rpm at (a) Branch (b)Pipe Downstream	182

NOMENCLATURE

Symbol	Description	Units
A	Area	$[m^2]$
A_{rHPi}	Valve plate area open to discharge port	$[m^2]$
A_{rLPi}	Valve plate area open to suction port	$[m^2]$
A_L	Area of the duct	$[m^2]$
A_N	Area of the Neck	$[m^2]$
A_o	Area of the Orifice	$[m^2]$
B	Constant	$[-]$
B_L	Isothermal wave speed	$[s/kg\ m^2]$
a_k	Piston Acceleration	$[m/s^{11}]$
C	Characteristic equation (used in MOC line model)	$[-]$
C_c	Capacitance	$[N \cdot s/ m^4]$
c	Speed of sound	$[m/s]$
D	Line diameter	$[m]$
E	Young Modulus	$[Pa]$
e	Wall Thickness	$[m]$
F	Force	$[N]$
F_{ai}	Piston's acceleration force	$[N]$
F_{DCi}	Displacement chamber force	$[N]$
F_{Ns}	Force normal to the swash-plate	$[N]$
F_{Ti}	Friction force	$[N]$
f	Frequency	$[Hz]$
f_{DW}	Darcy friction coefficient	$[-]$
I	Number of pistons	$[-]$
$Index$	Rotation kit index	$[^\circ]$
K	Fluid bulk modulus	$[Pa]$
K_f	Equivalent loss factor	$[-]$
k	Spatial frequency (wave number)	$[rad/m]$

L	Length of the Tube	[m]
L_N	Length of the neck	[m]
l	Inductance	[N·s/ m ⁴]
M_x	Swash plate moment about X axis	[N·m]
M_y	Swash plate moment about Y axis	[N·m]
M_z	Swash plate moment about Z axis	[N·m]
m	Number of displacement chambers	[-]
m_i	Empirical coefficient	[-]
m_N	Mass of the neck	[Kg]
n	Rotational speed	[rpm]
p	Pressure	[Pa]
p_i	i th displacement chamber pressure	[Pa]
p_{HP}	High pressure port pressure	[bar]
p_{LP}	Low pressure port pressure	[bar]
Δp	Pressure differential	[bar]
Q	Flow rate	[m ³ /s]
Q_s	Volumetric loss flow rate	[m ³ /s]
Q_{SB}	Gap flow through VP and CB	[m ³ /s]
Q_{SG}	Gap flow through slipper and swash plate	[m ³ /s]
Q_{SKBG}	Total flow from the gaps	[m ³ /s]
Q_{SK}	Gap flow through piston and cylinder block	[m ³ /s]
Q_r	Flow from ports to DC	[m ³ /s]
R	Resistance	[N·s/ m ⁴]
R_b	Cylinder block pitch radius	[m]
r	Radius	[m]
t	Time	[s]
V	Volume	[m ³]
V_c	Cavity volume	[m ³]
V_i	Derived displacement chamber volume	[m ³]
V_{dead}	Displacement chamber dead volume	[m ³]
v	Fluid velocity	[m/s]

y	Variation of velocity	[m/s]
Z	Impedance	[N·s/ m ⁴]
z	Position	[m]
α_D	Orifice coefficient of discharge	[-]
α_N	Neck length correction coefficient	[-]
β	Swash plate angle	[°]
ΔM_x	Amplitude of swash plate moment M_x	[N·m]
ΔM_y	Amplitude of swash plate moment M_y	[N·m]
ΔM_z	Amplitude of swash plate moment M_z	[N·m]
μ	Dynamic viscosity	[Kg/(m·s)]
λ	Wave length	[m]
ρ	Density	[kg/m ²]
τ	Shear Stress	[Pa]
ω	Angular velocity	[rad/s]
ϕ	Piston angular position	[rad]
ψ	Pressure propagation fixed phase shift	[rad]

LIST OF ABBREVIATIONS

Abbreviation	Description
ABN	Airborne noise
CP	Coupled pumps
DC	Displacement chamber
FBN	Fluid Borne Noise
FIR	Finite-impulse response
HIL	Hybrid-in-the-loop
HP	High pressure
HST	Hydrostatic transmission
IDC	Inner dead center
LP	Low pressure
LMS	Least mean square
LSI	Load simulator
MOC	Method of characteristics
MSH	Mode switching hybrid
ODC	Outer dead center
ODE	Ordinary differential equation
PDE	Partial differential equation
PCFV	Pre-Compression Filter Volume
SBN	Structure borne noise
SH	Series hybrid transmission
Δ	Difference

ABSTRACT

Hydraulic systems have many applications in the construction, transportation, and manufacturing sectors. Recent design trends involve systems with higher working pressures and more compact systems, which are advantageous because of power density increase. However, these trends imply higher forces and larger vibration amplitudes while having lesser mass and damping, leading to higher noise levels. Meanwhile, hydraulic machinery started prospecting new applications with tighter noise regulations, a trend which was also pushed by the electrification tendency in several fields of transportation and agriculture. One method to attain noise mitigation is passive-noise canceling techniques have the advantage of not introducing energy to the system. This approach arranges pressure ripple waves in a destructive pattern by projecting a hydraulic circuit's geometry, configuration, and features.

This dissertation aims to predict fluid-borne noise sources and investigate passive noise-canceling solutions for multiple operations conditions targeting to impact many hydraulic systems and a broad range of operating conditions. Primarily a coupled system model strategy that includes a one-dimensional line finite element model is developed. The line model predicts pressure wave generation and propagation. The model features versatility since parameters like line diameter and material can be discretized node by node. Simulations are compared to measured data in a realistic novel hydraulic hybrid transmission for validation.

Subsequently, an extensive numerical investigation is performed by setting fixed parameters along the hydraulic lines' length and comparing several isolated geometric properties in simulation. The developed line model is also used to study the influence of line features such as diameter and extent of the conduit. Cost-effective and simple passive solution solutions such as Quincke tubes (parallel lines), expansion chambers, and closed branches are selected and investigated on simulation. Four target pressure ripples are chosen as indicators for summarizing passive line elements behavior. The frequency-domain behavior of the pressure ripple peaks regarding the line's length is identified and isolated in simulation at the 50-5000Hz frequency spectrum. An experiment test rig is designed to implement these solutions and the experiments show three developed passive elements as practical and effective solutions for reducing fluid borne noise sources. The selected designs

yielded noise source attenuation over most of the frequency spectrum measured with piezoelectric pressure variation sensors and accelerometers in different positions in the hydraulic circuit. Sound pressure measurements detected reductions over 3dB in the best cases.

Also, a passive interference approach based on the principle of secondary source flow ripple cancellation was conceptualized, modeled, and implemented in a tandem axial-piston unit. The strategy consists of setting the phase between the two synchronous units to accomplish destructive interference in targeted unit harmonics. Two indexing strategies are investigated first analytically and then on simulation. One of the indexing strategies was implemented in a pre-existent commercial axial-piston tandem unit. Experiment results confirmed effectiveness for the first and third unit's harmonics, where reductions over 15dB on pressure ripple were measured.

Finally, a fluid-structure interaction based on the poison coupling principle is developed using the method of characteristics. Transfer functions of the pipeline accelerations versus the pressure ripples on lines calculated on simulation and later obtained experimentally to highlight a critical vibration band from 2000Hz to 3000Hz with high acceleration response.

1. INTRODUCTION

This chapter gives a brief review of noise, its generation, and propagation both in hydraulic units and in hydraulic circuits as a whole. It also presents the motivations for this work and the organization and original contributions offered by this manuscript.

1.1 Background

Hydraulics is a technology based on transferring mechanical power input to mechanical power output by utilizing positive displacement machines and pistons as power converters and valves as power regulators. Fluid power systems are mainly used to transmit energy from one source to various kinds of actuators or drives. It is employed in multiple applications, such as construction equipment, mining equipment, aerospace, agriculture, automotive vehicles, and many industrial applications. Usually, the hydraulic energy is created by a positive displacement pump, which receives mechanical energy from combustion engines in mobile applications or electric motors in industrial systems. The output can be transformed in either a rotary or translational mechanical movement where power can be continually distributed into efforts (force, torque, pressure) and flows (velocity, angular velocity, flow). Therefore, fluid-power is a versatile field that is the optimal technological solution in many engineering applications.

Compared with mechanical drives, hydraulic drives simplify the design of many applications, as rigid mechanical connections between driving and consuming units are avoided. This is particularly advantageous when driving and consuming units are located remotely from each other. Another advantage is that a rotational driving source can be used for linear actuation without fragile and discontinuous crankshaft solutions. Moreover, continuous transmission ratios can be obtained even for high torque operations. Competing electrical-based technologies have some of these advantages; however, one of the main advantages of hydraulics compared to its electric counterparts is high power density, which makes it more suitable for many types of vehicles. Also, electrical linear actuators are extremely limited for maximum power capacity when compared to hydraulic cylinders.

The most recent fluid power design tendencies rely on systems with higher working pressures necessary to further increase power density. However, the corresponding reductions of mass and dampening of the components lead to the generation of higher noise levels. Solutions to attain low noise levels requirements compared to competing technologies are required.

Recently, these requirements became even more crucial because of the noise improvements in concurrent technologies. In the last two decades of the 20th century, combustion engines had reduced noise at a faster rate than hydraulic systems, thus making the hydraulic noise more apparent in many engine driven systems. Later, the trend of electrification for mobile applications reduced overall machinery noise even further. The tendency of electrification and noise reduction is to continue to advance. Taking small on-road vehicles as an example, since the year 2000, hybrid electric vehicles sales are growing an average of 47% a year (Weiss et al., 2012), and electric vehicles are presented as solutions to decrease noise pollution, tightening legislation even further (Weiss et al., 2015). Therefore, the hydraulic system noise will keep becoming more and more perceptible for the machine users, thus becoming the bottleneck regarding noise emission in many applications.

In the context of noise generation, some hydraulic components are more significant than others. Two of the most fundamental elements of hydraulic systems that produce vibrations actively are hydraulic pumps and motors. A hydraulic motor is a positive displacement machine used to transform fluid power into mechanical power. A hydraulic pump is also a positive displacement machine with the opposite function. Most of the positive displacement machines have a finite number of displacement elements and, therefore, also the finite number of displacement chambers (DC). This causes a periodic flow pulsation, also called flow ripple, which propagates through the hydraulic system. The pulsating flow produces pressure pulsations, which are further converted into structural vibrations and eventually transmitted as air-borne unwanted sound. Besides, pulsating forces inside the positive displacement machines produce vibration of the structure and thus generate additional noise. Also, forces inside the positive displacement machines directly produce vibration in the structure and thus generate extra noise.

Another factor to consider is that there are many different components in hydraulic systems that can influence the system noise generation, e.g. valves, fittings, elbows. For example, the length of any given hose in the system can result in different noise levels. This implies that system developers have a very demanding job: finding the most suitable combination of components that together make a low overall noise level. Moreover, hydraulics can suffer from a phenomenon called cavitation, which occurs if pressure drops below atmospheric pressure level, causing the formation and implosion of gas bubbles, leading to very noticeable noise and machine damage.

From a legal perspective, the national and international legislation on noise emissions in urban areas is becoming stricter. The requirements governing working conditions in industrial environments are likewise increasing. For example, the European Council published several documents setting legislation for the noise level of various machinery categories, determining stricter levels for the noise produced by outdoor equipment (Johansson, 2005). These regulations are aimed to protect both workers and citizens from insalubrious noise levels. American legislation also defines maximum noise levels for each construction equipment (Chanaud, 2014), both to the operator and at 50 feet distance, which represents the distance common public will be from the noise source.

1.2 Motivation

1.2.1 Noise Generation

According to Edge (1999), there are three types of noise in a hydraulic system: fluid-borne noise (FBN), structure-borne noise (SBN), and air-borne noise (SBN). Structure-borne noise is mainly generated through mechanical forces acting in structural surfaces connected to elements with pressure variation, such as the displacement chambers. These forces create vibrations in the hydraulic circuit surface. For example, in a hydraulic axial piston unit, the exciter is the piston, generating both a stream of flow and oscillating forces. The pump housing and the connected structure are the resonant systems. When the fluid inside the displacement chamber and ports is rapidly pressurized, the sound intensifies at higher frequencies. This effect is not observed with gradual pressurization of the liquid.

Fluid-borne noise refers to noise generated oscillating flow and pressure fluctuations by the system, which is originated from pumps or motors with a finite number of displacement chambers at most times. The flow pulsation encounters the fluid inertia originating a pressure ripple. The pressure ripple interacts with the hydraulic lines and the structure to which the lines are connected, generating dynamic movements of the mechanical structure, creating further vibrations. Since fluid and structure have interacting surfaces through all the system, fluid and structure interact with each other such as structure-borne noise will be transmitted to the liquid and fluid-borne noise will be transferred to the structure. Eventually, the vibrations of the outer structure will be irradiated to the air. As vibrations interact with the surrounding air, the air begins to vibrate, and air-borne noise develops. Structure-borne and fluid-borne sources can be evaluated either on the time-domain (quantifying peak to peak amplitudes of swash plate moments, flow, and pressure ripple) or on the frequency-domain (separating and evaluating each harmonic of the oscillations).

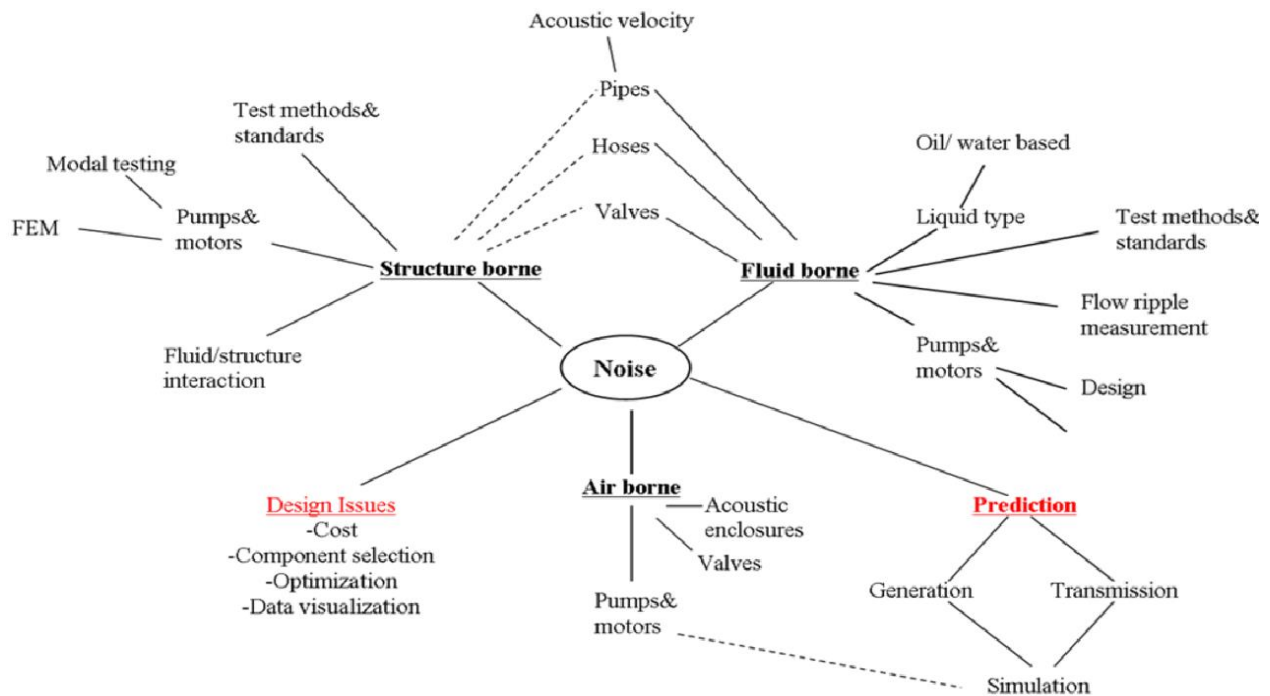


Figure 1.1 Hydraulic noise areas of study (Edge, 1999)

The amount of noise generated depends on the surface's size, the interface between the body and the ambient air, and the vibrations' nature. The perceived noise by humans depends not only on the measured noise level but also on the frequency distribution of the pressure waves in the air. For example, at an isophonic curve, the observed noise level is constant for different frequencies,

although the measured sound level is not (Boden et al., 1999). The perception of noise or humans depends not only on the acoustic response of the anatomic hearing system but also on the subjectivity of comfort on noise which is covered by the field of psychoacoustics.

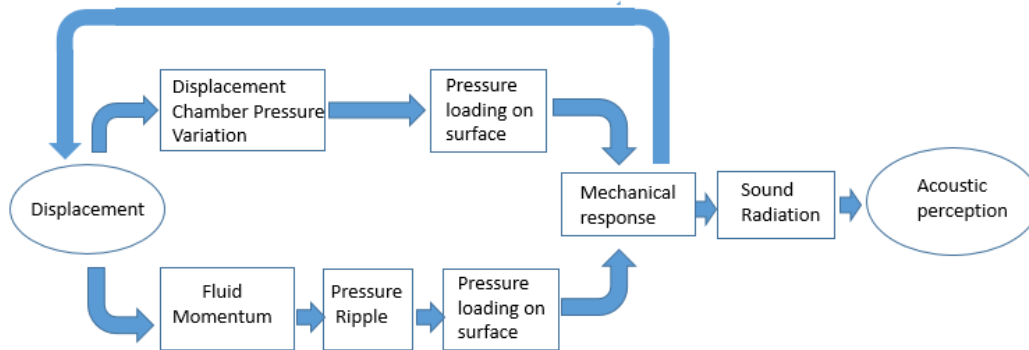


Figure 1.2 Noise generation, transmission, propagation, radiation, and preception

While the path from a noise source to a hearable airborne noise source is complex, expressive results with measure air-borne noise sources can give evidence of the most effective methods to reduce noise. Very recently, Ichiyanagi et al. (2015) affirmed a 33% reduction in amplitude of the noise source pressure ripple would result in a 3.5 dB reduction in noise level. Harrison and Edge (2000) claimed reducing flow ripple and thus pressure ripple is the most effective method to minimize air-borne noise. To support this claim, Harrison and Edge presented a mechanism called high damping check valve capable of reducing pressure ripple and achieving up to 6 decibels measured air-borne noise source reduction and mentioned Rebel's work of Rebel (1977).

Rebel (1977) introduced an active servo-valve control for a three-piston axial piston pump, a maximum speed of 2000 rpm, and accomplished up to 9 dB FBN reduction with open-loop control and up to 17 dB reduction with closed-loop control aiming the lower harmonics of the unit. However, Rebel concluded that the system was not commercially viable due to the system bandwidth limitations (50 hertz). There was also an efficiency compromise in this strategy. The commercial regulations are even more clear when recalled most hydraulic units have more than three displacement chambers. The fundamental harmonic of a unit spinning at speed n in rpm with the number m of displacement chambers is given by equation (1.1). For example, a nine-piston pump axial piston running at 2000 rpm will have a first fundamental harmonic of 300 Hz.

$$f_{1st\ harmonic} = \frac{n\ m}{60} \quad (1.1)$$

Adding an actuator to accomplish noise cancelation is called active noise cancelation, and the bandwidth limitation of the actuator is a known imitating factor. Lower frequencies are also easier to implement feedback control as the actuator phase can be more accurate. However, passive noise cancelation techniques are known to be effective in high frequencies, as will be described further in section 2.1.

1.2.2 Noise in Swash-plate Axial Piston Units

There are many different types of positive displacement machines, such as gear machines, radial piston machines, vane type machines, bent-axis machines, and axial piston machines. The working principle remains the same: When working as a pump, the inlet flow is taken from the port while the displacement chambers (DC) volumes are increasing. The inlet flow is divided into chambers and delivered to the outlet line while the DCs volumes are decreasing. The process is reversed while working as a motor. Swash-plate type axial piston machines are often selected for vehicle transmissions because they operate at high pressures, high speeds, high efficiency and are still reasonably compact.

At a swash-plate type axial piston pump, the rotation parts consist of the cylinder block, slippers, pistons, and the shaft. As a cylinder rotates, the piston goes back and forth, causing a displacement of fluid inside the displacement chamber result in the intake and outtake flow. In case the hydraulic unit is working at pumping operation, the great majority of intake and outtake flow will be on the low pressure (LP) port and high pressure (HP) port respectively.

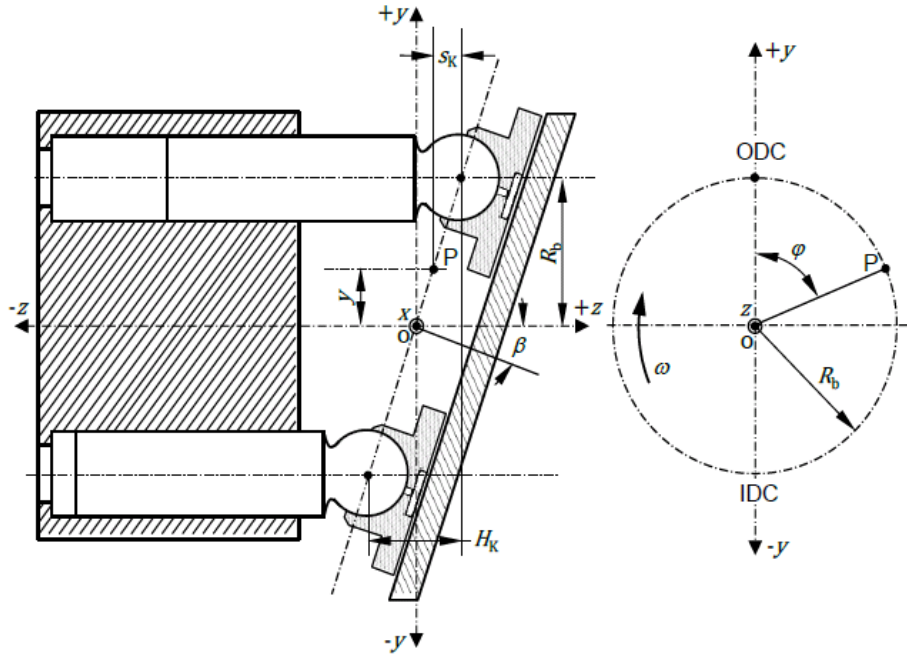


Figure 1.3 Cross-section and angle reference for the swash-plate type axial piston unit(Ivantisynin and Ivantysynova, 2001)

The total flow delivered at the HP port and LP port will be proportional to the value of the summation of all the HP ports flows into every chamber Q_{rHPi} , and LP ports flow into every chamber Q_{rLPi} . The number of displacement chambers and pistons is given by i . The total flow to each port is provided by the sum of all the individual flows, as shown by equations (1.2) and (1.3).

$$Q_{HP} = \sum_1^n Q_{rHPi} \quad (1.2)$$

$$Q_{LP} = \sum_1^n Q_{rLPi} \quad (1.3)$$

As each of these flows contains oscillations, the total flow delivered at the ports will also have a flow ripple. The discharge rate of a pump is affected by kinematic flow ripple, fluid compressibility, and cross-porting flow. HP flow (Q_{HP}) is strongly influenced by the compressibility of the fluid and the cross-porting that is determined by the design of the valve plate. Depending on this design, the displacement chamber can be connected to HP and LP simultaneously. The amount of fluid

exchanged between both ports during these instants directly influences instantaneous pressure buildup flow ripple in the displacement chamber (Kim, Kalbfleisch and Ivatysynova, 2014).

Valve Plate design also determines the timing of pressure buildup closes to outer dead center (ODC) and inner dead center (IDC) locations, which results in strong influences to flow ripple. At ODC, the displacement chamber (DC) transitions from LP to HP compresses fluid into the DC, creating back-flow for a short period. These rapid flow rate drops will happen every time a DC is opened to HP in the revolution; thus, for a nine-piston unit, as an example, there will be nine pressure drops throughout the revolution. At IDC, the DC transitions from HP to LP. If the valve plate's design allows the chamber to be opened to LP and HP simultaneously, cross-porting flow at the IDC will also create a sudden drop in flow rate since the fluid in the HP port is delivered to the LP port. If cross-porting occurs at the ODC the already existing backflow can be increased. However, since this backflow can make the displacement chamber to be pressurized at a slower pace, it can provide smoother compression of fluid, which possibly reduces the generation of high-frequency excitations content inside the displacement chamber.

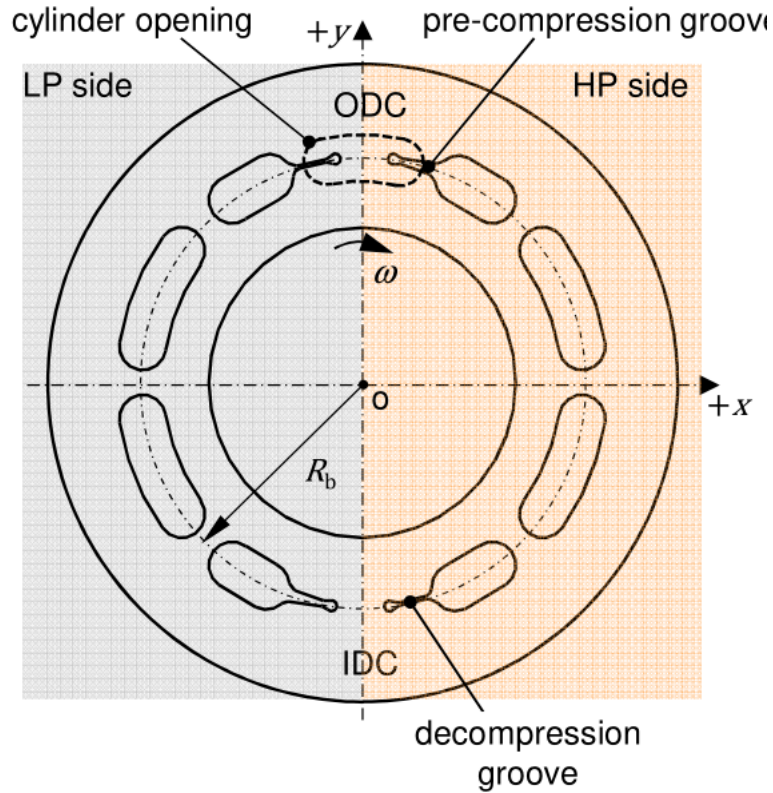


Figure 1.4 Valve plate schematic (Klop,2015)

Figure 1.4 shows the groove positioning of a valve-plate. The cross-sectional area of these grooves regarding the ports represents the orifice area in which the displacement chamber communicates to HP and LP. During most of the piston rotation, the angle ϕ the value of at least one of the areas is equal to zero, meaning the displacement chamber is connected to only one port.

At IDC and ODC, the cross-sectional areas increase slowly, representing the geometries of the relief grooves that influence the pressure of the displacement chamber. Remarkable work done with Valve-plate design and relief groove geometry to achieve noise source reduction was done by Palmberg(1989), and the usage of optimization techniques to reduce these sources was performed by Seeniraj(2009) and Kalbfleisch(2015).

1.2.3 Noise in hydraulic circuits

After being generated in units, both fluid and structure-borne noise will propagate through the hydraulic system, which impedance will influence the frequency response of the excitation and later affect the mechanical response of the system.

Therefore, in addition to pump-design solutions for reducing noise sources, there are also system design solutions. Some of the alternatives that affect the system's impedance, which can be mentioned, are the Helmholtz resonator and the closed end-pipe. Both components are referred to as side branch dampers, with well-defined resonance frequencies. Side branches use the principle of a hydraulic mass-spring system. The advantage of side branches is that they can be tuned easily for certain frequency regions. However, they cannot be adjusted outside of a relatively narrow bandwidth, limiting their practical use in modern systems that operate with widely varying pump speeds. These elements will be revisited in section 2.1.3.

Also, the hydraulic unit's housing material influences vibration and noise emission to the surrounding environment. One way to change the existing hydraulic response is tuning circuit component dimensions such as pipe lengths, housing shapes, volumes, and orifices properly. An ideal design minimizes the resonant response for the frequency ranges that coincide with the excitation energy. Moreover, insulation techniques can be applied with the hydraulic lines, pump cases, and other components, reducing transmission of the vibrations from the structure to the atmosphere.

Optimal sizing of components and circuit architecture can also achieve noise reduction. Klop et al. (2009) developed a model able to predict superimposed noise sources of the interacting pump, motor, and line dynamics. The same modeling approach was used to describe the impact of line lengths on pressure ripple (Klop and Ivantysynova, 2008). Later, the model was used to present noise-source reduction strategies based on line lengths to a case study (Klop, 2010) based on line lengths in a hydraulic line. A software called Transmodel was developed to simulate multiple architectures. This model compares noise sources for various configurations possible, allowing the system designer to choose compact and inherently quiet solutions.

One of the most challenging applications to obtain noise reduction is in hydraulic transmissions. The reason is that this application will have a wide range of operation conditions, compact packing (reducing mass and damping), and tight noise regulations. This challenge is even more defying if the noise reduction has to be accomplished by passive fluid-borne noise techniques, which are usually tuned for specific frequency bands and compromise other frequency bands. Such methods are covered in section 2.1.

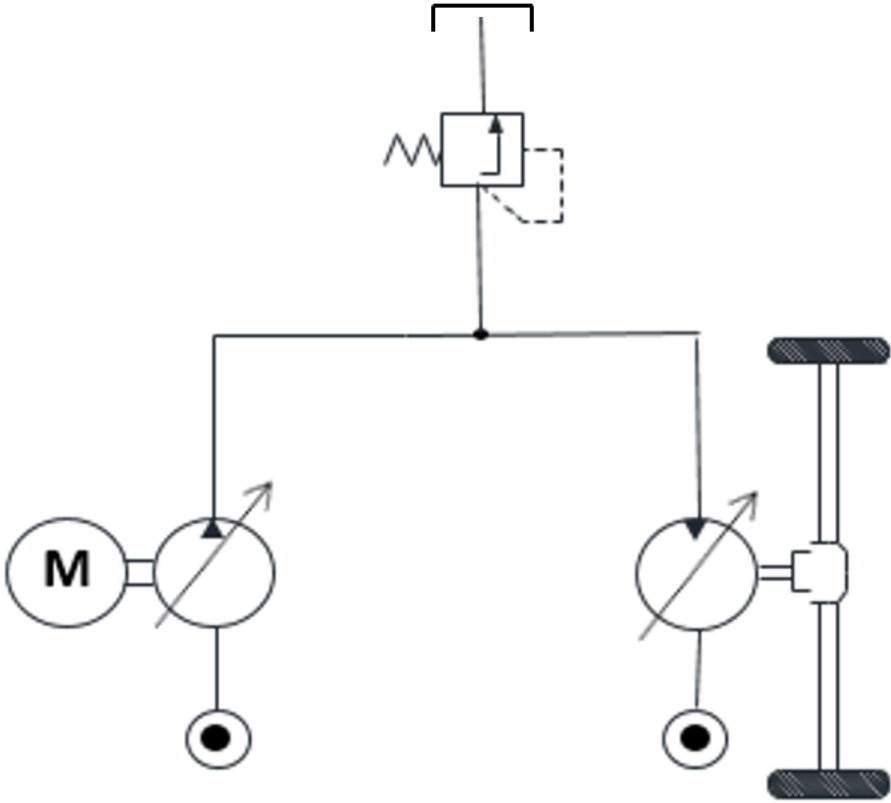


Figure 1.5 Simple example of unidirectional hydrostatic hydraulic transmission

However, it is essential to mention that predicting pressure oscillations with a non-empirical model in a realistic system is a defying but relevant task. To project lines that are inherently quiet, with curvatures, diameter changes, and discontinuities and without the necessity to perform several experiments to characterize the system behavior, better models are needed. Kojima and Shinada(1986) obtained outstanding pressure ripple behavior and transmission prediction using a frequency-domain approach combined with each hydraulic element's characterization through

experimental data. Klop(2010) got far better results predicting pressure oscillations in a controlled noise-source guided experiment than in real application transmission in a case study.

Calculating pressure ripples accurately for a realistic non-characterized hydraulic circuit is still a challenge to be overcome.

Reducing pressure ripple was claimed to be the most effective way to reduce system noise (Harrison and Edge,2000) when prototyping a heavily damped check valve mechanism achieved up to 6 dB air-borne noise reduction in the best case. Passive fluid-borne noise reduction has the potential to eliminate vibrations as early as possible, avoiding the complex task of modeling vibration propagation through complex three-dimensional structures with discontinuities. Also, several passive fluid-borne noise cancellation techniques have low cost, are easy to implement, do not require extra energy to be introduced to the system, and do not require feedback or any supervisory system. Moreover, structure-borne noise reduction may also be achieved by fluid-borne noise reduction since a passive technique consists of using the energy generated by the system itself to cancel undesired harmonics vibration, and one source of the oscillations in hydraulic systems is the pressure ripples of the pressurized fluid.

This dissertation focuses specifically on developing multi-operation condition passive fluid-borne noise source reduction strategies, expecting to impact the largest number of hydraulic applications as possible. For a broad frequency range, the frequency range chosen as scope to this works was 50-5000 Hz based on human's ear isophonic response, which suggests this frequency band is the most critical for human salubrity, in specifically c- weighting, which is the response for levels above 100 dB. A-weighting and C-weighting are frequency dependant curves that mimic the effects of human hearing, such as the ear drum's resonance, which is about 4000 Hz, causing higher sound levels.

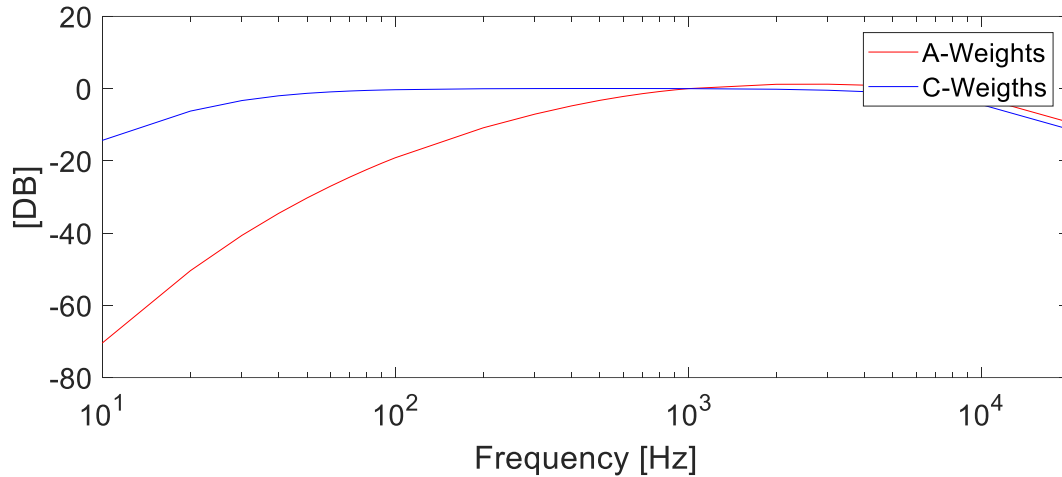


Figure 1.6 A-weights and C-weights regarding human ear perception

A secondary goal for this dissertation is to improve noise-sources simulation methods, which are possible with the introduction of new techniques, software, and hardware. Several noise-source predictions and reducing breakthroughs were obtained in literature by developing a simulation model either of generation or propagation of noise sources. In the 1980s, as computer technology became sufficiently robust, sophisticated models were developed to quantify the noise generated by flow ripples. This led to several new methods of reduction of FBN, including the introduction of the pre-compression filter volume(PCFV) by Pettersson et al. (1991), later studied by Ivantysynova et al. (2005), and crossing swash-plate angle by Johansson et al. (2002) and Manning and Dong(2004).

Dynamic models of pumps and motors were developed by Edge and Darling(1986), Palmberg(1989), Ivantysynova (1999), and Johansson and Werndin(2001), among others. In recent years, pump and motor models have been further developed using genetic algorithms with multiple objective functions to select an optimal design for given applications (Johansson, 2005)(Seeniraj, 2009)(Kalbfleisch, 2015).

While good noise reduction strategies were obtained with computer pump simulations, better models are required for system simulation. In 2000, Kojima and Ichiyanagi attempted to develop a transfer matrix-based computer simulation program to be a useful design tool for reducing fluid-borne noise on the pump discharge, only to find out the wave propagation would be dependent on

the upstream and downstream elements. Therefore, better tools capable of reproducing the interactions between pumps and motors with the hydraulic line are needed.

In this thesis, a model able to predict superimposed noise sources is developed and used to study the effect of passive fluid-borne noise reducers in lines and the impact of default line features, such as length, diameter, and duct material to these sources. The model is also used to develop new passive noise cancellation strategies using destructive interference patterns and investigate these proposed solutions.

1.3 Research Objectives

The objective of this thesis is to predict fluid-borne noise sources and propose passive noise cancellation solutions for developing quieter future hydraulic systems. The aim is not only to reach a better understanding of the interference patterns which are present in lines but also to evaluate strategies that passively use these interference patterns and may be useful in reducing fluid-borne noise sources without needing a high investment to be implemented. Passive-noise cancellation techniques have the advantage of not introducing energy to the system, not requiring feedback, and also being effective at high frequencies. Simultaneously, several passive fluid-borne noise reduction elements are low cost and easy to implement at existing and future hydraulic systems.

Consequently, findings regarding the effects of pipeline friction in hydraulic circuits and pipe wall resonance are a secondary goal to the dissertation. It is also an investigative contribution towards solutions that may effectively design hydraulic circuits to yield less audible noise to the people in the surroundings.

To accomplish effective noise source reduction solutions, this thesis's primary approach is to develop a versatile simulation model and use it to investigate strategies through simulation, thereby understanding how to design multi-frequency passive noise solutions. Finally, this study aims to propose, analyze, simulate, and measure feasible noise reduction solutions applied in practical hydraulic systems. The stages completed to seek this work are listed below:

- Development of a time-domain model capable of capturing superimposed pressure and flow pulsations dependent on the pump, motor, and system dynamics simultaneously. Therefore, the model will be able to simulate and propose fluid-borne noise source (FBNS)

reduction strategies taking into consideration the crossed influence between hydraulic lines and hydraulic components.

- Enhance stability and accuracy of the time-domain model to simulate “realistic’ hydraulic circuits, that is, hydraulic circuits with a considerable number of hydraulic elements and the presence of realistic often neglected features such as diameter variations, elbows, and line material variation.
- Design an experiment to validate this model and also to evaluate the impact of the varying parameters in a hydraulic line, such as duct material variation (steel, hydraulic hose), duct diameter, and also the presence of curvatures in the line.
- Propose a multi-operation condition passive fluid borne noise source reduction strategy for typical hydraulic applications. Specifically, in this study, a flow source replacement for coupled units to obtain destructive interference in targeted harmonics is proposed.
- Verify the performance of this strategy using the developed time-domain model to verify if the superposition of hydraulic elements crossed influence will affect the proposed strategy's effectiveness.
- Use the time-domain based model characterize via simulation hydraulic lines and typical passive hydraulic elements response on the frequency-domain. Compare the frequency-domain responses of the default line with passive elements to investigate strategies that can reduce the FBNS compared to the trivial line for the whole 25-5000 Hz spectrum to achieve effective strategies for multi-operation condition applications.
- Design of an experiment for verifying if the coupled units strategy is still useful in real-world applications. Compare its results with simulations.
- Design an experiment to verify some of the proposed strategies based on the replacement of default hydraulic lines for passive elements.

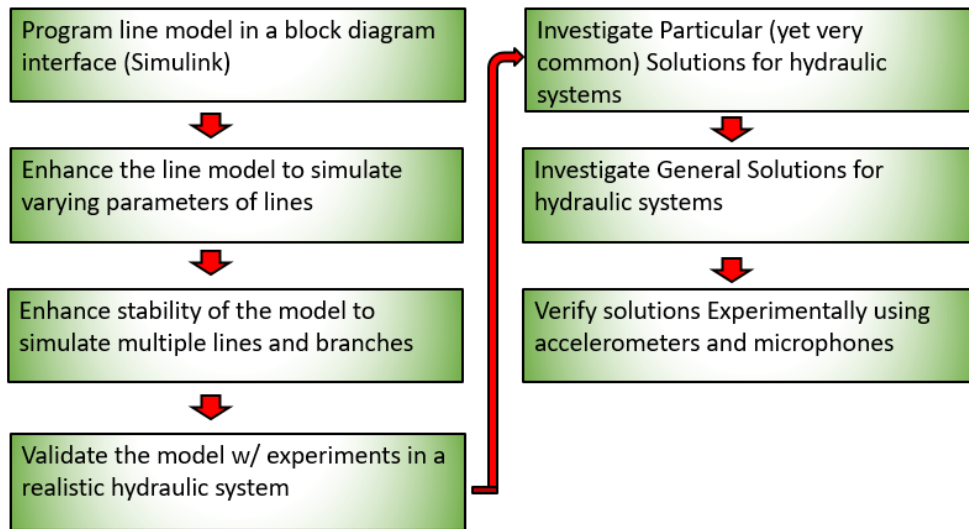


Figure 1.7 Research guidelines flowchart

1.4 Thesis Organization and Original Contributions

In chapter 2, a comprehensive review of noise reduction techniques employed in fluid power is presented, the advantages and disadvantages of each method are disclosed. An introduction to line models is also presented.

Chapter 3 presents the modeling approach, which is used in this thesis. The chapter describes each component of the model's mathematical approach and its assembling into a coupled hydraulic system model. The method of characteristics (MOC) line model in this study's main component is explained in detail. As shown in this chapter, the swash-plate type axial piston pump is chosen as the default hydraulic unit for this thesis's scope; however, the modeling approach can be extended for other types of units. While this chapter does not show any theoretical novelty, section 3.7.1 shows a state-of-art simulation regarding system complexity using the Method of Characteristics (MOC) as a line model. This was accomplished by selecting models for each component added to the solver strategy presented in the chapter. The method of characteristics based line model is further developed to support the line's discrete parameters, which is an original contribution of this dissertation. To evaluate this new model's accuracy, a mode switching hydraulic model architecture is presented, simulated, and then assembled to run experiments. Measurements are

conducted, and its results are compared to the simulation results to evaluate the influence of geometric and material parameters on pressure ripple in a hydraulic circuit.

Original contributions of this work are presented respectively in chapters 4,5,6, and 7 of this dissertation. In chapter 4, a holistic and comprehensive study of fluid-borne vibrations in hydraulic lines is developed. To accomplish this, hydraulic lines are isolated from the remaining system, and the frequency-domain behavior of the line is extracted by performing a set of time-domain simulations for isolated frequencies at the range of 25 Hertz to 5000 Hertz. In this study, passive reduction features are observed and compared to a reference line to develop fluid borne noise source reduction strategies and summarize these strategies in tools that application engineers can use to project their hydraulic circuits in a theoretical quieter manner.

In chapter 5, a novel passive noise source reduction strategy based on coupled units is presented. The method consists of replacing single units with a pair of units that can have targeted harmonic contents canceled by setting the pressure oscillations generated by both units into destructive interference. The strategy is investigated first analytically and followed by a simulation study using coupled hydraulic models.

Chapter 6 displays the experiment's design elaborated to evaluate the effectiveness of the strategies elaborated in chapters 4 and 5. A hydraulic circuit is designed, and a reference case is used as a baseline to represent a hydraulic circuit in which no technique is implemented. Then, the circuit is modified with the introduction of the proposed passive elements. The experiment also uses a tandem unit to evaluate the proposed destructive interference strategy. Chapter 7 shows the experiment results and the most findings of noise source mitigation effects the solutions can provide to the hydraulic power field. Finally, the conclusions of the experimental results are drawn in chapter 8.

2. STATE OF ART

This chapter presents a literature review of the state-of-art of the relevant subjects to achieve the objectives illustrated in chapter 1. Section 2.1 gives an overview of noise cancellation techniques and strategies used in hydraulic systems. Section 2.2 presents the numerical approaches used to model the propagation of pressure oscillations in hydraulic lines.

2.1 Noise Cancellation Overview

As vibration is an earlier stage of noise-generating, vibration canceling techniques are usually used to attempt to reduce overall audible noise. According to Franchek et al. (1994), there are four classifications of vibration control techniques: (1) passive; (2) active; (3) hybrid; (4) adaptive-passive vibration controls.

Passive techniques involve using reactive or resistive devices to change the acoustic impedance of a system, generally affecting a wide range of frequencies, thereby reducing vibration in particular regions for a given set of frequencies. Consequently, there are increases in vibration for other frequency bands. Passive techniques are known to have better performances in high-frequency conditions while having poor performances in low frequencies (Jiao et al.,2003).

Active methods achieve noise reduction using force actuators requiring external energy. This technique effectively reduces a single harmonic disturbance; the drawbacks are the cost, the energy requirements of an active control system, and the limitations when applied to high frequencies(Pingchao et al.,2006)(Wang and Johnson,2008).

Hybrid techniques integrate a passive approach combined with an active control strategy, achieving a reduction in a broader range of frequencies than any of the previous would achieve alone. Finally, adaptive–passive vibration control achieves an attenuation of harmonic excitations through dynamically tuning a passive device to the desired range of frequencies so that optimal performance is guaranteed regardless of the operation condition (Bernhard et al. 1992). Adaptive-

passive techniques resemble active techniques in the sense that there is a necessity for feedback control.

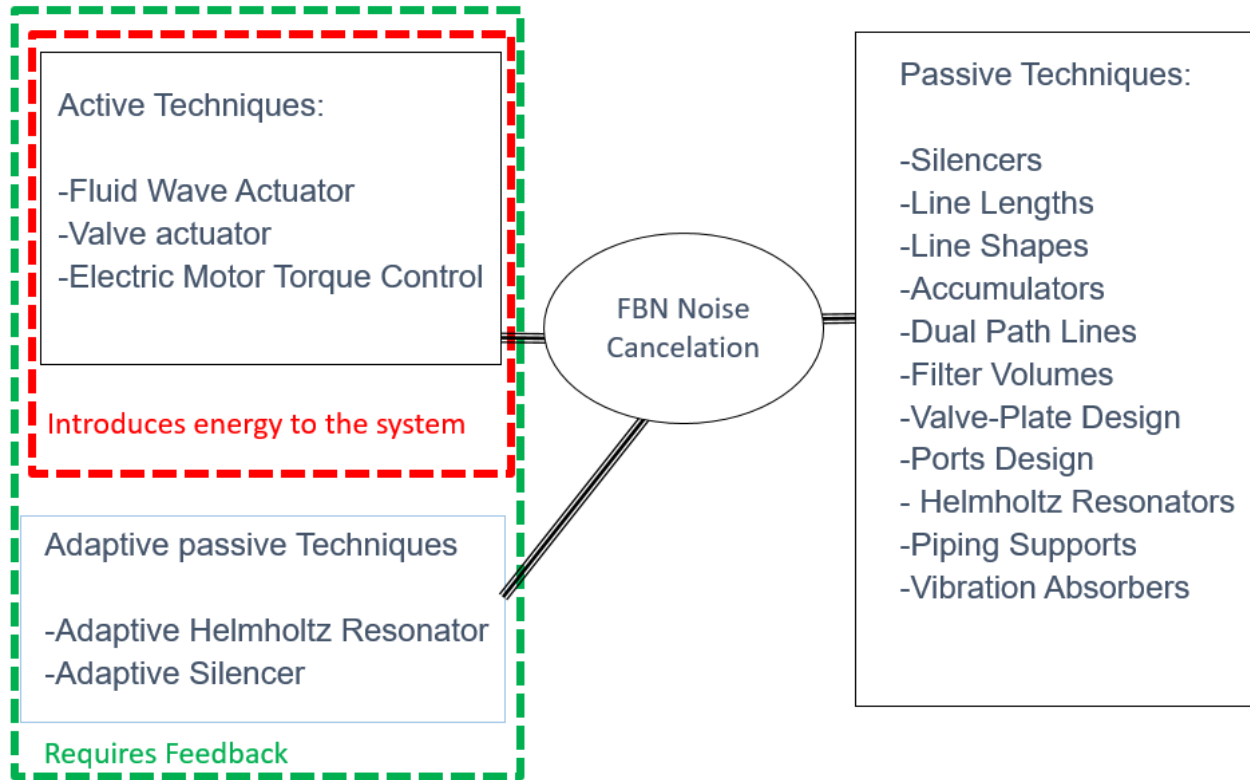


Figure 2.1 Types of Fluid-Borne Noise Cancellation

While active cancellation techniques cannot be used for higher frequencies due to the actuators' bandwidth limitations, passive techniques cannot be used for low frequencies because of size constraints. As frequencies get lower, the wavelengths become more extensive, thus requiring extensive components to influence the waves.

One example is the quarter wavelength side branch resonator, a closed-end tube with a length of one-quarter of the wave's length. This component is a ramification with a closed-end of the line inserted at the hydraulic circuit; the resonance modes of the standing waves of pressure and flow oscillations are the frequencies that fit a quarter-wave into the branch and its respective odd number harmonics (Ichiyanagi and Nishiumi, 2008). Considering, for instance, a wave with a frequency of 50 Hertz and a 1090 m/s propagation speed, the wavelength is equal to 21.8 meters,

and thus a 5.45 meters long tube would be required to reduce noise. In many engineering systems, both active and passive strategies are combined to cover noise reduction in a more extensive set of frequencies to achieve better performance overall.

2.1.1 Active Noise Cancellation

The principle behind active control is the addition of secondary source(s) to cancel the response generated by the primary source. Lueg(1934) first proposed an active control technique to reduce noise using the destructive interference of sound waves. The principle can be explained as a pressure wave propagating in space that can be canceled by adding an equal amplitude wave shifted by 180° phase, as shown in Figure 2.2. The inverted signal is called a destructive interference signal. In most cases, the fluid borne noise in hydraulic systems is caused by positive displacement units at multiples of the unit's fundamental frequency, also called the first harmonic. This harmonic amplitude tends to be directly proportional to the pump operating speed, resulting in a deterministic noise source. For example, a nine-piston axial piston running at 3000 rpm has a shaft fundamental frequency equal to 50 Hz. However, the unit has nine pistons, each opening a connection to the high-pressure port one time per revolution totalizing nine flow oscillations per shaft revolution, resulting in a first harmonic of 450 Hertz. Therefore, the pumping device's operating frequency can be used as a reference signal to the controller, which in turn generates secondary signals out of phase with the pump signals to cancel fluid-borne noise.

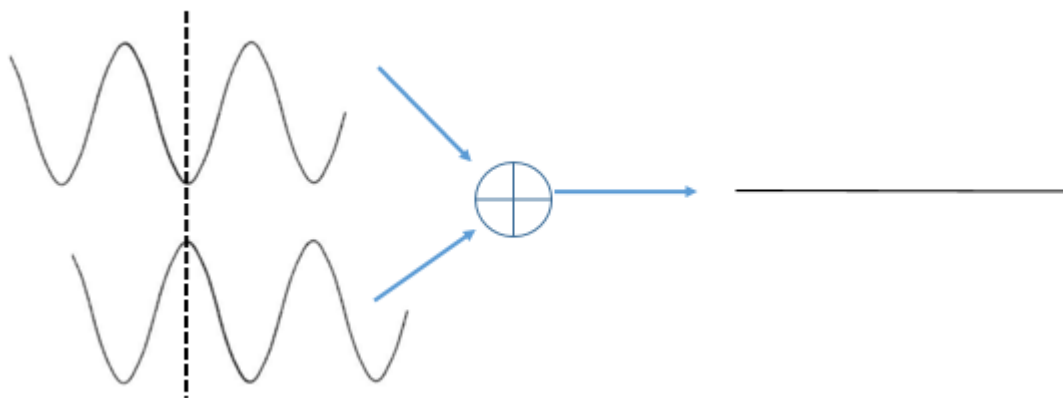


Figure 2.2 Two waves shifted by 180° to achieve a destructive interference pattern

A key element of active noise canceling is actuators, which need to provide the necessary control signal's amplitude, frequency, and phase for its application. High-frequency limitations affect even state-of-the-art actuator technology and are factors for implementing a given active noise cancellation strategy. Sensors and data acquisition must also be considered since these elements need to provide accurate measurements and avoid random and systematic errors(Wang and Johnson,2008). Also, the algorithms are a crucial point of active control. It is rather challenging to use traditional control techniques for this purpose. Due to the excessive phase lag obtained at such high frequencies, high gain is required, violating the stability margins (Johansson,2005).

Another among the most common active vibration reduction actuators is the piezoelectric actuator. The primary advantage of piezoelectric actuators is the high speed of operation. Maillard(1998) examined the potential for active control to reduce fluid pressure impulses generated by a system's hydraulic pump and motors. The target system was a hydraulic pipeline aboard a ship. Pressure pulses generated in the pipes from a hydraulic pump and a motor resulted in high noise levels. A non-intrusive structural actuator was implemented to control these pressure pulses actively. The actuator consisted of a peripheral ring of piezoelectric stacks vibrating on the pipe wall to produce an axisymmetric flat wave. The actuator was effective for all targeted frequency ranges, but the vibration reduction did not bring cancellation superior to 90% of the primary pulsation. Kartha(2000) assembled an experimental rig, filled with water at ambient pressure, and performed tests on the vibration and pressure reducing devices. Experiments were conducted using a combination of active and passive techniques: a Helmholtz resonator and a side branch with piezoelectric oscillator composites. Active control experiments were performed at three different frequencies: 70, 150, and 500 Hz. The measurements demonstrated vibration reductions from 15-30 decibel[dB]. Later, broad experiments from 0-500 Hz were performed and showed decibel reductions from 10-20 dB at the pressure sensors. An accumulator using a piezoelectric actuator to reduce high-frequency flow pulsations was developed and used in a range of 500Hz to 1kHz by Yokota et al. (1996). The method reduced flow pulsations well at the three target frequencies in the study.

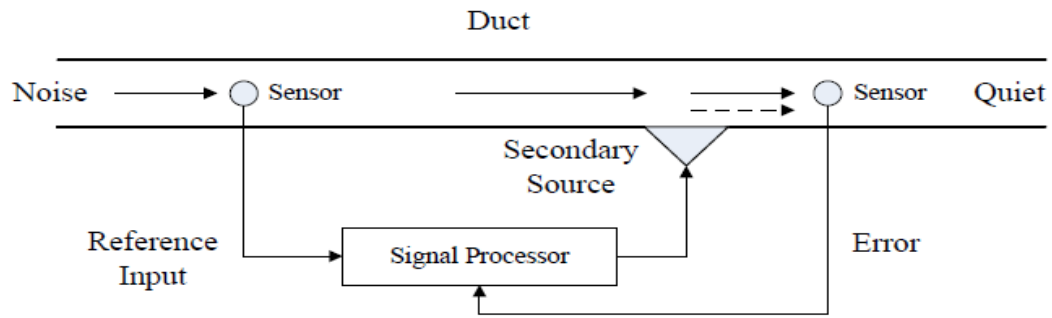


Figure 2.3 Example of a piezoelectric actuator acting at the fluid in a duct (Wang,2008)

Other actuators to be used are valves. Harrison(1997) used the rotary valve in which flow pulses were proposed to replace the lost flow from the delivery chamber of an axial piston pump, thus reducing the delivery pressure ripple. The actuator could operate up to 225 Hz but needed a feeding source to provide the flow. Unless a constantly filled-up accumulator was used, the feeding source had its ripple and reduced the device's effectiveness, which was concluded to be non-viable commercially. Servo-valves had been tested with good results in slightly higher frequencies. Jiao et al. (2003) used an orifice valve as a second source and achieved a 68% reduced rate at a frequency of 350 Hz.

Other actuators also can be used for active control strategy. A servo-cylinder was used by Kojima and Shinada(1986)(1992) to reduce pressure pulsations. The control strategy was a Finite-Impulse Response (FIR) filter and an analog compensating circuit, achieving 20 dB reduction of pressure pulsations ranging from 15 to 400 Hz harmonic signals. Harper and Leung(1993) employed a seven degree-of-freedom system and demonstrated a substantial decrease in low-frequency noise transmission at fluid-filled pipes. Six piezoelectric polymer PVDF cables were used as active actuators. The cables acted around a flexible section of the pipe. Also, a piezoelectric actuator operated directly into the fluid. An active orifice valve was developed by Jiao et al. (2003) to reduce pressure pulsations by controlling leakages of the system. The orifice valve used a piezoelectric actuator for this purpose. Specifically, in swash-plate axial piston units, Ohuchi et al. (2002) examined an open-loop swash plate control strategy to repress swash plate vibrations of a

22cc/rev, pump with an odd number of pistons, joining synchronized sinusoidal signals. The method indicated a maximum level of sound pressure reduction of 74 to 68dB.

Concerning active control, when an actuator is used to generate secondary oscillations in a system, the control strategy is crucial since there is the need to estimate and generate the correct frequency and phase of the respective oscillations. A repetitive controller, which uses the fact that pressure ripples at the present time are almost identical to the pressure ripples that appeared one period earlier, was employed by Hara et al. (1985). The controller was able to actuate the pulsation device before the pulse was detected by the sensors, introducing phase lead compensation. However, as the phase lead can vary depending on the situation, adaptive controls are more suitable for active techniques.

While many techniques rely on canceling the pressure ripple after it is generated on the line, some methods try to prevent its generation by adjusting the electric driving unit speed to compensate for the pump speed and avoid pressure ripple generation. This method was investigated for axial piston units by Minav et al. (2011), but no control logic was proposed. Later, O'Shea (2016) theorized and implemented a feedforward electric motor torque control algorithm to a gerotor to get 75 % pressure ripple reduction in the first harmonic, which had a frequency of 60 Hz.

Because of the time-varying nature of vibration, adaptive algorithms have been widely used in various active vibration/noise control applications. Active vibration control algorithms can be classified into three types: feedback control, feedforward control, and hybrid control that combines the former two (Kim,2017). Feedback algorithms use the error of the sensor feedback signal to generate a vibration suppression signal. Feedforward algorithms either use an extra reference sensor or create a new reference signal for the fundamental vibration frequency. The Least Mean Square technique (LMS) is very popular among adaptive algorithms due to its simplicity and stability (Elliott,2000). The FxLMS Filter (Filtered-x LMS) was introduced as a compensation for the secondary path between the filter output and the sensor's error (Kuo and Morgan, 1995). The technique is widely used in the automotive industry (Clark et al., 1998). FxLMS techniques were also used for servo-valves actuators (Pan et al., 2012,2013).

Kim(2017) was the first to use advanced adaptive control for swash-plate vibration reduction. The proposed active vibration control system was implemented and achieved vibration reductions measured with accelerometers at the case and at the swash-plate. Also, noise reduction was measured for some strategies. In this work, both a two-weight notch LMS filter with a delay unit compensation algorithm and a two-weight notch FxLMS were used.

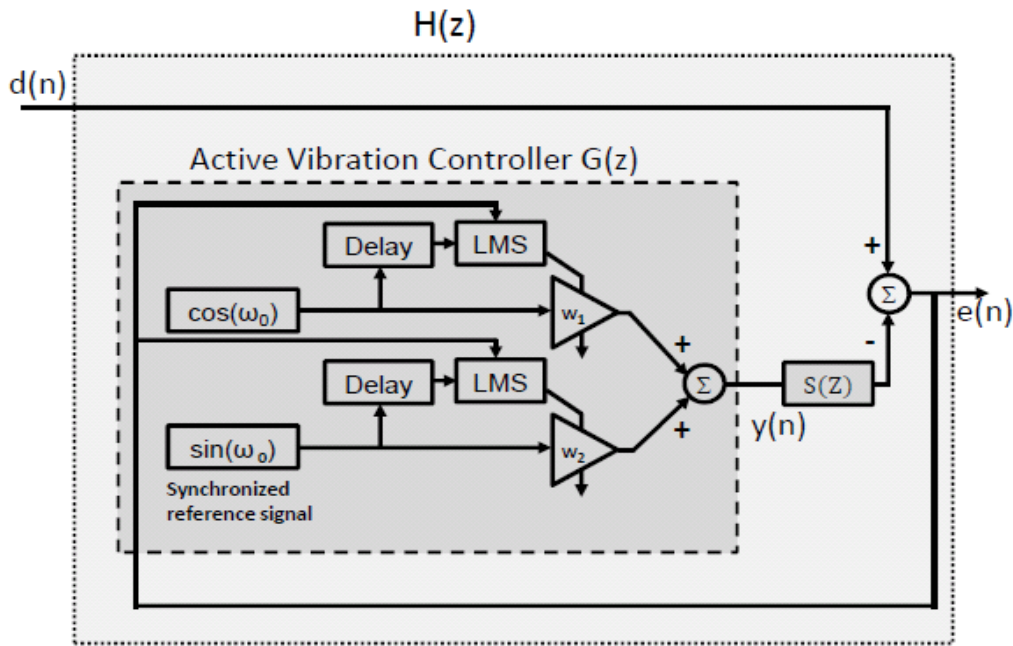


Figure 2.4 Two-weight notch LMS filter with delay unit compensation. (Kim,2017)

Wang(2008) did use line models to do a supervisory system for active control techniques. A FIR filter based two-weight LMS adaptive notch filter has been used using the method of characteristics to give an accurate description of pressure and flow ripple at any point along the pipe. Two strategies were suggested for noise cancellation methods to make the system stable. In simulation results, above 90 percent of fluid-borne noise was attenuated in simulation both for single and multiple-frequency cases.

2.1.2 Adaptive-Passive Noise Cancellation

Adaptive passive control techniques are characterized by tonal, time-varying stimuli and are an alternative between fully active and passive methods. Each approach has its drawbacks. If the noise fundamental frequency changes over time, a passive approach does not provide satisfactory

performance. Meanwhile, active techniques are limited to low frequencies and narrow bandwidths. A drawback of adaptive passive control is the requirement of online control, increasing the design's cost and complexity.

One adaptive-passive technique is semi-active pulsation dampers, a tunable vibration damper for harmonic vibration applications. The semi-active dampers are adjustable and passive. Therefore, the dampers do not actively reduce pressure waves, but the steady-state resonance response can be modified for good damping performance as the excitation frequency varies. A theoretical study of solid body dampers with tunable resonance frequencies was presented by Mikota et al. (2001). Adaptability to varying excitation frequencies is demonstrated. Experimental results were published (Mikota,2001), and the concept was patented later.

A more popular adaptive passive alternative is the adaptive Helmholtz resonator, a simple element frequently used in acoustic applications. A conventional Helmholtz resonator is a hydraulic component composed of a narrow neck and a large cavity volume, and it is ideally designed to have a single resonant frequency. Ideally, the volume should have a spherical shape to keep a more predictable frequency behavior. The resonator can be modeled very similarly to a mass-spring system. At the Helmholtz resonator's resonant frequency, the liquid mass travels within the resonator neck at high-velocity amplitudes. Consequently, the resonator's mouth sends back a high amplitude tone that is out of phase with the incident channel field and thus accomplishes destructive interference.

Nonetheless, the resonator loses efficiency as the applied excitation frequency moves away from the intended resonant frequency. An adaptive Helmholtz resonator can be tuned to the changing excitation frequencies because the resonant frequency can be modified by applying changes to the resonator geometry. The resonant frequency for a spherical Helmholtz resonator is given by equation (2.1)(Alster, 1972):

$$f = \frac{c}{2\pi} \sqrt{\frac{A_N}{V_c(L_N + \alpha_N)}} \quad (2.1)$$

Where V_c is the volume of the resonator, A_N is the area of the neck, and L_N is the length of the resonator neck. The factor α_N is a correction ratio used to calculate the neck's effective length, which value can vary from 1.5 for a flanged termination to 1.7 for an unflanged termination (Kinsler et al. 1982). To change the Helmholtz resonator's resonant frequency, both the area of the neck or the volume of the resonator cavity can be modified.

In an example of work done with variable volume adaptive Helmholtz resonators, Kela(2010) designed a piston-shaped Helmholtz resonator that could change its volume from 0.33 liters to 1.9 liters. The element achieved pressure rippled reduction up to 20 dB between frequencies of 35.6 and 46.4 Hertz. Another interesting strategy to change the volume is to insert a wall in a cylindrical cavity and change the cavity volume as the moving wall angle concerning the fixed wall changes such as the work of Bedout et al. (1996). However, this technique is much more popular in air applications since the moving walls may not be feasible to work with high pressure.

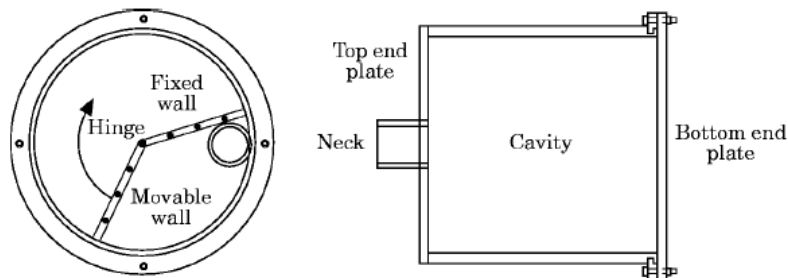


Figure 2.5 A variable volume Helmholtz resonator by the principle of a movable wall (Bedout et al.,1996)

Regarding the neck area, Kartha(2000) used a throttle valve in a Helmholtz resonator neck and thereby developed a tunable resonator with a range from 77 Hz to 278 Hz (neck 10% to 100% open). Nonetheless, the experiments using the tunable Helmholtz resonator did not obtain the expected results. In this work, it was pointed out that this could have been caused by air bubbles or first harmonic structural waves. Recently an adaptive Helmholtz silencer which could vary both its volume and neck area was proposed and designed (Ichiyanagi et al., 2013)

Adaptive-passive techniques can also be combined with active strategies. Kostek, Franchek, and Bolton(1998) combined a dynamic noise control system with adaptive-passive elements. The adaptive-passive element was a tunable Helmholtz resonator. The performance requirements for noise reduction for the system could not be achieved by either one of the parts alone. A tuning algorithm for the resonator was developed to deal with non-measured broadband vibrations. This enabled the adaptive-passive system to tune for several noise tones.

2.1.3 Passive Noise Cancellation

Passive-noise cancellation techniques rely either on changing the system's impedance as a whole or shifting the phase of predetermined frequencies. Most passive methods that act directly on structure-borne noise involve structural damping or insulation.

Measurements were conducted by Kartha(2000) to compare the response of a test rig with or without dampening line segment. The dampening segment was a rubber isolator comprising a fabric reinforced rubber hose clamped on two regular steel pipes with flanges at both ends. The rubber section embedded within the steel pipes created an alteration in the structural impedance. The component successfully stopped the transmission of structural waves on the test rig. Nevertheless, the working fluid, water, in this case, had low pressure and was stationary in these experiments. In this work, in hydraulic systems under high pressure, the performance of the tested elements can degrade. According to Maillard(1998), conventional vibration absorbers, like the rubber insulator, can become ineffective as structural vibration absorbers at high operating pressures.

A compact damping principle is known as the “solid body compensator” is based upon mechanical mass-spring resonance systems that absorb pressure ripples(Mikota,2000). Concerning the branches of the hydraulic side, the attenuation performance of the solid body compensator is restricted to frequencies around the mechanical resonance. Hence, the device is effective in a narrow bandwidth. However, differing serially mounted solid body compensators allow for a larger frequency region to be covered. (Johansson, 2005).

Another component, which works on the principle of wave-canceling, is the quarter-wavelength resonator. A quarter wavelength tube's length is selected to be an odd integer multiple of a quarter wavelength of the acoustic disturbance to be controlled. In Dodson et al.(1998), three quarter wavelength types were experimentally tested (flexible side branch, in-line, and rigid side branch) in an industrial-scale hydraulic system. It is important to note that these experiments' piping system was a flexible, reinforced rubber hose. Using one-dimensional acoustic theory, the behavior of rigid side branches was predicted correctly.

Efforts have been carried out to develop side branches with broadband attenuation. An example is a multi-volume resonator presented by Kojima and Ichiyanagi(1998). The principle is based upon several side branches in series, giving rise to multiple mass-spring systems with different oscillating frequencies. The complex tuning process required for proper performance (Mikota, 2000) is the main problem with the multi-volume resonator concept.

Already mentioned in section 2.4, Helmholtz resonators are components often used in applied acoustics. A simple Helmholtz resonator essentially encompasses a cavity volume and a neck with defined area and length. The neck's fluid also acts as the mass element, while the stiffness element is provided by the acoustic pressure inside the cavity. At the resonant frequency, the Helmholtz resonator's mouth radiates out of phase with the incident duct pressure field, thus reflecting the vibration back to the source. Such a resonator can reflect the sound wave of a specific frequency: the resonant frequency. Since a non-adaptive resonator does not need to have variable volume, ideally, the resonator should shape a perfect sphere, such as in Figure 2.6. Recently, other shapes, such as hemispherical vessels, have been tried for hydraulic applications (Ichiyanagi et al., 2017). Accumulators used for storing power in hydraulic systems can also be successfully used as Helmholtz resonators(Larsson,1989)(Ortwig,2005).

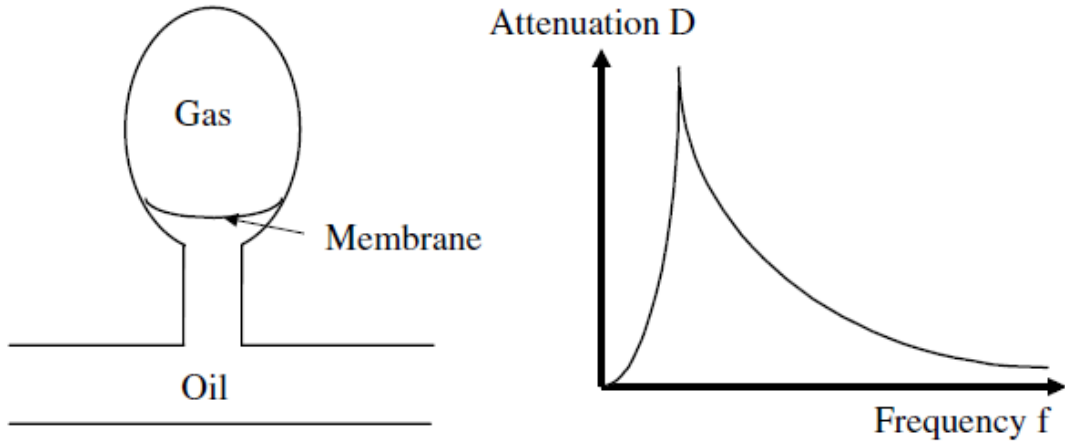


Figure 2.6 Helmholtz resonator schematics and its attenuation frequency response trend (Ortwig,2005)

Another famous passive pulsation damper is the expansion chamber attenuator, which allows efficient and broadband attenuation at low cost (Weddfelt et al. 1985)(Larsson,1989) and is widely used in ventilation systems. In multi-volume expansion chamber attenuators, the attenuation frequency range has a lower frequency limit because of the mass-spring resonance from the pipes between the chambers. However, they usually give better attenuation at higher frequencies. The downstream attenuation of this technique is generally very good. Thus, it is crucial that these dampers are mounted very close to the pump and that the diameter of the hose joining the pump and the damper is as large as possible to prevent severe upstream pressure ripples, i.e., between the pump and damper (Rydberg, 2001).

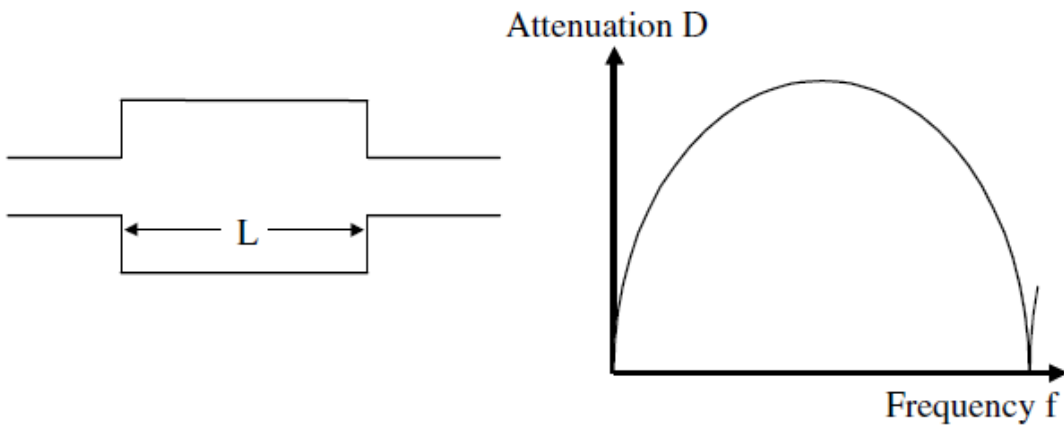


Figure 2.7 Expansion chamber schematics and its attenuation frequency response trend (Ortwig,2005)

Quincke was the first to introduce the idea of unequal acoustic path lengths in a branched duct to eliminate propagating waves by destructive interference. With a so-called Quincke tube, the flow is separated into two parallel paths of different sizes. The pressure ripples in both courses are thereby phase-shifted 180 degrees for a set of frequencies. As the flows are combined, their pressure waves cancel to some extent. According to Johnston and Edge(1989), the Quincke tube attenuation might be efficient, but it is hard to tune. Nonetheless, in a more recent work, pressure ripple reduction for a single speed (1000 rpm) bent axis pump was obtained using parallel lines (Kim et al., 2005). It was observed that the phase between the pressure wave of both units was 180°, which was possible to achieve because the pump's speed was well defined.

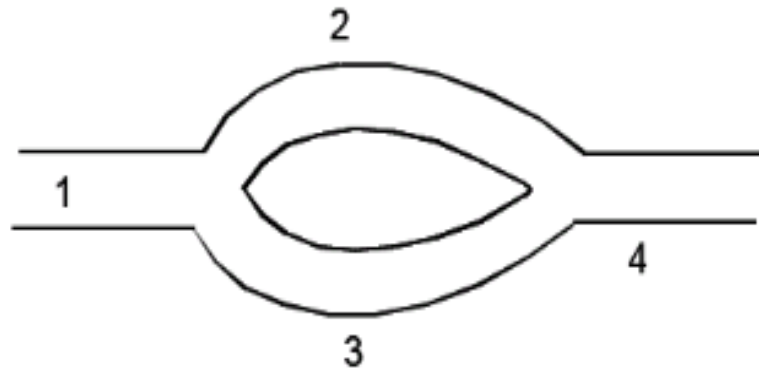


Figure 2.8 Quincke tube example: Segments 2 and 3 have interference patterns among each others frequency content

2.1.4 Hydraulic Unit Design for Pressure Ripple Mitigation

Fluid-borne noise sources can be reduced by understanding its behavior and tackling its generation at units' design: the displacement chamber's pressurization. One early scientific work was performed in 1967 by Helgestad(1967) for axial piston units. Later, Hegelstad et al. (1973,1974) presented the importance of pressurization of the cylinder volume and described ideal timing and the relief groove's pressure effects at the displacement chamber pressurization process. Becker(1970) presented the influence of valve plate timing on displacement chamber pressurization and delivery flow fluctuations in 1970. Ideal timing is setting the valve plate timing so that the displacement chamber and high-pressure port will have the same pressure as the valve plate is opening the connection among the respective volumes. Ideal timing is determined by the

swashplate angle and delivery pressure and, therefore, cannot be used for a wide range of operating conditions.

Orifice area management techniques such as the valve-plate grooves design (in swash-plate axial piston units) also are useful for reducing fluid borne noise sources. According to Palmberg(1989), the decrease of pressure oscillations with grooves in valve-plate can reduce both SBN and FBN in axial piston units. Since the orifice regulates the flow strokes' timing and magnitude to the unit ports, the flow ripple at the ports can be regulated, and then the pressure ripple. Hydraulic unit design focusing on flow ripple reduction also can be extended to other types of hydraulic units such as external gear pumps (Devendran and Vacca,2013) and vane pumps (Zanetti-Rocha et al.,2013).

There are also examples of passive noise source reduction using the pressure of the displacement chamber to accomplish destructive interference. In particular, for swash-plate axial piston units, Masuda and Ohuchi(1996) made use of a passive swash plate control on a pump with an even number of pistons by joining displacement chambers and control cylinders. The passive method exhibited sound pressure reductions from 71 to 64.5dB in the best case.

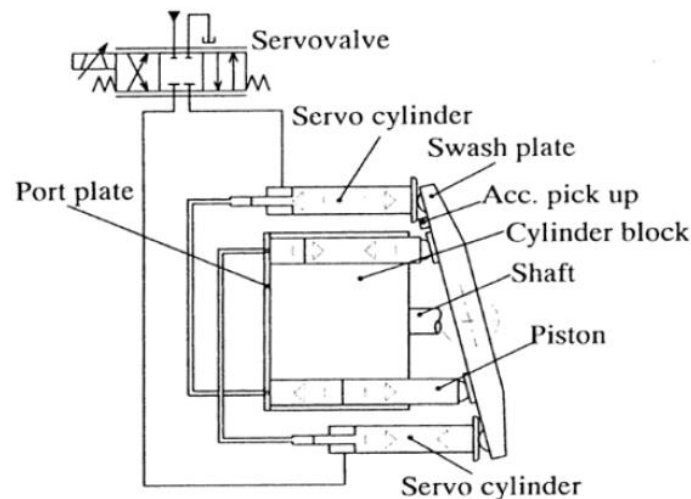


Figure 2.9 Passive vibration control system (Masuda and Ohuchi [1996])

Novel architectures had been elaborated for reducing the flow ripple by reducing the number of displacement chambers in hydraulic units. Achten et al. (2004,2017) developed an axial-piston unit architecture that was conceptualized using the floating cup principle. The unit architecture has a centralized double-ring with mirrored pistons. This configuration allows a low tilt angle, cancelation of the forces, and a high number of displacement chambers. Great efficiency was shown by this configuration due to the low friction compared with the slipper-type pumps. Also, the barrel tipping torque reduction allows high-speed operation. Experiments showed a strong reduction in flow pulsations due to the high number of pistons and the floating cup principle of this unit(Plazer et al., 2004). Other examples of innovations in other types of units, such as gear units, are the dual flank pump design (Negrini,1996), or the non-involute pump design (Mitome, 1983).

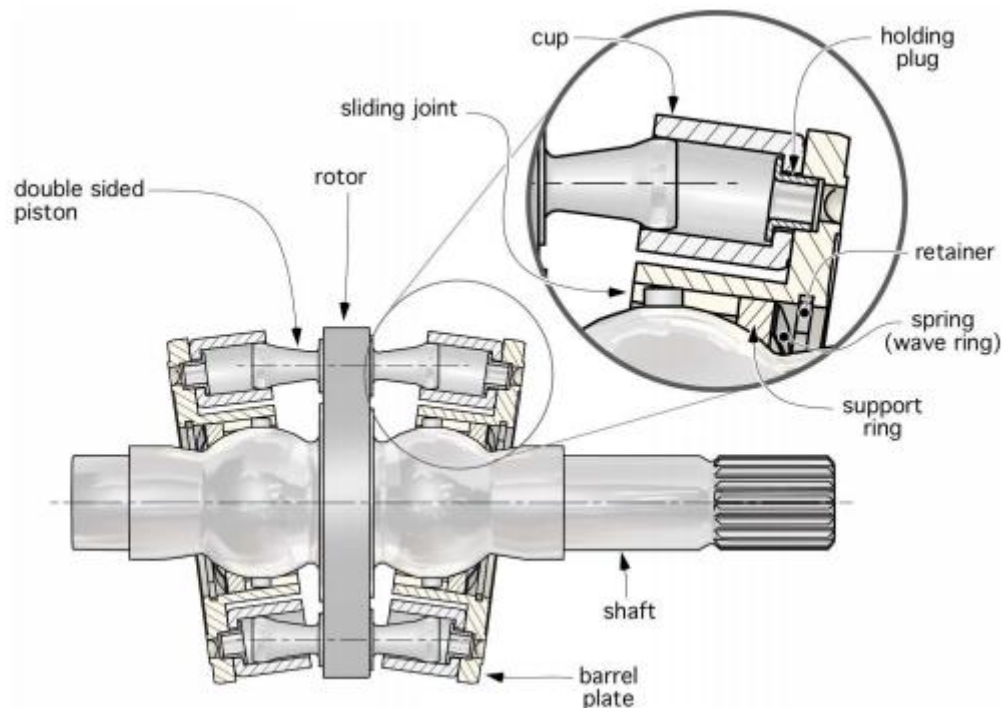


Figure 2.10 Cross-section of the rotating parts of the floating cup machine (Achten [2004])

Once the number of displacement chambers is reduced, a second principle can be added to reduce the flow ripple even further: anti-phasing. Anti-phasing is accomplished by displacing the two units creating a 180° phase shift at the fundamental first harmonic. For gear units, flow ripple

cancellation using the anti-phasing principle has been attempted by the Dowty 1P3000 series (Lipscombe, 1987). The application of these principles in other hydraulic unit architectures, such as axial piston tandem units has not been much studied.

2.2 Line Models Overview

There are many approaches to model hydraulic lines in a hydraulic circuit. There are two major groups of modeling approaches: the ones which simulate the line behavior on the time-domain and the ones that simulate the line behavior on the frequency-domain.

The frequency-domain methods can be utilized in modeling hydraulic systems to examine the sources of noise. These techniques depend on evaluating the source's flow and the source's impedance of either motor or pump. The source impedance of the pump is a transfer function representing the frequency-dependent relationship between pressure and movement at the pump port. Each frequency has a particular transfer function. The pump source movement(flow) describes the unit's flow identified by the unit's kinematics, free of the system's remaining parts.

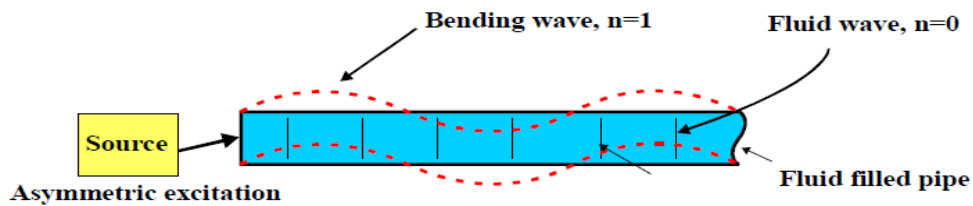
An alternative to frequency-domain methods is time-domain methods. The simplest time-domain form is a lumped parameter model. Implementing lumped parameter models is comparatively easy; however, some criteria must be met: one-directional flow, constant fluid velocities, and constant pressures in the middle of each lumped volume. The line capacitance, fluid inertia, and resistance must be formulated such time response of the system will be outputted. In some models set up a range of transfer functions representing the line, based on the line impedance (Karnopp,1972)(Kassem,1988)(Rabie,2007). When based on empirical data, lumped parameter standards can describe both turbulent and laminar flow.

A more complete form of the time-domain line model was introduced by Wylie and Streeter(1978) using the Method of Characteristics (MOC) to linearize two partial differential equations, the continuity and momentum equations, into four ordinary differential equations, called characteristic equations. As a discrete one-dimensional model, some parameters can be discretized, which defines the model as a distributed parameter model. A vital element of this particular model is a precise calculation of friction that may be dependent on frequency. Zarzycki and Kudzma(2004)

created weighting function standards for two-dimensional wall shear stress appropriate in both turbulent and laminar regimes. This method has likewise been applied successfully to study water hammering effects (Wiggert et al., 1985)(Adamkowski and Lewandowski,2006)(Klop,2010). The benefits of the MOC include simplicity when implementing boundary conditions and finite element methods. One disadvantage of this approach is that it can solve mathematical formulations computationally expensive for very complicated systems that have many elements included.

While the method of characteristics shows efficiency in characterizing the propagation of excitations through the fluid path, there are also propagations throughout the mechanical paths, e.g., the line walls, couplings, and fittings. Kartha(2000) detected the presence of first harmonic structural bending waves at the rig response for his experiments performed at low pressure. It was necessary to eliminate the structural waves with rubber line segments. Structural waves could be generated due to test rig discontinuities or by asymmetric excitation at the sources. This asymmetric excitation can be caused by structure-borne vibrations of the sources that can be propagated from the boundaries of the duct's structure.

a)



b)

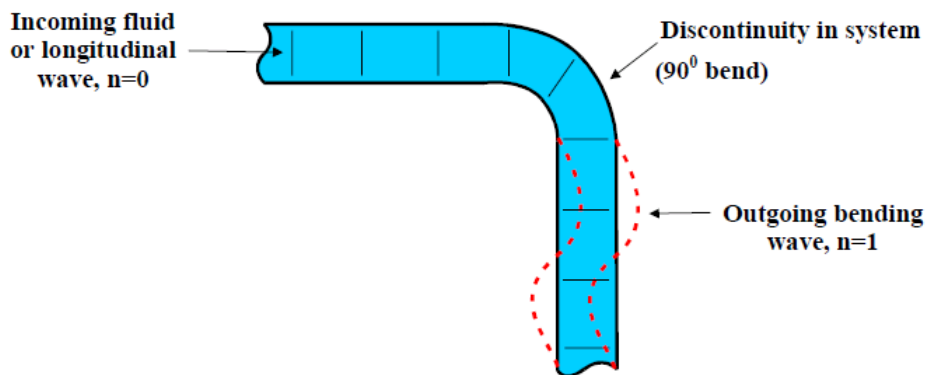


Figure 2.11 Two examples of bending waves propagating into the structure of a duct: a) source vibrations. b) curvatures(Kartha,2000)

To measure the one-dimensional flow for pipes carried by bending, longitudinal, and torsional waves, Verheij(1980) formulated cross-spectral density methods. Usually, these waves are in the low-frequency range. At these frequencies, the complex dispersion of waves in pipes approaches simple rod and beam models. Through simplification of the models, the line becomes a homogeneous one-dimensional surface model that can be used to estimate energy propagations of the vibrations. Pavic(1992) was the first to decompose the flow and structural excitation waves in fluid-filled pipes by applying acoustic structural intensity measurement methods.

However, for high-pressure applications, most of the cancellation techniques for structural vibrations are dubious (Maillard, 1998). The necessity to maintain high pressure requires the lines to be stiff, and thus damping techniques became ineffective. Two consensus guidelines to reduce these vibrations would be to make the lines as straight as possible and to minimize structure-borne noise at the hydraulic units.

2.2.1 Lumped Parameter Models

The most straightforward approaches to evaluate the pressure oscillations in a line are lumped parameter models. A popular method is to calculate the hydraulic capacitance, resistance, and inductance of the line separately and then join the three together to determine the total impedance of a line in a circuit analogous to electrical systems. For this system, voltage, as an effort, is directly comparable to fluid pressure and current is comparable to fluid flow. This technique can be extended to even more complex systems such as hydrostatic transmissions containing pumps, motors, and lines with respective impedances. The pump, which can be modeled as a flow source, has a theoretical flow characterized by the pump's kinematics only.

A pressure ripple can be used as a voltage source, or a flow ripple can be used as a current source for an electrical circuit. The pressure analogy is an electrical potential, and the fluid volume is an analog to charge. For a straight long hydraulic line, the capacitance R , inductance l , and resistance C of the line are respectively calculated by equations (2.2), (2.3), and (2.4) (Akers et al., 2006).

$$R = \frac{8\mu L}{\pi r^4} \quad (2.2)$$

$$C_c = \frac{V}{K} = \frac{L\pi r^2}{K} \quad (2.3)$$

$$l = \frac{\rho L}{\pi r^2} \quad (2.4)$$

Where K is the bulk Modulus, ρ is the density, and μ is the viscosity of the fluid. While this method seems trivial, it can still achieve noise reduction up to this date. In recent work, Akers et al. (2006) present a case study where the electrical circuit analogy is used to reduce noise sources in a medium-size agricultural tractor's hydraulic system. After the mathematical model representing the system was developed, an attenuator was sized and incorporated in reducing both noise and system instability.

Lumped models can further be extended for more sophisticated approaches. Rabie(2007) did propose a lumped model to predict water hammer in hydraulic transmission lines and then suggested the usage of accumulators to prevent it. The model would split the transmission line into four connected lumps to calculate the model's transfer matrix and simulate the transients of a line with good experimental matching.

2.2.2 Transfer Function Approaches

Frequency-domain line models are often chosen because of their simplicity and ability to capture superimposed pressure and flow pulsations. The most popular approaches are based on the transmission line method (TLM).

This method is simple, elegant, and computationally inexpensive; however, this approach presents some drawbacks. One is the aspect that the displacement chamber pressure and discharge flow rate are not dependent on the entire system's dynamics. Therefore, the model does not reflect the interrelated dynamics between the pump and motor. A second limitation is that the model assumes no fluid compressibility, which is considered a primary factor influencing flow and pressure oscillation magnitudes. Finally, efforts are still necessary to accurately quantify the friction effects in the line. Advances have been made with the TLM approach, like the estimation of frequency-dependent friction (Johnston,2012,2014)(Manhartgruber,2019). At the same time, the calculation

of friction is achieving good accuracy for simple straight lines, the estimation for more complex lines still in progress.

The line models are dependent not only on the impedance of the line but also on the hydraulic units' impedances. A remarkable work using this method was done by Kojima and Shinada(1986) who developed a model capable of predicting the superimposed pressure and flow pulsations in a high-pressure line. The source impedances of both units were determined by independent measurements. A four-pole transfer matrix was determined for calculating superimposed pulsations in the hydraulic system. For the line, a transfer matrix based on the wave equation was used. To calculate this transfer matrix, a constant diameter pipe fluid flow is calculated using the undamped wave equation. The general solution for this equation can be described by equation (2.5) (Kinsler et al., 1982), where ω is the angular frequency, k is the spatial frequency, λ is the wavelength, and the B terms are constants to be defined.

$$p(t, x) = B_1 e^{-j(\omega t + kx)} + B_2 e^{j(\omega t + kx)} \quad (2.5)$$

$$k = \frac{2\pi}{\lambda} \quad (2.6)$$

At the instant when time is equal to zero, the time-dependent terms of the equation go away, and the pressure value is only dependent on the position z within the respective duct. The flow Q concerning position z can be derived by the linearized Euler equation:

$$p(0, z) = B_1 e^{-jkz} + B_2 e^{jkz} \quad (2.7)$$

$$Q(0, z) = -\frac{A}{j \cdot \omega \cdot \rho} \frac{\partial p}{\partial z} = \frac{A}{\rho \cdot c} (B_1 e^{-jkz} - B_2 e^{jkz}) \quad (2.8)$$

A one-dimensional, constant diameter pipe is described in the following picture Figure 2.12, which shows the section of a straight line with propagating waves in the positive and negative directions at the instant of zero seconds. The start of the pipe is considered the position where z is equal to zero and the end is the position where z is equal to the length L . Based on these boundaries, four

boundary conditions are met, which are respectively, the pressure and the flow at the start and the end of the pipe.

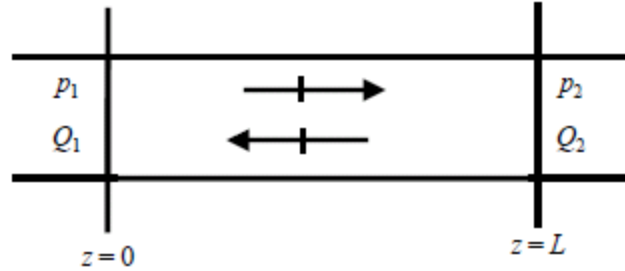


Figure 2.12 Cross-section of duct

By rearranging the terms and finding the relations between the constants A and B, a transfer function capable of describing the relationship between the pressure and flow of the pipe's start and end can be calculated. Furthermore, this technique can be extended to calculate pressure and flow at any given position of the line, by replacing the value L with a given position z .

$$\begin{bmatrix} p_1 \\ Q_1 \end{bmatrix} = \begin{pmatrix} \cos k L & j \frac{\rho \cdot c}{A} \sin k L \\ j \frac{A}{\rho \cdot c} \sin k L & \cos k L \end{pmatrix} \begin{bmatrix} p_2 \\ Q_2 \end{bmatrix} \quad (2.9)$$

Transfer function approaches also can be used to model passive noise-cancellation components to project acoustic filters for a given application. Kinsler, Frey, Coppens, and Sanders(1982) describe expansion chambers as low-pass filters, orifices as high-pass filters, and Helmholtz resonators as band-pass filters. All these elements can be modeled through transfer functions. An expansion chamber can be simply described by equation (2.9), however, with a different value of cross-section A. The Helmholtz resonator and orifice can be described by the transfer function given by (2.10) where Z_b is the respective impedance of the element:

$$\begin{bmatrix} p_1 \\ Q_1 \end{bmatrix} = \begin{pmatrix} 1 & 0 \\ \frac{1}{Z_b} & 1 \end{pmatrix} \begin{bmatrix} p_2 \\ Q_2 \end{bmatrix} \quad (2.10)$$

Where the impedance of the orifice is given by equation (2.11) in which A_o is the area of the orifice and L' is the corrected length of the neck:

$$Z_b = \frac{j\rho L'\omega}{\pi A_o^2} \quad (2.11)$$

For a Helmholtz resonator, Z_b can be calculated by an equation dependent on the neck area A_N ; the neck corrected length L' , the mass of fluid at the neck m_N :

$$Z_b = \frac{j}{A_N^2} \left(\omega m_N - \frac{A_r}{\omega} \right) \quad (2.12)$$

$$m_N = \rho A_N L' \quad (2.13)$$

$$A_r = \frac{\rho c^2 A_N}{V} \quad (2.14)$$

Finally, several components can be coupled together, and the frequency-domain response of a whole system can be calculated. This method can be used to present frequency content attenuation solutions for line systems by introducing, removing, or modifying existing components of the line. The frequency-domain response of the coupled system is different than the total summed response of all transfer functions.

$$\begin{bmatrix} p_{in} \\ Q_{in} \end{bmatrix} = [T_1][T_2] \dots [T_n] \begin{bmatrix} p_{out} \\ Q_{out} \end{bmatrix} \quad (2.15)$$

2.2.3 Time-Domain Line Models Derived with the Method of Characteristics

The method of characteristics (MOC) line model is a time-domain approach in which the pressure buildup in a line is calculated by solutions from the momentum equation and the continuity equation which are partial differential equations. Firstly, the two partial differential equation are simplified into four ordinary differential equations and then the finite element approach is used so the line is split into a unidimensional grid in which the pressure buildup of each node can be

calculated based on flows and pressures of the adjacent nodes of the previous time step. This method will be covered in detail in section 3.2

3. COUPLED-SYSTEM MODELING

This chapter will present the modeling approach to make a time-domain non-characterized coupled system model capable of calculating fluid borne noise sources generation and propagation within a hydraulic system. This section will cover the derivation of each of the necessary blocks necessary to assemble a mid-complex hydraulic system, the system solver strategy. It will present an example of a multi-function Hydraulic circuit that can be simulated by this modeling approach to demonstrate the model's stability and versatility.

3.1 The relevance of a coupled system model

Mapping the isolated behavior of lines in the frequency-domain is useful; however, to assure the model and proposed vibration reduction solutions will be effective, it is necessary to couple the MOC model with the other hydraulic system's components.

One of the main advantages of a coupled system transmission model using a MOC line model is the non-necessity of characterization of the components, which would require several measurements to be performed and still be impacted by the incompleteness of impedance models. Also, the model is capable of covering structure-borne noise sources such as the vibrations of the swash-plate. Hence this modeling is more suitable for optimization techniques. Also, it covers a more significant number of noise sources. The greatest the number of covered operation conditions is, the better the optimization is. Also, the experimental characterization of components is not possible in optimizations and computational investigations.

The time-domain coupled system can simulate dynamic effects in the line to some extent as in an accelerating hydraulic transmission. Yet, there is no apparent practical use to evaluate the model with varying frequency. Finally, in a MOC coupled hydraulic system, the friction effects on the line will impact the whole system, and this behavior will be able to be quantified.

Firstly, however, it is necessary to evaluate how many components are necessary to model to be able to compose a hydraulic system with relatively high complexity. Taking as an example the simple unidirectional hydrostatic hydraulic transmission of Figure 1.5, the system contains two hydraulic units and a relief valve, installed to avoid the line to over pressurize in case the wheel meet unexpected high torque.

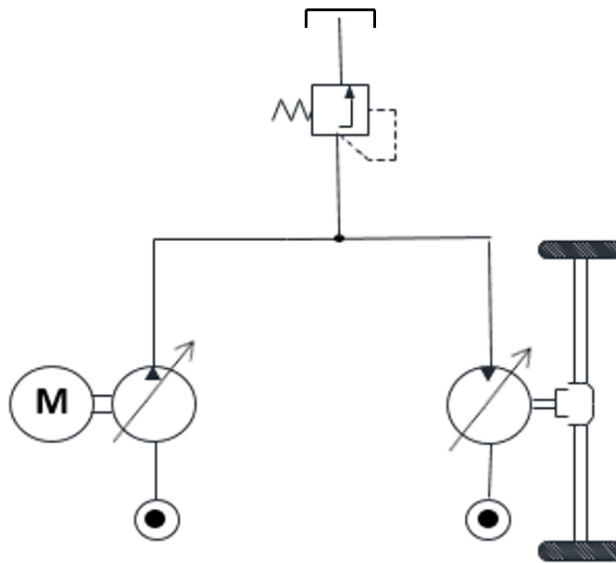


Figure 1.5 Simple example of unidirectional hydrostatic hydraulic transmission

To reproduce the pressure ripple within the transmission within the simple system, it is necessary first to have a model capable of simulating its generation in their respective hydraulic units and a model capable of calculating its propagation inside the hydraulic lines. It is important to notice three hydraulic lines connected to a branch, and the pressure wave will travel in all directions. Therefore it is also necessary to develop a branch model capable of simulating how the fluid vibrations in each segment of the line will influence each other. Finally, an ordinary valve model based on the orifice equation is also needed.

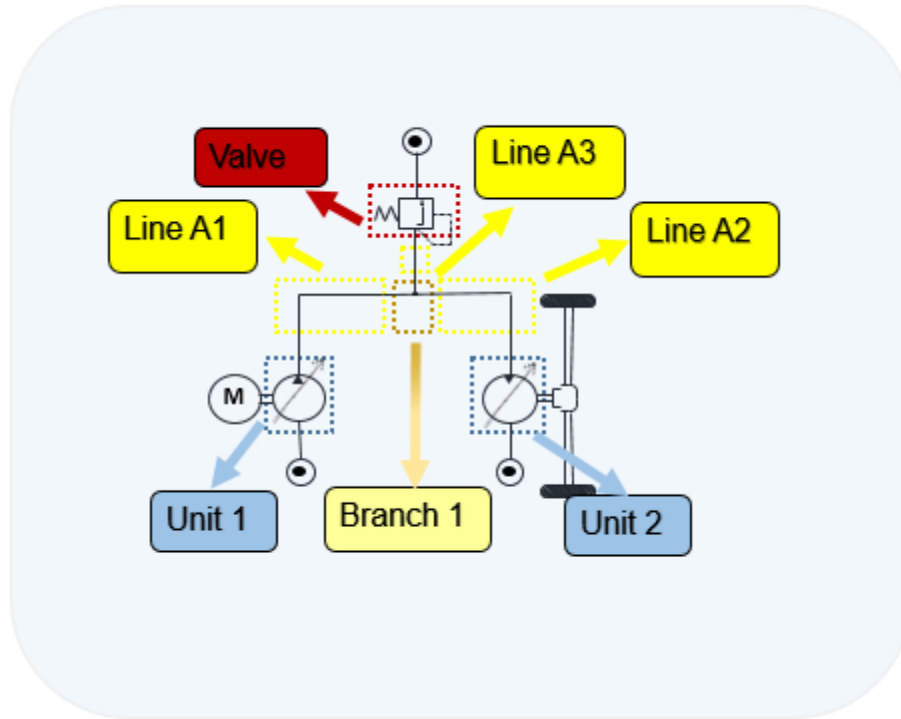


Figure 3.1 Necessary blocks for simulating pressure ripple generation and propagation

Then, the boundary conditions of the hydraulic elements must be defined. A lumped hydraulic model based on Wieczorek and Ivantysynova's (2000) work can calculate the intake and outtake flow of a hydraulic unit if the following inputs are given: Pressure of both ports, unit speed, and swash-plate's displacement. The model will calculate the displacement chamber volume variation from the speed and displacement; the ports' pressure on its turn will be necessary for the calculation of both external flows.

The MOC-based line model will calculate the pressure build-up caused by the fluid momentum and the pressure drop caused by the fluid's transient shear stress in the wall. Therefore, this model needs flow as input and can give pressure as output, which is complementary for the unit model's inputs and outputs. The branch model will need to be given the values of the characteristic equations' parameters, which are outputted from the hydraulic lines the branch is connected to. After this stage, the branch model can calculate the flow which will be supplied to each segment of the line. For the block diagram's sake, as these parameters are used to calculate pressure build-up, they are represented as pressure.

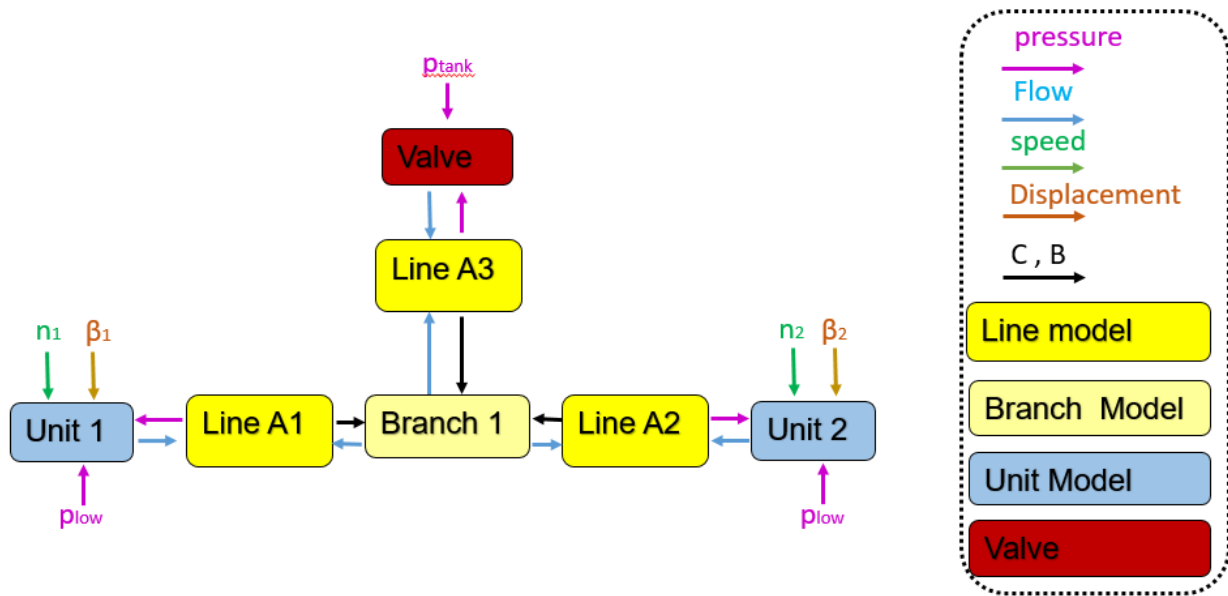


Figure 3.2 Necessary blocks for simulating pressure ripple generation and propagation

In the case of hydraulic transmissions, the motoring unit is usually connected to an inertia model, which will receive the torque of the unit and calculate the speed both the inertia and the unit are rotating. These elements won't be covered as they are beyond the scope of this work. Much more complex hydraulic circuits can be modeled by this approach, as will be seen in section 3.7.1.

3.2 Method of characteristics based line model

For this work, a time-domain one-dimensional line model was selected as a reliable model capable of calculating flow and pressure oscillations at any given position at the line, at any given time. This versatility makes possible to evaluate the effects of coupled systems: The upstream and downstream of the lines can be coupled to hydraulic units and valves. Thus the pressure and flow excitations at the whole model can be evaluated. Also, this approach allows the possibility to select any given point of the one-dimensional grid to compare pressure ripples of these respective nodes to measurements made by a sensor in the given position, an important feature since the behavior of waves is dependent both on time and space. The line model is solved by the method of characteristics (MOC). This is a mathematical method that discovers curves called characteristic curves in partial differential equations (PDE) that becomes an ordinary differential equation (ODE). For the modeling of flow and pressure oscillations in a tube, the characteristic method was

originally used by Wylie and Streeter(1978), applying it in the equation of momentum (3.1) and the equation of continuity (3.2).

$$L1 = \frac{1}{\rho} \frac{dp}{dz} + \frac{dv}{dt} + \frac{2}{\rho \cdot r} \tau = 0 \quad (3.1)$$

$$L2 = \frac{dp}{dt} + \rho c^2 \cdot \frac{dv}{dz} = 0 \quad (3.2)$$

This model also allows applying discrete elements, such as applying nonlinear friction and variable parameters in the line, such as diameter and material. As previously mentioned, another advantage is that it makes it possible to simulate coupled systems and how each component of the system influences the other. For example, a large pressure drop in the line at an instant of time may cause the unit to provide higher flow and increase a higher pressure peak at the same line a few moments later. Then, this higher pressure peak in the line may cause the unit to provide a slightly smaller flow at another instant and result in deeper pressure valley instants later.

For modeling flow and pressure oscillations in a tube, the method of characteristics couples both the momentum equation and continuity in one linear equation equal to zero using multiplier λ elevated to the square power. A characteristic curve is found for a specific value of gamma, and four ordinary differential equations can be deduced from the equation the solution:

$$\left. \begin{aligned} \frac{1}{\rho c} \cdot \frac{dp}{dt} + \frac{dv}{dt} + \frac{2}{\rho \cdot r} \tau = 0 \\ \frac{dz}{dt} = +c \end{aligned} \right\} C^+ \quad (3.3)$$

$$\left. \begin{aligned} -\frac{1}{\rho c} \cdot \frac{dp}{dt} + \frac{dv}{dt} + \frac{2}{\rho \cdot r} \tau &= 0 \\ \frac{dz}{dt} &= -c \end{aligned} \right\} c^- \quad (3.4)$$

Where c is the velocity of sound propagating in the fluid and τ is the shear stress of fluid acting at the duct wall and fluid. According to Wiley and Streeter(1978), for a flexible tube with a diameter much smaller than the wavelength, the value of c is given by equation (3.5) containing the density and bulk modulus of the fluid, the properties of the line are considered, E is Young's modulus of the line material, d is the diameter and e is the wall thickness of the line.

$$c = \frac{\sqrt{\frac{K}{\rho}}}{\sqrt{1 + \frac{K \cdot D}{E \cdot e}}} \quad (3.5)$$

The equation demonstrates the influence of the duct wall at the speed of sound of the fluid, especially for flexible materials. Klop(2010) studied the influence of the young modulus on the wave model was noticed as experiments with steel pipes had different values than experiments with hoses. As the stiffness of the hose was not yet known, experimental measurements were compared to several simulations considering different values for the speed of sound in the hose, and by selecting the minimum error both in phase and magnitude for oscillation values, the speed of sound in hoses was estimated between 1080 and 1100 m/s. The Young modulus of the hose was backwards calculated as 19 Gigapascal, which is an order of magnitude smaller than steel. According to the equation (3.5), as the wall thickness or Young modulus becomes too large, the speed of sound gets dependent only on the bulk modulus and fluid density, which is the behavior of the speed of sound in a free medium.

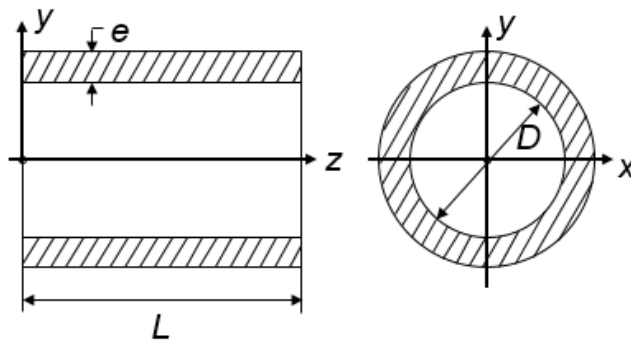


Figure 3.3 Diagram of a hydraulic line node

Using finite element methods at the four characteristic equations can be used to calculate pressure propagation in both directions for a one-dimensional grid. The $C+$ equations represent a characteristic line describing the flow in the upstream-downstream direction, and the $C-$ equations describe flow upstream. The solution results show that pressure and flow at a particular node of the line depend only upon the flow and pressure of both adjacent $(i + 1)$ and $(i - 1)$ nodes in the previous step.

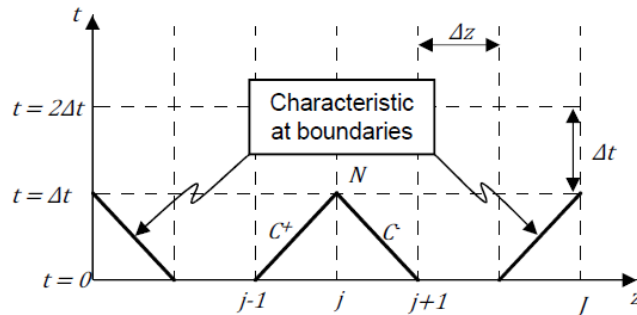


Figure 3.4 One Dimensional Line Grid Solution

The characteristic equation $C+$ represents the pressure traveling in the positive direction of the grid, and $C-$ represents the pressure traveling in the negative direction of the grid. For the boundary nodes, where only one direction exists, the pressure is calculated as the average of the pressure traveling in the remaining direction and the pressure for the node at the previous time step.

$$C_P = p_{j-1} + B_L \cdot Q_{j-1} - \frac{2 \cdot \Delta z \cdot \tau_{j-1}}{r} \quad (3.6)$$

$$C_M = p_{j+1} + B_L \cdot Q_{j+1} - \frac{2 \cdot \Delta z \cdot \tau_{j+1}}{r} \quad (3.7)$$

$$B_L = \frac{\rho c}{A_L} \quad (3.8)$$

Where r is the inner radius of the line, and A_L is the inner pipe area. The flow at the boundaries are the inputs of the model and are updated at every time step. The flow for inner nodes is calculated after the pressure, as a function of the pressure difference between each node and the isothermal wave speed B_L . Flow components traveling in the positive and negative directions are calculated, and the node speed is determined as the average of the two.

$$Q_j = \frac{1}{2} \left(\frac{C_p - p_j}{B_L} + \frac{p_j - C_m}{B_L} \right) = \frac{C_p - C_m}{B_L} = \quad (3.9)$$

Besides the isothermal wave speed and pressure in the adjacent nodes, the characteristic equations are given by equations (3.6) (3.9), and (3.7) also depend on friction. These friction terms are calculated at every computational node along the pipe and at every time step. This procedure increases the computational effort greatly and yet tends to result in a higher fidelity of the model. The variable component of the friction in the time-domain is the shear stress, which permanent components can be given by:

$$\tau_{steady,j} = \frac{1}{8} \cdot \rho \cdot f_{DWj} \cdot v_j \cdot |v_j| \quad (3.10)$$

Where the v_j terms are the speed of flow at each node and f_{DWj} is the Darcy-Weisbach friction factor at each node. The friction factor is calculated based on empirical data. For laminar flow, it behaves linearly inverse to the Reynolds number Re . For turbulent flow, the friction factor it is less sensitive to Reynolds number variation:

$$f_{laminar,j} = \frac{64}{Re_j} \quad (3.11)$$

$$f_{turbulent,j} = \frac{0.316}{Re_j^{0.25}} \quad (3.12)$$

$$Re_j = \frac{\rho \cdot v_j \cdot D}{\mu} \quad (3.13)$$

However, the friction factor f can be strongly frequency-dependent as the wall shear stress is dependent not only on the mean flow speed but also on the flow acceleration. Fifty years ago, a straightforward approach to describe the wall shear stress was described by Zielke(1968). However, Zielke's model required the whole vector of past velocities. Thus the model was very expensive computationally and, also, was valid when the Reynolds number was low (Vardy et al., 1993). In the later years, many other more sophisticated transient friction models were developed (Vardy et al., 1993) (Vardy and Brown,1995) (Duan et al.,2010)(Schohl,2010)).

Klop(2010) developed a time-domain hydraulic transmission model with the inclusion of a sophisticated friction model responsible for calculating the frequency-dependent friction component. The model is based on a modified convolution integral solution and verified by empirical data and developed by Schohl in (2010). Simplified weighting functions were used to determine the transient friction parameters acting at the fluid flow. The value of the unsteady shear stress can be given by (3.14) where m_i is a series of coefficients and y_{ij} is an updated value representing a change in velocity at previous time steps for each node.

$$\tau_{unsteady,j} = \frac{2 \cdot \rho \cdot v_j}{r} \sum_{i=5}^5 m_i \cdot y_{i,j}(t) \quad (3.14)$$

For hydraulic circuits which line have a reasonable diameter, the pressure build-up coming from the upstream and downstream is dominantly influenced by the isothermal wave speed (3.8). The isothermal wave speed can be analyzed even further in (3.15).

$$B_L = \frac{4\sqrt{\rho K}}{\pi D^2 \sqrt{1 + \frac{K \cdot D}{E \cdot e}}} \quad (3.15)$$

One can notice that if friction is neglected, a lower isothermal wave speed can reduce the magnitude of the pressure ripple. Since variables such as the bulk modulus and density vary with operating pressure and temperature, the speed of sound and isothermal wave speed depends on the operating condition. Lower operating pressures, lower working flow density, lower bulk modulus, and higher working temperatures should reduce the oscillations but are impractical for some fluid power applications. Flexible duct materials and thinner wall thickness also will get the desired results but will be constrained by the necessity of resilience of the duct, which should be able to contain high pressure. Nonetheless, several of these trends are supported by the literature. Wylie and Streeter (1978), in chapter 10 of their book, gave suggestions on reducing the wave-speed by bleeding air into the system or by using flexible hoses. Ngah and Edge (2001) demonstrated the sound power levels would be more sensible to increasing speeds than to increasing pressures, and the same trends were later verified by Klop in (2010), where sound power and sound intensity levels were measured for an axial piston pump in an anechoic chamber, and it was verified higher pressures and higher frequencies would lead to higher noise levels.

In a very recent work, Kim (2017) detected swash plate vibration changes for different temperatures. A large decrease at the x-axis swash-plate acceleration measured by accelerometers and maximum 4 dB noise reduction was obtained as the case temperature in the study increased from 25.79 C ° to 62.67 C °. Ichiyanagi et al. (2015) verified in experiments that the speed of sound decreases for higher temperatures, however, significant pressure ripple drop was not detected.

3.3 Discretized Parameter Hydraulic Line Model

In most hydraulic circuits, several line parameters will vary over the length of the line, also resulting in a change at the speed of sound which propagates in the fluid. Hydraulic circuits usually contain steel segments, hose segments, the variation of diameters, elbows, and curvatures that can influence both the transient and non-transient components of flow and pressure.

To improve the accuracy of the previously existing method of characteristics line model and to evaluate the impact of variable parameters in the line for propagation to the amplification of pressure oscillations in hydraulic systems, a discrete parameter line model was developed. The model allows simulating variations of diameter, hydraulic hose segments, and metal pipes, as well as the elbows and bends of the line.

The MOC approach for calculating pressure ripple was adapted in lines that can simulate varying parameters in a line, which to evaluate the generation in lines with particular geometries. Each node has its own wave speed and resistance. Wylie and Streeter (1978) state that “A system with numerous minor changes in property may be approximated by use of “equivalent” uniform reach length that spans minor discontinuities.” To calculate each equivalent length, the time step is fixed and the grid has variable lengths corresponding to the distance the speed of sound at the respective node will travel during the onetime step. The chosen time step for the line model was equivalent to 10 microseconds which results in a resolution smaller than one centimeter since the speeds of sound for pressurized working fluid in hydraulic systems are usually higher than 1000 m/s.

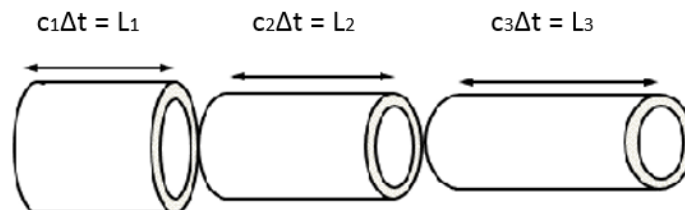


Figure 3.5 Approximation to variable-property series system

Wylie and Streeter(1978) also warn about possible instabilities on the model in case the speed of sound varies more than 15% from a node to an adjacent other. Therefore, the usage of this technique can make the simulations more unstable, which will require reliable solver strategies, specially to insert the line model in a coupled system and evaluate the vibrations of this system.

The model also decouples the permanent and non-permanent flow of the system. In this way, it is possible to evaluate the impacts of frictional influence on the pressure separately. The presence of curvatures and elbows in the line increases the pressure drop in the fluid in the upstream-downstream direction. However, Walker and Phillips(1975) it is observed that in the case of pressure variations in the millisecond range, the radial inertia is insignificant. This observation was empirically demonstrated in Wiggert et al. (1985), which simplified a line with high curvature for a 4-equation model of the method of characteristics and obtained good comparisons of the experimental results with the simulations made.

However, in a composite system, the pressure drop can change the behavior of the flow oscillations generated by the hydraulic units, which in turn can alter the pressure oscillations contained in the line. The equivalent length method was used to simulate the influence of the component line curvatures on the pressure transient. In this method the pressure drops through a curvature can be described as equivalent to pressure drop in a straight tube. In theory, the pressure drop across the fitting is equivalent to the pressure loss through a certain length of tubing at that corresponding flow rate. The ratio between these lengths is given by a factor K_f , and thus the pressure drop can be calculated by:

$$p_{Loss} = K_f \cdot f \frac{L \cdot \rho \cdot v^2}{2D} \quad (3.16)$$

Menon(2004) provides a full table for the values of the factor K_f calculated empirically from ambient pressure water hydraulics. The kind of fittings needs to be taken into consideration and also the ratio between the curvature ratio Rc and the line diameter D . Sharper curvatures will result in a longer equivalent length increasing the pressure drop considerably when compared to a straight line or even smoother curvatures.

Table 3.1 Equivalent Factor for different line discontinuities(Menon, 2004)

Fitting	Types	K_f
----------------	--------------	-------------------------

90° Elbow Curved, Threaded	Standard Radius ($R_c/D = 1$)	30
	Long Radius ($R_c/D = 1.5$)	16
90° Elbow Curved, Flanged/Welded	Standard Radius ($R_c/D = 1$)	20
	Long Radius ($R_c/D = 2$)	17
	Long Radius ($R_c/D = 4$)	14
	Long Radius ($R_c/D = 6$)	12
90° Elbow Mitered	1 weld (90°)	60
	2 welds (45°)	15
	3 welds (30°)	8
45° Elbow Curved, Threaded	Standard Radius ($R_c/D = 1$)	16
	Long Radius ($R_c/D = 1.5$)	8
45° Elbow Mitered	1 weld 45°	15
	2 welds 22.5°	6

3.4 Line branches Model

In hydraulic systems, branches divide fluid into several paths that will naturally occur. To evaluate the propagation of waves in branches, a branch model is needed. Branches can be modeled according to Wiley and Streeter (1978). In this model, the branch is considered a node that connects a number k of nodes from other lines, and it has a common pressure p_{cn} at the center of the branch. The isothermal wave speed B_k and characteristic equations coefficients C_k are inputs for the model.

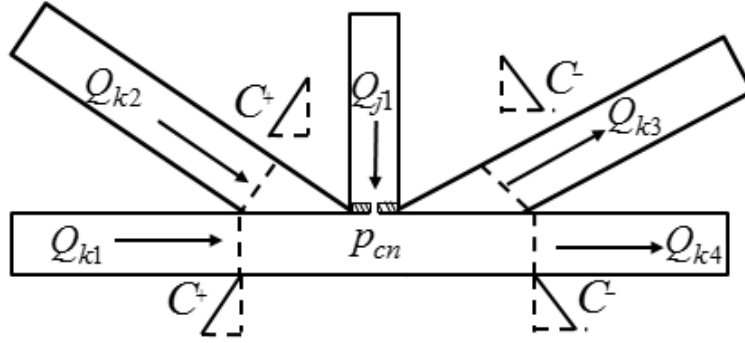


Figure 3.6 Diagram of a branch approximated to a line node

The conservation of the mass principle is used to calculate the branch pressure according to (3.17). Then, the flow for each line is solved with the usage of (3.18), which is analog to (3.9).

$$p_{cn} = \frac{\sum_{k=1}^n \frac{C_k}{B_k}}{\sum_{k=1}^n \frac{1}{B_k}} \quad (3.17)$$

$$Q_k = \frac{C_k - p_{cn}}{B_k} \quad (3.18)$$

In equation (3.19), this model has been further expanded to include a number j of external flows called Q_j to represent branches that are connected to elements other than ducts, such as orifices and valves. This alteration makes it possible to implement the line model in more complex line configurations in hydraulic systems.

$$p_{cn} = \frac{\sum_{k=1}^n \frac{C_k}{B_k} + \sum_{j=1}^m Q_j}{\sum_{k=1}^n \frac{1}{B_k}} \quad (3.19)$$

3.5 Axial piston unit model

3.5.1 Pressure and flow calculation model

A swash plate type axial piston machine, the machine can be divided into two main groups: a rotating group and a non-rotating group. The rotating group consists of the rotating elements of the unit, which includes the cylinder block, pistons, and slippers, while the non-rotating group includes the fixed elements such as the swash plate, the valve plate, and the end case.

A swash-plate axial piston machine can be operated either in pump mode or motoring mode. In pump mode, an external power source drives the shaft, which transmits the torque to the cylinder block through gears. The cylinder block, pistons, and slippers will rotate on the z-axis while the non-rotating elements remain stationary. As the cylinder block rotates, the pistons change their position, and as the swash-plate remains stationary, each piston is dislocated in and out of the cylinder block, takes liquid from the inlet port, and delivering liquid at the outlet port. That displacement is dependent on the angle of the swash-plate, which is fixed for fixed-displacement units. However, in the case of variable-displacement units, the swash-plate angle can be varied, changing the fluid displacement of the unit, which turns the unit into a very versatile machine. Since the unit is pumping, the outlet pressure will be set by the load of the application the machine is performing and thus can reach high values. Therefore, this is defined as the high-pressure (HP) port, and the inlet port is then called low pressure (LP) port.

Using the z-axis as a reference, the angle ϕ is the piston angular position where the displacement chamber achieves maximum volume is called the outer dead center (ODC) and defined as $\phi = 0$. At a half revolution ($\phi = 180^\circ$), the piston enters the cylinder block the most leaving the smallest achievable volume in the displacement chamber, called the dead volume (V_{dead}). This location is referred to as the inner dead center (IDC).

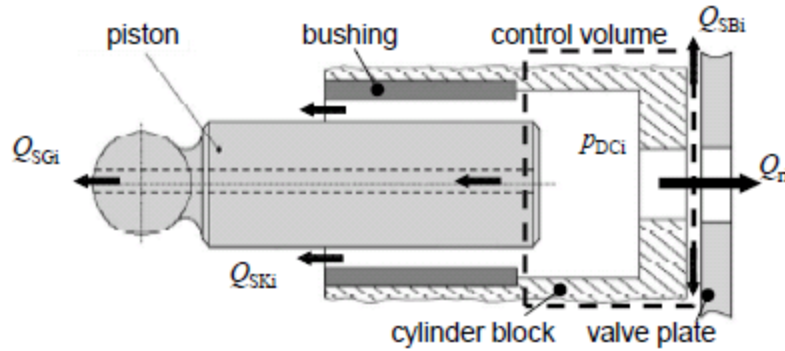


Figure 3.7 Cross-sectional view of a piston in a displacement chamber

The method for modeling the axial piston unit dynamics is based on a lumped parameter approach developed by Wieczorek and Ivantysynova(2000). The hydraulic unit is divided into separate displacement chambers, one for each piston the unit has, it is possible to derive the instantaneous pressure through the pressure buildup equation by using the value of the flows that enter and leave the chamber and the variation of the volume of the same as equation (3.20) shows.

$$\frac{\partial p_i}{\partial t} = \frac{K}{V_i} \left(Q_{ri} - Q_{SKi} - Q_{SBi} - Q_{SGi} - \frac{\partial V_i}{\partial t} \right) \quad (3.20)$$

The flows Q_{SKi} , Q_{SBi} , Q_{SGi} , are the flows occurring between the interfaces of the movable components of the axial piston hydraulic unit, respectively the interface between the piston and the cylindrical block, the interface between the cylindrical block and the valve plate, and the interface between the piston and the slipper see fig Figure 3.7. These leakages will result in volumetric losses for the unit. Two other sources of volumetric losses are compression losses and cross-porting flow. Compression losses are the change of fluid volume by the effect of the pressurization, which reduces the effective outlet volume flow. Cross-porting is the simultaneous exchange of fluid among the displacement chamber, low-pressure port, and the high-pressure port.

The volumetric losses of a unit were obtained empirically by mounting the hydraulic unit in an experimental setup instrumented according to ISO 4409 to capture velocity, torque, flows,

temperatures and pressures simultaneously. Steady-state measurements for a full range of speeds n , pressures p , and displacements β resulting in a map for the value of flow loss Q_s . This data is interpolated by using fit to least-squares polynomial interpolation and then fit in a polynomial surface. To estimate the sum of the values Q_{SKi} , Q_{SBi} , Q_{SGi} the cross-porting flow and compression losses, which can be calculated inside the model are subtracted from the values of Q_s . The remaining value can be used in equation (3.21), as a term Q_{SKBGi} , which will replace the sum of values Q_{SKi} , Q_{SBi} , Q_{SGi} .

$$\frac{\partial p_i}{\partial t} = \frac{K}{V_i} \left(Q_{ri} - Q_{SKBGi} - \frac{\partial V_i}{\partial t} \right) \quad (3.21)$$

The term Q_{ri} represents the volumetric flow coming from the ports of the unit a single displacement chamber Q_{ri} is calculated in Equation (3.22) where Q_{rHPi} represents the volumetric flow coming from the high-pressure port and Q_{rLPi} is the flow coming from the low-pressure port. For modeling's sake, the convention of the flow must be determined. Liquid flowing into the displacement chamber is represented as a positive flow, and liquid flowing out of the displacement chamber is represented as a negative flow.

$$Q_{ri} = Q_{rHPi} + Q_{rLPi} \quad (3.22)$$

These flows, Q_{rHPi} and Q_{rLPi} , are assumed to be turbulent and thus modeled using the orifice equation (3.23)(3.24), where K and ρ are the bulk modulus and fluid density respectively and α is the discharge coefficient empirically added to the orifice equation.

$$Q_{rHPi} = \alpha_D \cdot A_{rHPi} \sqrt{\frac{2}{\rho} |p_i - p_{HP}| \cdot \text{sign}(p_{HP} - p_i)} \quad (3.23)$$

$$Q_{rLPi} = \alpha_D \cdot A_{rLPi} \sqrt{\frac{2}{\rho} |p_i - p_{LP}| \cdot \text{sign}(p_{LP} - p_i)} \quad (3.24)$$

The bulk modulus and density vary with changes of pressure and temperature and thus need to be updated at every iteration of the unit model. Figure 3.8 and Figure 3.9 show the temperature and pressure dependence of this bulk Modulus and density, respectively, for HLP 32 fluid.

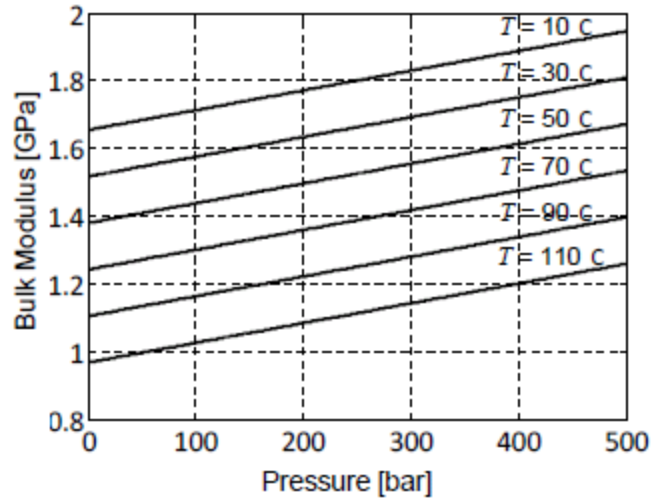


Figure 3.8 Bulk Modulus HLP 32

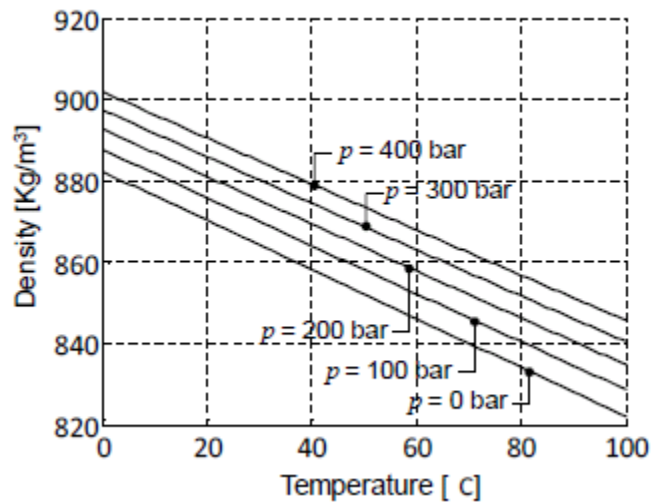


Figure 3.9 Density HLP 32

Volumetric and torque losses are obtained empirically, and then polynomial models are used to describe losses at all points of operation. Thus it is possible to obtain the effective torque and effective flow of a hydraulic unit. Finally, the areas A_{rLPi} and A_{rHPi} are respectively the areas of the orifices to which the displacement chambers are open for the low and high-pressure chambers. The value of these areas is defined by the unit's valve-plate geometry. For this simulation, a Sauer

Danfoss S-90 standard plate-valve model was chosen, a valve plate consolidated by the Market. As discussed previously, the valve plate is one of the main internal components of the unit capable of characterizing the oscillation of flow and pressure that the unit has.

The model can predict both fluid-borne noise sources and structure-borne noise sources. Structural noises are generated from the moments resulting from forces on the swash plate, while noises from the fluid are caused by pressure oscillations due to kinematics of fluids and compressibility effects. In theory, these noises can be reduced by identifying the sources and modeling and designing a valve plate with a pressure module modeled to reduce undesirable effects and to meet the requirements demanded, such as the magnitude of force specific output that projects to the unit.

3.6 Solver

For this thesis research, the developed line model includes the MOC line model, the lumped parameter model for positive displacement machines, the branch model other trivial models such as simplistic valve models and an adiabatic accumulator. These models were all developed in Matlab/Simulink environment. This strategy uses the versatility of the block-diagram-based software, so flow and pressure ripple propagation solution can be implemented and simulated for several architectures.

The main simulation is where all the hydraulic circuit elements communicate with each other. The model was implemented in Matlab/Simulink Simulink's functions blocks with inner loops. The outer simulation layer uses the fixed step Euler method solver with a time step of 50 microseconds. The size of the steps affects the precision of the simulation. The main simulation time step needs to be small enough, such as the valve-plate Geometry is reflected in the system, and oscillations frequencies up to 5000 Hertz are reflected in simulation. With a 50 microsecond time step, the main system simulation sample will be 20000 Hertz, and the Nyquist frequency will be equal to half of this value: 10000 Hz. Therefore, the simulation should represent oscillations for the target band this project is interested tot tackle.

The positive displacement machine model also must solve for each displacement chamber pressure and flows at every iteration. However, this model needs a much smaller time step to reach the solver stability region. Each axial piston unit has a nested Euler method solver with a time step of 0.1 microseconds to accurately simulate the pressure buildup inside the displacement chambers. The choice of the time steps (and thus, number of loop interactions) was based on checking convergence for the units' highest power operation demand (3400 rpm, 420 bar), and then a safety factor of 3 was considered. The boundary inputs of the units are the pressures in each port and the unit speed. The units calculate the displacement chamber pressures also using the Euler method with equation (3.21) to calculate the pressure build-up rate. After the pressure is updated, the loop is repeated 500 times, the flows on the ports are calculated according to the summation of the flows entering and exiting each displacement chamber, which are described by equations (3.22) and (3.23).

The line model contains a $10\mu\text{s}$ inner time step. The line model has a particular time step for two reasons: spatial resolution and boundary stability. One of the most trivial variables to evaluate the generation of pressure and flow oscillations into the lines is the speed of sound. The length of the node will be given by the time-step value multiplied by the speed of sound in this given node. As the speed of sound is in the range of ~ 1000 meters per second time step of 10 microseconds will result in node lengths slightly smaller than 1 centimeter, a good resolution for representing the line features variations. The pressure at each node is calculated with the average of equations (3.6) and (3.7), while the flow is updated according to equation (3.9). After the hydraulic line model is completed, five times the pressures at the extremities are provided to the boundaries. The flowchart in Figure 3.10 describes the simulation of a hydraulic circuit with several units and model lines.

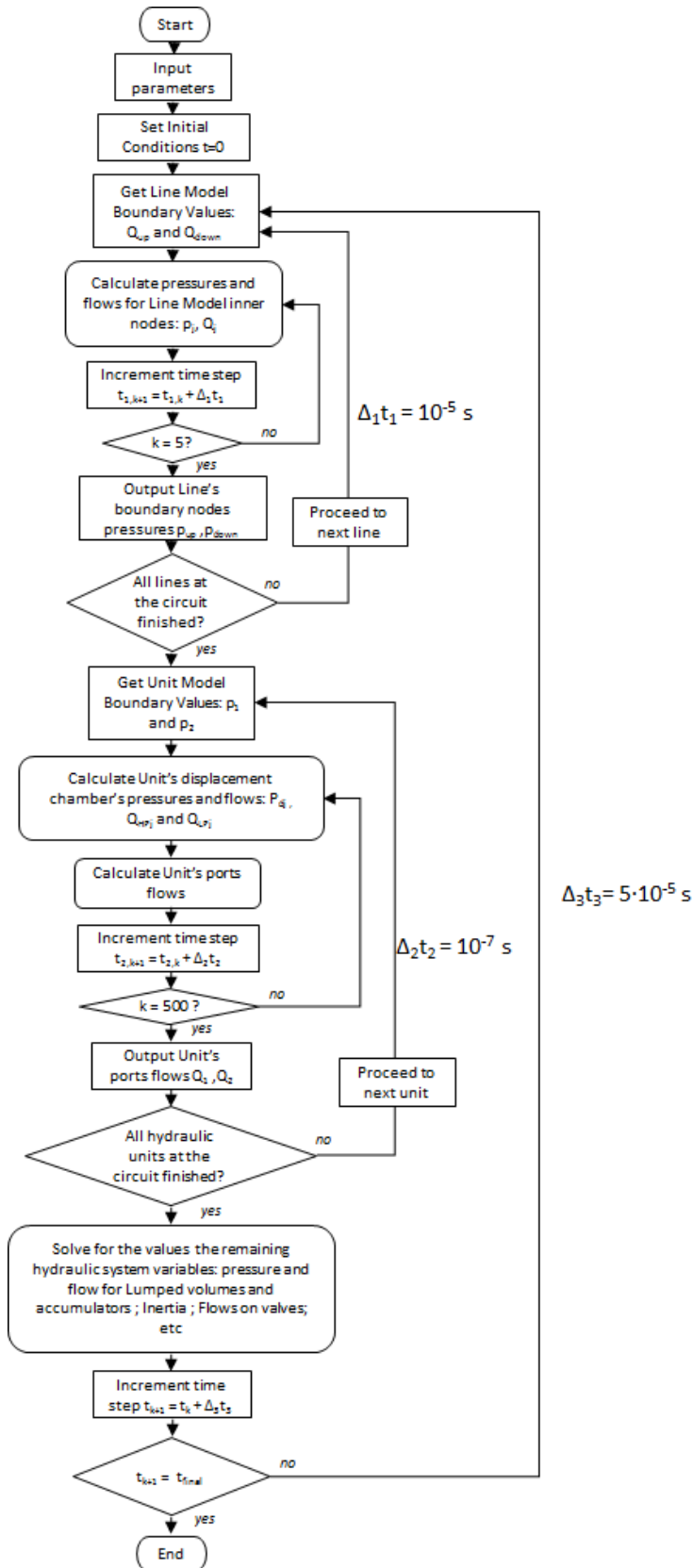


Figure 3.10 Hydraulic system model solver flowchart

3.7 Validation

To validate the solving strategy and its capability in characterizing practical hydraulic circuits, the model was employed to simulate a modern hydraulic circuit: the novel Maha Switching Hybrid (MSH) circuit was assembled as a compact and practical test rig, resulting in the presence of diameter variations, hose segments, and elbows in the circuit. The simulation model accounts for the effect of these asymmetries. Measurements were conducted, and the results were compared to the simulation results.

3.7.1 Example of a coupled system simulation

To test the accuracy of the coupled hydraulic system model in predicting realistic hydraulic circuit oscillations, a set of measurements were conducted in a full bench hybrid-in-the-loop (HIL) hydraulic transmission experimental test setup. The design allows for testing different hydraulic transmission operating modes for off-and-road vehicles.

The transmission test circuit can switch among three different architectures: hydrostatic transmission (HST), hybrid serial transmission (SH), or mode switching hybrid (MSH). The latter is an architecture developed at the Maha Fluid Power Research Center to manage energy consumption efficiently. Figure 3.11 shows the circuit of the HIL test platform. Appendix A gives a detailed circuit with sensors, and power supply included, while Appendix B gives the data acquisition schematics of the experimental setup.

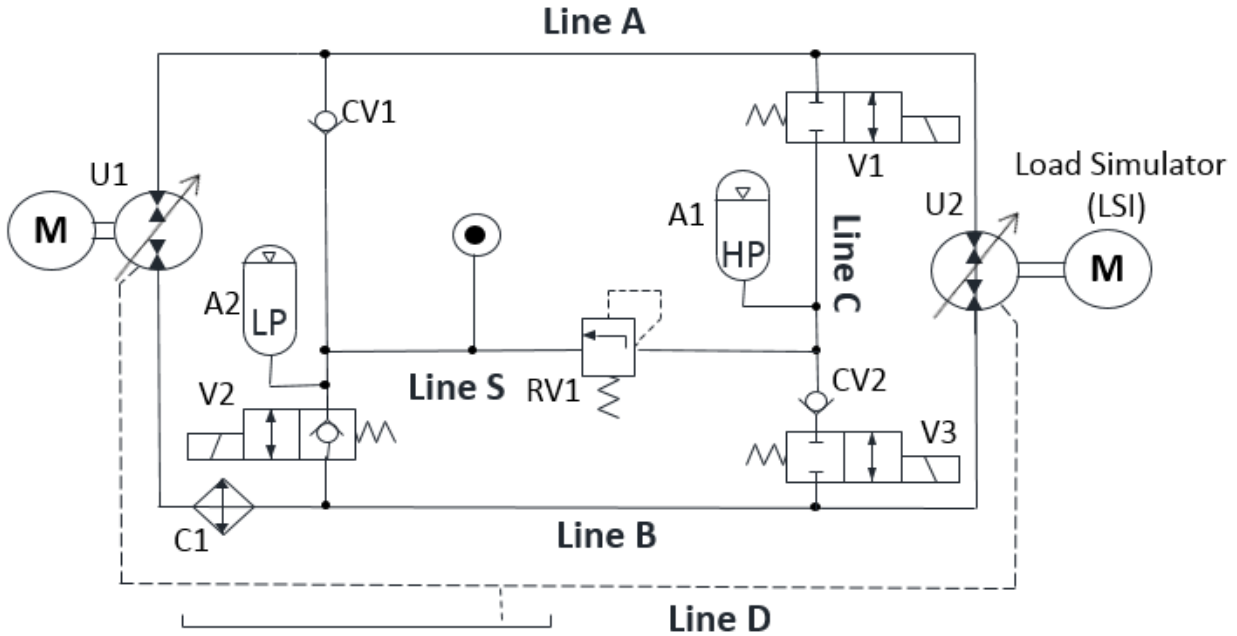


Figure 3.11 Hybrid-in-the-loop hydraulic circuit

The circuit contains three valves that are used to switch the circuit architecture. Valve 1 (V1) is the enabling valve that connects or disconnects the high-pressure accumulator (A1) to the high-pressure line (line A), giving the high-pressure line a much larger capacitance and the capability of storing energy or using already stored energy. Valve 2 (V2) connects the low-pressure accumulator (A2) low-pressure side of the (line B). Valve 3 (V3) opens a flow path from line B to the high-pressure accumulator. Once V2 is open, if line B has a higher pressure than the high-pressure accumulator, oil flows through the check valve (CV2), and line B feeds the energy in the high-pressure accumulator. The test equipment will be on the HST when setting V1 and V2, and V3 are all closed. SH configuration is achieved when V1 and V2 are open, and V3 is closed. MSH configuration requires the cooler (C1) in line B to be removed and replaced by a pipe connection. Furthermore, to close valve 2, valve 3 must be opened. Valve 1 is actively controlled: it opens the accumulator to Line A when regenerative power is used and will remain closed when it is not.

Unit 1 (U1) is a 42cc and unit 2 (U2) 75 cc swash-plate axial piston machines. These are variable displacement swash-plate type axial piston units. They have 8 operating quadrants and can function as a pump or a motor. The displacements are controlled using servo-valves. A current

source from 0 to 100 mA is used to control the servo valve. A 20-80 mA signal changes the swash-plate tilt from 0 to 100% displacement. The high-pressure and low-pressure accumulators are both bladder type with the capacity for 20 liters. The pre-charge pressure in the high-pressure accumulator is 80 bar, and the pre-charge pressure of the low-pressure accumulator is equal to 14 bar. The low pressure is connected to a central hydraulic supply, and therefore the system is not fully independent. If line A or B pressure is lower than the supply power pressure fluid will flow to the lines through valves CV1 and V2, respectively. Table 6.1 describes the hydraulic elements of the circuit.

3.7.2 Simulation

A single line Model was used to represent line A while line B was considered to be a lumped model since it has low pressures, which are not the scope of this study and also the lack of piezo-electric sensors installed on it, which means the pressure ripples of line B are not being measured on the test rig. Different combinations of speed and pressure were measured to validate the model in a considerable operating range.

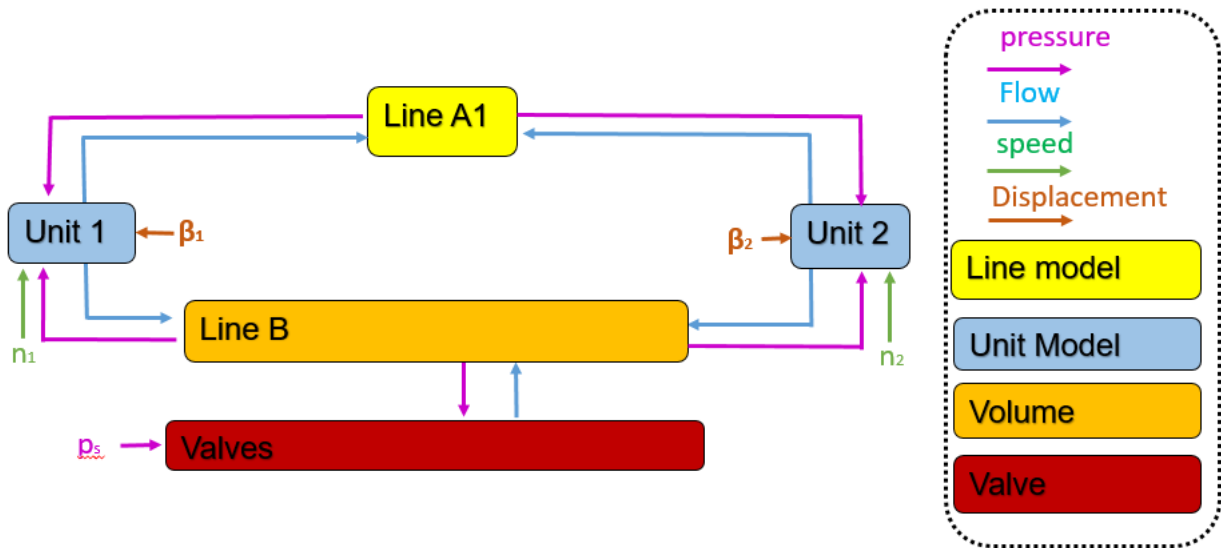


Figure 3.12 Hybrid-in-the-loop test rig model using the coupled hydraulic system model

Table 3.2 illustrates the main measured parameters for all five operating conditions measured. All experiments were conducted at the maximum pump and motor displacement and at hydrostatic transmission mode. Also, line A oil temperature was controlled to be equal to 55°C. The speed of

the pumping unit was controlled by the electric motor, while the speed of the motoring units was determined by the inlet flow and inner losses. At simulation, the volumetric losses were calculated from the experimental data rather than using the polynomial loss model.

Table 3.2 Experiment Operating Conditions

<i>Test</i>	<i>Operating conditions</i>		
	<i>Unit 1 Speed (rpm)</i>	<i>Mean High pressure (bar)</i>	<i>Mean Low Pressure (bar)</i>
1	2000	100	24
2	2000	200	24
3	2000	300	24
4	3000	100	24
5	3000	200	24

Four simulations ran for all five operating conditions. Each model improves describing the line features in Figure 3.14 by one level. These models are described by the following labels:

- **Standard:** All line is made of steel, no curvatures, and a constant inner diameter equal to 19 millimeters.
- **Material:** the line has steel and hydraulic hose segments. Still it does not have any curvatures and a constant diameter;
- **Mat+Elb:** The line has steel and hose segments, curvatures are represented on the model, inner diameter remains constant
- **All Det:** All line features shown in Figure 3.14 are represented. The line has hose and steel segments, curvatures, and variable diameter.

3.7.3 Experimental Setup

For model validation, the experimental setup shown in Figure 3.11 was assembled at Maha Fluid Power Research Center of Purdue University using two Sauer Danfoss S90 swash plate axial piston-type positive displacement units. The assembled test bench is shown in Figure 3.13. The pumping and motoring units were respectively sized at 42cc and 75cc. The main hydraulic components can be verified in Table 3.3. This transmission was derived from novel transmission

architectures designed for utility vehicles (Sprengel, 2015) and specifically installed in an experimental setup for energy management algorithms (Williams & Ivantysynova, 2019) . This design is focused on mid-power, high-density hydraulic functionalities for road vehicle applications, which have strict noise regulations

Table 3.3 HIL Hydraulic Components

<i>Component</i>	<i>Specification</i>
Unit 1 (pump)	42 cc
Unit 2 (motor)	75 cc
High-pressure accumulator	20 liters (bladder type, pre-charged at 80 bar)
Low-pressure accumulator	20 liters (bladder type, pre-charged at 14 bar)
High-pressure relief valve	350 bar
Low-pressure relief valve	24 bar

The test platform is also connected to software capable of representing the hydraulic transmission while using mathematical representations for subsystems such as motor vehicle dynamics tires, road conditions, brakes, and other factors. The load simulator (LSI) can replicate various characteristics of a road, such as jerks and bumps and suspension impact, vibration, etc. It also facilitates a high level of control.

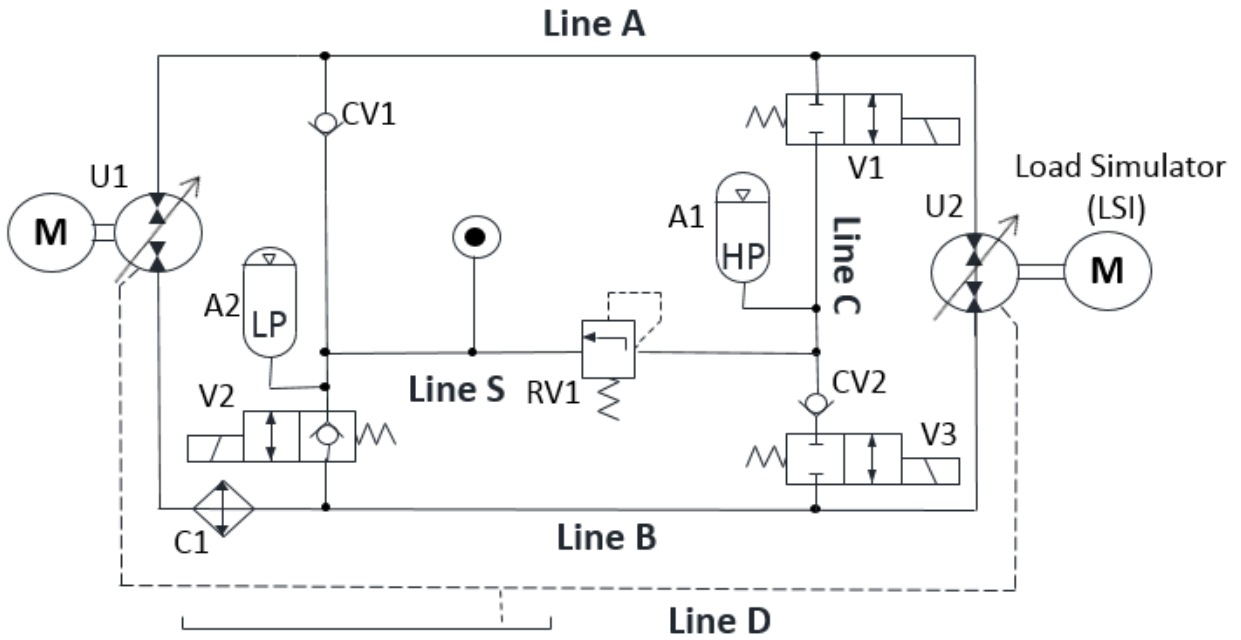
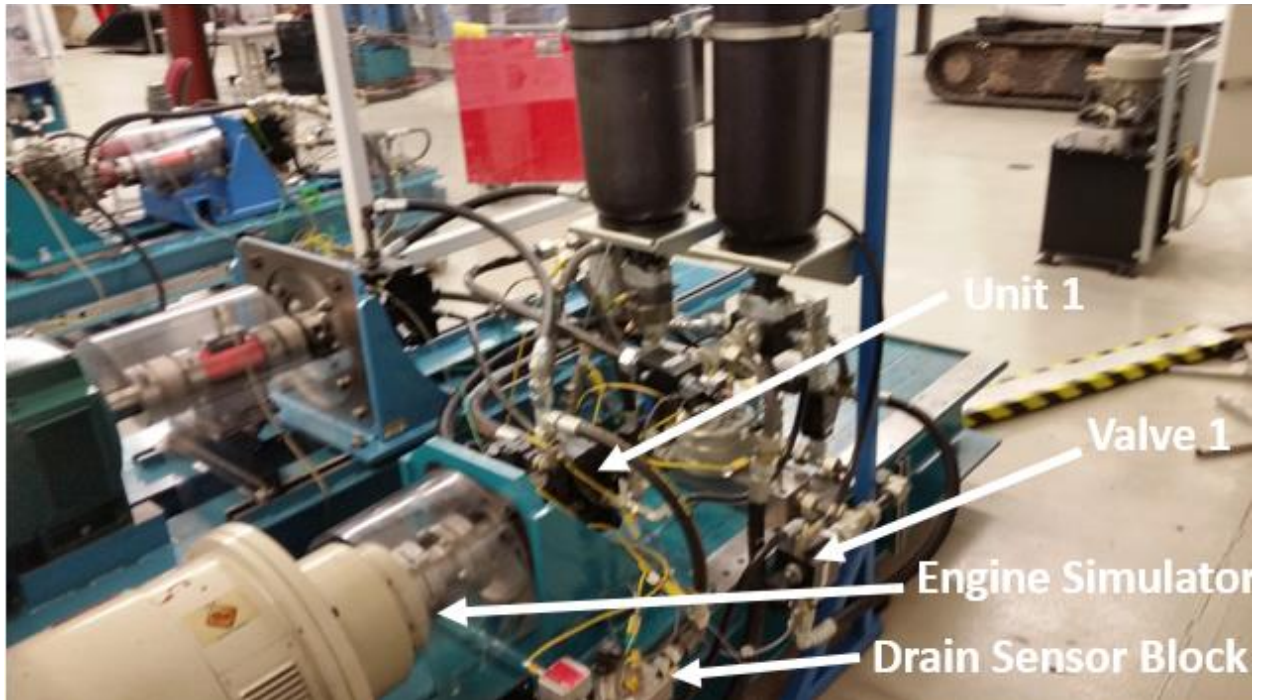


Figure 3.11 Hybrid-in-the-loop hydraulic circuit

a)



b)

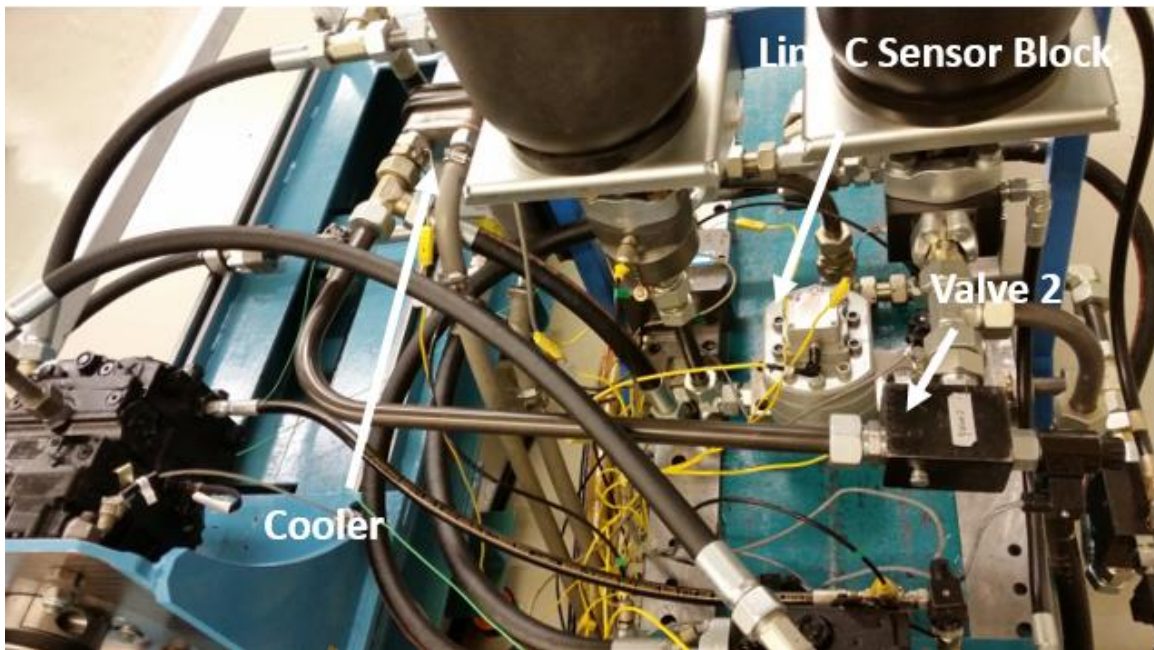


Figure 3.13 Hybrid-in-the-loop Experimental Bench

Figure 3.13 continued

c)

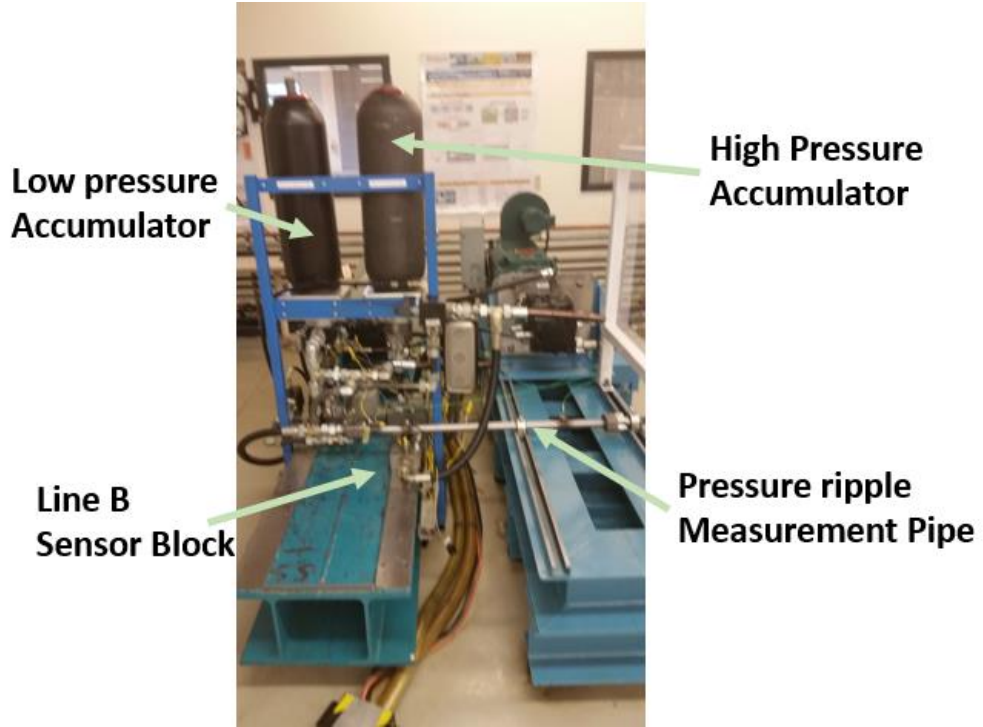


Table 3.4 describes the instrumentations used at the test rig to measure relevant data. The mean pressure of each line is obtained by five piezo-resistive sensors, while the pressure variation is obtained at three different locations of line A by three Kistler 603B type piezoelectric sensors. Flows are measured at the outlet of unit 2 in line B, at the drain line, and at line C just before the accumulator. Two torquemeters and two tachometers provide respectively the torque and the speed of the engine and the load simulator to the supervisory system, which is mainly important for control and energy management issues. The exact location of the sensors can be verified in Appendix A, and the data acquisition of the system can be check-in Appendix B.

Table 3.4 HIL Test rig Hydraulic sensors

<i>Sensor</i>	<i>Location</i>	<i>Manufacturer</i>	<i>Range</i>
Piezo-resistive pressure sensor	Line A	WIKA	0-400 bar
Piezo-resistive pressure sensor	Line B	WIKA	0-5000 psi
Piezo-resistive pressure sensor	Line C	WIKA	0-8000 psi
Piezo-resistive pressure sensor	Line D (Drain)	WIKA	0-25 bar
Piezo-resistive pressure sensor	line S	Hydac	0-60 bar
Piezo-electric pressure sensor	Unit 1 Downstream	Kistler 603B	0-1000 bar
Piezo-electric pressure sensor	Pipe upstream	Kistler 603B	0-1000 bar
Piezo-electric pressure sensor	Pipe downstream	Kistler 603B	0-1000 bar
Type K thermocouple	multiple locations	Omega	0-1200 C
Flowmeter	line C	VSEVS4	1-250 l/min
Flowmeter	line B	VC Kracht5	1-250 l/min
Flowmeter	Drainage	VSE VS02	0.1-120 l/min
Torquemeter	Engine	Schenck	500 Nm
Torquemeter	Load	Staiger Mohilo	500 Nm
Tachometer	motor	Hubner	0-12000 rpm
Tachometer	Load	Staiger Mohilo	0-420 Hz

Figure 3.14 describes Line A profile along its length and the placement of the three piezoelectric sensors. Sensor 1 is placed as close as possible from the outlet of unit 1, being 14 centimeters apart from it. Sensor 2 is installed upstream of a 25.4-millimeter diameter pipe, while sensor 3 is installed downstream of the same pipe.

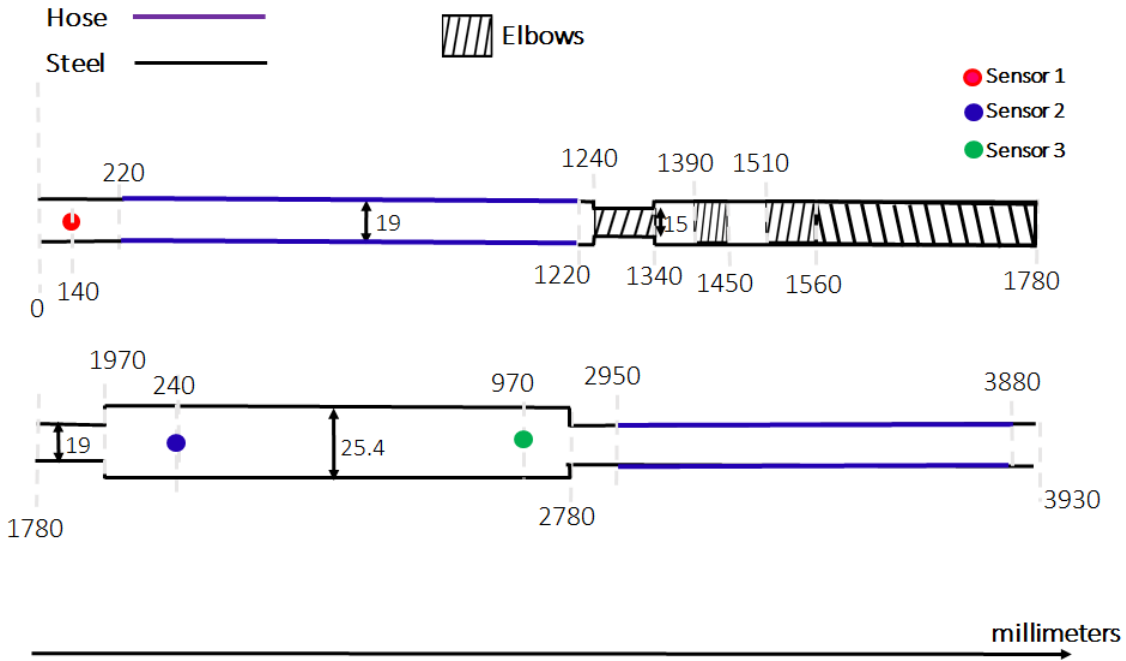


Figure 3.14 Line A₁ features and sensor placement

3.7.4 Comparative Results

Figures 3.15, 3.16, and 3.17 illustrate measured and simulated pressure ripple at the time-domain in the high-pressure line for all three piezoelectric sensors positions for tests 4 , 1, and 5, respectively. All four simulated models are represented in the pictures. It is possible to notice, as a sensor is closer to a unit, the simulations provide better matching with experimental data than in a sensor position further from the units.

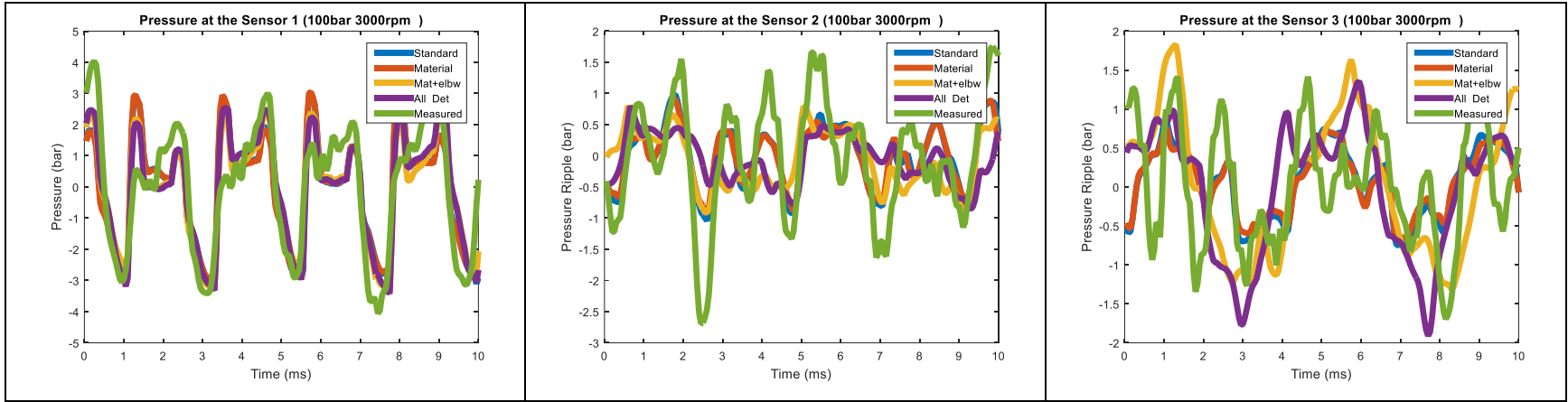


Figure 3.15 Measurement vs four simulation models time-domain results at 100 bar, unit 1 speed equal to 3000 rpm, unit 2 speed equal to 1387 rpm

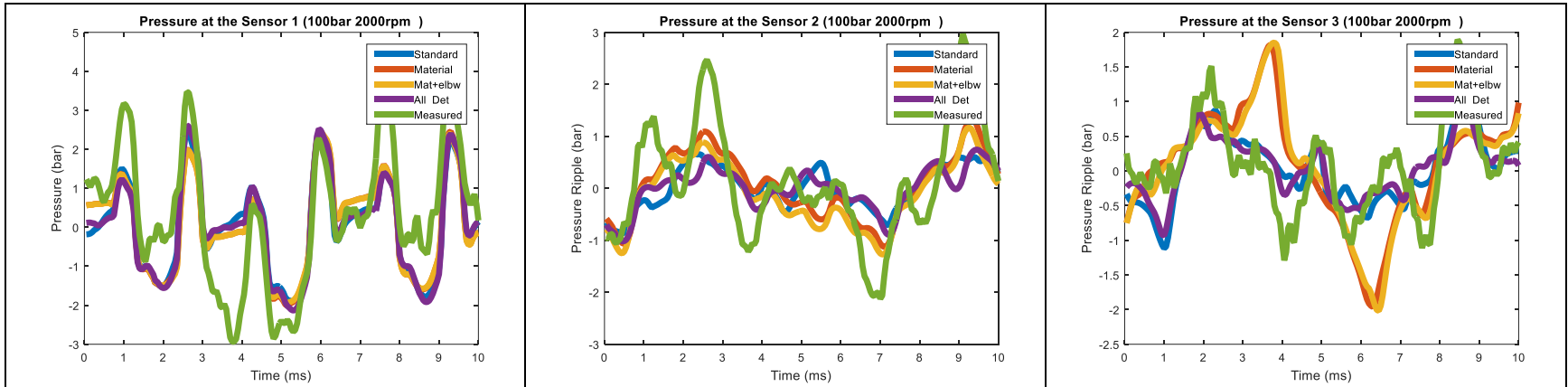


Figure 3.16 Measurement vs four simulation models time-domain results at 100 bar, unit 1 speed equal to 2000 rpm, unit 2 equal to 915 rpm

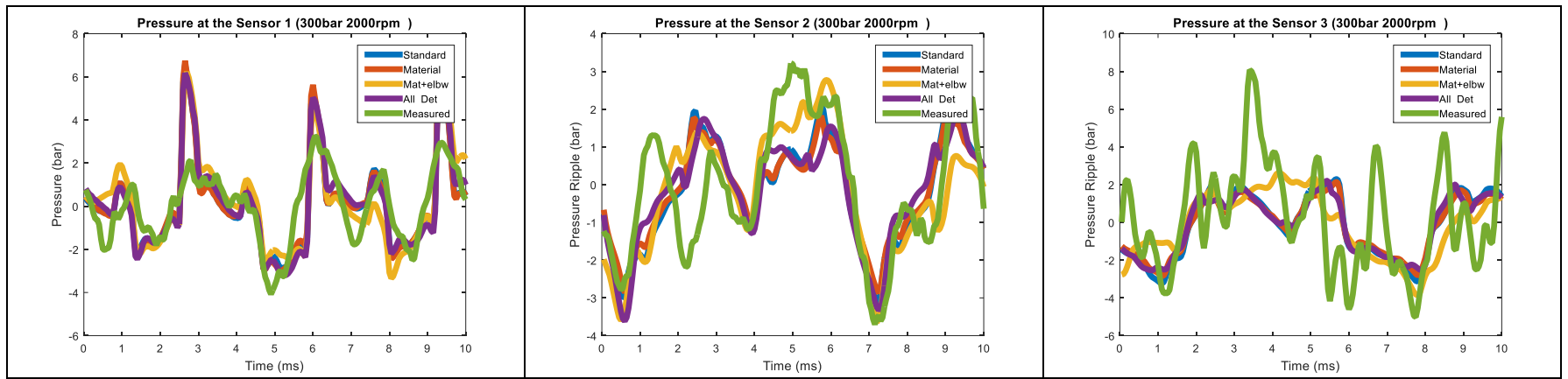


Figure 3.17 Measurement vs four simulation models time-domain results at 300 bar, unit 1 speed equal to 2000 rpm, unit 2 speed equal to 818 rpm

Figures 3.18 and 3.19 represent the frequency-domain magnitude for pressure ripple on all three sensor positions for tests 4 and 3 respectively. The fundamental frequencies of a unit depending on the speed of the unit n in rpm and the number of displacement chambers in on the unit.

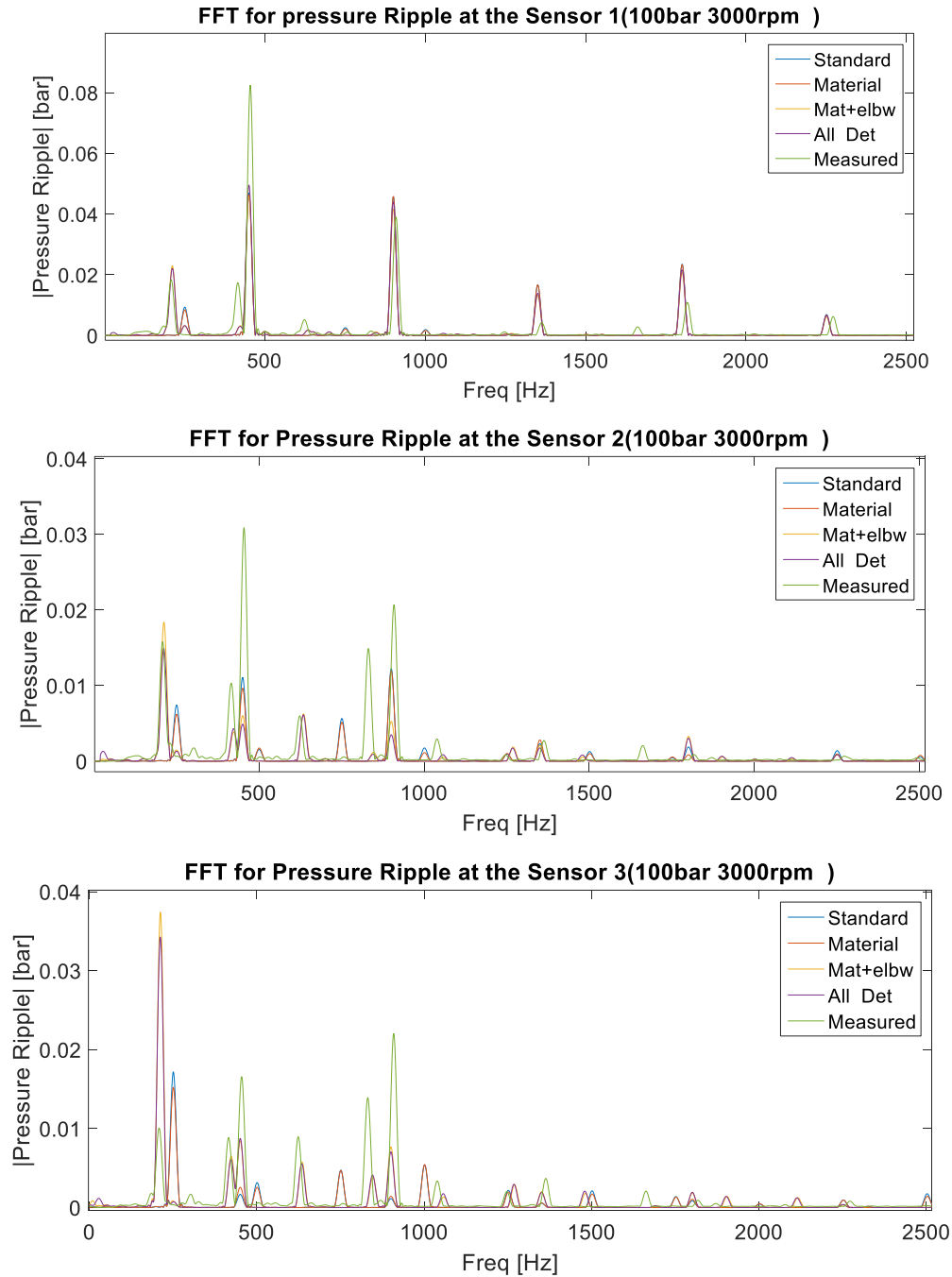


Figure 3.18 Measurement vs four simulation models fast Fourier transform at 100 bar unit 1 speed equal to 3000 rpm, unit 2 speed equal to 1387 rpm

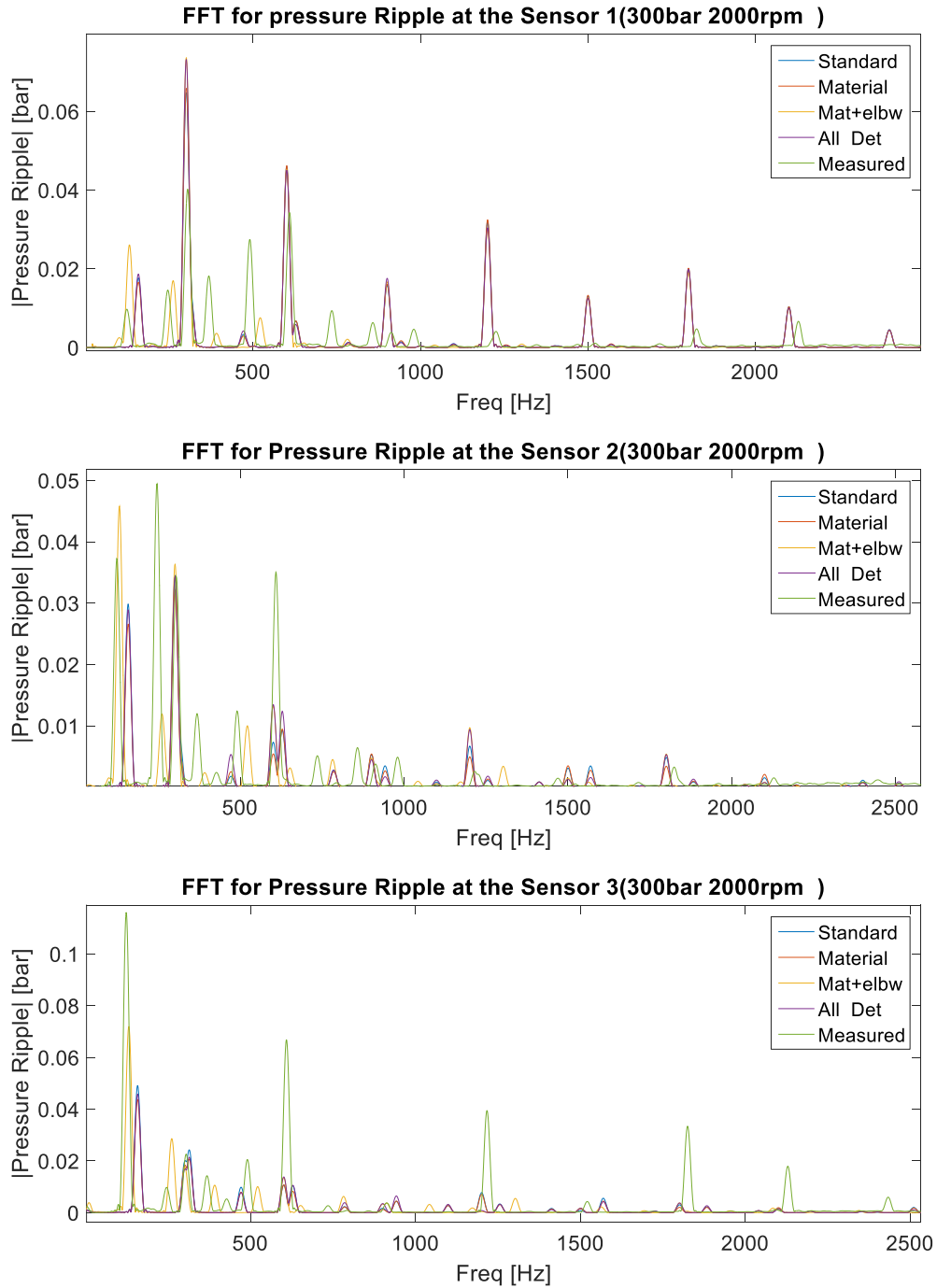


Figure 3.19 Measurement vs four simulation models fast Fourier transform at 300 bar unit 1 speed equal to 2000 rpm, unit 2 speed equal to 818 rpm

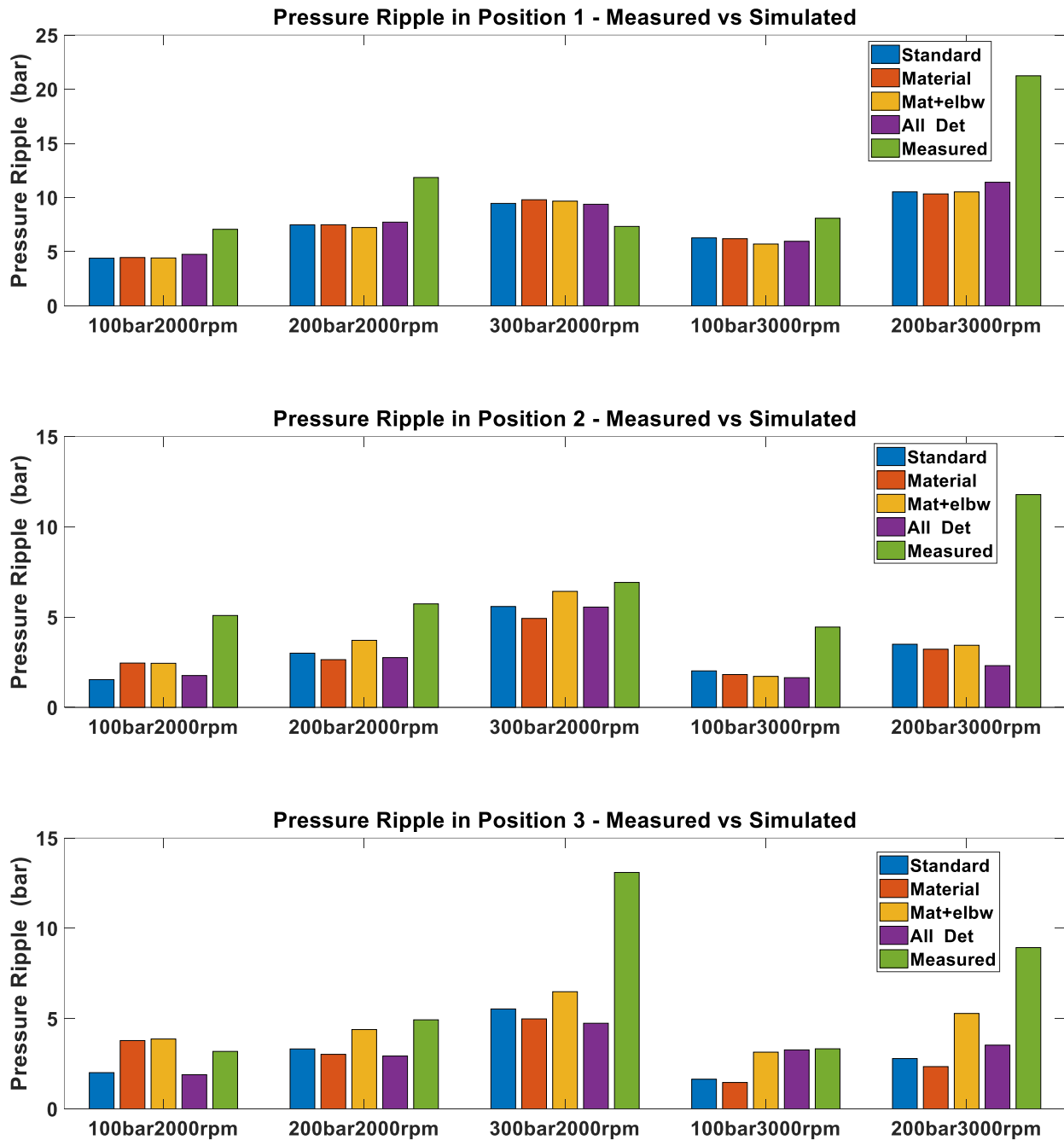


Figure 3.20 Pressure ripple magnitude for four simulated models compared to the measured data

Overall the pressure ripple magnitudes predicted by the model were decently close to the magnitudes measured by the experiment. Considering all three sensors, the model with material and curvatures representation but with a constant diameter, had the best matching. At Sensor 1, The best matching was given by model **All Det** with an average error of 34.3%, and the worst was

Mat+Elb with an average error of 38.2%. For sensors 2 and 3 however, **Mat+Elb** obtained the best results with 50.6% and 31.1% average errors respectively. The worst matching at Sensor 2 location was given by **All Det** (59.6% average error) and the greatest average error of sensor 3 was equivalent to 53.4% by the model **Material**.

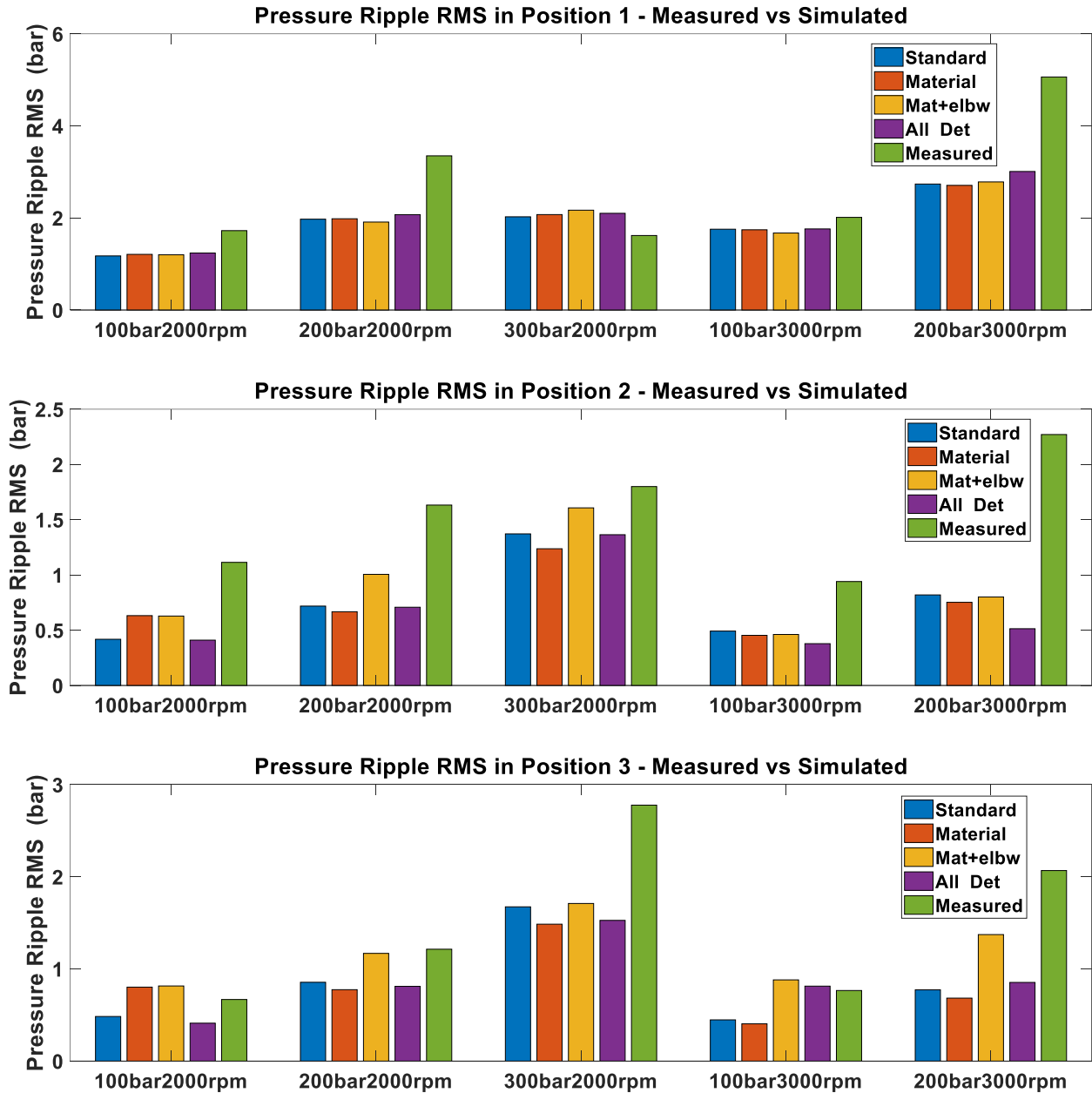


Figure 3.21 Pressure ripple RMS for four simulated models compared to the measured data

4. A HOLISTIC COMPREHENSIVE METHOD FOR USING THE MOC MODEL AT THE FREQUENCY-DOMAIN

This section introduces a holistic study on hydraulic lines' passive elements and aims to find FBNS reduction solutions based on replacing elements that are purely reactive and do not introduce energy in the system. Four indicators (target pressure ripples) are chosen to be reduced by the replacement of a common hydraulic line with a featured one. This method is then summarized in graphical tools to be used in applied engineering without the need for experimental characterization. This strategy tends to be effective for multiple operating conditions through reducing the proposed element's frequency response (in comparison to the default element) for a given target indicator and a whole 25-5000 Hz frequency spectrum. To obtain the reactive elements' frequency domain response accounting for fluid friction effects, a time-domain line model was used, and multiple isolated frequency simulations were performed one at a time.

4.1 Model and methodology

In this project, the method of characteristics model was also used to conduct studies on line behavior in the frequency domain. When compared to a standard transfer function based frequency domain methodology, the method of characteristics presents the advantage of simulating the line's transient and non-transient friction influence. Since it is no trivial to find a passive FBNS reduction strategy that is effective for a broad frequency band, this study requires evaluating as many factors as possible that are likely to increase or reduce pressure ripple.

Also, this study aims at impacting as many hydraulic circuits as possible. Therefore, the less the variables depend on the upstream and downstream elements, the better. The inputs for the models are two flows (initial pressure has also to be defined), while the transfer function method uses two pressures and two flows. Since the pressure, in this case, will depend on the boundary condition such as an orifice, valve, hydraulic unit, or pipe termination, the isolated behavior of the line alone cannot be evaluated.

One of the possible reasons this model inputs depend only on boundary flow and not on the boundary pressure may relay in a physical interpretation standpoint. In this interpretation, it is considered that the pressure oscillation will be created by a flow's water-hammer effect being held in the line because of the fluid momentum. Actually, the pressure rise and pressure decline would be at first generated in the boundaries line nodes, and only then, the boundary pressure should be affected by the line pressure. So the pressure on the boundaries would be the effect, not the cause of the pressure in the line extremities, and therefore, the pressure ripple of the boundary nodes would be the 'earliest source' of fluid borne noise to be transmitted through the system, including back to the units. There is, however, another earliest noise source, which is the interior of the units' displacement chambers. This source has its behavior due to different frequency contents behavior since the displacement chamber pressurization has large high-frequency content.

The excitation response for each frequency is considered important in the study of noise that can result in unhealthiness for humans working with hydraulic machinery. The hydraulic system can have multiple resonant modes in the fluid that will cause force excitations to the structure, which will have, consequently, new resonant modes. At the next step, these vibrations will be transmitted to the atmosphere, and the transmission will depend on the direction of the incidence's waves and angles at the interfaces. Finally, the human ear responds differently to each frequency, being more sensitive to some frequencies than others, this sensitivity also varies with sound level; all these factors combined make the correlation of fluid-borne oscillations and noise quite unpredictable both in time and frequency domain.

Therefore, despite using the time domain model to account for as many factors as possible, it is necessary to develop a simple test capable of evaluating the pressure oscillation in an isolated given line for a given frequency, Figure 4.1 describes this standardized simulation. An oscillation at a given frequency is inserted both upstream and downstream, resulting in a homo-harmonic pressure oscillation. A default value of 50 liters per minute was chosen for the mean flow to account for friction's effects on the model.

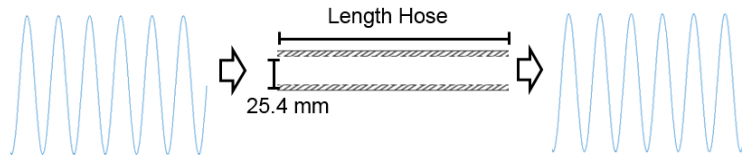


Figure 4.1 Hydraulic line with upstream and downstream excitation

After being excited, each inner node of the line will have a pressure oscillation that will be related to the magnitude of the upstream and downstream excitation. Line characteristics may result in very high or very low oscillations when compared to the excitation magnitude. The oscillation magnitude will also vary from node to node as a consequence of the existence of standing waves created by the line model. Once the line model stabilizes, the amplitude of the oscillation at each node can be determined by measuring the maximum and minimum value the pressure reaches at each node in a sampling period higher than the wave period. This value can be called Δp .

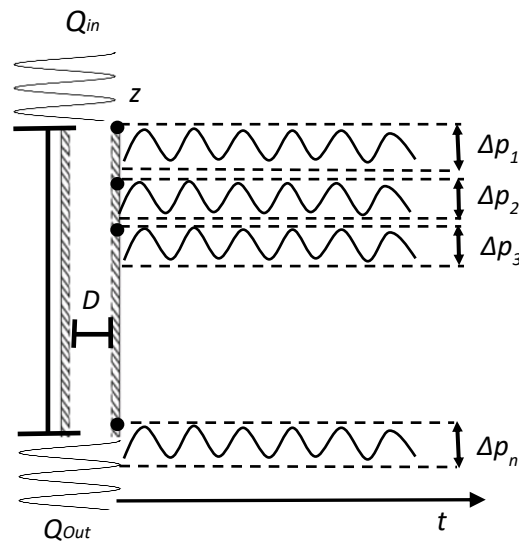


Figure 4.2 Amplitude of the pressure oscillations in each node of the line

In the context of fluid borne noise sources, some oscillations are more relevant than others. The upstream and downstream nodes are often connected with other hydraulic components, active or passive, and the pressure oscillation at these nodes results in forces that will act as excitations for these components. These excitations can be magnified, transmitted, and propagated very efficiently in these components, resulting in unwanted noise levels. In other applications, there is

utter focus on the downstream ripple, since usually, the sources are too far from the human operator. However, in hydraulic lines, many times the upstream, downstream, and line are close to human operators, and solutions that reduce the ripple but compromises the other may not achieve good noise reduction results.

From the statistical point of view, the mean amplitude summarizes the magnitude of the pressure oscillations in the line as a whole in just a single variable. The maximum amplitude among the nodes highlights the highest excitation in the system, which can be determinant for noise generation since noises are often generated transmitted in a non-linear manner. Therefore, the max, mean, upstream, and downstream pressure ripples can be highlighted to study the behavior of fluid-borne noise in a line. Thus, the default model is chosen to be a standard hydraulic line, 25 mm diameter, steel made, and the boundary conditions are pure flow inputs in both directions.

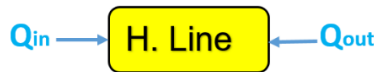


Figure 4.3 Default model used for the study

4.2 Line length influence

Despite considering the line model will react differently for every frequency of Q_{in} and Q_{out} it is also necessary to consider the hydraulic lines can have several lengths and that usually these lengths are constrained by the hydraulic circuit packing. Often, a proposed replacement of this line will have severe limitations in changing length. To verify the line length influence in a default line, 2900 simulations were performed as showed in

Table 4.1 .

Table 4.1 Default Simulation bounds

<i>Parameter</i>	<i>Lower Bound</i>	<i>Upper Bound</i>	<i>Increment</i>
Length(m)	0.2	3	0.1
Frequency(Hz)	50	5000	50

Plotting the target pressure ripples concerning line length and frequency results in a three-dimensional plot. Figure 4.4 shows respective highlighted pressure ripples in a regular duct with 25 millimeters diameter, the mean pressure was set at 300 bar and mean flow to 50 l/m.

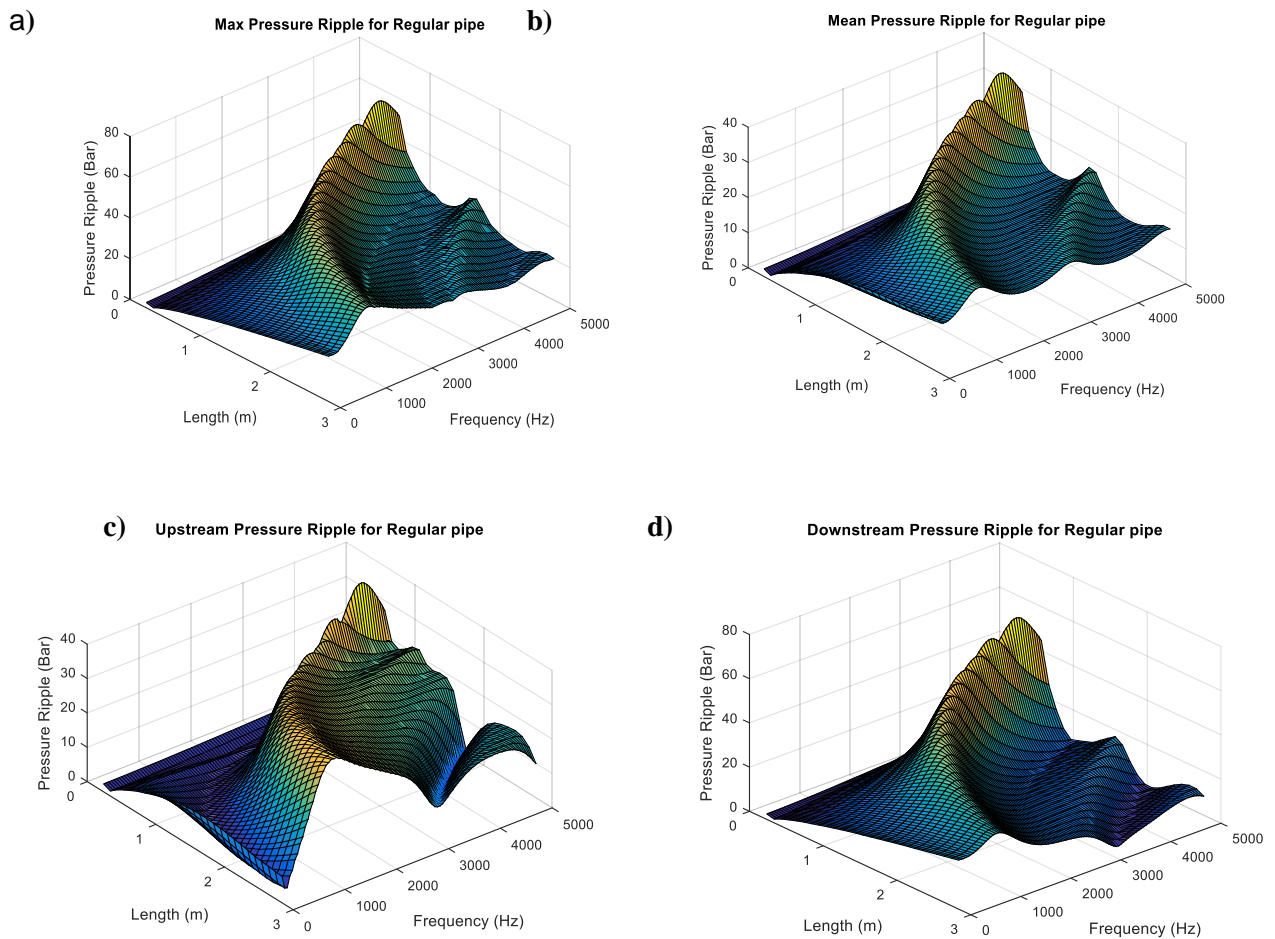


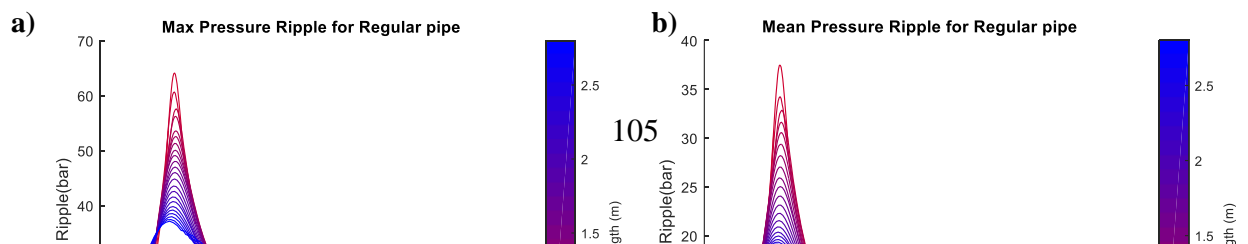
Figure 4.4 Targeted amplitudes of the pressure oscillations in a 25 mm diameter line: a) Max pressure ripple; b) Mean pressure ripple; c) Pressure ripple at the Upstream ; d) Pressure ripple at the downstream

In Figure 4.4 it is possible to notice that the line has a resonance mode that changes to a suitable length. The resonance however does not depend exclusively on the length of the duct, but on the total phase shift the wave translates inside the tube, therefore it depends on the length and speed of the sound. To determine the value of this resonance mode, it is necessary to understand the influences of the oscillation frequency in the space plane using the spatial frequency k instead of the angular frequency ω and time-frequency f . A similar approach is to deduce how many wavelengths λ fit inside the duct for each excitation frequency. According to Kinsler et al. (1982), the wavelength λ and spatial frequency k can be calculated from the frequency f and speed of sound c (given by equation (3.5)) using respectively equations (4.1) and (4.2).

$$\lambda = \frac{c}{f} \quad (4.1)$$

$$k = \frac{2\pi}{\lambda} \quad (4.2)$$

Using these two variables, it is possible to represent the three-dimensional plots such as in Figure 4.4 in two dimensions where color represents different hose lengths. Two different hose lengths will have the same phase shift inside the duct for different values of the frequency f . Figure 4.5 demonstrate pressure ripples for different lengths in respect to the angular phase shift kL within the tube. It is possible to verify the consistent trend the pressure ripple has in respect to the angular phase shift despite of hose length. Nonetheless, also local divergences can be found in some frequencies which may be a consequence of the line capacitance and friction losses divergence for different hose lengths. These two factors are remarkable but act on a smaller scale than the influence of line length. It is also possible to notice that upstream pressure ripples are far more affected by the phase shift than the line capacitance.



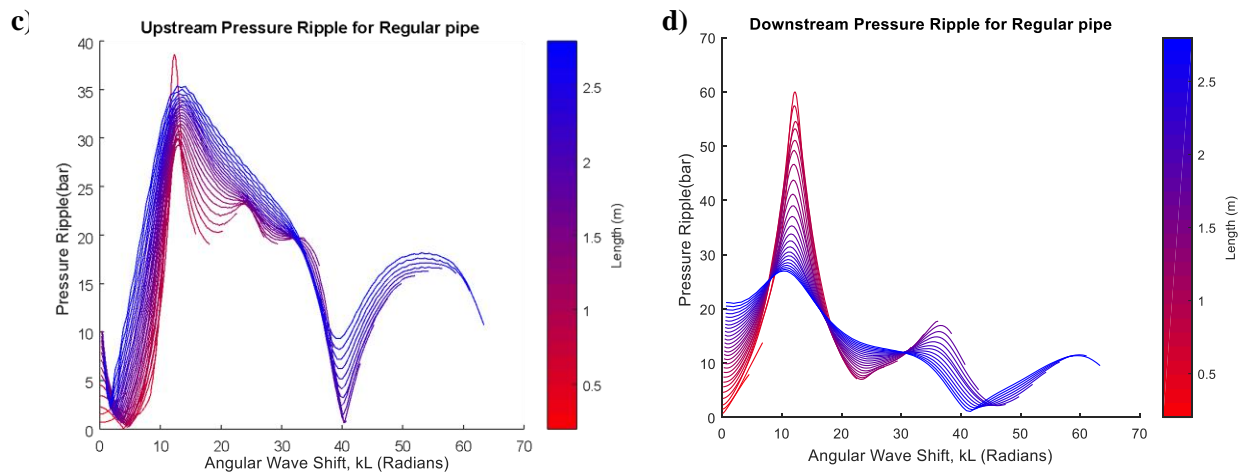


Figure 4.5 Influence spatial frequency at the a) maximum, b) mean, c) upstream and d) downstream pressure oscillations in a 25.4-millimeter diameter steel pipe

The length of 4π radians or two full wavelengths fitting the pipe demonstrates large pressure oscillations' amplification. For a very short duct, even a very high frequency will not result in a large shift; therefore, the resonant mode will be translated out of the 0 to 5000 Hertz frequency range. Choosing a short line can be a solution for noise in multiple operating conditions if it is possible to select such a short component in its respective hydraulic system.

Transfer function-based frequency-domain simulations suggest a pipe, closed in both has resonant modes as multiple of $n\pi$ of the fundamental harmonic. Figure 4.6 displays this trend also for the MOC-based simulations if friction effects are neglected. Also, the magnitude of the pressure oscillations is high. The friction time-domain simulations suggest the 4th harmonic of this

resonance being the most critical. The 12th harmonic is the second most critical. Thus, according to the simulations, there are evident effects of the line length, which should be a consequence of the different frictional losses as of the different line capacitance as well as of the different line capacitance. As lines get longer, the higher line capacitance and friction dampening also result in a reduction of the pressure ripple in the resonant modes.

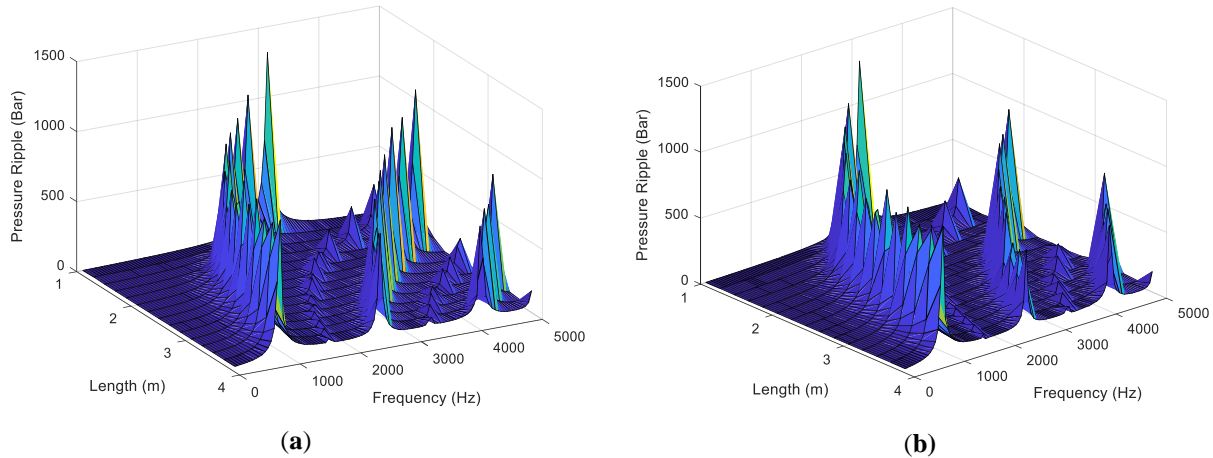


Figure 4.6 Amplitudes of the pressure oscillations in a 25 mm diameter line neglecting friction effects: (a) Max pressure ripple (b) Pressure ripple at the upstream

Understanding the pipeline behavior is important to design the passive FBNS reduction elements this study is aiming for. It is possible to conclude from simulations that the presence of friction effects simplifies the problem-tackling investigation for a fluid-borne noise source mitigation solution for hydraulic lines.

For only a single operating condition, some additional specific solutions can be taken. The length of 12.5π radians (six and a quarter wavelengths) greatly minimizes pressure oscillation in the upstream and downstream. These two positions are often connected to hydraulic components which may be generating a lot of noise. It is important to mention nevertheless that flow excitations may behave differently up to some level for different boundary conditions. The current boundary conditions were chosen as the default for this study based on the relatively small pressure ripple changes verified in section 4.3 and due to the symmetry property.

4.3 Major influencing parameters

By performing an analytical analysis of equations (3.6), (3.7), and (3.8) it is possible to verify that neglecting the value of the isothermal wave speed and friction will have a key influence on the pressure build-up from a node to an adjacent other. The isothermal wave speed B_L depends on fluid density, duct diameter, and sound speed. On its side, sound speed is calculated according to equation (3.5)(3.8) which shows dependence on wall stiffness, diameter, and bulk Modulus. Simplifying the isothermal wave speed to equation (3.15) is possible to evaluate the weight of each of these factors on pressure oscillation magnitude. A strong inverse quadratic relation to the diameter can be verified as a dominant factor.

$$B_L = \frac{4\sqrt{\rho K}}{\pi D^2 \sqrt{1 + \frac{K \cdot D}{E \cdot e}}} \quad (3.15)$$

One idea to reduce pressure ripple magnitude is to reduce isothermal wave speed. However, because friction also plays a role, it is necessary to run simulations and verify if, for the given circuit dimensions that are the scope of the study, the isothermal wave speed will dominate the pressure ripple build up. The MOC line model is very appropriate for this evaluation.

Since variables such as the bulk modulus and density vary with operating pressure and temperature, the speed of sound and isothermal wave speed depends on the operating condition. Lower operating pressures, lower working flow density, lower bulk modulus, and higher working temperatures should reduce the oscillations but are impractical for some fluid power applications. Flexible duct materials and thinner wall thickness also will get the desired results but will be constrained by the necessity of duct resilience which should be able to contain high pressure. Nonetheless, several of these trends are supported by the literature.

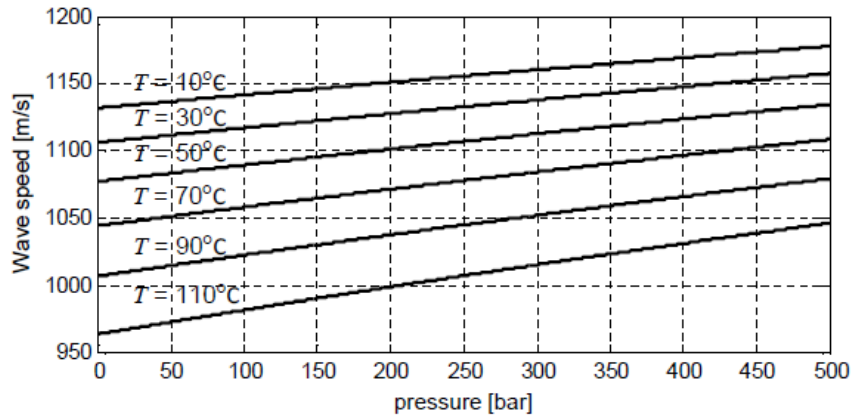


Figure 4.7 Speed of sound in steel duct of 25.4 mm internal diameter and 31.75 mm external diameter (Klop,2010)

Nonetheless, in equation (3.15), the most noticeable factor to influence pressure ripple is the line diameter. Despite the consequence of higher costs and a heavier hydraulic system, in many cases, this is a practical solution. Figure 4.8 shows simulation results: for a 50 l/min mean flow with 20 l/min flow ripple, there are considerable advantages in using at least 19 mm diameter lines in hydraulic systems. The reduction of diameter reduces the pressure ripple for every frequency from 25 to 5000 hertz.

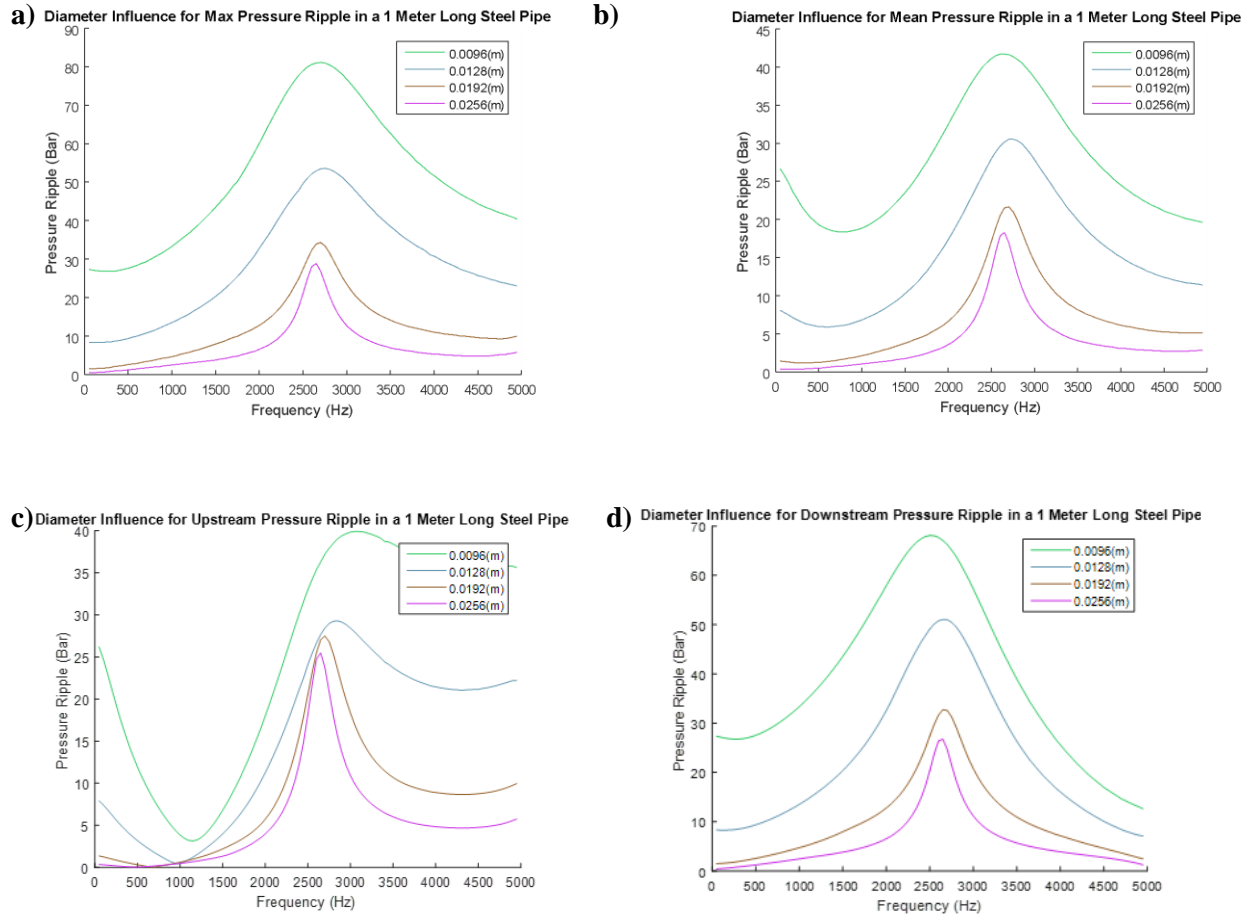


Figure 4.8 Influence of the diameter on the magnitude of the a) maximum, b) mean, c) upstream and d) downstream pressure oscillations in a 1-meter long duct with 50 l/min mean flow and 20 l/min flow ripple

Another property that also influences fluid velocity is the flow oscillation magnitude, this flow magnitude variation demonstrates an almost linear variation in the mean pressure ripple, and the behavior of the frequency domain is the same for upstream and downstream pressure ripples.

Flow Excitation Magnitude Influence over Mean Pressure Ripple in a 1 Meter Long Steel Pipe

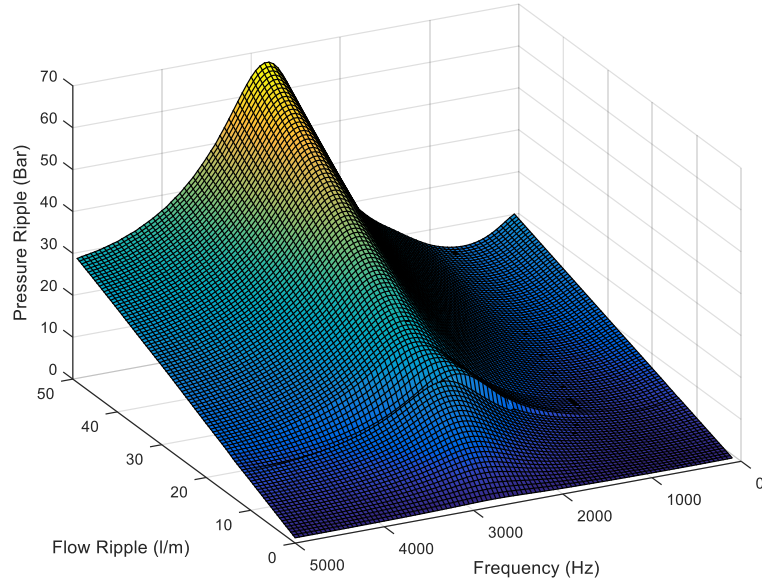


Figure 4.9 Influence of fluid oscillation magnitude at mean pressure oscillations in a 1 meter long, 25.4 millimeter diameter steel pipe

Flow Excitation Magnitude Influence over Upstream Pressure Ripple in a 1 Meter Long Steel Pipe

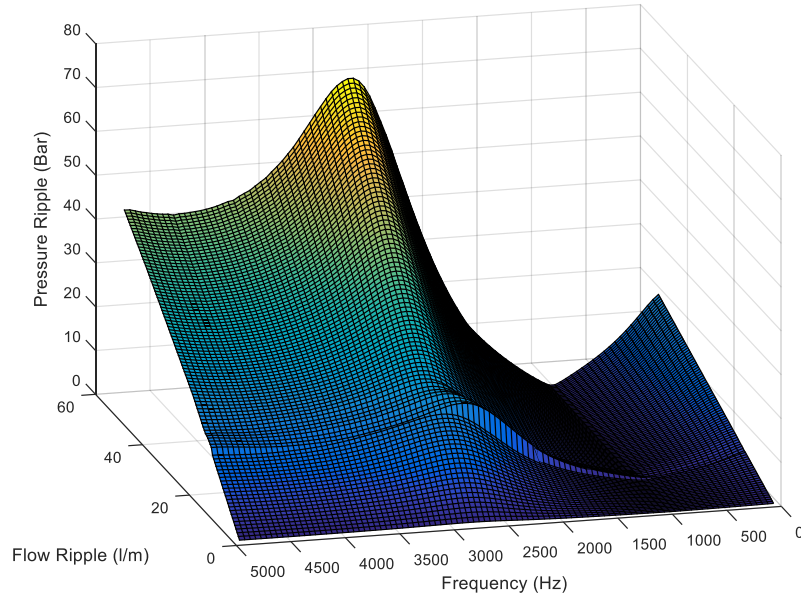


Figure 4.10 Influence of fluid oscillation magnitude at upstream pressure oscillations in a 1 meter long, 25.4-millimeter diameter steel pipe

A value of 20 l/min was chosen for the peak-to-peak flow oscillation, while a 50 l/min was chosen as mean flow throughout the duct. For all the simulations of this study, an operating pressure of 300 Bar and a temperature of 55 C° were chosen. This pressure is not only widely used in high power applications but also has a high noise level as pressure fluctuations increase and sound speed goes up with higher pressure. The increase of sound speed also results in different oscillation modes for the line, which results in a shift in the frequency oscillation peaks in the frequency domain. As Figure 4.10 shows, the magnitude of resonant mode variation is not very significant, however, as pressure increases the resonant mode of the line is translated for lower frequencies becoming thus more noticeable and the average ripple magnitude at the 0 to 5000 Hertz raises. The increase in average excitation forces for the noticeable range may result in higher noise levels.

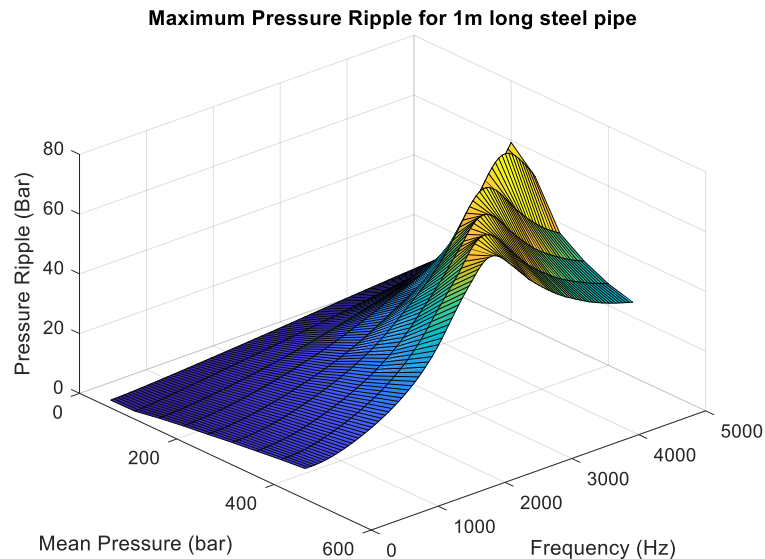


Figure 4.11 Influence of the mean pressure at the maximum pressure ripple in a 1 meter long, 25.4-millimeter diameter steel pipe

4.4 The downstream magnitude and phase influence

The boundary conditions of the system are a crucial factor since the interaction in the line model boundaries will have a great influence on the behavior of the pressure oscillations at each position. In equation (2.5) for example, for many systems the values of the constants B_1 and B_2 can be calculated from the boundary conditions, and different conditions will affect the position of the standing waves' peaks and valleys in a pipe. The advantage of evaluating the pipe behavior with

two equal oscillations sharing the same phase both upstream and downstream is the symmetry of the system. If the mean flow is equal to zero, the system should be symmetric and the upstream and downstream pressure should be equal at every instant of considering the pipe has a constant parameter. Since there is also fluid flowing across the pipe, the mean flow is different than zero and the upstream and downstream pressure oscillation will demonstrate different behavior. The usage of symmetric excitations makes this difference more evident.

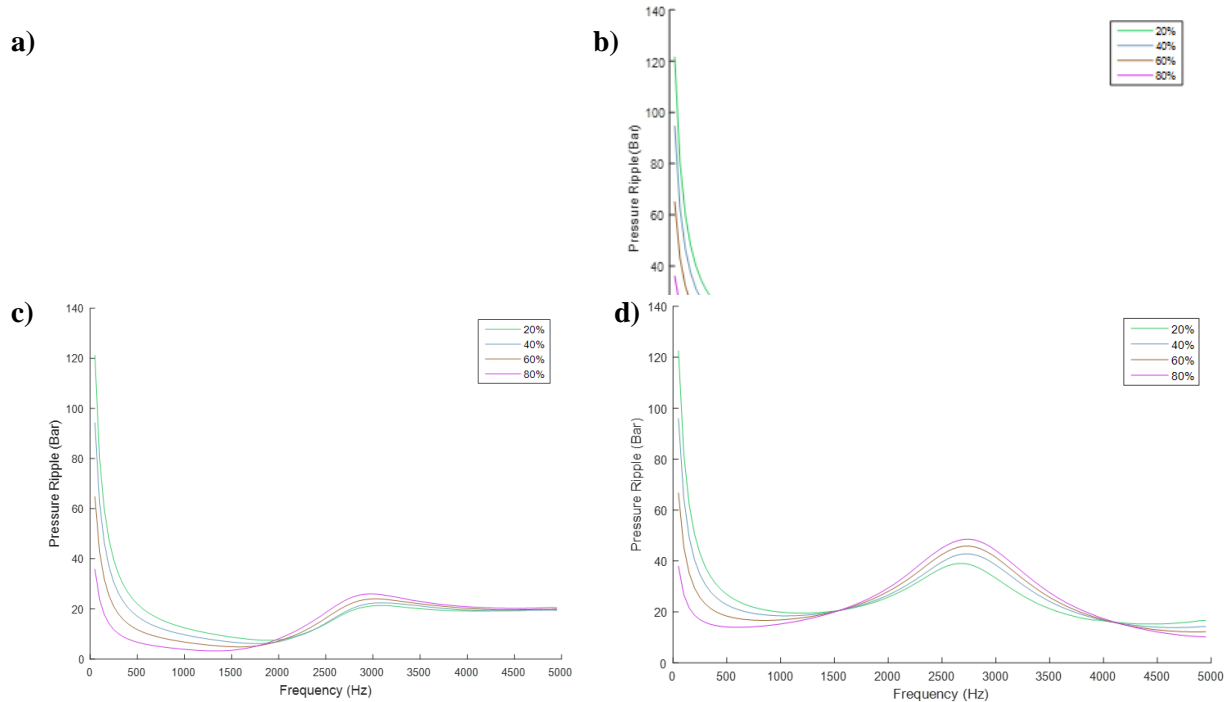


Figure 4.12 Influence of downstream flow ripple magnitude in proportion to upstream flow ripple magnitude at a) maximum, b) mean, c) upstream and d) downstream pressure oscillations in a 1 meter long, 25.4-millimeter diameter steel pipe

Once the pipe is inserted in a hydraulic system, it won't have such simple behavior. Valves, pumps, motors, and asymmetric terminations will have different magnitudes and phases than the upstream excitation.

Figure 4.12 demonstrates that for a downstream excitation, equal both in frequency and phase to the upstream, a downstream ripple magnitude reduction will increase oscillations that have a frequency that is lower than the resonance of the pipe. However, pressure ripples for frequencies higher or equal to the resonant of duct frequency will increase. The resonant frequency of the pipe will not be affected by the alteration in the magnitude of the downstream flow.

The downstream phase influence is comparable to the magnitude influence. A positive shift of downstream phase flow will behave like a reduction of the downstream flow magnitude in addition to the fact that the resonant frequency of the duct is shifted to lower frequencies. A negative phase-shift will act with inverse alterations when compared to the positive phase shift. The pressure ripple augmentation is very noticeable for very low frequencies but for this very slow flow variation, the flow difference between the source and the sink should be enough to influence the pressure buildup in the pipe, therefore, a part of this pressure ripple is a consequence of the non-transient component of the flow and not the transient effects which are the interest of this study. Also, for passive hydraulic elements, small phase shifts should be more realistic since these components will react to pressure rising by also increasing outlet flow.

Figure 4.13 demonstrates the downstream excitation phase shift influence at the standard 1 meter long, 25.4 millimeters diameter steel pipe. Overall, for frequencies superior to the resonant frequency, the maximum and mean pressure ripples are very similar, while the lower frequency content will increase for most cases. For upstream and downstream excitation, the phase shift will also increase pre-resonant frequency content, however, for the higher frequency; a positive phase shift will increase the downstream oscillations and decrease the upstream ripples. A negative phase-shift will have the inverse effect.

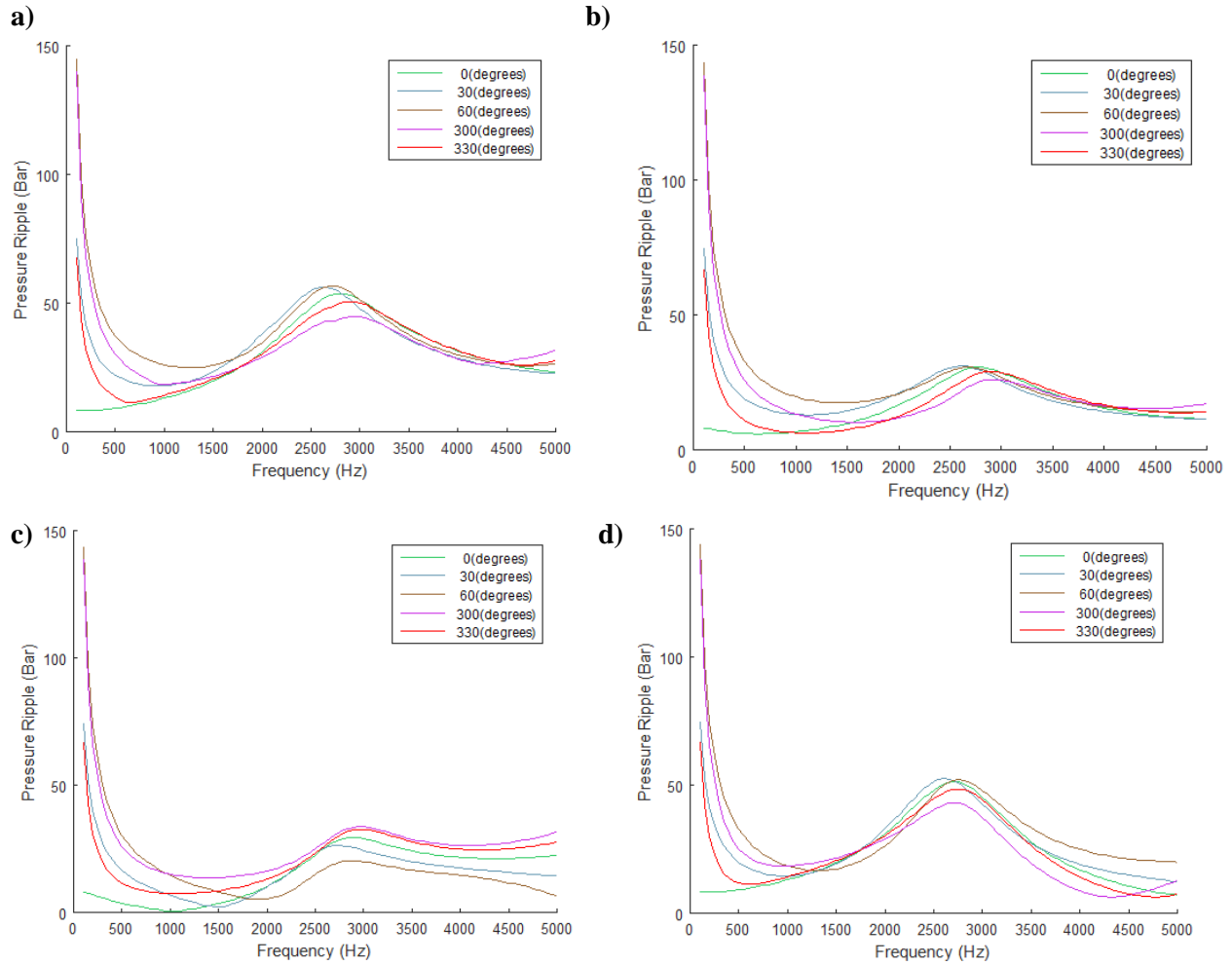


Figure 4.13 Influence of downstream flow ripple phase shift in respect to upstream flow ripple at the a)maximum,b)mean, c) upstream and d)downstream pressure oscillations in a 1 meter long, 25.4-millimeter diameter steel pipe

4.5 Passive fluid-borne noise elements influence

4.5.1 Duct Profiles

One of the possible solutions to reduce pressure oscillations in a hydraulic system can be the implementation of the diameter variation along the line. The line model, as already explained, is stable enough to simulate line diameter variations.

An alternative to reduce the isothermal wave speed is to increase the diameter, however, because hydraulic lines have standardized coupling and fittings for line variations, usually this diameter

will have to be reduced back to a standard diameter. A strategical usage of line shaping may be an alternative for reducing the pressure ripple.

For this study, some line-shaped variations along the line were tested. Restricting line shapes, to which the line diameter was first reduced to before increasing back to the original size, increased the pressure ripple drastically in most cases. Expanding shapes, however, showed promising results. For these shapes, line diameter is increased by 50% from an extremity up to half of the line and then decreased back to its original diameter, the speed of sound will gradually decrease along the line and then increase again. The pace in which the speed variation occurs will also be an important factor of this line shapes. The aim is to compare the pressure oscillation performance of these shapes with the standard pipe. A normalized value of pressure ripple is capable of demonstrating the relation in a summarized manner as shown in equation (4.3) is displayed by Figure 4.14.

$$\Delta p_{Norm} = \frac{\Delta p_{Solution}}{\Delta p_{Default}} \quad (4.3)$$

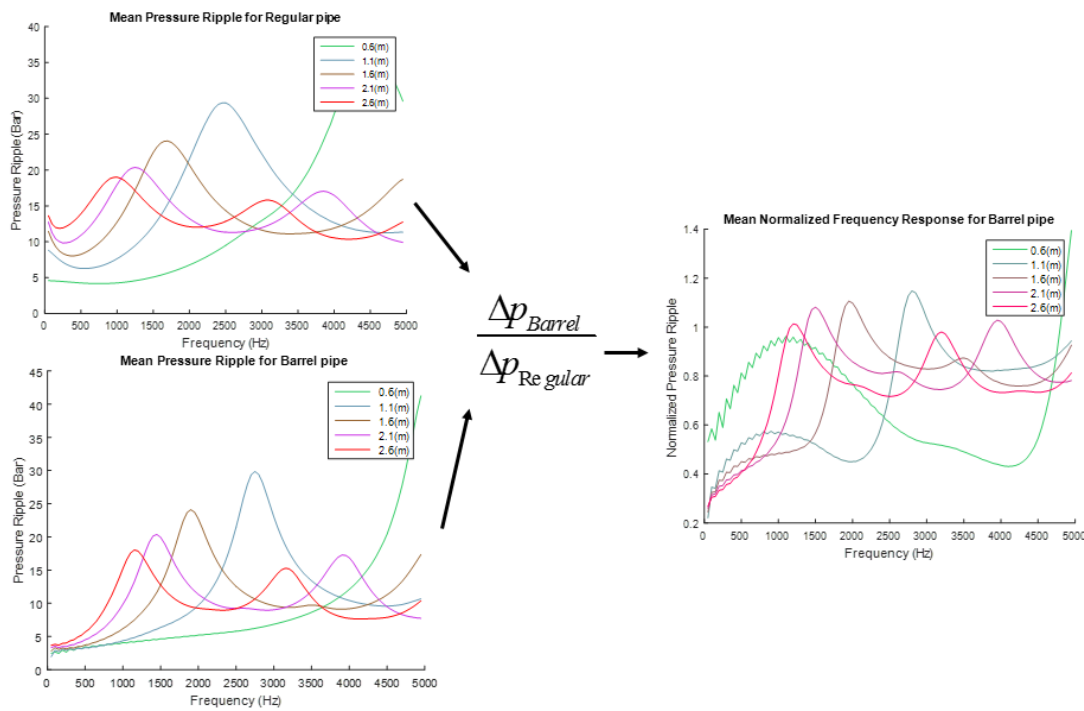


Figure 4.14 Pressure variation normalization from a special featured line to a standard line

Along the simulated line-shapes, two profiles distinct out as having the best performance when compared to a standard pipe: A barrel-shaped line which will increase the diameter quickly and decrease slowly, and a barrel-cornet pipe cornet which increases and decreases the line diameter slowly. Both shapes are described in Figure 4.15.

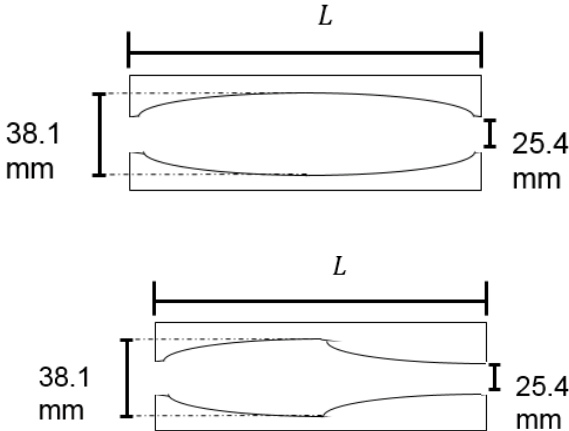


Figure 4.15 Line profile in barrel format and barrel-cornet format.

While special profiles amplify the oscillations around resonant frequency, lower frequency ripples are minimized. For very short lines (less than 0.5 meters in length), a barrel-shaped line can reduce the maximum, mean, and downstream pressure oscillations but the upstream ripple is greatly amplified for a given band. The barrel profile frequency content for the maximum, mean, upstream, and downstream pressures are shown in Figure 4.16.

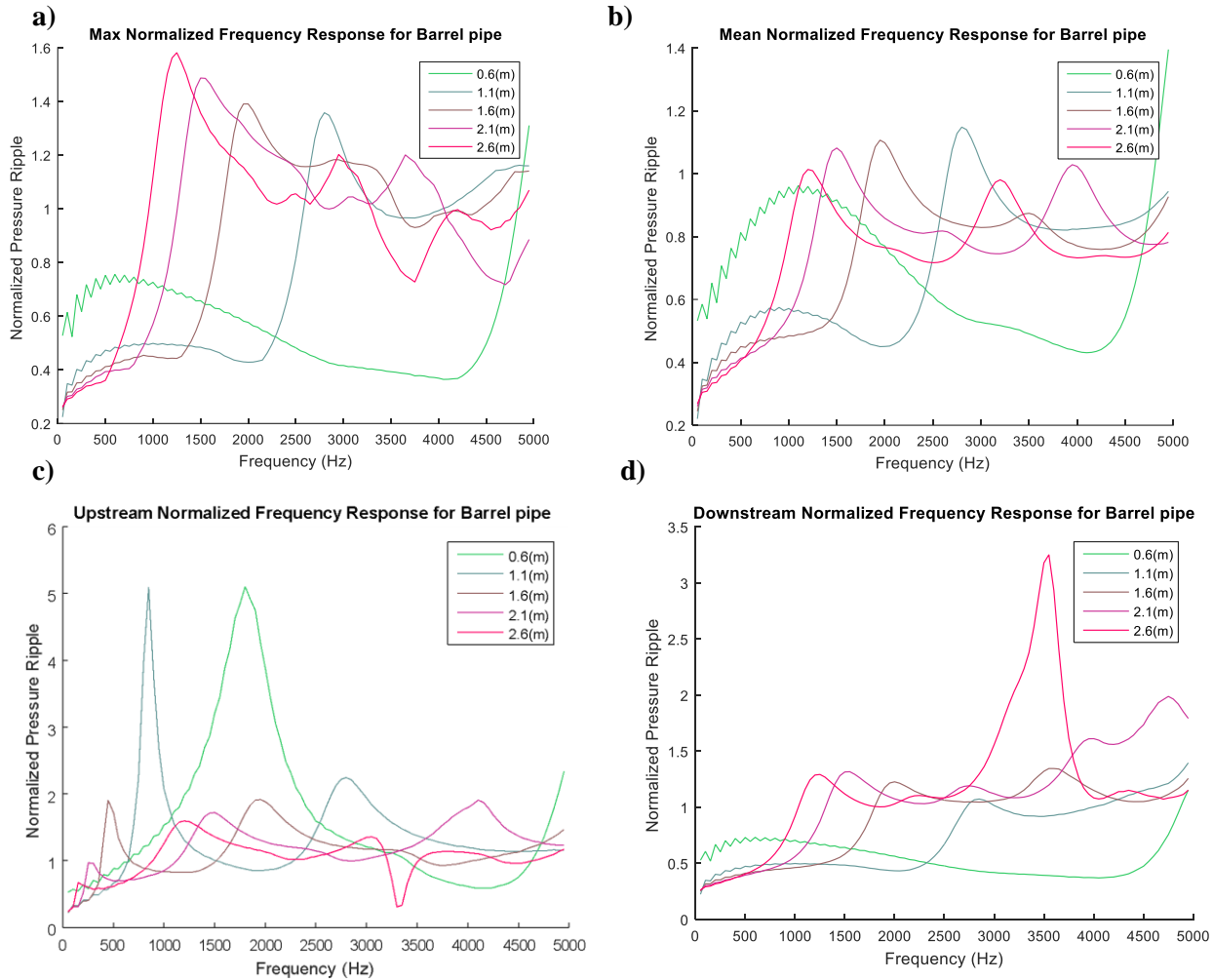


Figure 4.16 Normalized response of a barrel shape profile to a default profile response in respect to: a) maximum, b) mean, c) upstream and d) downstream pressure oscillations

The barrel-cornet shape obtained even further reduction than the barrel shape, also deserving to be in the scope of solutions for the same application. The main advantage when compared to the barrel profile, however, is the fact that the upstream ripple's highest amplification is reduced, which minimizes the disadvantages of this feature when compared to a standard line. The barrel-cornet profile line however is not symmetrical, which means that it will behave as a cornet-barrel if flow changes direction. Also, it may have higher manufacturing costs than the barrel shape due to its higher geometric complexity.

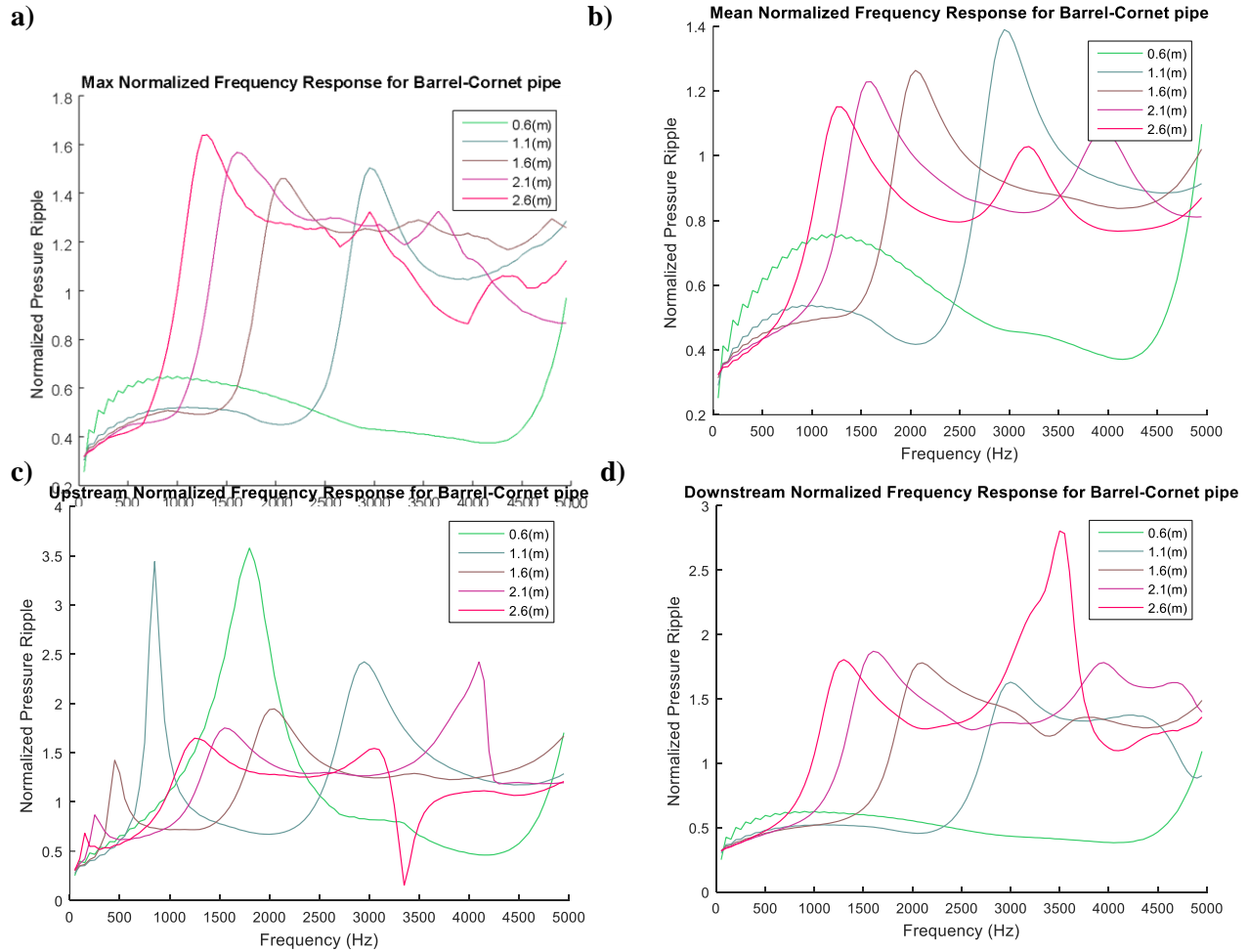


Figure 4.17 Normalized response of a barrel-cornet shape profile to a default profile response in respect to: a) maximum, b) mean, c) upstream and d) downstream pressure oscillations

4.5.2 Side branch closed-end silencers

Closed-end side-branches had long been used as fluid-borne noise source reduction solutions for either a single frequency or defined band. If a single frequency is chosen to be attenuated, the two most used branch lengths are the quarter-wave silencer and the three-quarters wave silencer. These two specific lengths will assure that the pressure excitation in the branch will travel in the positive direction to the end of the silencer, and then be reflected to the branch with a 180° phase shift capable of destroying the original excitation. To develop a multi-frequency side-branch based strategy capable of achieving pressure ripple attenuation in the whole 0 to 5000 Hertz range, the behavior of an isolated line is observed in Figure 4.5 and it is concluded that the most critical

situation the pipe will face is when the duct is two full wave-lengths long or phase shift is equal to 4π . Therefore, a quarter-wave side branch is selected that results in a side branch that has $1/8$ of the original line length.

Table 4.2 Side branch simulation bounds

<i>Parameter</i>	<i>Lower Bound</i>	<i>Upper Bound</i>	<i>Increment</i>
Length(m)	2	5	0.1
Frequency(Hz)	25	5000	25
Position ratio (n/8)	1/8	7/8	1/8

A second factor to consider is in which position of the mainline the branch must be included. For the resonance case, there will be a standing wave peak at one eighth the length of the tube, an inflection point at quarter length of the tube, a valley at three eights, and another inflection point at half of the pipe. The pattern is repeated for the second half of the tube resulting in the presence of seven interesting points along the pipe, which are candidates to accomplish the best overall performance.

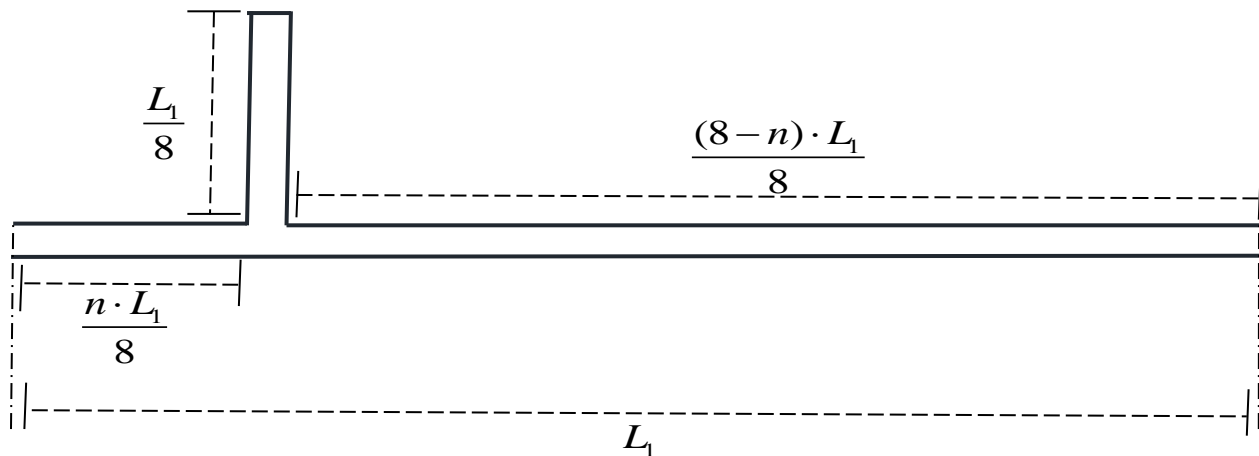


Figure 4.18 A closed-end side-branch, with the line length ratio proposed for multiple frequency pressure ripple reduction

A cohesive manner of representing the behavior of a special features line compared to the standard line for all line length range is to use a normalized version of the spatial frequency-based graphs

presented in section 0. The behavior of the proposed side-branch ratios showed in Figure 4.18 is demonstrated in Figure 4.19. For example, when $n=4$ means the side-branch is at the center of the line. One can see both maximum and upstream pressure ripples are reduced in most of the frequency range. However, there is a high amplification band both at $kL=12\pi$ and $kL=13\pi$ respectively for the maximum and upstream pressure ripple. As the lines get longer, this apex decreases, eventually hitting a normalized value lower than for lengths superior to 3.5 meters. In practice, this means that according to simulations, the suggested solution is better than a standard line for any line longer than 3.5 meters, concerning maximum and upstream pressure ripples.

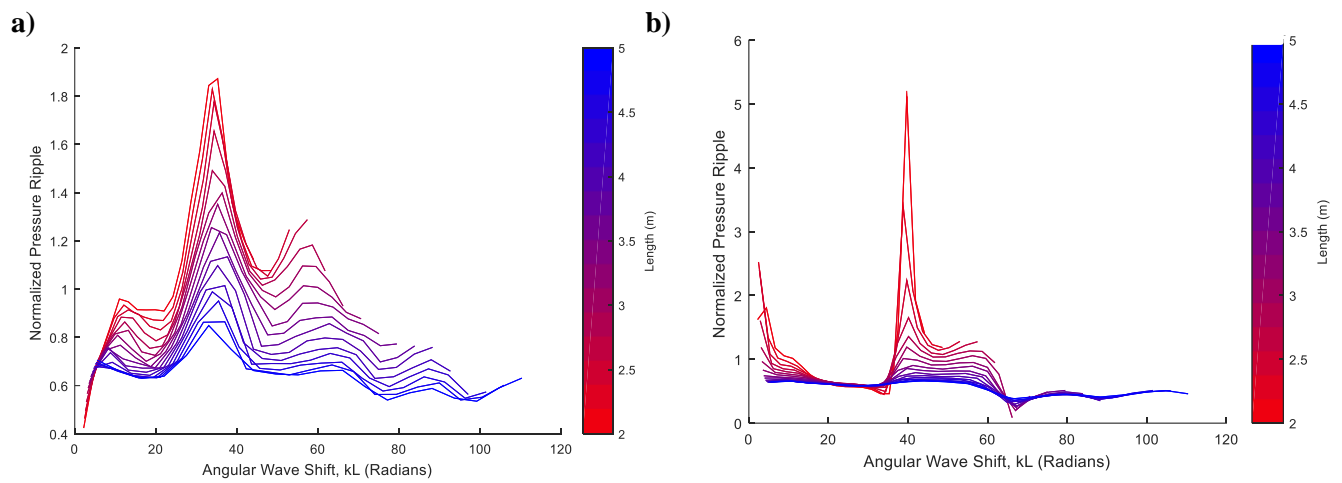


Figure 4.19 Spatial response of a line with a 1/8 length side-branch silencer placed in the center of the line($n=4$) normalized to the response of a default profile in respect to the a)maximum,b)upstream, pressure oscillations

Nonetheless, the greatest impact of the proposed feature was the downstream pressure ripple in which there was a massive reduction when compared to a standard line for any length tested. The centered side-branch line showed a downstream pressure ripple attenuation that is superior to 80% in most of the cases.

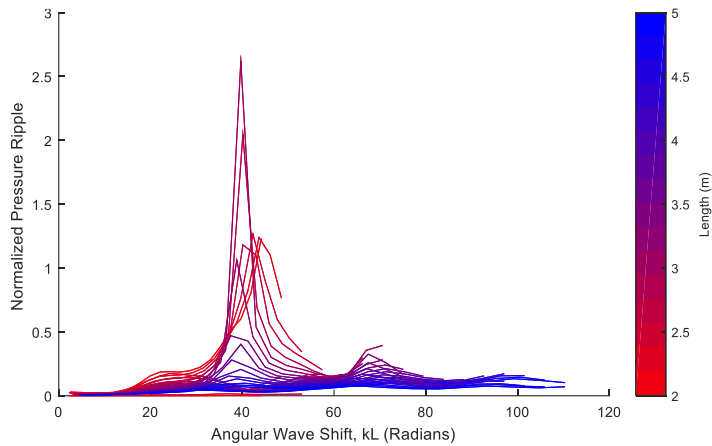


Figure 4.20 Spatial response of a line with a 1/8 length side-branch silencer placed in the center of a line normalized to the response of a default profile in respect to the downstream pressure oscillations

When compared to other 1/8 length ratio side-branches with different placements, the centered side-branch placed case is the only case with a significant reduction at the downstream. About the maximum pressure ripple, the centered case also has the best overall performance. Figure 4.21 demonstrates the downstream pressure ripple of the centered case $n=4$ normalized to the closest upstream case $n=1$.

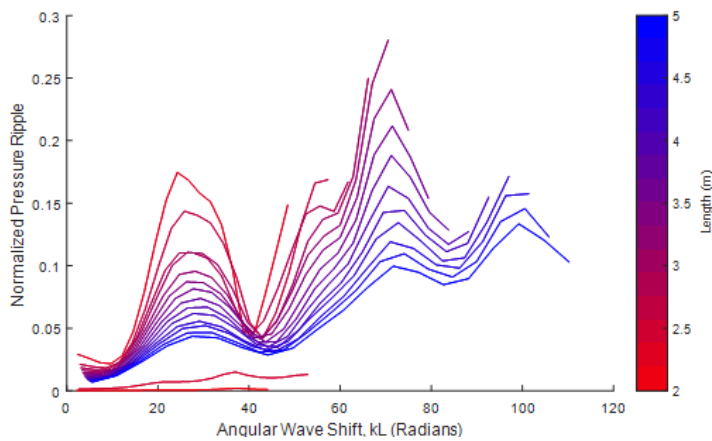


Figure 4.21 Downstream pressure ripple spatial response of a line with a 1/8 length side-branch silencer, at $n=4$, normalized to $n=1$

However, concerning the upstream pressure ripple, for the seven placement spots tested as the side-branch approaches the upstream, upstream pressure oscillations are further reduced. The $n=1$

case has the overall best performance for long lines. This configuration also has a “sweet spot” in which the upstream pressure ripple is reduced by more than 90% for a value of $kL = 13\pi$. This was the highest upstream excitation reduction found by this study, although it is valid only for a single frequency.

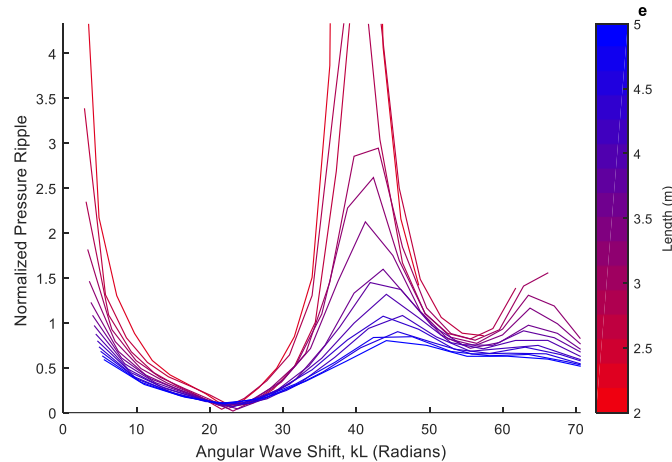


Figure 4.22 Response of a line with a 1/8 length side-branch silencer in place at 1/8 of the line extension profile normalized to the default profile response in respect to the upstream pressure oscillations

4.5.3 Quincke tube

Quincke tubes are a parallel arrangement of two ducts yielding multiple frequency noise attenuation through destructive interference. Generally, this configuration's behavior is hard to predict when dealing with a band of frequencies, therefore, the goal is to find a whole 0-5000 Hertz band attenuation design using parallel ducts. While using the method of characteristics model line to find this solution may be a good way, the fact that this configuration has the presence of two branches leads simulation to instability in many cases. In order to evaluate the pressure oscillations of this feature for the whole frequency spectrum, it was necessary to input the only oscillatory components of the flow into the line model. Therefore, the standard mean of 50 l/m flow was not considered for this study.

A design with the Quincke tube place of the line center was chosen to accomplish symmetry based on the success of the centered side-branch design. The shorter path of the tube was fixed at 80 centimeters while the longer path L_2 was varying in the range of 0.5 to 1.5 meters.

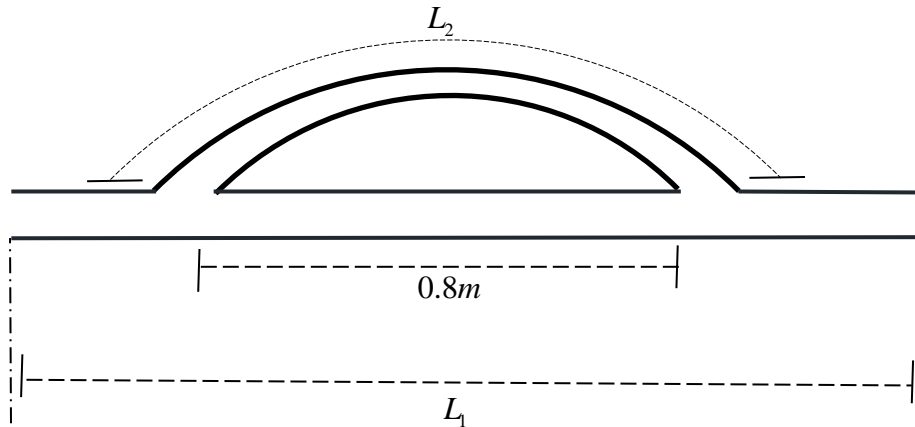


Figure 4.23 A standard Quincke tube dimension proposed for multiple frequency pressure ripple reduction

Overall, the shorter path tends to dominate the behavior of the Quincke tube, while the longer path will influence small peaks and valleys for different constructive and destructive interferences. It is somewhat difficult to compare the best size for L_1 . However, $L_2=1.2$ meters had the best performance on average.

Table 4.3 Quincke tube simulation bounds

<i>Parameter</i>	<i>Lower Bound</i>	<i>Upper Bound</i>	<i>Increment</i>
$L_1(m)$	2	5	0.1
Frequency(Hz)	25	5000	25
$L_2(m)$	0.5	1.5	0.1

Figure 4.24 shows the response of the maximum pressure ripple for $L_2=0.7$ normalized to the maximum pressure ripple at $L_2=1$ meter. The total length, represented by the colors describes the length of the hydraulic component from upstream to downstream using the shortest path.

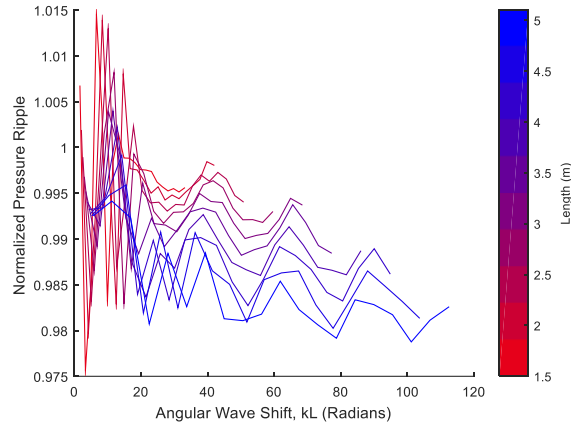
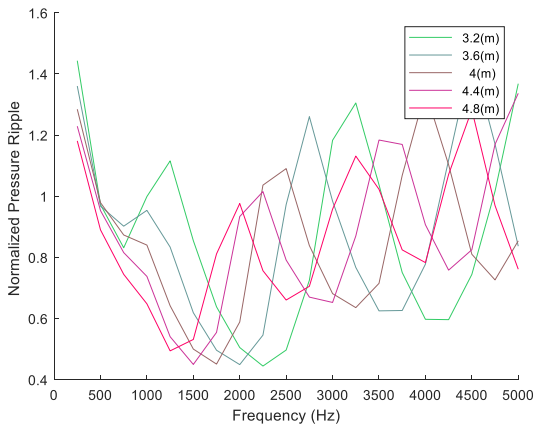
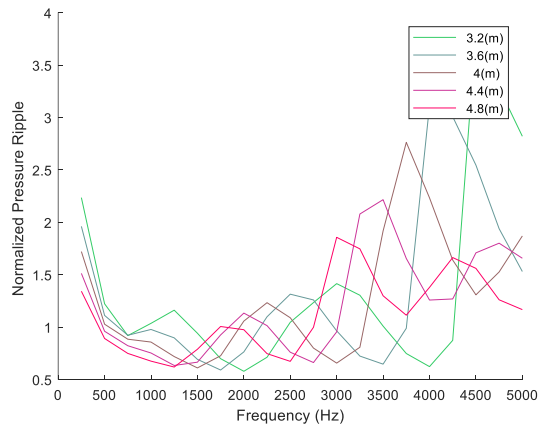


Figure 4.24 Normalized response of a line with a shorter quinke tube ($L_2=0.7$ meters) versus a larger quinke tube ($L_2=1.0$ meter), both placed at the center of the line, concerning the maximum pressure oscillations

When compared to a standard line, the selected Quinke tube had lower maximum, upstream, and downstream pressure ripples for long lines. From what the graphics say, the length of the Quinke tube is considered to be the shortest throughout the path. Figure 4.25 shows the normalized response of a Quinke tube ($L_2 = 1.2$ meters) when compared to a standard line.



a)



b)

Figure 4.25 Normalized response of a line with a default Quinke tube placed at the center ($L_2=1.2$ meters) versus default profile response in respect to the a) maximum, b) upstream

4.6 Fluid borne noise source reduction summary

After studying a large set of design features that are better than standard lines at the whole 0 to 5000 Hz frequency domain, it is interesting to summarize possible design features' solutions into a compact and elegant engineering tool that could be used to design the hydraulic system better.

The range of flow in our study was around 10 to 150 l/min, and for pressure; it was about 100 to 450 Bar, and that includes several operating conditions used in industry and vehicle hydraulics.

The major conclusions of the study were:

- Lines must be projected to be as flexible as possible and have the diameter as large as possible.
- If possible, project the line shorter than 0.6 meters to avoid resonant frequencies.
- For a short line (typically < 0.6 meters), a barrel-shaped profile can reduce maximum, mean, and downstream Pressure ripple to any desired frequency from 0-5000 Hertz. The Barrel-Cornet shape provided results that were better than the barrel shape's although this profile is more complex to manufacture.
- Specific ratio closed-end side-branches show effective pressure at a reduction in many cases for given frequency bands.
- The Quincke tubes accomplished diminution at all frequency bands for maximum, upstream, and downstream pressure when compared to a regular pipe.

Also, the selection of a passive fluid-borne noise source reduction method depends on the focus of the engineer. Different hydraulic systems will have different noise generation focuses and the component, which is generating a higher amount of sound power may vary. Therefore, it is very important to be able to know, or at least suspect where the noise and/or vibrations are the most critical in a given hydraulic system. After determining that component, a passive noise reduction strategy could be implemented. There are three main focuses: the downstream hydraulic component, the upstream hydraulic component, and the line itself. Figure 4.26 is a flowchart that can help in decision making to select a feasible and practical passive fluid borne noise source reduction based on simulations performed in this study. The flowchart should be read starting on top towards the down end. As the path is followed according to the hydraulic circuit characteristics,

all the solutions in blue found through the path of the flowchart can be used by the application engineer.

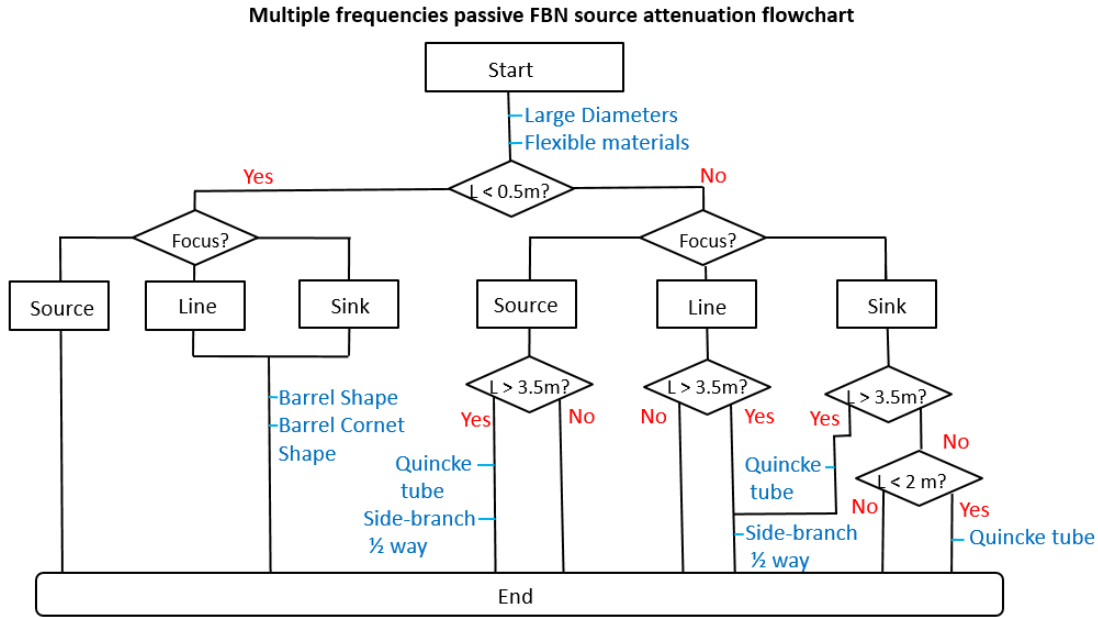


Figure 4.26 Generic hydraulic system passive solution implementation flowchart for a multiple frequency fluid borne noise source reduction

Also, the study has found a solution that accomplishes considerable reduction for specific frequencies at very high levels of frequency. Content reduction in one single frequency may compensate for the compromise of increasing the frequency response for several other frequencies. Therefore, for an application that has a well-defined frequency response, a single frequency solution might be as shown by the flowchart in Figure 4.27.

In order to implement a single frequency solution, the target frequency has to be known and then used with equation 6.4 in order to calculate the value of k.

$$k = \frac{2\pi f}{c} \quad (4.4)$$

Single frequency passive FBN source attenuation flowchart

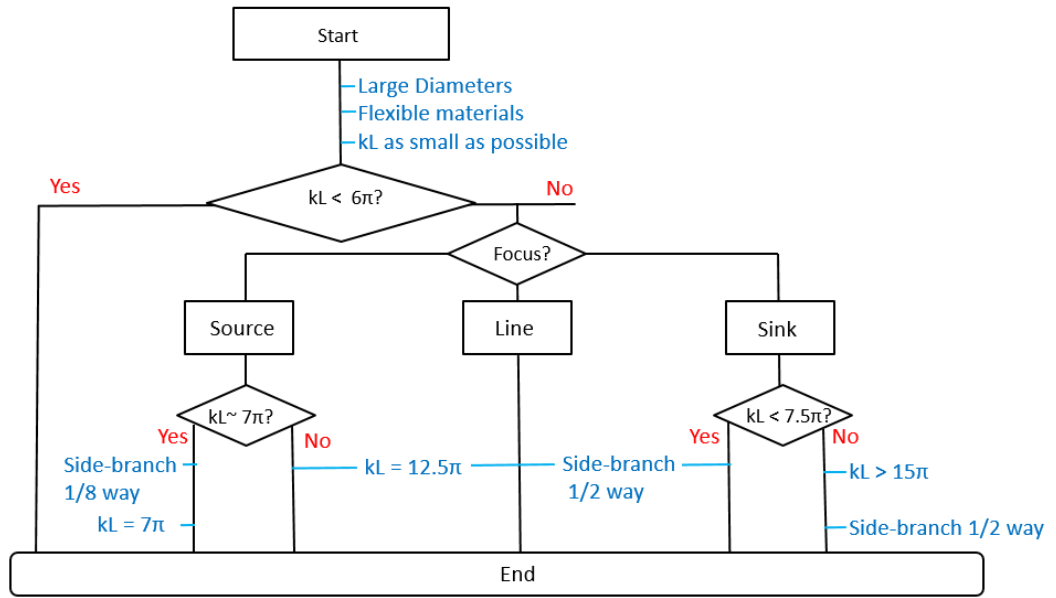


Figure 4.27 Generic hydraulic system passive solution implementation flowchart for a single frequency fluid borne noise source reduction

5. SOURCE FLOW RIPPLE REDUCTION STRATEGY BASED ON SECONDARY SOURCE

This chapter introduces a multi-operation condition passive FBNS reduction strategy for an element that introduces oscillatory energy in the system; a flow source as an example. A single unit used as a flow source is suggested to be replaced by smaller coupled units (sharing the same shaft), these units are arranged to achieve destructive interference for targeted harmonics generated pressure ripple. This solution also has better energy efficiency in many cases. Simulations are made with a time-domain coupled system model to verify the proposed solution functionality.

5.1 A noise reduction method based on alternative component sizing

Both pumping and motoring units can generate multiple frequency content which will be propagated into the line very efficiently becoming thus a great generating noise candidate. Therefore, this technique can be used both for pumping and motoring units in a broad range of applications. As a default application, a trivial flow source will be studied in which two swash-plate axial piston units connected through the same shaft will gather flow from a 20 bar low-pressure line to supply a high-pressure one. This configuration will be called coupled pumps (CP) or dual pump configuration.

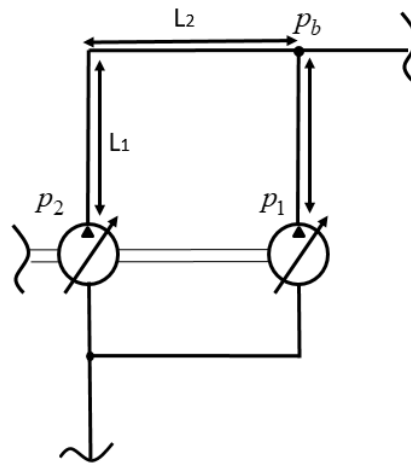


Figure 5.1 Modeling flow source with two units connected to the same axis

5.2 Destructive interference arrangement

Interference works by superposition of waves and it can be classified either as incoherent or coherent interference. At incoherent interferences, the relative phases among the waves are constantly changing while at coherent interference, the pattern is stationary, the waves will add up or subtract with the same phase all the time. Constructive interferences are waves that combine and add up to a bigger irradiance than the original waves, having its max value at 0° phase shift. Destructive interference waves combine and subtract each other to a smaller irradiance than the original waves. Same magnitude waves that combine 180° out of phase cancel out and yield zero irradiance. The desired interference pattern for a noise reduction strategy is destructive interference; therefore, the value of the phase between the pressure ripples generated by both units must be constant and equal to 180° .

Since in the given example the two axial piston units are connected by the same shaft and considering the torsional deformation of the shaft negligible, the rotation phase between both units will remain constant, hence, the units will be synchronized and coherent interference is possible.

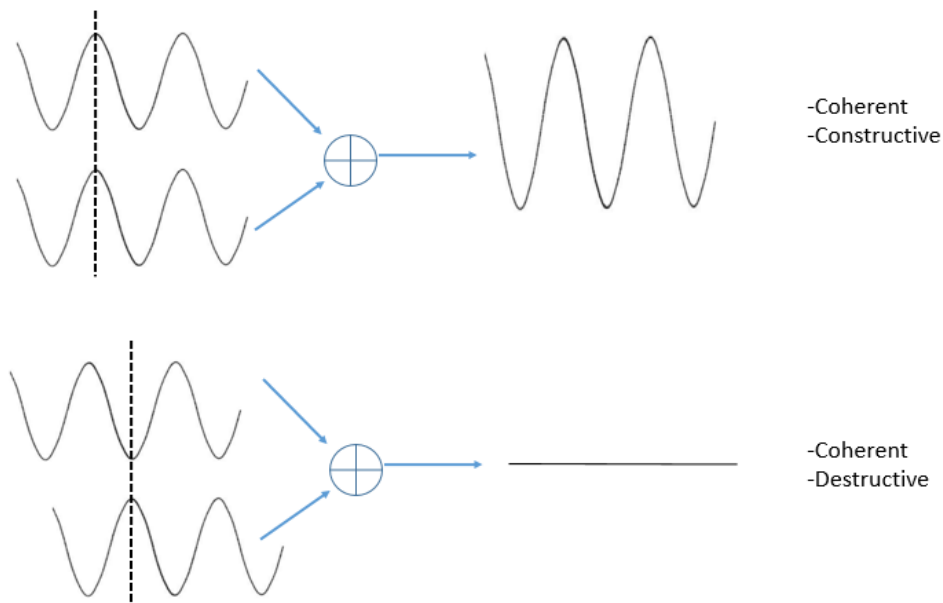


Figure 5.2 Coherent interference patterns: Constructive interference and destructive interference

Each unit contains a rotating kit consisting of the inner shaft, cylinder block, pistons, slippers, and all the components that rotate with each revolution of the hydraulic unit. When connecting two units on the same axis, the kits of both units are not necessarily aligned so that the center of each piston must be overlapped on the z-axis. Rotating on the z-axis, the angle between the centers of the piston from one unit to the center of the piston of another is the index of the Index rotation kit.

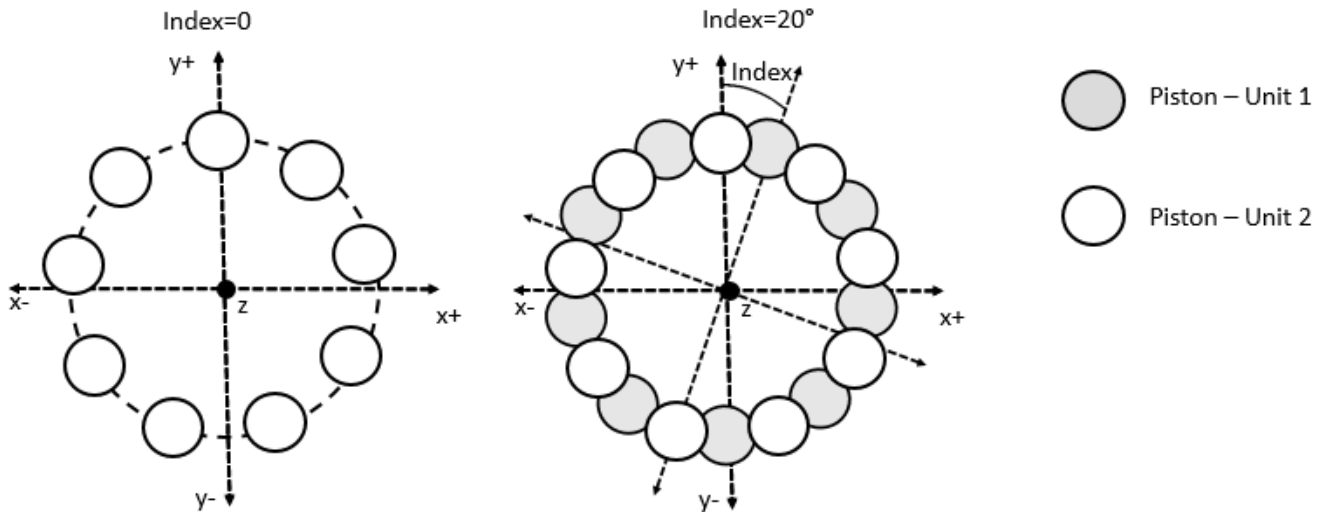


Figure 5.3 Rotating kit index

As the harmonics for a nine-piston unit are nine times faster than the rotational speed of the shaft, a nine-piston unit rotation kit index of 20° is equivalent to a 180° phase for the first harmonic frequency, and the index of rotation kit of 10° is equivalent to a 90° phase for the first harmonic frequency. In general, the index for a unit with m displacement chambers, to achieve a phase-shift of ψ will be given by (5.1).

$$Index = \frac{\psi}{m} \quad (5.1)$$

From the solution proposed in Figure 5.1, one needs to evaluate how the pressure oscillations will propagate through the lines. The pressure traveling from unit 1 to the branch can be recalled by equation (2.5). This is a general solution for pressure wave which is also valid for ducts:

$$p(t, x) = B_1 e^{-j(\omega t + kx)} + B_2 e^{j(\omega t + kx)} \quad (2.5)$$

For the pressure propagating from unit 1 to the branch, the value of x is replaced by the line segment length L_1 . For the traveling pressure of unit 2, the value x is equivalent to $L_1 + L_2$. The wave-number k is dependent on the speed of sound c and angular frequency ω . The variable ψ describes the phase shift between the rotation kit of both units which is defined by the index between the units rotating kits as it was described before.

$$p_{b1}(t, L_1) = B_1 e^{-j(\omega t + \frac{\omega}{c}L_1)} + B_2 e^{j(\omega t + \frac{\omega}{c}L_1)} \quad (5.2)$$

$$p_{b2}(t, L_1 + L_2) = B_3 e^{-j(\omega t + \frac{\omega}{c}L_1 + \frac{\omega}{c}L_2 + \psi)} + B_4 e^{j(\omega t + \frac{\omega}{c}L_1 + \frac{\omega}{c}L_2 + \psi)} \quad (5.3)$$

The terms B_1 , B_2 , B_3 , and B_4 depend on the flow and pressure generated at the source. Since the units are equivalent and have the same displacement, the term B_1 is considered equal to B_3 and B_2 equal to B_4 . The relative phase between pressure oscillations depends on the value of L_2 , the speed of sound, the angular frequency, and the fixed phase shift ψ which is defined by kit index rotation among the units. This phase shift is assumed to be fixed since it is set by rigid a mechanical path.

The angular frequency depends on the unit's drive speed while the speed of the sound has to do with the bulk modulus, density, Young's modulus, and thickness of the line material. Therefore, the relative phase between the two units will vary depending on the unit's speed, line pressure, oil temperature, and even line manufacturer thus having a different value for each application. A key element to accomplish coherent destructive interference is to keep a constant phase among oscillations. However, by setting the value of L_2 to zero, and assuring the lines have the same specifications, the relative phase between the pressures will only depend on the value of ψ . Since this value is set by a mechanical connection only, the interference pattern will be coherent. When the value of ψ is equal to 180° or simply π , the units can mutually cancel each other's pressure oscillations as shown by equations (5.4) and (5.5). The cancelation will remain for every position after the branch. Another advantage of depending solely on the shaft angle is that the phase value stays constant even during dynamic conditions.

$$\begin{aligned}
 p_{b2}(t, L_1) &= B_1 e^{-j(\omega t + \frac{\omega}{c} L_1)} e^{-j\pi} + B_2 e^{j(\omega t + \frac{\omega}{c} L_1)} e^{j\pi} \\
 &= -B_1 e^{-j(\omega t + \frac{\omega}{c} L_1)} - B_2 e^{j(\omega t + \frac{\omega}{c} L_1)}
 \end{aligned}
 \tag{5.4}$$

$$p_{b2}(t, L_1) = -p_{b1}(t, L_1)
 \tag{5.5}$$

The fluid displacement from the units will generate oscillations of flow and pressure in several frequencies that are multiples of the first harmonic, therefore it is important to have strategies that can cancel a considerable number of harmonics. Figure 5.4 demonstrates that a first harmonic phase shift angle of π or 180° , configures destructive interference not only the first harmonic, but all $1 + 2n$ harmonics, or simply odd harmonics. This happens because after removing the complete wave periods from the phase-shift, the remainder equals $\pi/2$ or 180° .

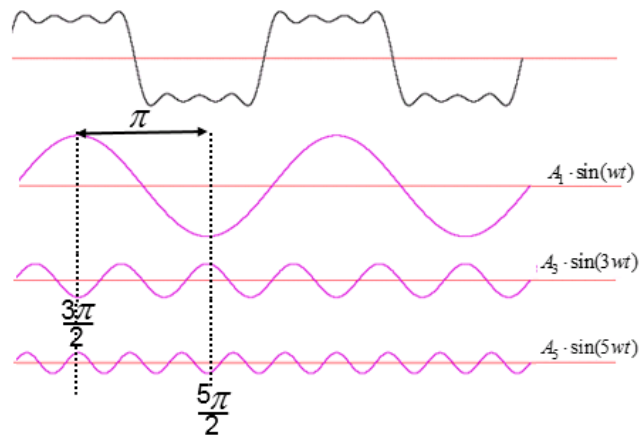


Figure 5.4 Phase-shift for different harmonics

Similarly, all $2 + 4n$ harmonics can be canceled by selecting a 90° equivalent phase shift. A 60° phase shift will cancel the $3 + 6n$ harmonics and so on subsequently. Since no rotating kit index angle allows destructive interference to all existing harmonics, it is also necessary to observe the remaining harmonic components. For instance, for a phase shift of 180° , the even harmonics will be maintained in complete constructive interference because the translation results in multiple complete periods. On the other side, a 90° phase shift will set odd harmonics out of complete constructive interference; therefore, the level frequency content will see some cancellation.

Thus, by placing the angles in terms of rotation of the shaft rate, as shown by equation (5.1), a rotation kit index of 20° will allocate all the odd harmonics in the maximum destructive interference, but also will maintain all even harmonics in maximum constructive interference. On the other hand, a 10° rotation kit index puts all $2 + 4n$ harmonics at a maximum destructive interference and (at least) puts odd harmonics out of maximum constructive one. Harmonics of order $4n$ stay at maximum constructive interference.

5.3 Verification through simulation

Despite the fact the interference pattern can be described analytically, it is necessary to verify if it is going to hold in a line model coupled by two axial piston units' lumped models that would be capable of simulating the pressure ripple and the flow these units will produce.

Table 5.1 Simulated sources

<i>Name</i>	<i>N° of units</i>	<i>Unit Size(cc)</i>	<i>Index(°)</i>	<i>Displacement(%)</i>
130cc	1	130	Does not apply	100
0 degrees	2	75	0	86
10 degrees	2	75	10	86
20 degrees	2	75	20	86

To do that, an experiment was set up to simulate the generation of pressure oscillations by two units, and analyze possible ways of canceling these oscillations. In this simulation, two nodes were highlighted: the branching node, where the interference happens, and the downstream node which is used to verify if any harmonic cancellation will propagate to the end. Two 75 cc units were chosen using 86.6% displacement.

For the proposed system model, all lines were defined as 1 meter long. Lines A_1 and A_2 were set for 25 mm of diameter and line A_3 was set for 38 mm diameter. These values were chosen, firstly because they are standard values for line diameters and thus the suggested solution can be implemented with existent market components. Secondly, to keep the average flow speed as constant as possible after the merge of the branch and, as a result, focus the evaluation on transient

components of the flow. A base model containing only one hydraulic unit providing flow for a 2-meter line and 38 millimeters diameter throughout all its extent was also simulated. By symmetry, the nodes chosen for comparison were positioned at 1 meter and 2 meters from the beginning of the line. The hydraulic unit of the base model was a 130 cc unit with 100% displacement.

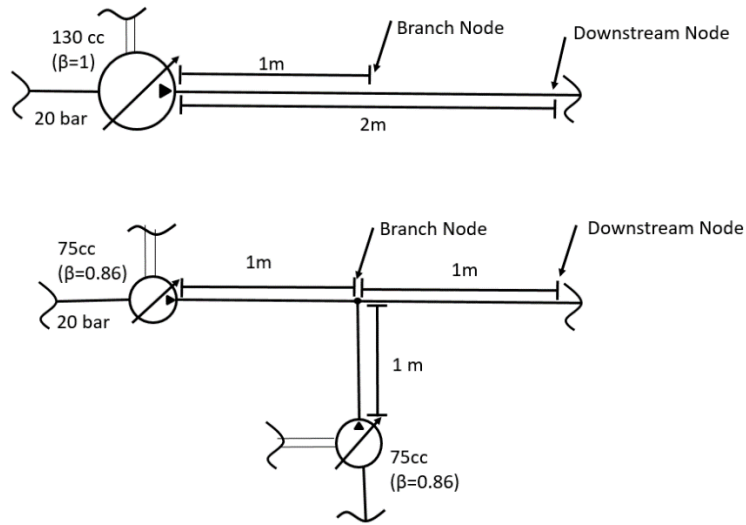


Figure 5.5 Hydraulic diagrams for baseline system and proposed system

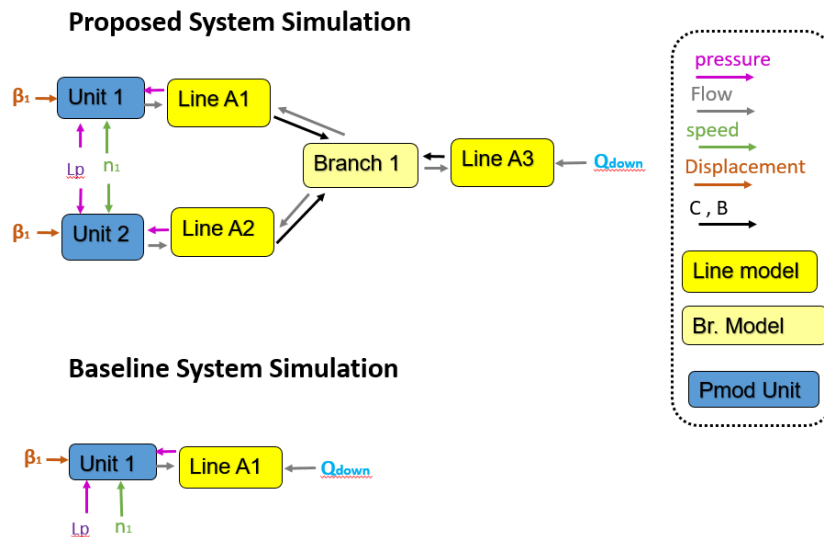


Figure 5.6 Simulation Schematics for baseline and proposed system

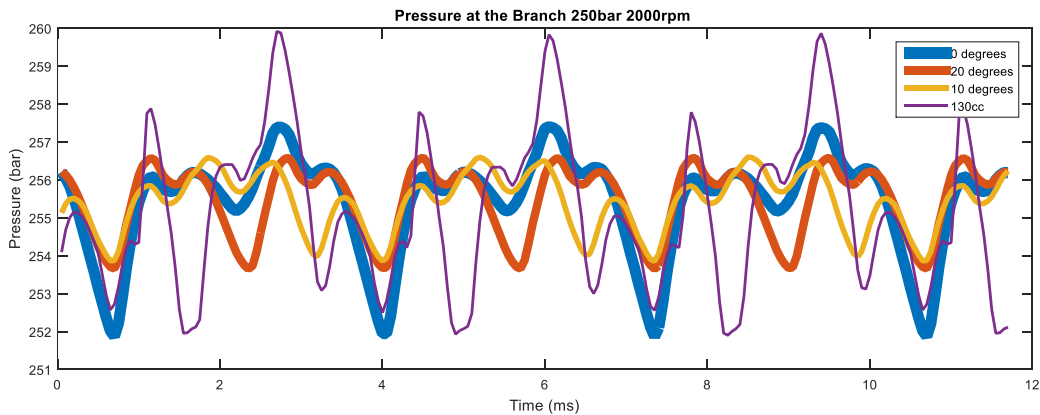
5.4 Results

Nine operating conditions were simulated at three different speeds and three different pressures. The simulated speeds were respectively 2000, 3000 and 3400 rpm, the latter one being the highest operating speed of the 130 cc unit. The three chosen pressures were 250, 300 and, 420 bar, the latter one represents the highest constant pressure both units can handle.

Table 5.2 Operation conditions

<i>Number</i>	<i>Speed(rpm)</i>	<i>High pressure (bar)</i>
1	2000	250
2	2000	300
3	2000	420
4	3000	250
5	3000	300
6	3000	420
7	3400	250
8	3400	300
9	3400	420

Figure 5.7 shows the pressure oscillations in the time-domain for the branching and downstream in the operating condition of 250 bar and 2000 rpm.



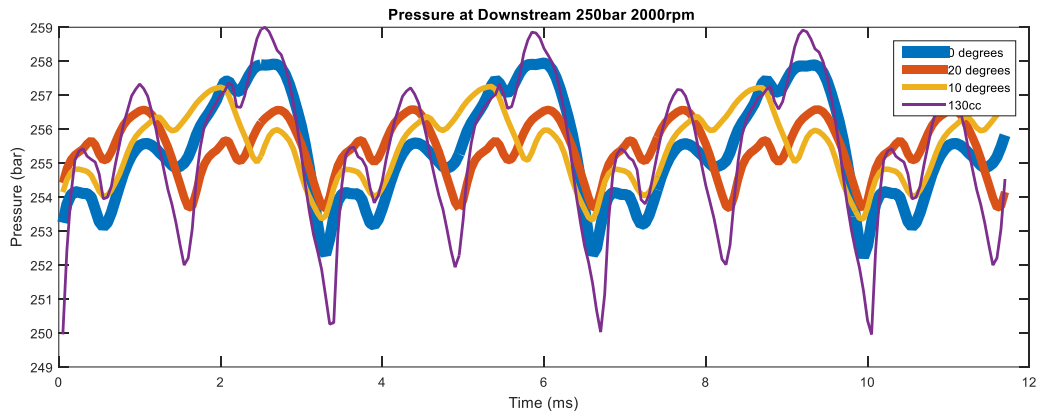


Figure 5.7 Pressure oscillations at the branch & the downstream nodes at 250 bar 2000 rpm

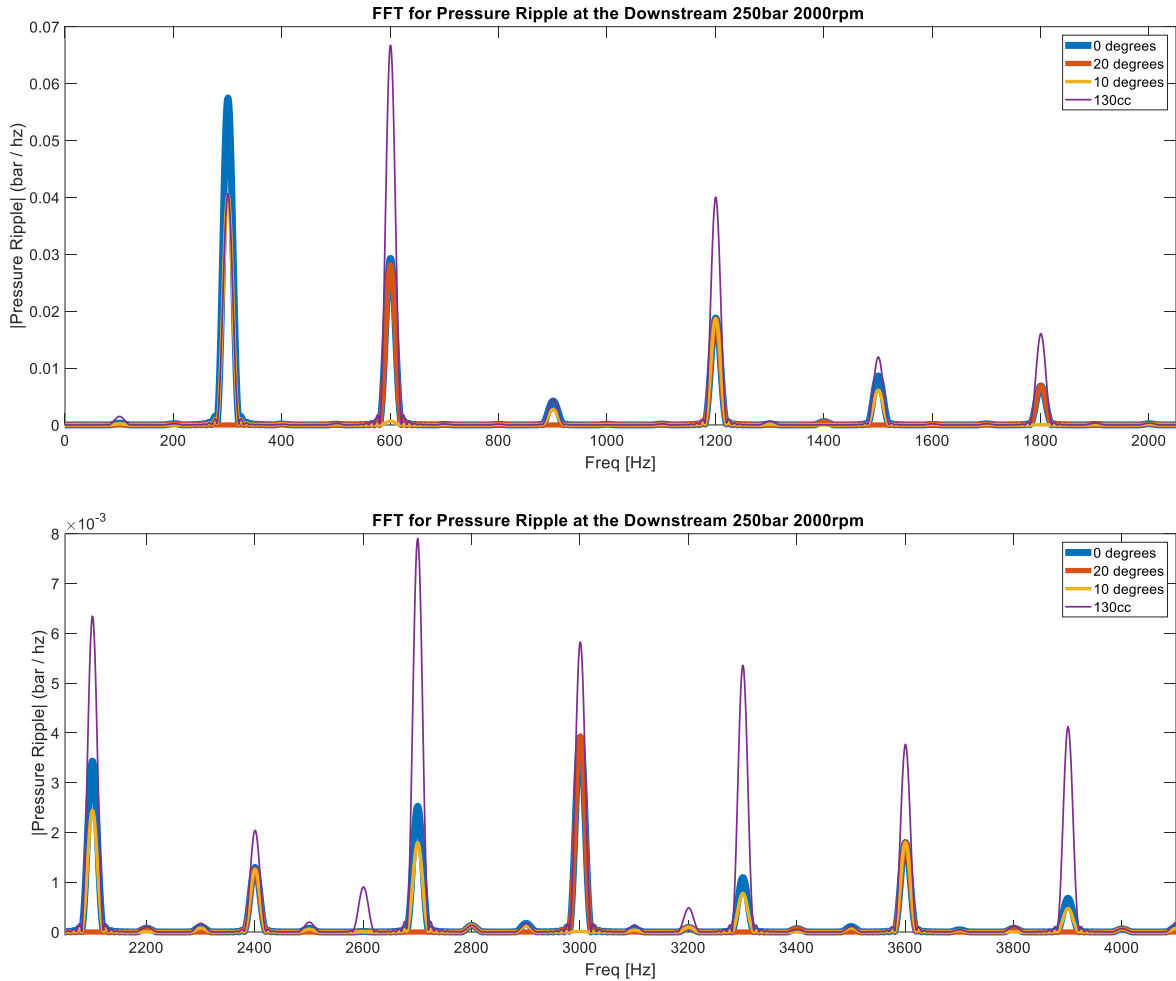


Figure 5.8 Pressure oscillations fast Fourier transform at the branch & downstream nodes at 250 bar 2000 rpm

Time-domain pictures show that when the dual unit group has a rotating group index close equal to zero the pressure ripple shows some resemblance to the pressure ripple of the 130cc unit. In the frequency-domain, it is possible to verify that the interference standards deduced analytically are verified in the simulation. Figure 5.8 describes how the 20° rotation index canceled the odd harmonics and maintained constructive interference in pairs. The 10° rotation rate canceled the harmonics $2 + 4n$, and maintained maximum constructive interference in harmonics $4n$. This phenomenon happened in every simulated operating condition. Therefore, the behavior deduced analytically was demonstrated in simulation. Generally, the 130cc single unit simulation had the

largest pressure ripple both at the branch and at the downstream, followed closely by the 0° indexed dual unit supply.

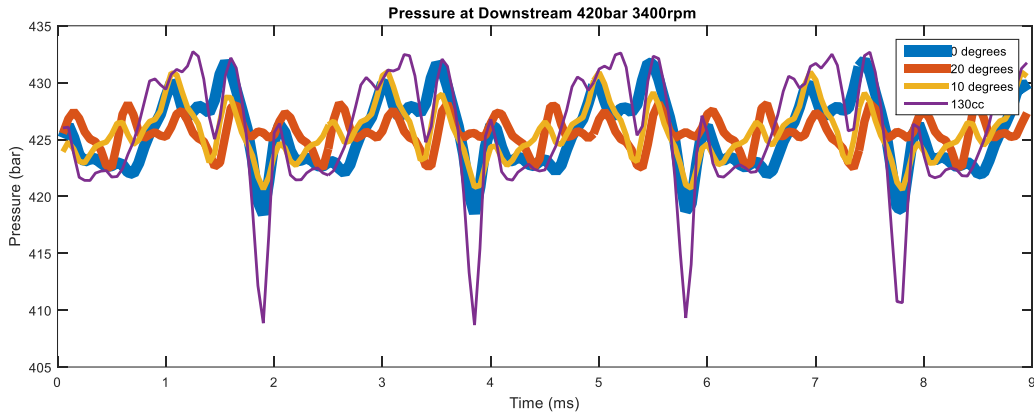


Figure 5.9 Pressure oscillations at the downstream nodes at 420 bar 3400 rpm

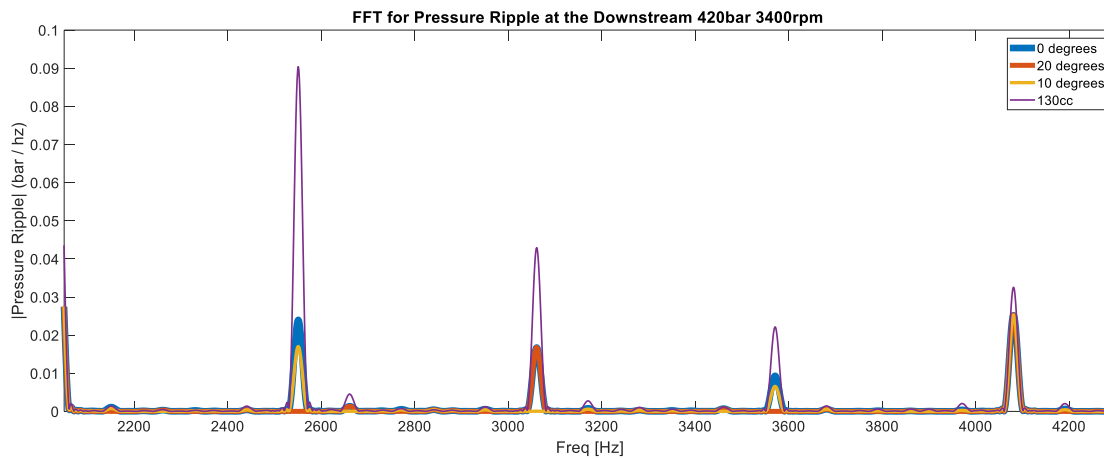
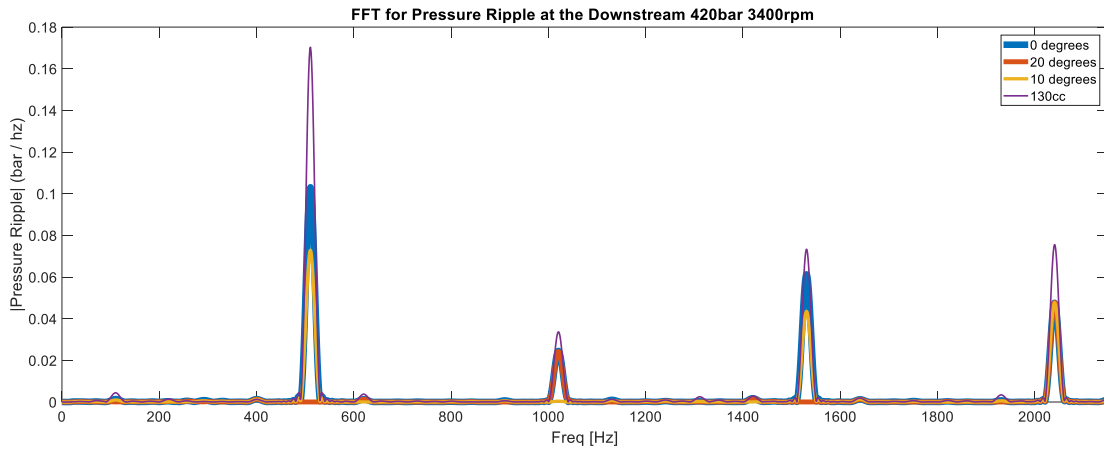


Figure 5.10 Pressure oscillations fast Fourier transform at the branch and at the downstream nodes at 420 bar 3400 rpm

Overall, the 20° index dual unit configuration had the best performance in reducing pressure ripple followed by the 10° index configuration. Nonetheless, the 10° configuration accomplished the lowest pressure ripples for some positions and frequencies at the branch when the units are at 3000 rpm. On average, when compared to the baseline at the branch the coupled-units accomplished 27%, 62.1%, and 62.8% pressure ripple reduction for the 0°, 20° and 10° respectively index angles. At the downstream, the respective angle shifts mean minimization of the oscillations was equal to 47.5%, 76% and 62.3% when compared to the baseline.

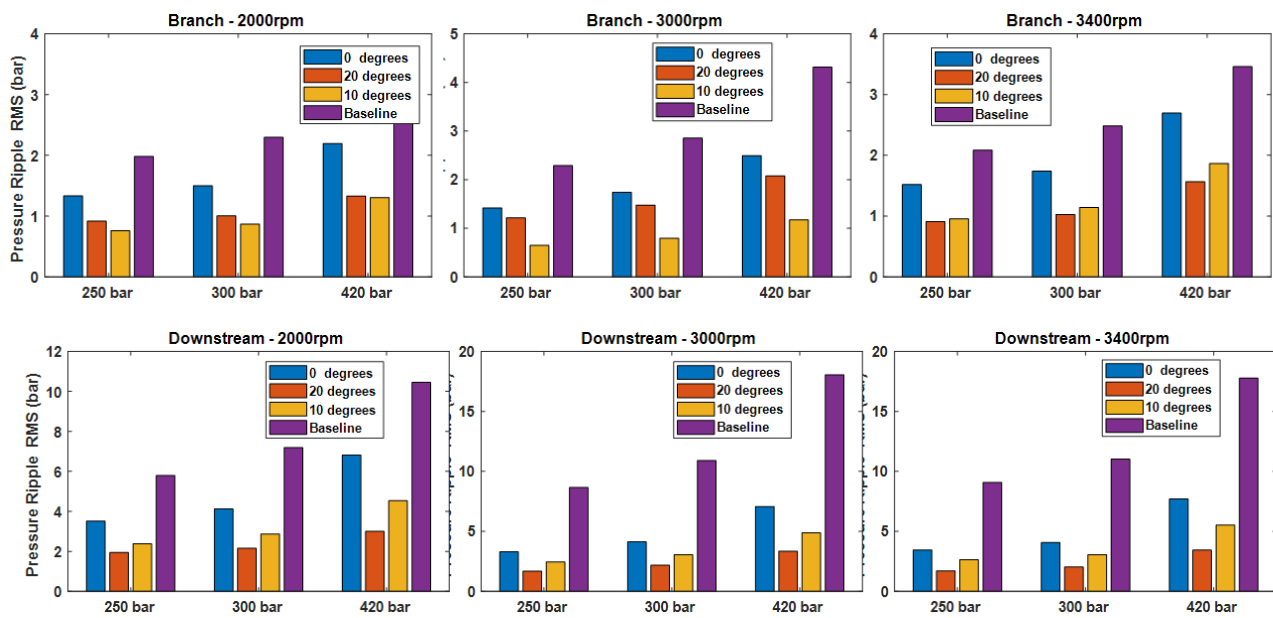


Figure 5.11 Pressure ripple root mean square value for the baseline and three coupled units rotating group index angles strategies for the branch and downstream nodes

The pressure oscillation magnitude in a position will be given by the over-position of the unit's harmonics standing waves including the spatial phase shift of the lines. Therefore, for a generic downstream pressure ripple reduction in a given application, the line length has also to be accounted for to decide which Index is the best to use; the 10° index only cancels half the harmonics the 20° index does, however, it does target a different set of harmonics which the 20° index method will not influence.

According to the simulations, the replacement of the hydraulic unit alone could reduce the pressure ripple in comparison to the baseline. The 0° index technique had a smaller pressure ripple than the baseline in every condition tested. One of the reasons that could explain these results maybe scaling effects at the units, which had proportional but different volumes and valve-plates areas than the baseline's. Nevertheless, some of the pressure ripple reduction might be due to the characteristics of the line such as a larger capacitance or the presence of a branch. Therefore, to understand the isolated contribution of the replacement of the hydraulic unit, a different line configuration was tested as shown in the next section.

5.5 Symmetrical lines results

It is not possible to give both systems the exact same line configuration; the goal is to enhance the line similarity to a maximum level. On this configuration, the baseline was given a close end branch which acts as a silencer for the system. Hence, if at the dual unit configuration, the branch is also causing the cancellation of a given harmonic from a unit to the very same unit, this factor will be covered by the configuration of the baseline as well. The line capacitance of both setups is very convergent, but still, it is different because line diameters are different between the upstream(s) and the branch. To both reduce the effectiveness of the baseline silencer and make the line capacitances more similar; the branch was brought closer to the sources.

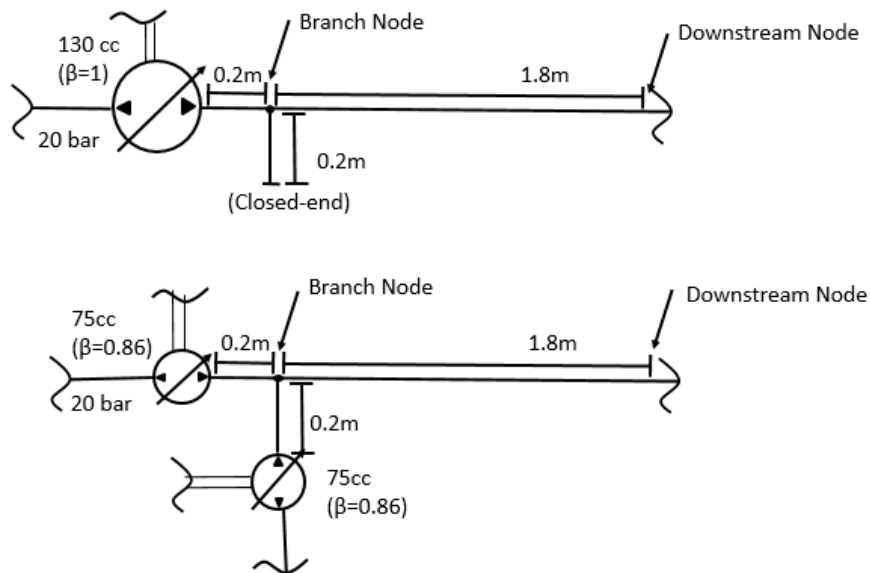


Figure 5.12 Hydraulic diagram for the proposed system and similar lines sized baseline

The same nine different conditions were simulated with three chosen different speeds, respectively 2000, 3000, and 3400 rpm, and three different pressures: 250, 300, and 420 bars. Figure 5.13 describes the pressure oscillations in the time domain for the branching and downstream in the operating condition of 250 bar/2000 rpm respectively in the time domain, while Figure 5.14 shows the same variable at the frequency domain.

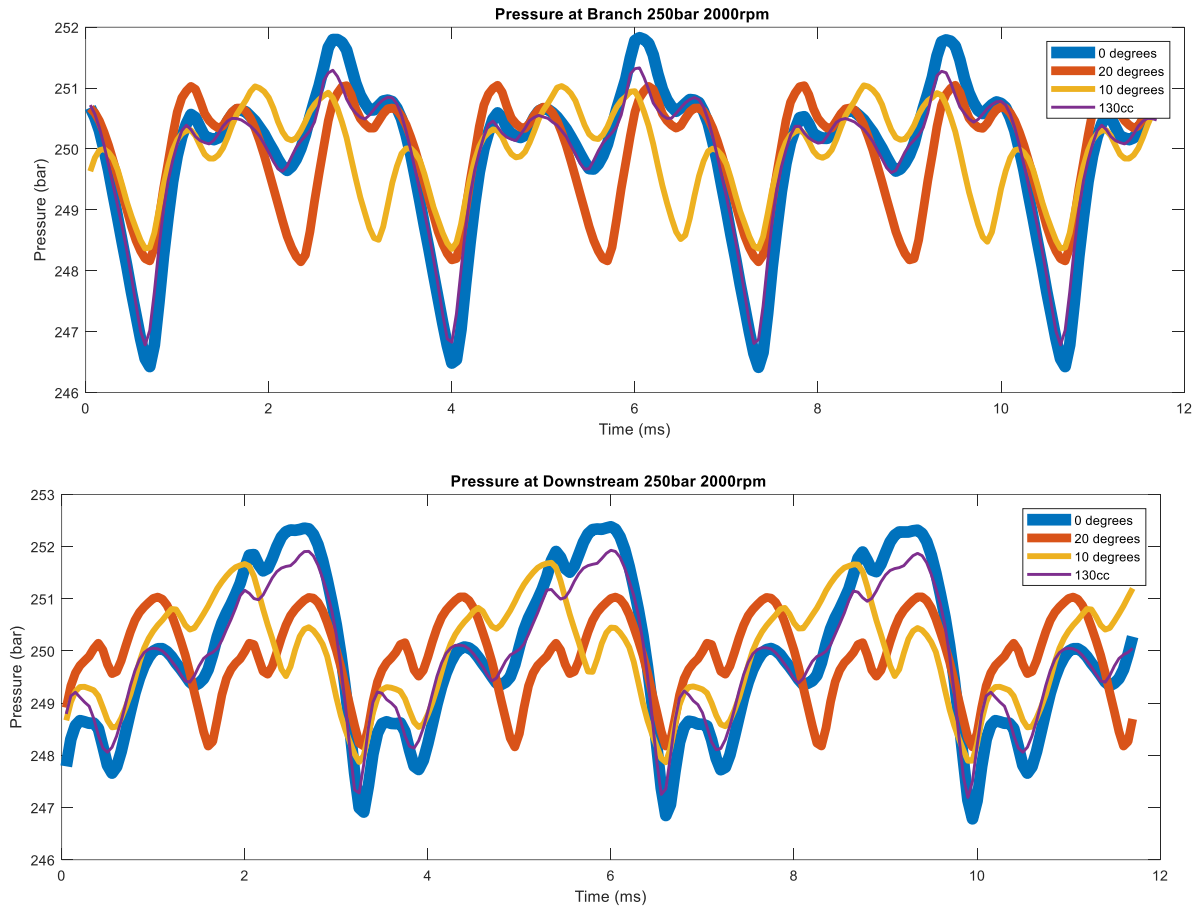


Figure 5.13 Pressure oscillations at the branch and the downstream nodes at 250 bar 2000 rpm for the similarity-guided design lines.

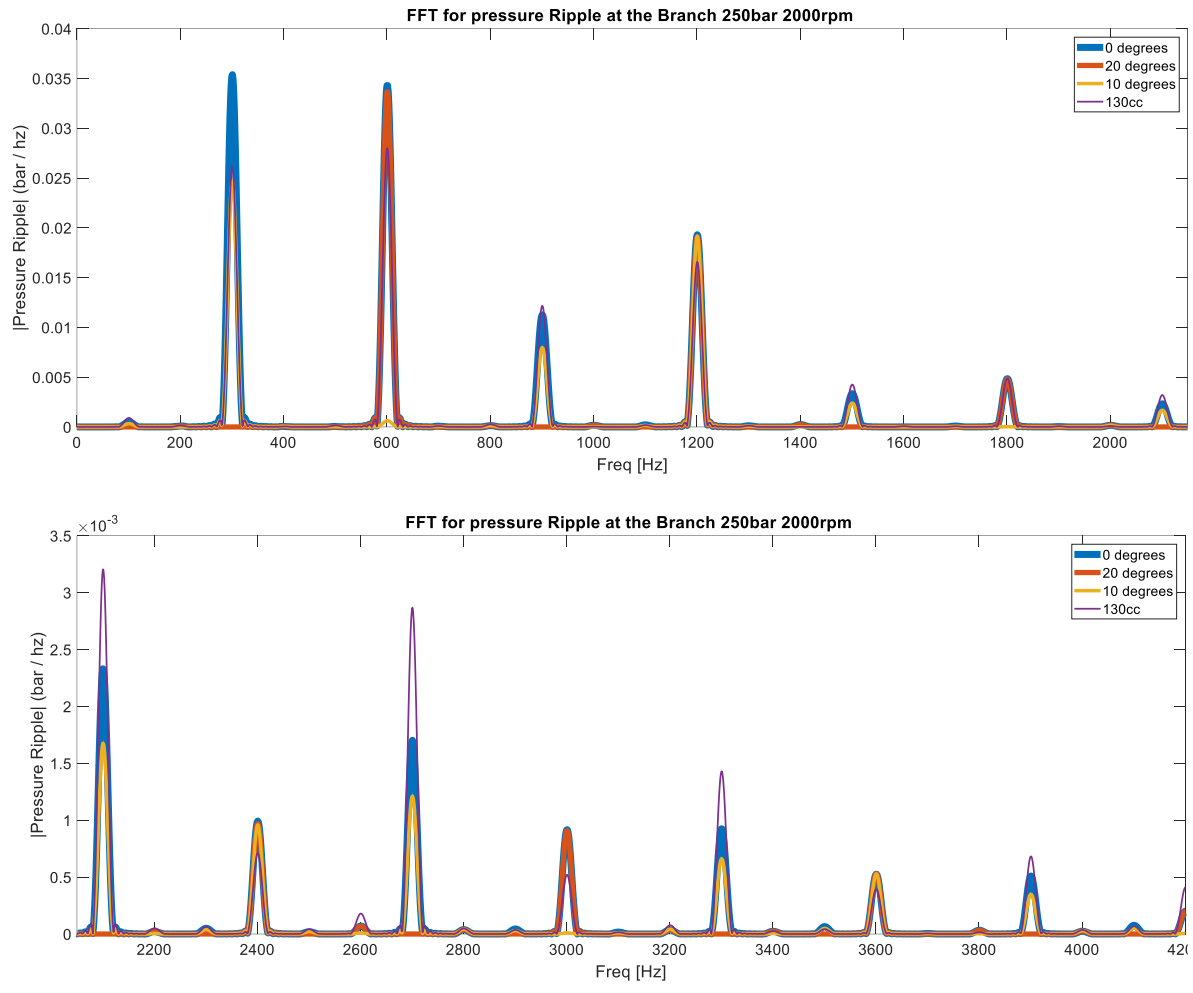


Figure 5.14 Pressure oscillations fast Fourier transform at the branch and & downstream nodes at 250 bar 2000 rpm for the similarity-guided design lines

Overall, the model simulations for these configurations have shown the same trends predicted by analytically influencing harmonics, and thus, provide flexible ways of reducing pressure undulation under various operating conditions. Generally, the dual-unit strategy with a 20° index had the best performance in reducing pressure ripple.

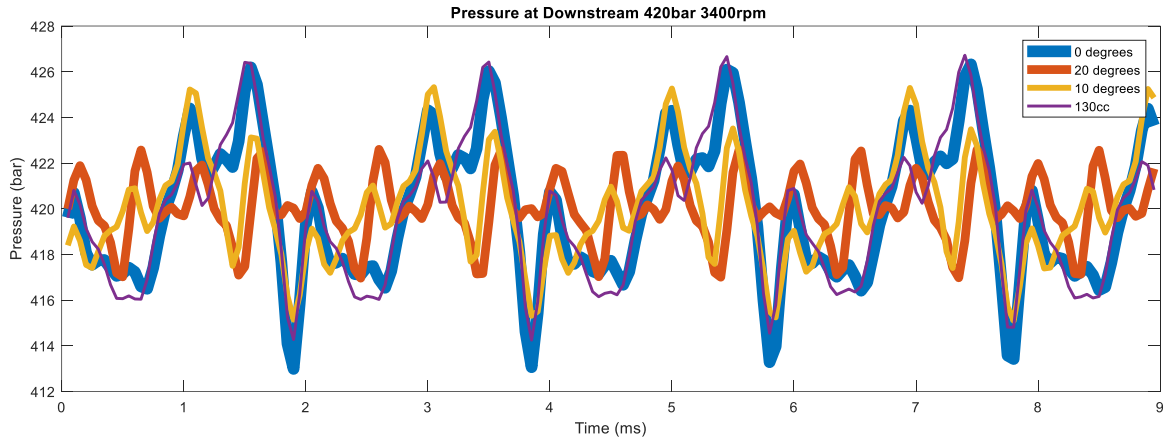


Figure 5.15 Pressure oscillations at the downstream nodes at 420 bar 3400 rpm for the similarity-guided design lines

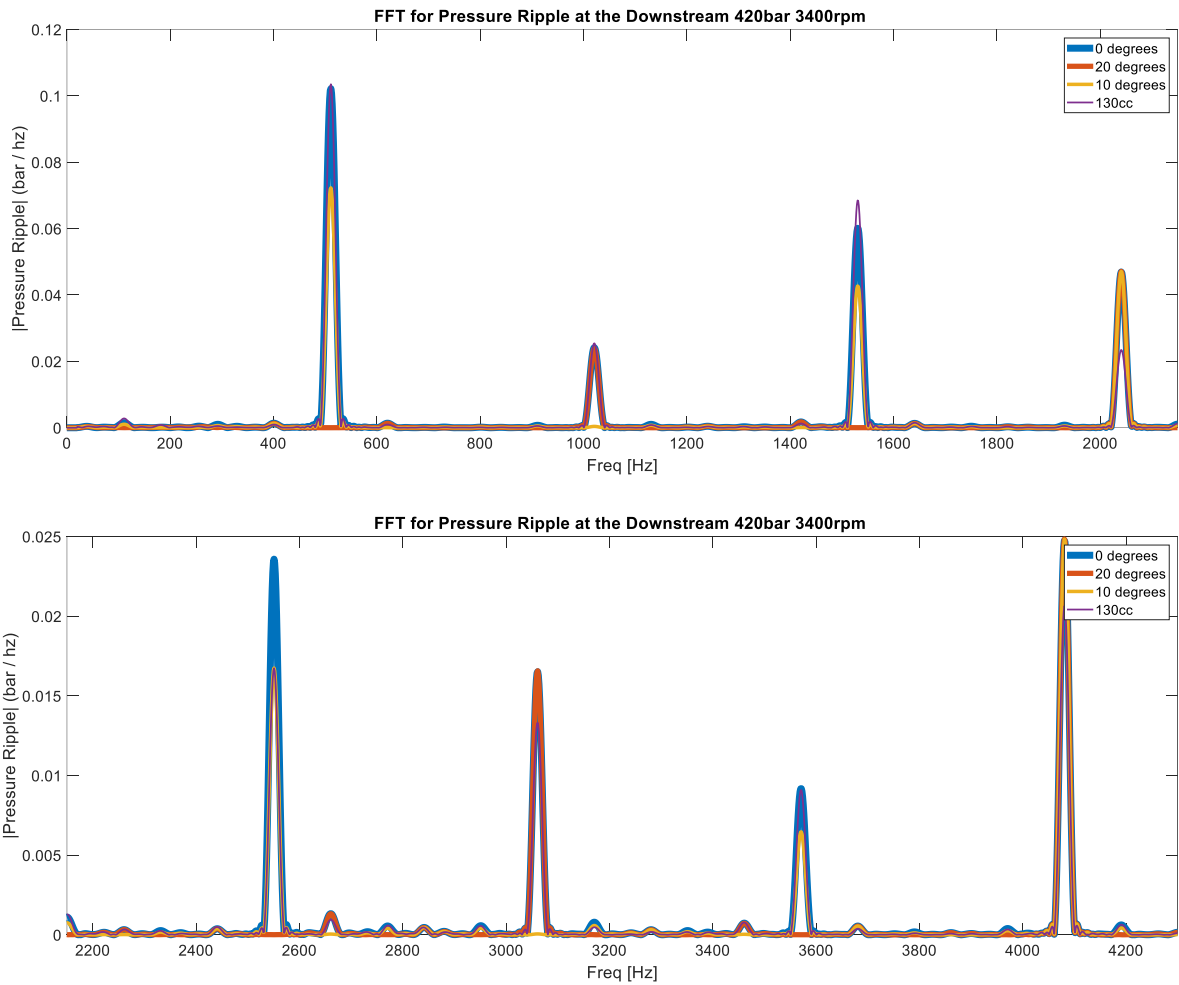


Figure 5.16 Pressure oscillations fast Fourier transform at the branch & downstream nodes at 420 bar 3400 rpm for the similarity-guided design lines

The coupled pumps average reduction for the 20° and 10° index angles were respectively about 36.5% and 40 % at the branch, while the decrease was equal to 55.2% and 29.78% at the downstream. The 0° mechanical phase shift resulted in an actual 18.43% increase at the pressure ripple in the branch and a 2.1% decrease at the downstream on average for all the nine different operating conditions. The average decrease for the downstream was mostly influenced by 3400 rpm scenario where the baseline oscillations were considerably higher than at the previous operating conditions.

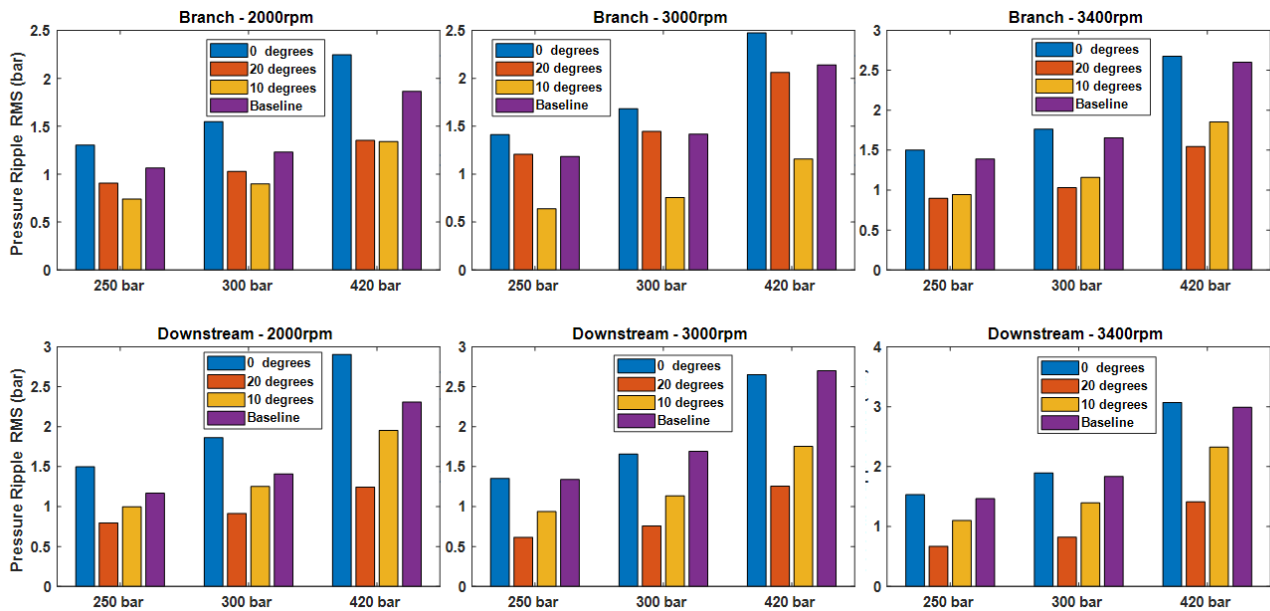


Figure 5.17 Pressure ripple rms value for the baseline and three coupled units (Cp) rotating group index angles strategies for the branch and downstream nodes for the similarity-guided design lines

The great advantage of the indexed dual unit system is that it does accomplish harmonics canceling regardless of the different circumstances, which would classify this method as a multi-operating strategy. Multiple conditions Noise reduction is desirable for applications in which lines are set to a wide range of pressures are, and units are set to a large range of speeds. Another advantage is related to sound quality; as the suggested system will have fewer harmonics, there would also be a small number of simultaneous force excitations at the system, which generates a “softer” noise to any people around the machinery, and thus, resulting in a sound comfort improvement that would be interpreted as a noise reduction by the human brain.

6. EXPERIMENT DESIGN FOR PROPOSED PASSIVE ELEMENTS EXPERIMENTAL EVALUATION

This chapter displays an experimental design to evaluate the effectiveness of passive fluid-borne noise source reduction strategies, which were introduced in sections 4 and 5. The focus of the experiment is to measure pressure ripple and vibrations but also a microphone for sound pressure measurement as a simple reference for future work.

6.1 Experimental Setup

For this experiment, two simple circuits were designed. A tandem unit, which contains in-built relief valves, was chosen to supply flow in both experiments. In Figure 6.1, only one side of the tandem unit Bosh-Rexroth A22 m is used to supply flow to the load, while in Figure 6.2, both units of the same tandem pump were used for this purpose. The in-built valves of the unit allow simplifying the circuit load. Since the relief valves, need for safety reasons and check valves needed to avoid cavitation, are included in the unit, the element at circuits downstream is just a needle valve used to regulate system pressure. The flowmeter influence in the line was avoided by installing the output flowmeters after the throttle valve. Therefore pressure and temperature sensors were needed both before and after the throttle valve to correct the flow output of the unit. SAE 32 oil, the same model used in the simulation, was chosen as the operating fluid at all times, while the inlet temperature was set between 52C° and 53C°. Two independent hydraulic supply lines provided flow to the supply pressure and servo valve pressure. The supply pressure and servo valve pressure were controlled to be set to 30 and 21 bar, respectively, at the supply line.

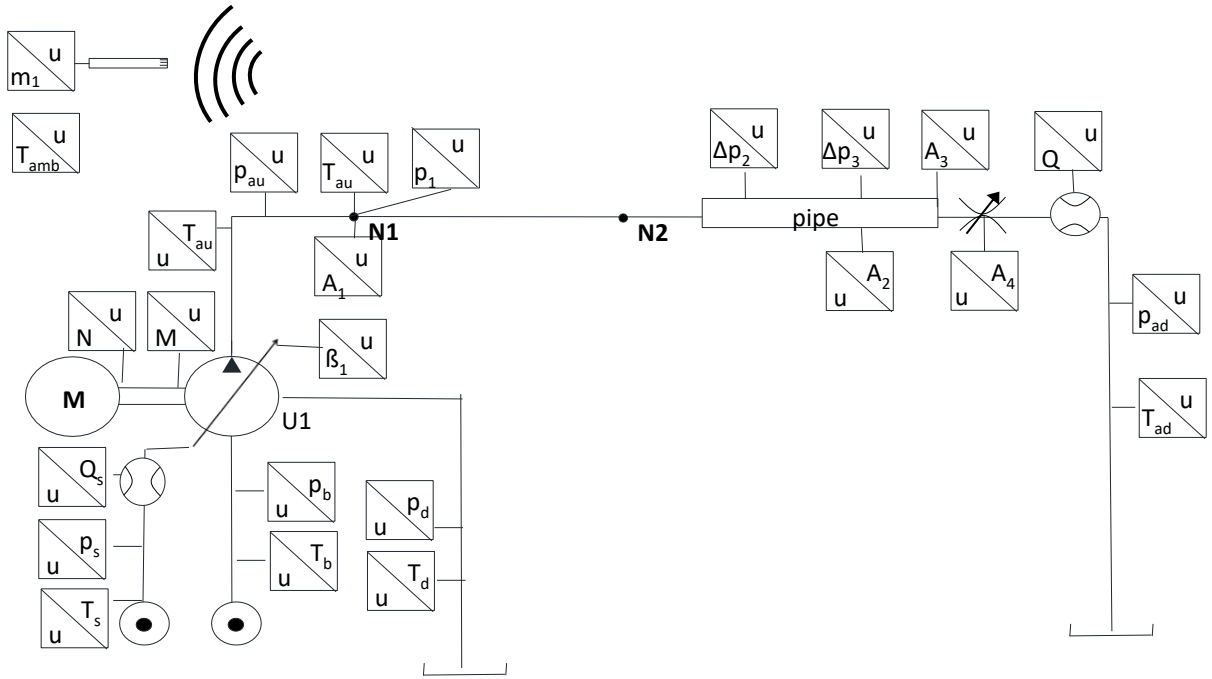


Figure 6.1 Single unit hydraulic circuit schematics

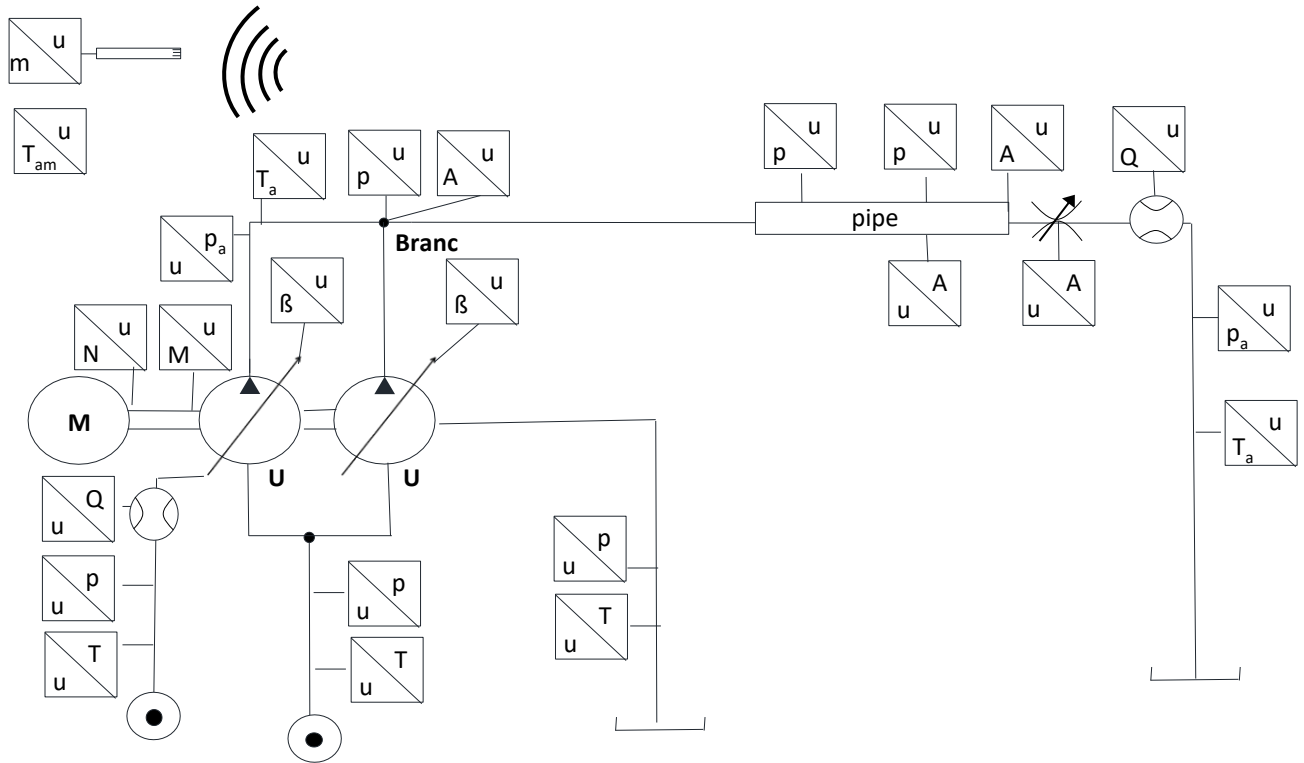


Figure 6.2 Tandem unit hydraulic circuit schematics

While having the minimum number of elements at the circuit load, it is still very important to control the line properties to be as similar as possible to the concurrent setups to isolate only the effects of the newly added element. The line will have five main configurations (Figure 6.4); the first four will use only one of the two units from the tandem pump. The latter configurations will use both units. To make the line configurations as comparable as possible, some default line segments are defined (Figure 6.3). Also, it makes the configuration change of the test rig much easier to handle.

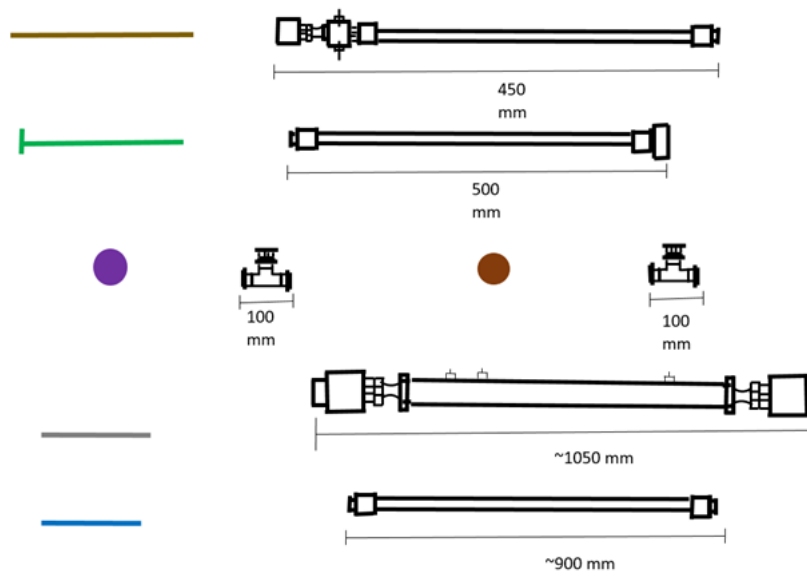


Figure 6.3 Segments of the hydraulic load

All configurations were projected to have a constant 25 mm diameter and a total 4-meter length from the outlet of the unit to the relief valve. After construction, the final length of the circuit was 403 centimeters.

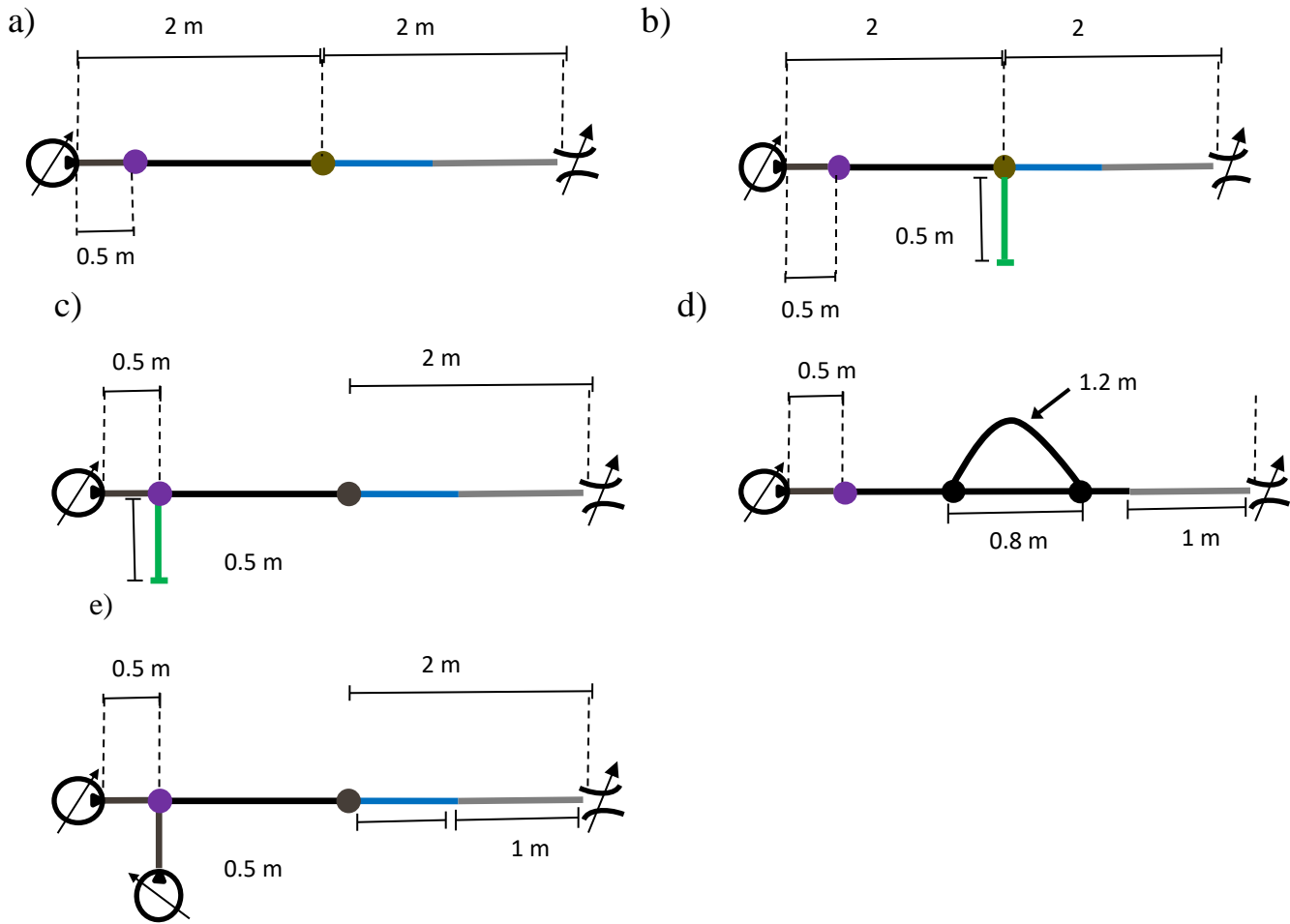


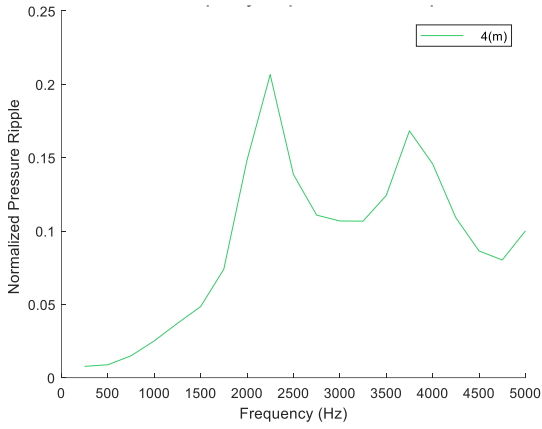
Figure 6.4 Configurations of the hydraulic line; a) Baseline; b) Halfway Silencer; c) Eightway Silencer; d) Quincke tube; e) Tandem unit arrangement

According to the simulations, the quarter-wave side branch resonator installed in the middle of the two-wave long pipe (halfway silencer) is the only element for a 4-meter line which can reduce the pressure ripple for all metrics developed (upstream, downstream, max, and mean) for almost all 0-5000 Hz frequency band as shown by Figure 6.5.

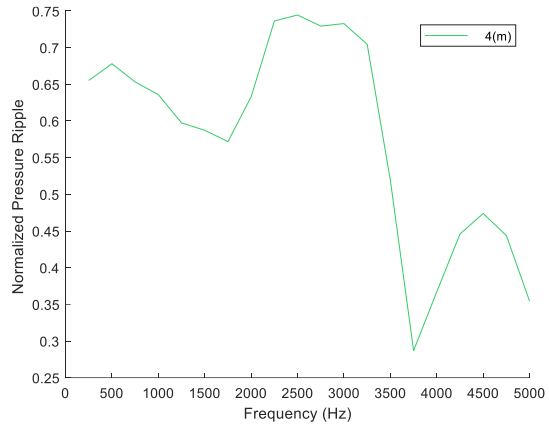
Meanwhile, Figure 6.6 shows the same element installed at 0.5 meters after the source (eightway silencer) will have a much better pressure ripple reduction in the upstream than the downstream. Since the element in the downstream is simply a needle valve, the comparison of these two strategies should give a notion on how much the is the relevance of the upstream and downstream on audible noise, at least for a system where the upstream element is much more complex and larger than the downstream one. Configuration D is also interesting because while the upstream

response is reduced by the Quincke tubes, the downstream response is greatly compromised in the low-frequency range.

a)



b)



c)

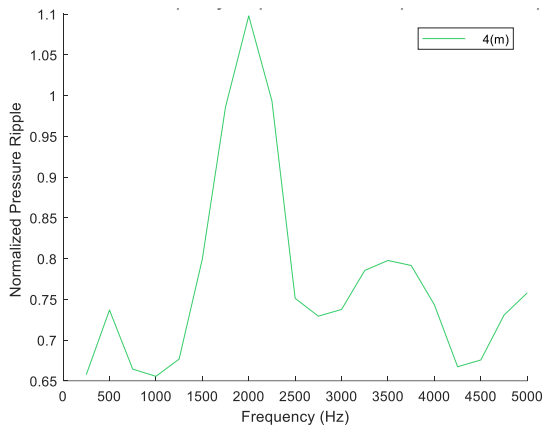


Figure 6.5 Halfway silencer normalized to baseline load with a line length of 403 cm and 25 mm diameter; a) Downstream; b) Upstream; c) Maximum;

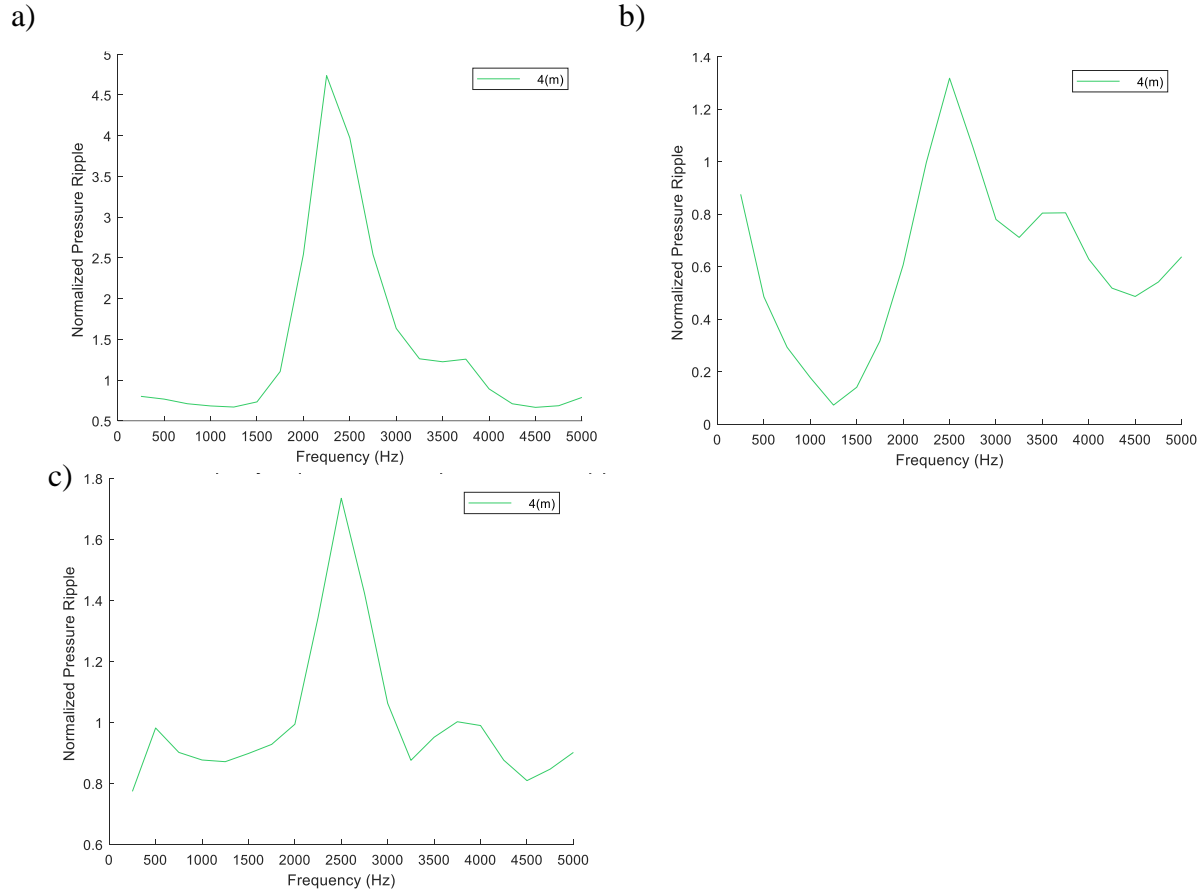


Figure 6.6 Eightway silencer normalized to baseline load with a line length of 403 cm and 25 mm diameter; a) Downstream; b) Upstream; c) Maximum;

6.2 Sensors and Components

It is important to assure steady-state conditions to measure the system oscillations in a comparative manner. To achieve this goal, pressure sensors and temperature sensors were installed according to Table 6.1. Three piezoelectric pressure sensors were installed along the pipeline to measure pressure ripple, while four accelerometers were installed along the line. Also, a G.R.A.S 40AO microphone, dynamic range from 20dB to 163dB, was installed 1.5 meters above the center of the circuit to obtain sound pressure measurements. The distance of 1.5 meters is greater than 0.5 m; thus should avoid the field is being affected by near field intensity circulation.

Table 6.1 Sensors installed at the tandem unit circuit

Tag	Name	Sensor	Range
p _s	Pressure Source	Hydac	60 bar
p _{au}	Pressure A (HP)	Wika	550 bar
p _d	Pressure Drain	Keller	30 bar
p _{ad}	Pressure A (LP)	Wika	25 bar
p _b	Pressure B	Wika	100 bar
Q _a	Flow Line A	VSE	250 L/Min
Q _s	Source Drain	VSE	40 L/Min
M	Torque	Staiger-Mohilo	0-500 N.m
N	Speed	Staiger-Mohilo	0-12000 rpm
β ₁	Displacement U1	In-Built	4-20 mA
T _{au}	Temp. A (HP)	Omega	K-type Thermocouple
T _s	Temp. Source	Omega	K-type Thermocouple
T _d	Temp. Drain	Omega	K-type Thermocouple
T _{ad}	Temp. A (LP)	Omega	K-type Thermocouple
T _{amb}	Temp. Ambient	Omega	K-type Thermocouple
Δp ₁	Pressure Ripple 1	Kistler	-30 – 30 bar variation
Δp ₂	Pressure Ripple 2	Kistler	-30 – 30 bar variation
Δp ₃	Pressure Ripple 3	Kistler	-30 – 30 bar variation
m ₁	Microphone	G.R.A.S 40AO	5Hz to 12.5kHz
A ₁	Accelerometer 1	PCB 356A16	±50 g
A ₂	Accelerometer 2	PCB 356A16	±50 g
A ₃	Accelerometer 3	PCB 356A16	±50 g
A ₄	Accelerometer 4	PCB 356A16	±50 g

Once the sensors are influenced by the physical parameters, voltage or electric current is outputted. Signals must be directed through signal conditioning boxes such as the flowmeters pulse counter of the Kistler 5023 amplifier, which is used by the piezoelectric sensor to amplify the original output. Then, the signals are sent NI cards, which are installed in the NI cDAQ-9178. The cDAQ communicates with the computer via the serial bus and is acquired by the software LabVIEW,

which linearizes and records the measurements. The piezoelectric pressure transducers and accelerometers require a high sampling rate of 25600Hz are routed to the module NI 9234 while the remaining signals, sampled at 1000Hz, are routed to an NI 9205 analog input card. Thermocouple signals are inputted into a NI 9211 module. Figure 6.7 shows the signal routing of the sensors into the data acquisition system.

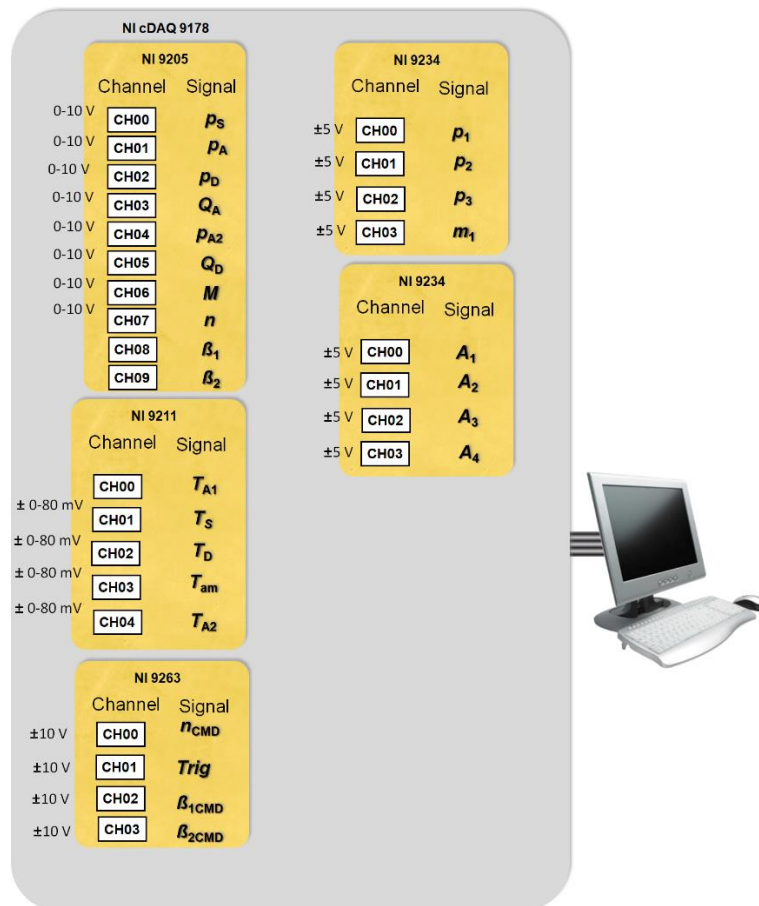


Figure 6.7 cDAQ-9178 and main modules used for the experiment

The Rexroth A22 tandem axial piston unit was selected because it is a nine-piston tandem unit in which the cylinder block's inner shaft has exactly 18 splines, as displayed by Figure 6.8. Because of this property, the rotation kit index between both pumps of the tandem unit can be shifted by 20° intervals. Thus, indexes of 0° or 20° can be achieved in this unit. The 0° index achieves the set-up in which all harmonics are set to full constructive interference. The 20° index sets destructive interference to all 1 + 2n harmonic while the even harmonics still are kept in

constructive interference. Thus the experiments for configuration E were split into two groups: E_1 where the tandem unit has a 0° index and E_2 , where the tandem unit has a 20° index.



Figure 6.8 Selected tandem unit display; **(a)** Closed case; **(b)** Rotation kit;

When disassembling the Bosh-Rexroth A22, the rotating kit of each side can be easily accessed by opening its respective endcase. Firstly, the endcase of unit 1 is opened. A spline aligned to the piston slipper's inner circle was identified and then rotated to a reference position using a bolt hole, as shown by Figure 6.9. Subsequently, the end case of unit 1 is closed. The hydraulic unit is turned around and opened on the other side, where the same piston/spline alignment pattern was found. Then, the rotating kit of unit 2 is removed and reattached in such rotating index kit configuration is desired. During the first disassemble, the valve-plate and rotating kit geometry will be measured. It is important to simplify the unit disassembly to preserve the case properties. Bolt torque also was controlled with the usage of a torque-wrench when reassembling the unit.

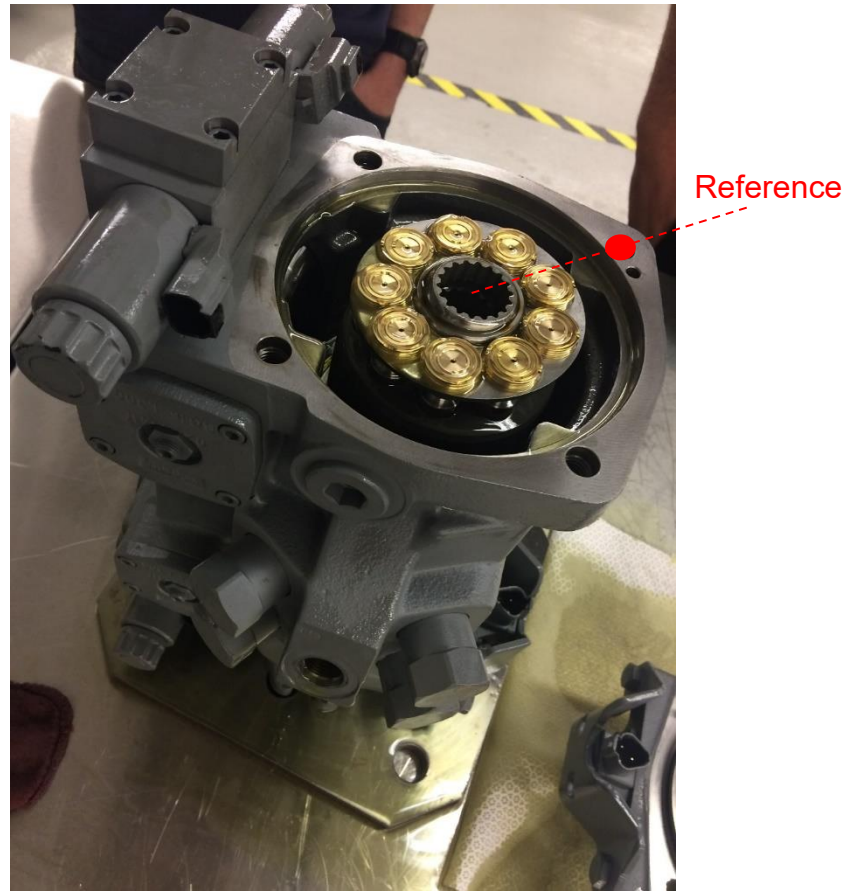


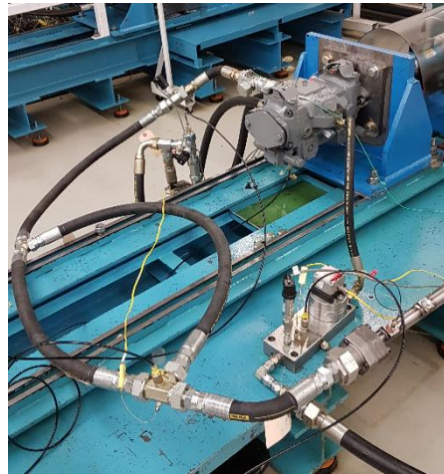
Figure 6.9 Tandem unit indexation reference

6.3 Test rig Assembly

The test rig was constructed at the facilities of Maha Fluid Power Research Center in Lafayette, Indiana. The circuit total line length from the pump's hydraulic unit's outlet to the line's downstream, which is the throttle valve, is equal to 403 cm. Line diameter was kept constant at 25.4 mm from upstream to downstream. The hydraulic circuit was adaptable for the installation of the passive elements with minimum intervention. Circuit configuration B and C could be achieved by adding closed-end branches in the nodes N_1 and N_2 from Figure 6.1, respectively. These nodes were placed 50 cm and 201 cm from the pump outlet, respectively. For configuration D, the middle tee was removed, and then two tees were installed respectively 160 cm and 240 cm from the pump outlet. The Quincke tube's parallel line was connected to these two tees to another and was 120 cm long. Figure 6.10 and Figure 6.11 shows the assembled circuit with configurations B, C, and D.

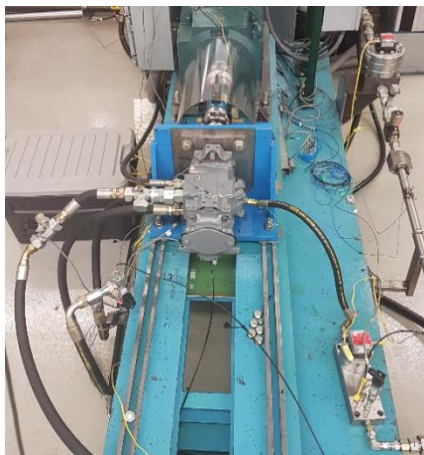


(a)



(b)

Figure 6.10 Candidate passive elements in the hydraulic circuit; (a) Configuration B - Halfway silencer; (b) Configuration D - Quincke tube



(a)



(b)

Figure 6.11 Assembled test rig with Configuration E ; (a) Tandem Unit; (b) Hydraulic circuit

Piezoelectric sensor, Δp_1 was installed 50 cm after the pump outlet. Piezo-electric sensors 2 and 3 were placed 720 millimeters apart from each other in a steel pipe. The distances from Δp_2 and Δp_3 to the unit downstream are equivalent to 295 cm and 368 cm. Four accelerometers were installed to measure structural vibrations; Accelerometers 1 and 2 and 3 are respectively installed close to piezoelectric sensors 1 and 3 to measure pipe surface acceleration close to the pressure ripple

measurements. Figure 6.12 shows the accelerometer's positions. The last accelerometer, A_4 was installed in the throttle valve top to measure vibrations at the circuit downstream.

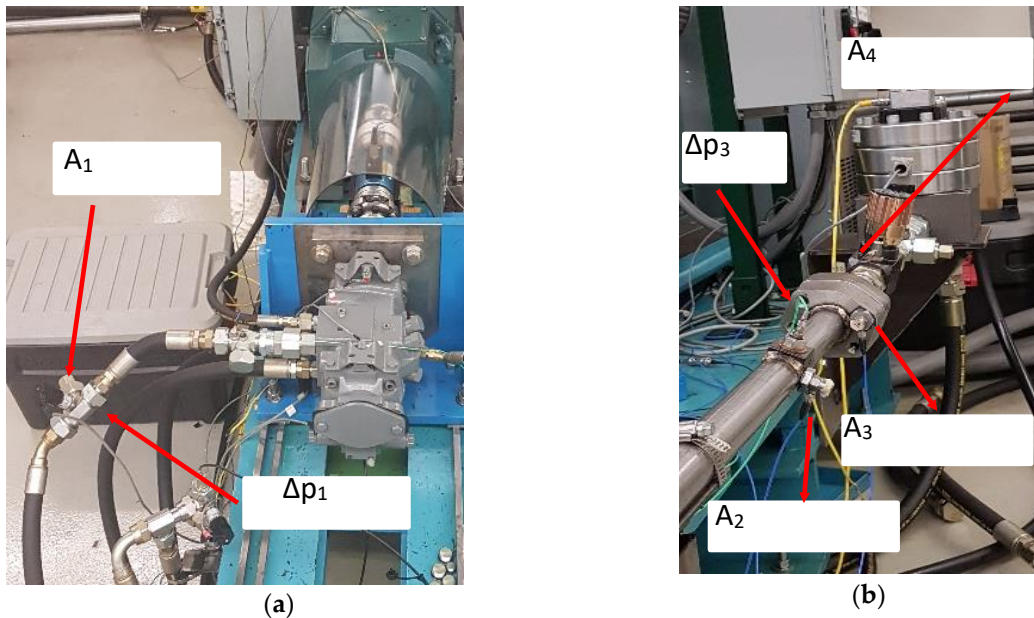


Figure 6.12. Accelerometers positioning the hydraulic circuit

6.4 Measured Operation Conditions

The operation conditions are chosen to cover different operating speeds, pressures, and unit's displacement. The speeds are selected so the unit first 20 harmonics will sample the frequency band 0 -5000 Hertz nicely, to calculate the frequency response function for the several line configurations and evaluate insertion loss of the proposed solutions. For testing the passive elements the speeds of 1200 rpm and 1940 rpm were chosen, while for evaluating the tandem unit antiphasing, 1200 rpm and 1660 rpm were chosen since the flow demand of the tandem unit is higher. Figure 6.13 shows the frequency harmonics of the units at 1200 rpm and 1920 rpm.

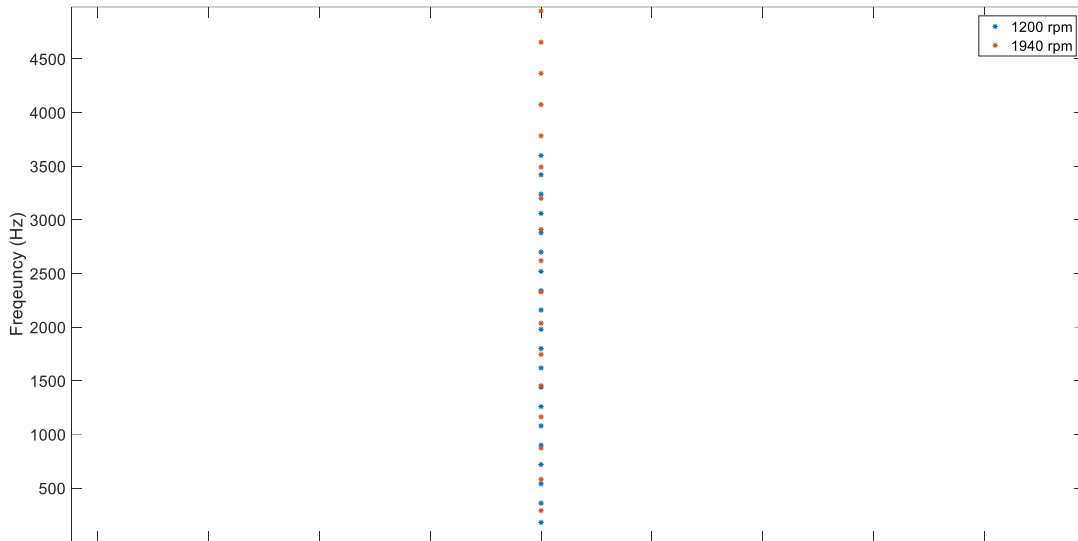


Figure 6.13 First 20 harmonics for 1200 rpm and 1940 rpm speeds

Two sets of eight operation conditions were chosen as showed in Table 6.2 and Table 6.3. These eight operation conditions include two different speeds, two different line displacements, and three different pressures. At each operation condition, five back to back measurements were performed. For each measurement, the pump inlet pressure was controlled to be equal to 30 bar while the inlet temperature is controlled to be between 52° and 53 C°. As Table 6.4 the measurements for the configurations A, B, C, and D will use the operation condition set 1, while The measurements for set E1 and E2 will use the operation condition set 2.

Table 6.2 Operation condition set 1

Set 1			
	U_1 Speed(rpm)	High Pressure (bar)	Displacement(%)
1	1200	100	100
2	1200	175	100
3	1200	250	100
4	1940	100	100
5	1940	175	100
6	1940	250	100
7	1200	100	50
8	1940	100	50

Table 6.3 Operation condition set 2

Set 2			
	U₁ Speed(rpm)	High Pressure (bar)	Displacement(%)
1	1200	100	100
2	1200	175	100
3	1200	250	100
4	1660	100	100
5	1660	175	100
6	1660	250	100
7	1200	100	50
8	1660	100	50

Table 6.4 Measurements sets and configuration summary

Measurement	Line Configuration	Opcon Set	Units Rotating kit Index
1	A	Set 1	-
2	A	Set 1	-
3	B	Set 1	-
4	C	Set 1	-
5	D	Set 1	-
6	E ₁	Set 2	0°
7	E ₂	Set 2	20°

After the measurements are obtained, comparisons will be made to verify discrepancies and noise source attenuation from different hydraulic system configurations. The comparison sets are summarized in Table 6.5. Measurement batteries 1 and 2 will be used to verify the repeatability of the experiments. Measurement 1 will also be the reference baseline to verify the passive element's influence on pressure ripple and structure acceleration. Measurement battery 7 is the reference to verify the coupled unit indexing strategy to attenuate source pressure ripple attenuation. The two sets of eight operation conditions were chosen as showed by Table 6.2 and Table 6.3

Table 6.5 Comparison Study

Study	Test Compared
Repeatability	1 vs 2
Tandem unit antiphasing	7 vs 6
Passive Line Elements Transmission loss Strategies	3,4,5 vs 1

6.5 Repeatability

Two different measurement batteries were selected to check the repeatability of the experimental testing results. Five measurements were performed at each operating condition present on set 1. The repeatability study did not find significant differences for the pressure ripple and acceleration measurements. The sound pressure measurement showed a divergence of 1.5 dB verified in the worst case. The periodic patterns in pressure ripple and acceleration can be verified in each operation condition. Figure 6.14 shows the pressure ripple at node N1, while Figure 6.15 shows the pressure ripple at the pipe upstream. The acceleration at node N1 is showed by Figure 6.16, while Figure 6.17 shows the acceleration verified at the pipe wall.

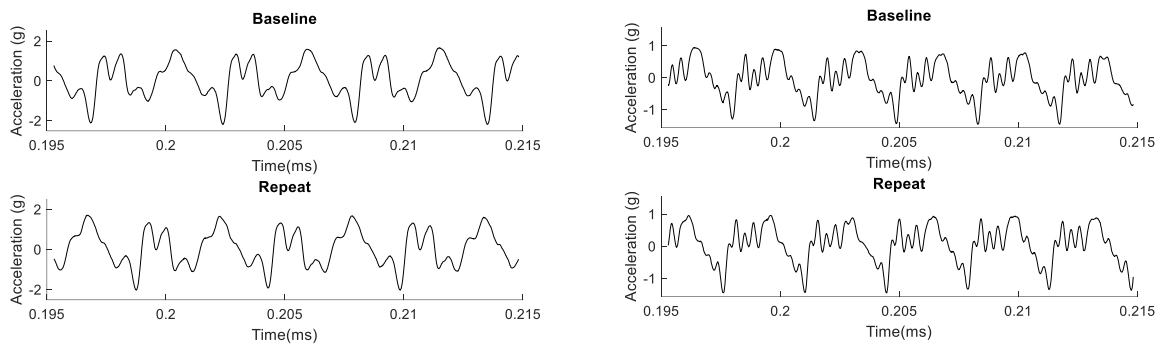


Figure 6.14 Measured pressure ripple Δp_1 at 170 bar (a) 1200 rpm (b) 1920rpm

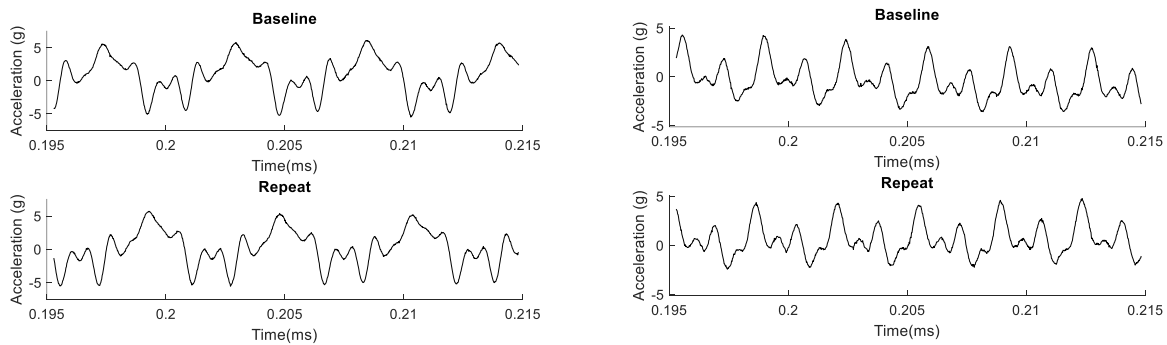


Figure 6.15 Measured pressure ripple Δp_2 at 170 bar (a) 1200 rpm (b) 1920rpm

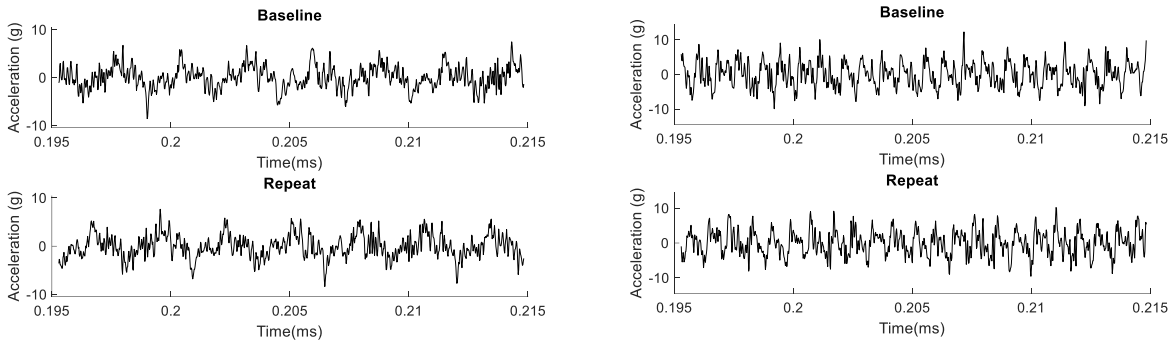


Figure 6.16 Measured Acceleration A_1 at 170 bar (a) 1200 rpm (b) 1920rpm

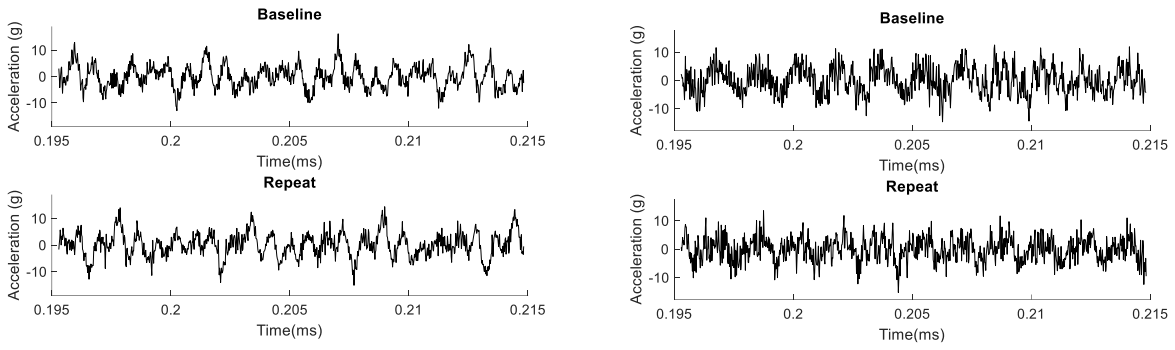


Figure 6.17 Measured Acceleration A_2 at 170 bar (a) 1200 rpm (b) 1920rpm

7. EXPERIMENTS WITH THE PROPOSED PASSIVE TECHNIQUES

This section shows the experimental results of the experiment it was performed to verify the effectiveness of the noise source attenuation strategies elaborated on chapters 4 and 5. This model introduces the effects of discrete parameters along the connecting lines. In section 7.1 measurement battery 1 will be used as a baseline since it has the configuration without the introduction of vibration attenuation passive elements. In section 7.2 measurement 7, which is the tandem unit with a 0° rotation kit phase-shift, is used as a reference since it has the index which keeps all pump harmonics in a constructive interference pattern.

7.1 Passive Elements Experimental Results

To evaluate the effects of the proposed passive elements on attenuating noise source metric needs to be defined. Power spectral density S of the signals is usually used to represent power in the frequency-domain. To represent transmission loss given variable x to a given variable y , the powers spectral density of both variables of the first is divided by the latter, thus resulting in a spectral power ratio (SPR) as shown by equation (7.1) shows. To represent the transfer function from an input to an output for one given unit speed, the value of the four operation condition power spectral density is averaged. Also, at each operation condition, five different measurements were performed for a total of $m=20$ measurements to reduce the inaccuracies of random errors due to the precision of the sensors.

$$SPR = \sum_{m=1}^{20} \frac{|S_{xx,m}|}{|S_{yy,m}|} \quad (7.1)$$

Figure 7.1 and Figure 7.2 shows how a transfer function between variable x and y is represented by the spectral power ratio. Pressure ripple Δp_1 was chosen as input x and Δp_2 was chosen as input y at

Figure 7.1. Pressure ripple Δp_2 was chosen as input x , and Δp_3 was chosen as output y on Figure 7.2. Since for all the four circuit configurations, the pipe in which piezoelectric sensor 2 and electric sensor 3 to is the same, the transfer function among the two remained very consistent.

However, the frequency response function between Δp_1 and Δp_2 has changed considerably after passive elements are installed.

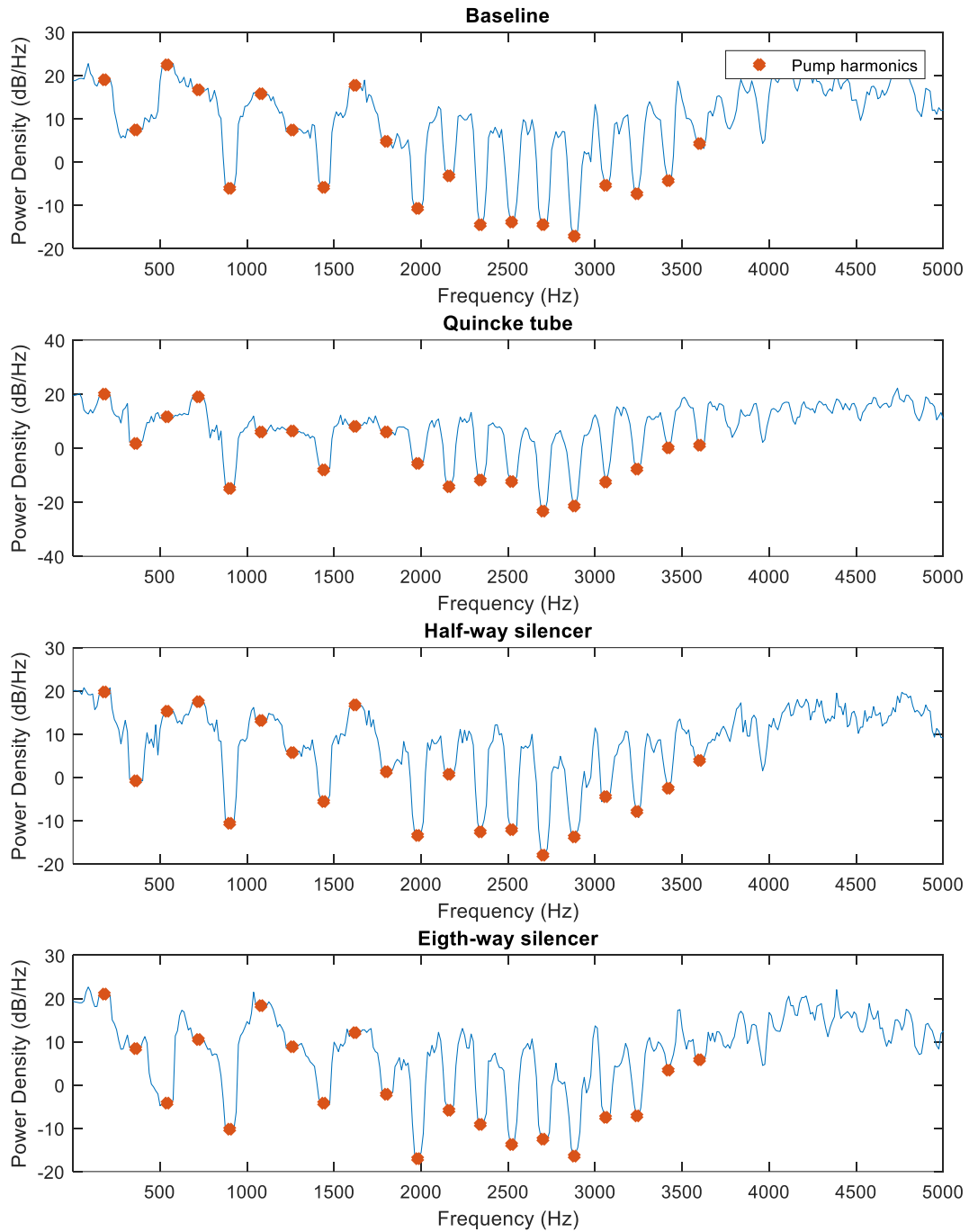


Figure 7.1 Spatial power ratio with unit 1 at 1200 rpm, configuration A; $x = \Delta p_1$ $y = \Delta p_2$

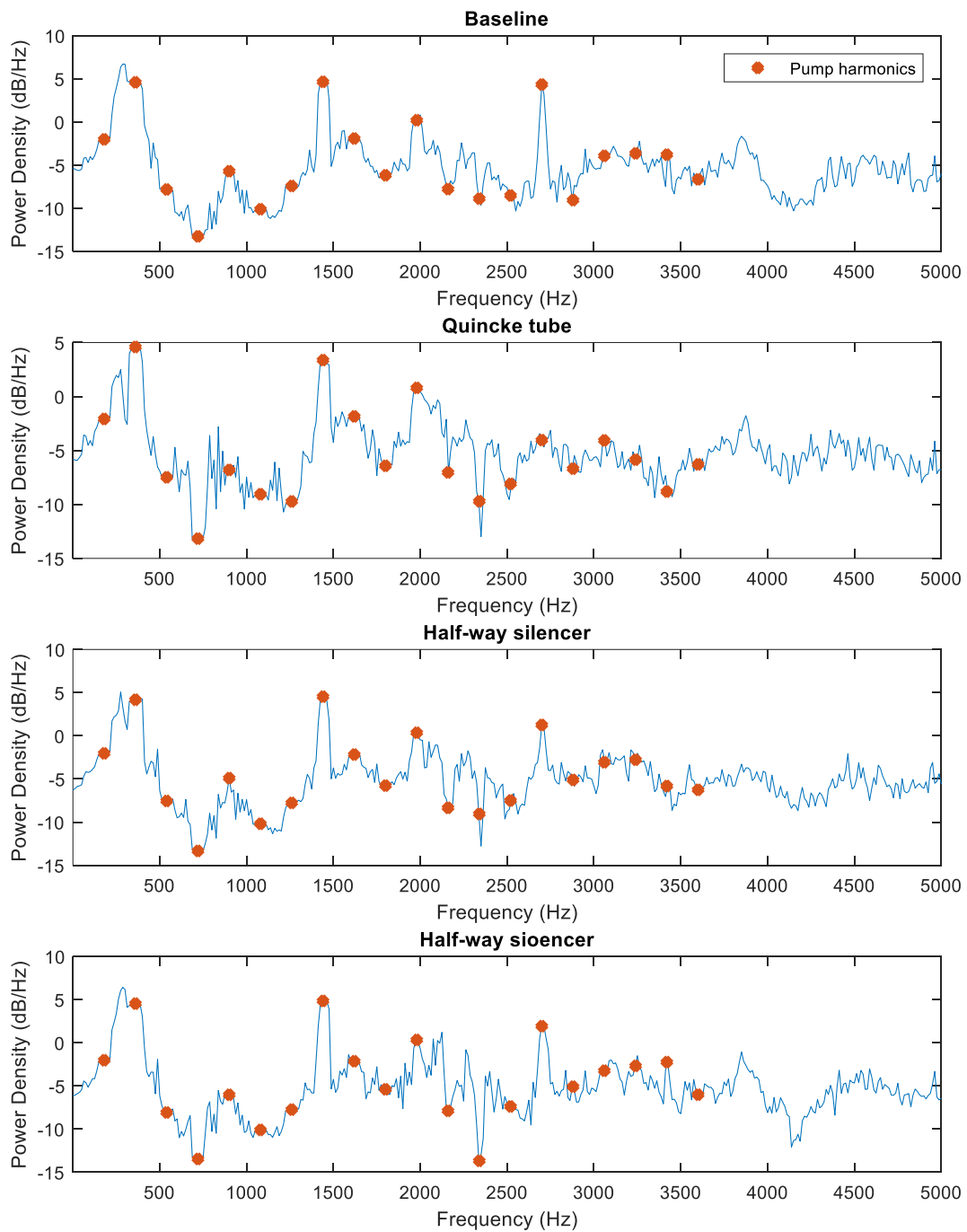


Figure 7.2 Spatial power ratio with unit 1 at 1200 rpm, Configuration A; $x = \Delta p_2$ $y = \Delta p_3$

To enhance the differences in the transfer functions from a line configuration that contains the candidate passive element to the baseline, a normalization based on the baseline is proposed as

equation (7.2) to calculate a Normalized Power Spectral Ratio (NPSR). One advantage of this approach is that each pressure transducer signal is divided by the same transducer signal in other hydraulic circuit configuration. Therefore, systematic errors in the pressure transducer and accelerometer will be absent in the final result.

$$NPSR = \sum_{m=1}^{20} \frac{|S_{xx,m,baseline}| |S_{yy,m,element}|}{|S_{yy,m,baseline}| |S_{xx,m,element}|} \quad (7.2)$$

Figure 7.3 shows NSPR that represents the passive element effects on the pressure ripple and the pipe wall acceleration. It is possible to verify none of the candidate design accomplished attenuation for the whole 50-5000Hz frequency range suggested by the simulations. However, the passive elements still achieve vibration power reduction in the majority of the frequency range. When evaluating the spectral power divergence from Δp_1 to Δp_2 the Quincke tube shows 10 dB attenuation in several frequency bands a while the eightway silencer achieved 27 dB attenuation for the pressure ripple at ~550 Hz. However, this metric alone cannot serve as the indication of the actual pressure ripple reduction by the noise solutions since it does not consider the initial differences in the magnitude of Δp_1 . Concerning the accelerations, surprisingly the Quincke tube achieved noticeable downstream vibration reduction which was not predicted on simulation.

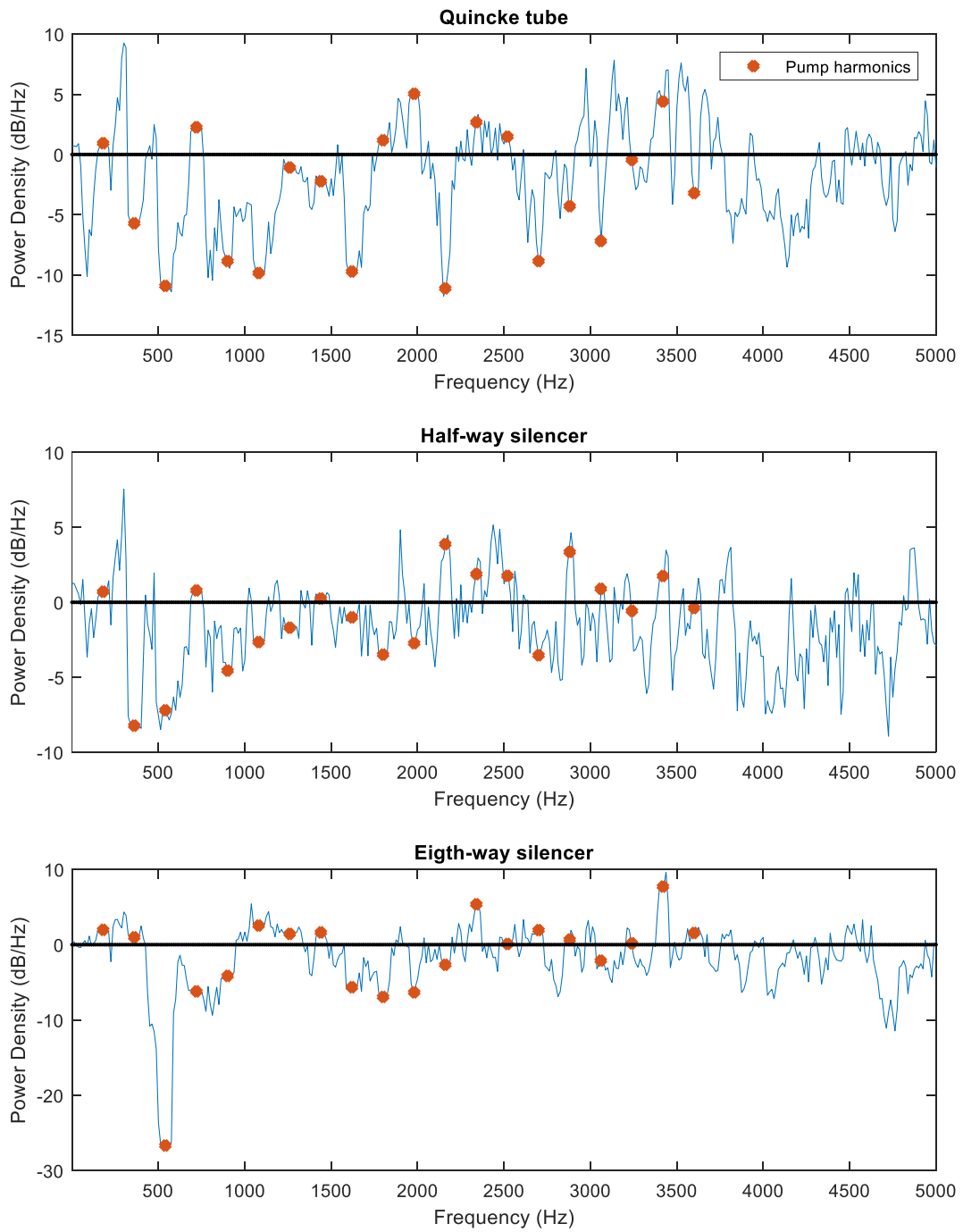


Figure 7.3 Normalized Spatial power ratio with unit 1 at 1200 rpm; $x= \Delta p_1$ $y= \Delta p_2$;

If a given variable is the most critical for noise reduction, one can evaluate the passive element impact in this variable alone by simply dividing the power spectral density of the variable by the same variable measured with the baseline conduit. This method is analog to Insertion Loss with the exception that line length is conserved, and the average of many measurements contribute to reducing random errors. The systematic errors were once again eliminated by this approach called Modification Spectral Power Ratio or MSPR (7.3).

$$MSPR = \sum_{m=1}^n \frac{\|S_{xx,m,element}\|}{\|S_{xx,m,baseline}\|} \quad (7.3)$$

Figure 7.4 to Figure 7.9 shows MSPR for the pressure ripple, downstream acceleration, and sound pressure measurements obtained by the microphone. With this simplified metric, it is possible to verify the reduction of pressure ripple and pipe wall acceleration for most of the frequency content. However, an inferior correlation of the measured sound power with these two parameters is possibly a result of the sound pressure having multiple sources including several oscillating structures that are not being measured, including the source's.

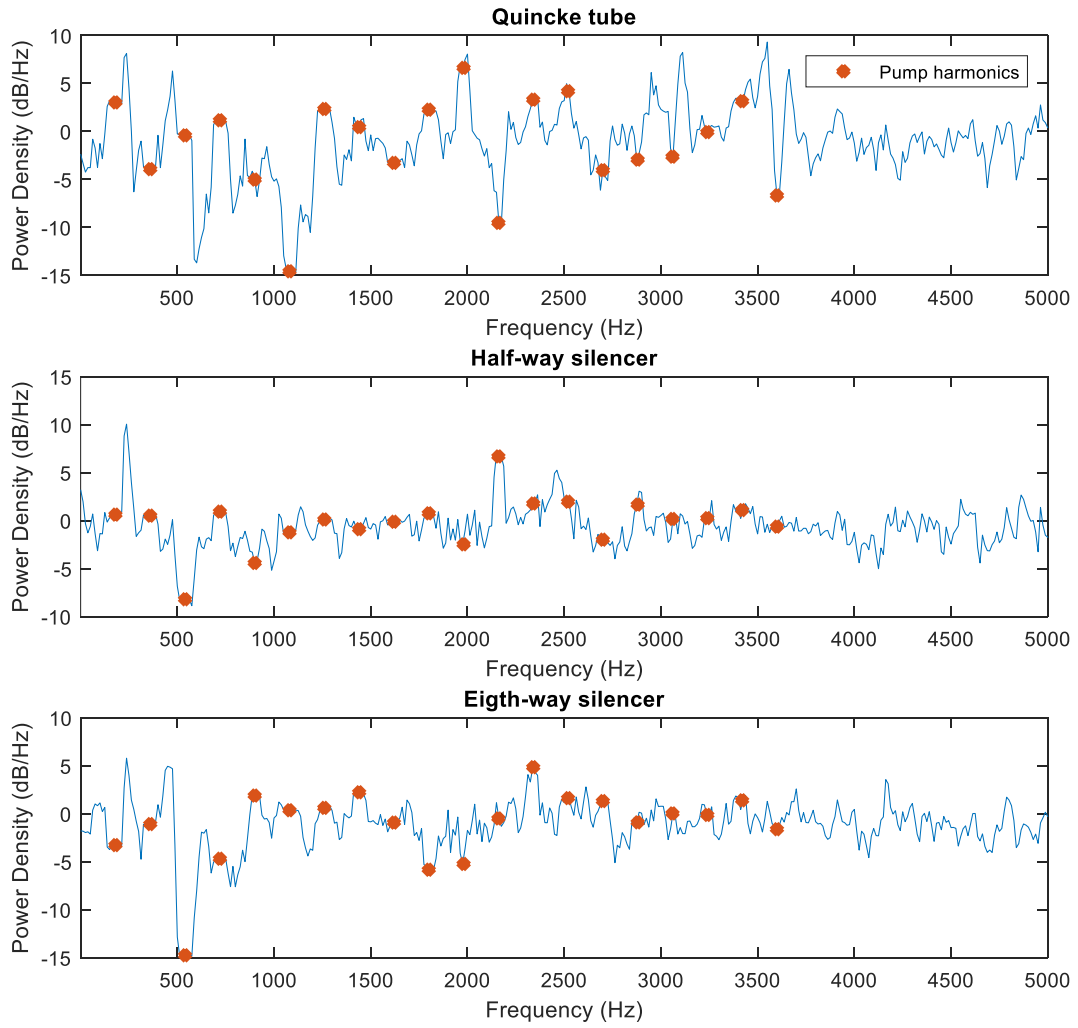


Figure 7.4. Modification Spectral Power Ratio for p2 at 1200 rpm

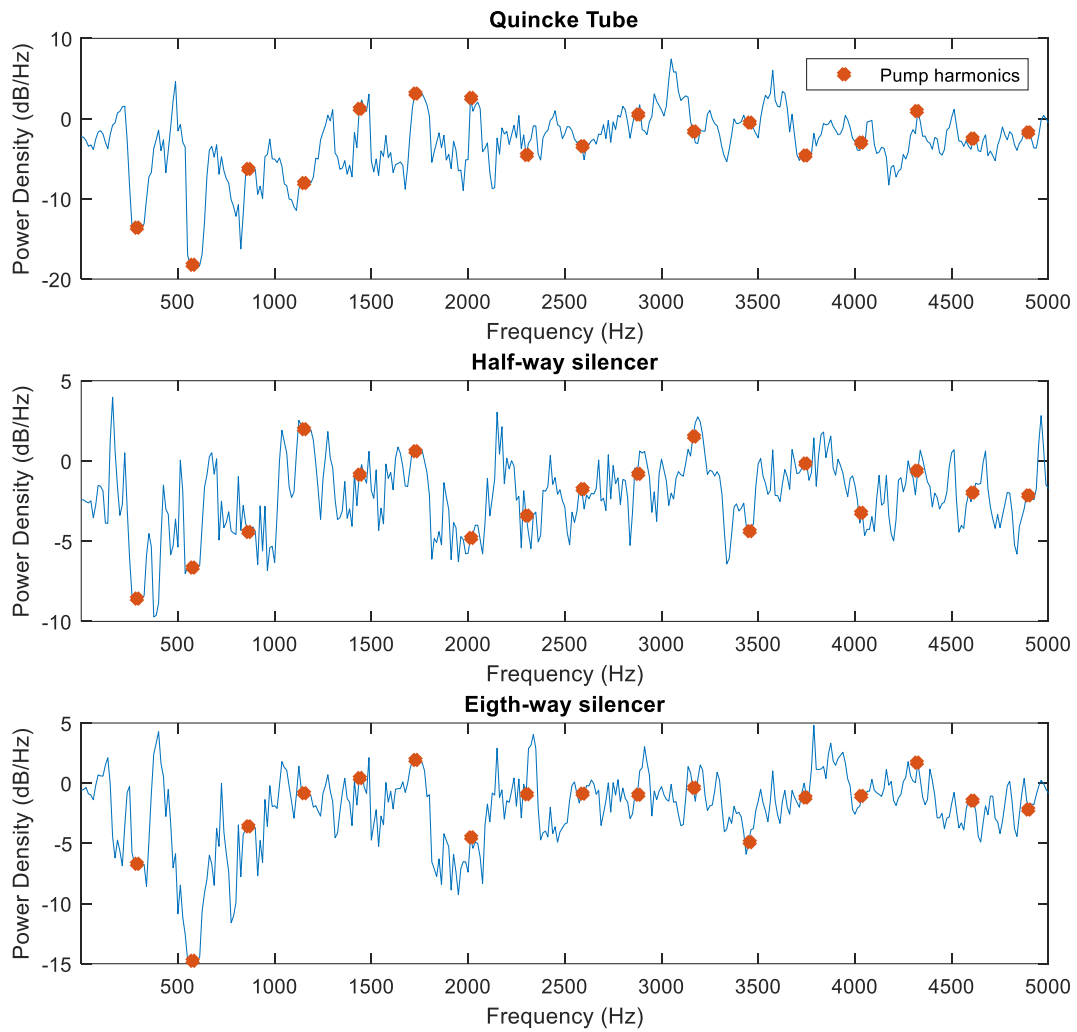


Figure 7.5. Modification Spectral Power Ratio for Δp_2 at 1940rpm

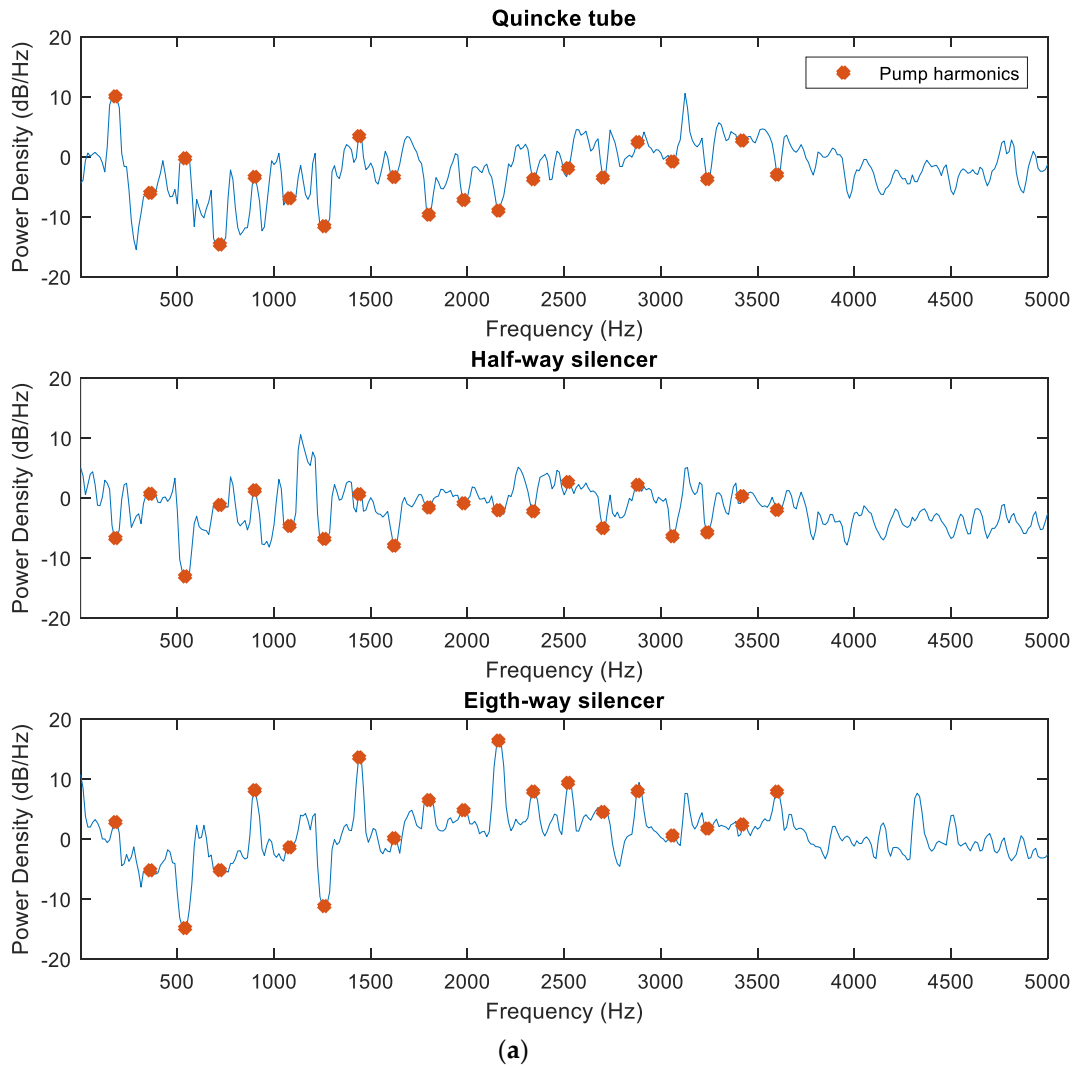


Figure 7.6. Modification Spectral Power Ratio for A4 at 1200 rpm

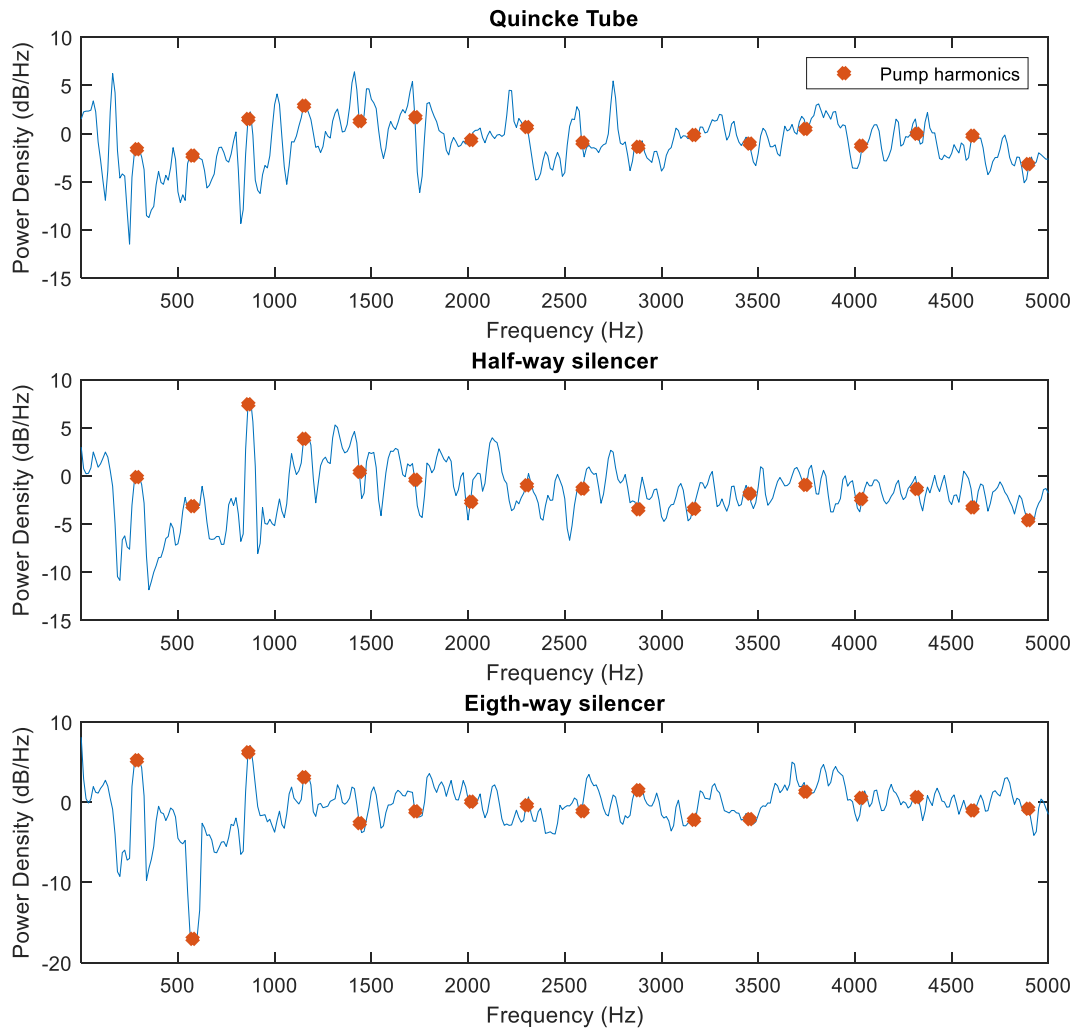


Figure 7.7. Modification Spectral Power Ratio for A4 at 1940rpm

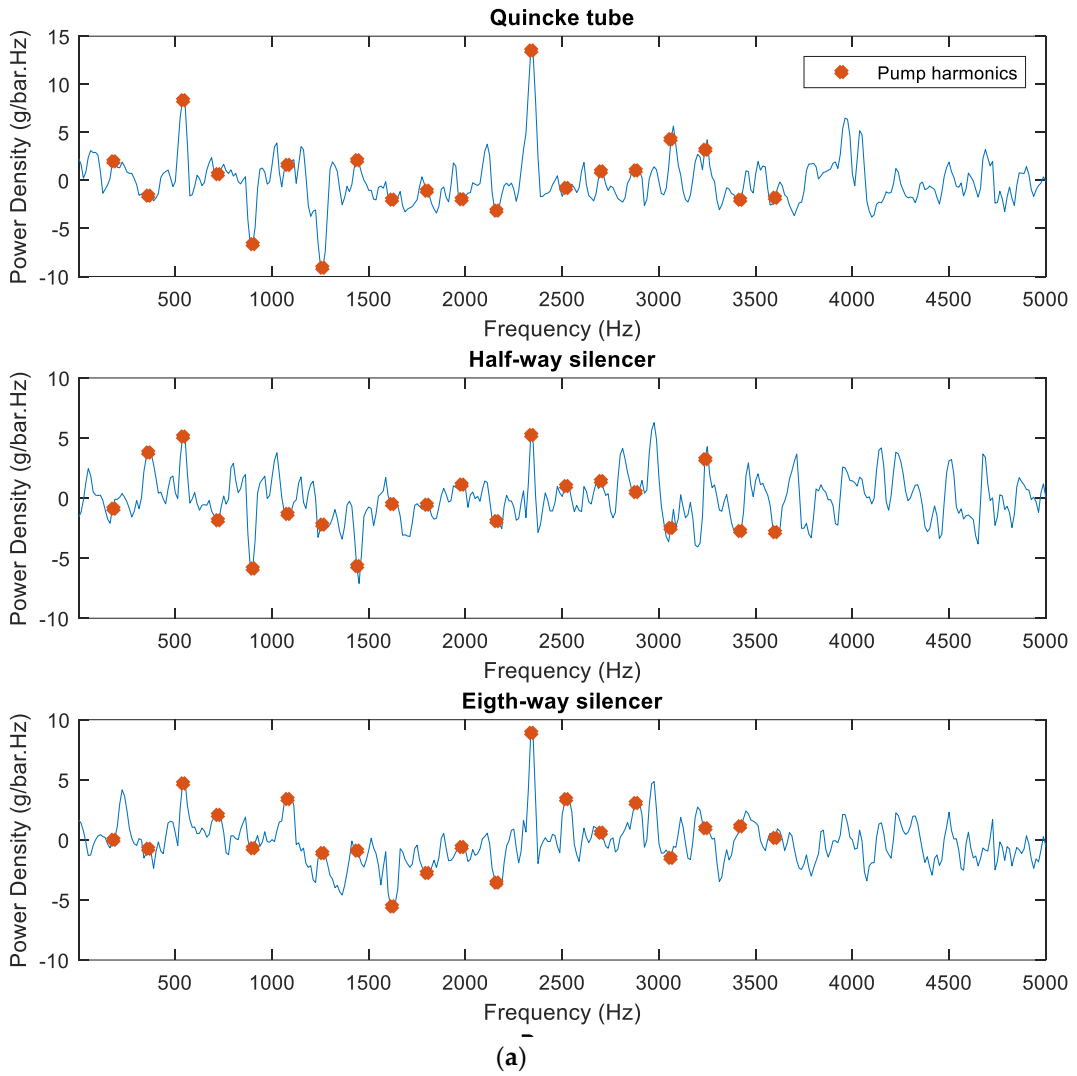


Figure 7.8. Modification Spectral Power Ratio for Measured Sound Pressure at 1200 rpm

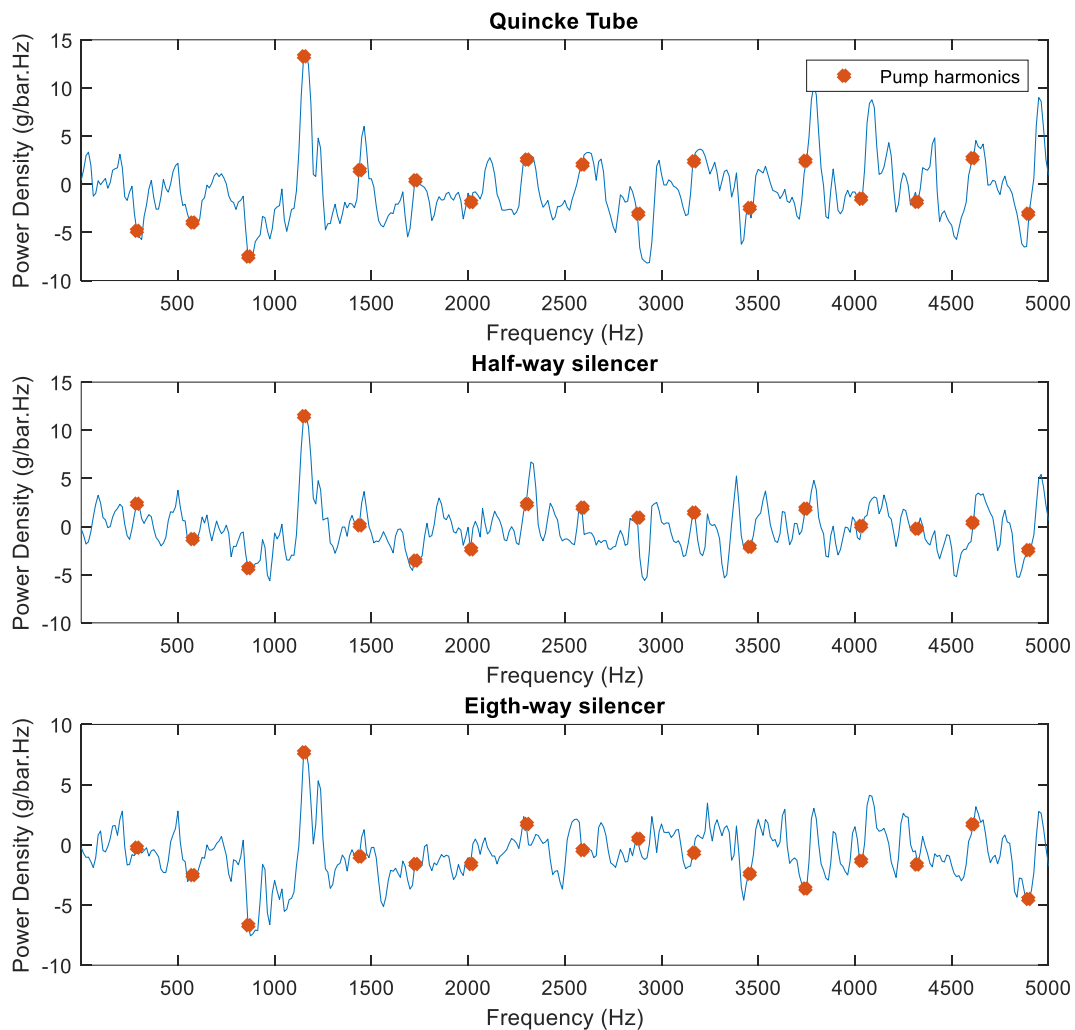


Figure 7.9. Modification Spectral Power Ratio for Measured Sound Pressure at 1940rpm

Time-domain graphics are showed from Figure 7.10 to Figure 7.15. The first four figures show pressure ripples Δp_1 and Δp_2 . As the position where Δp_2 is measured is at the downstream of each of the introduced massive elements noticeable peak to peak ripple reduction was obtained in each operation condition. Therefore the ripple mitigation on the majority of the frequency domain is also reflected at the time domain.

Meanwhile, while the wave shape of pressure ripple Δp_1 has changed, for most operating conditions the peak to peak time-domain pressure ripple has either kept very similar. Thus the goal of the passive elements of reducing pressure ripple at the downstream without compromising the upstream was partially achieved, However as neither solution was capable of reducing the frequency response at all 0-5000 Hz band, the noise source mitigation cannot be guaranteed. However, data show noise source reduction will happen often. The accelerations measured at the hydraulic circuit showed the same trends of the pressure ripple, had it been reduced in positions after the position of the introduced element and maintained similar magnitude for positions before the element.

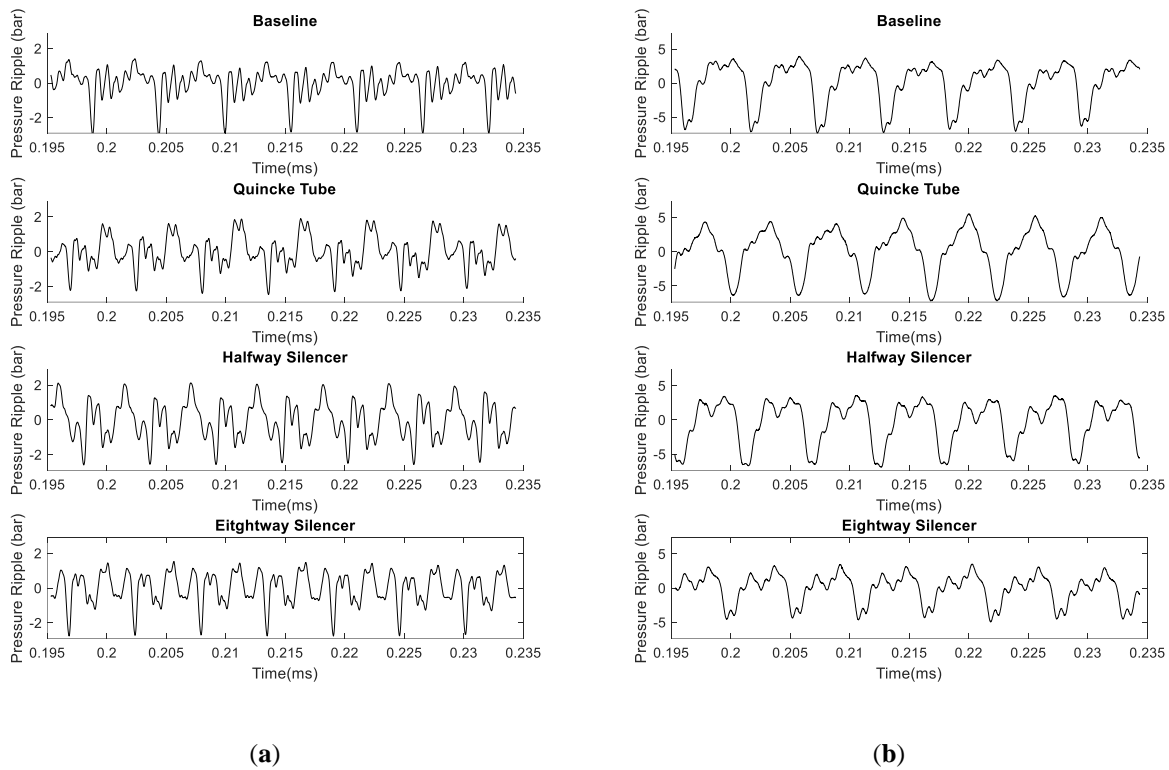
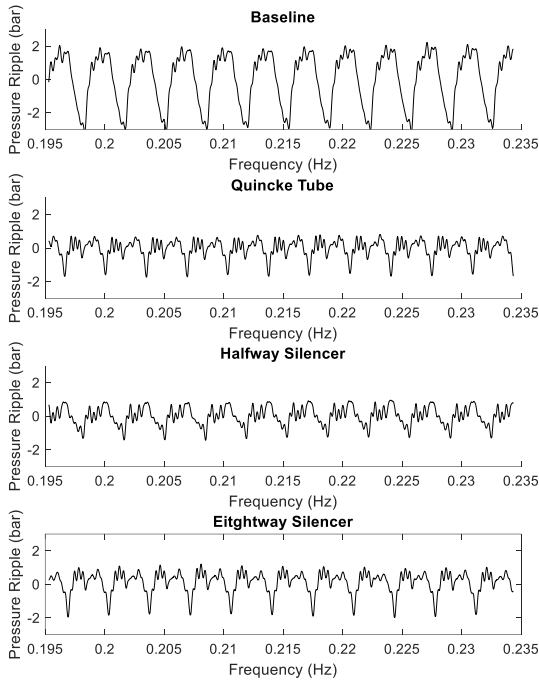
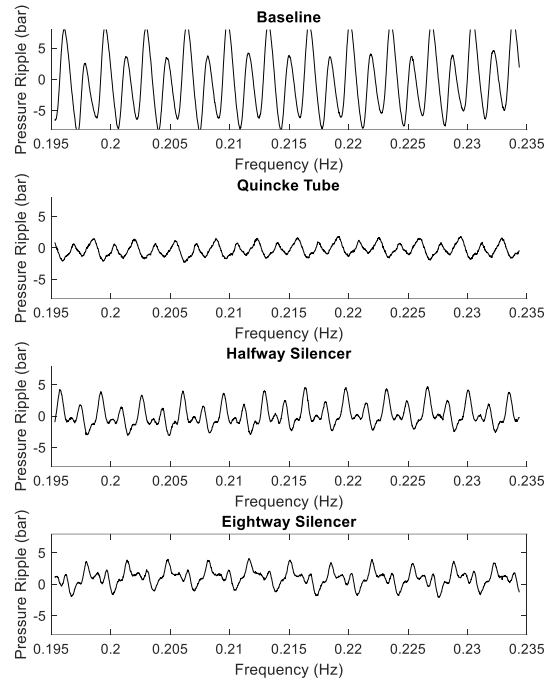


Figure 7.10 Measured pressure ripples at 1920 rpm 170 bar (a) Δp_1 (b) Δp_2

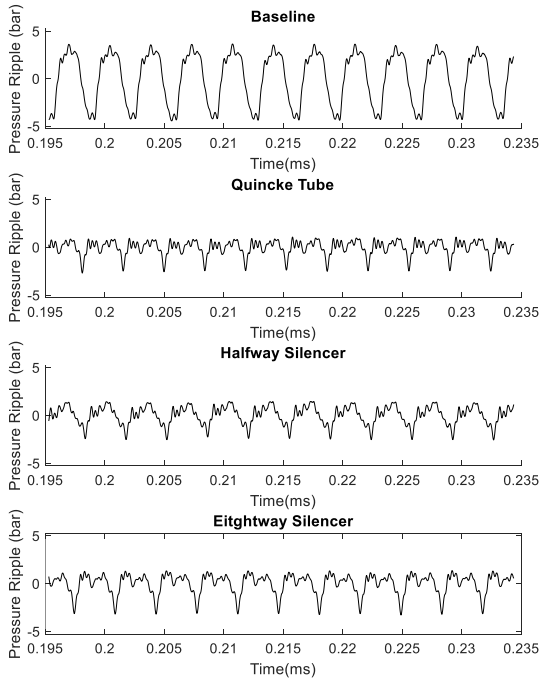


(a)

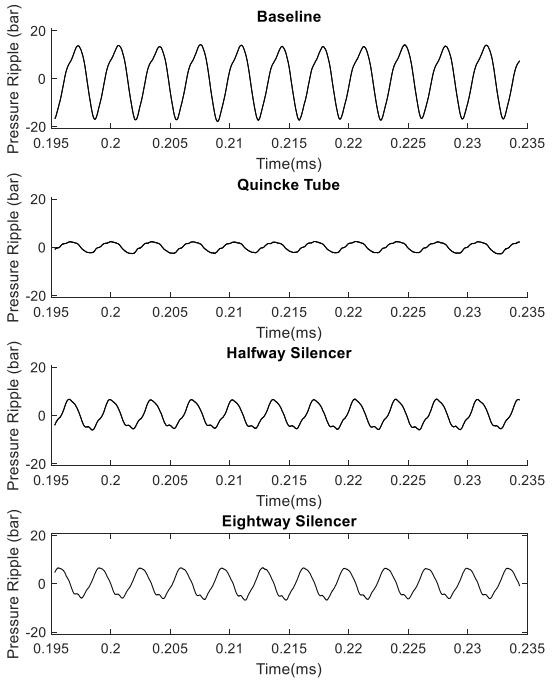


(b)

Figure 7.11. Measured pressure ripples at 1200 rpm 250 bar (a) Δp_1 (b) Δp_2

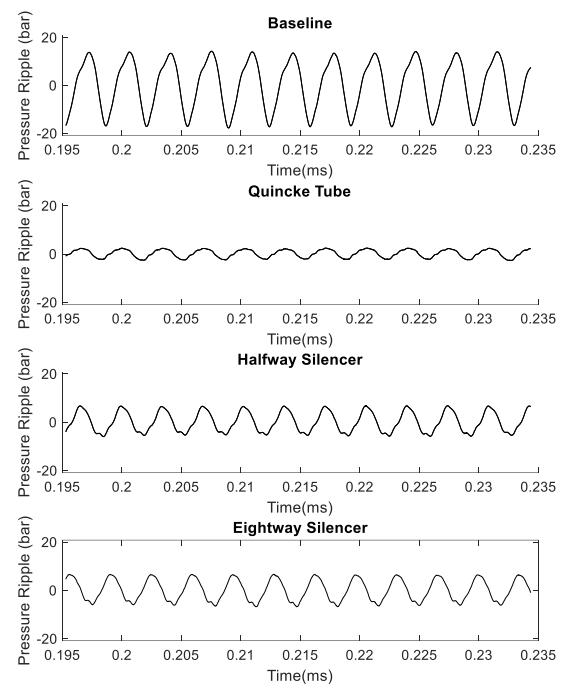
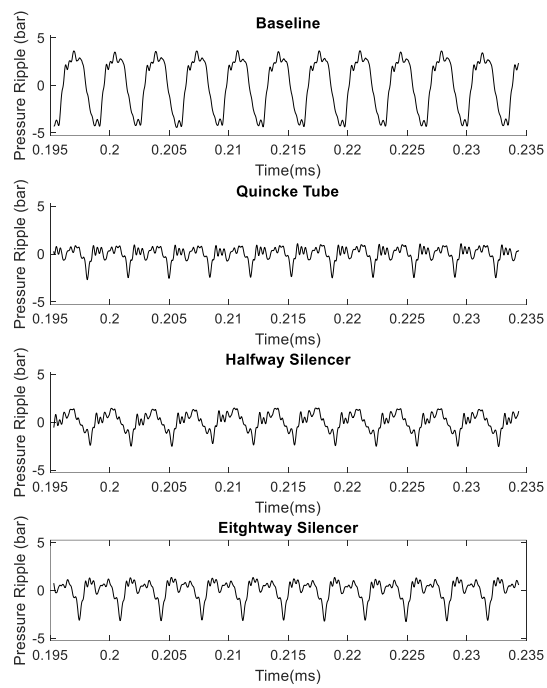


(a)



(b)

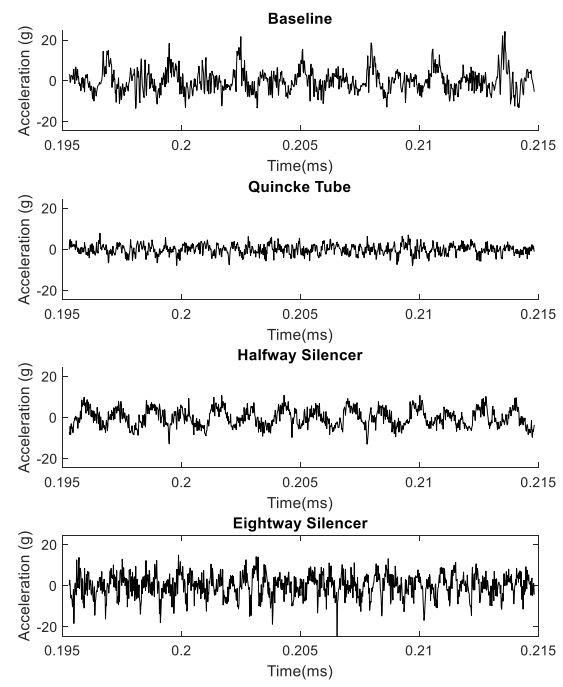
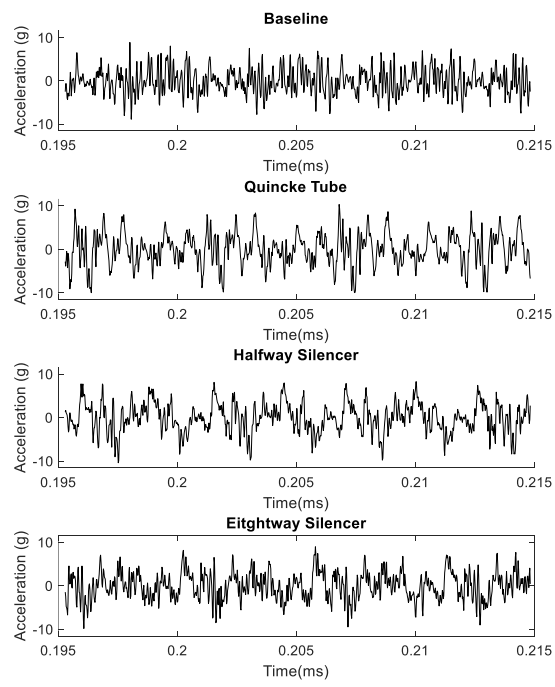
Figure 7.12. Measured pressure ripples at 1920 rpm 250 bar (a) Δp_1 (b) Δp_2



(a)

(b)

Figure 7.13 Measured pressure ripples at 1920 rpm 250 bar (a) Δp_1 (b) Δp_2



(a)

(b)

Figure 7.14. Measured accelerations at 1200 rpm 250 bar (a) A_1 (b) A_4

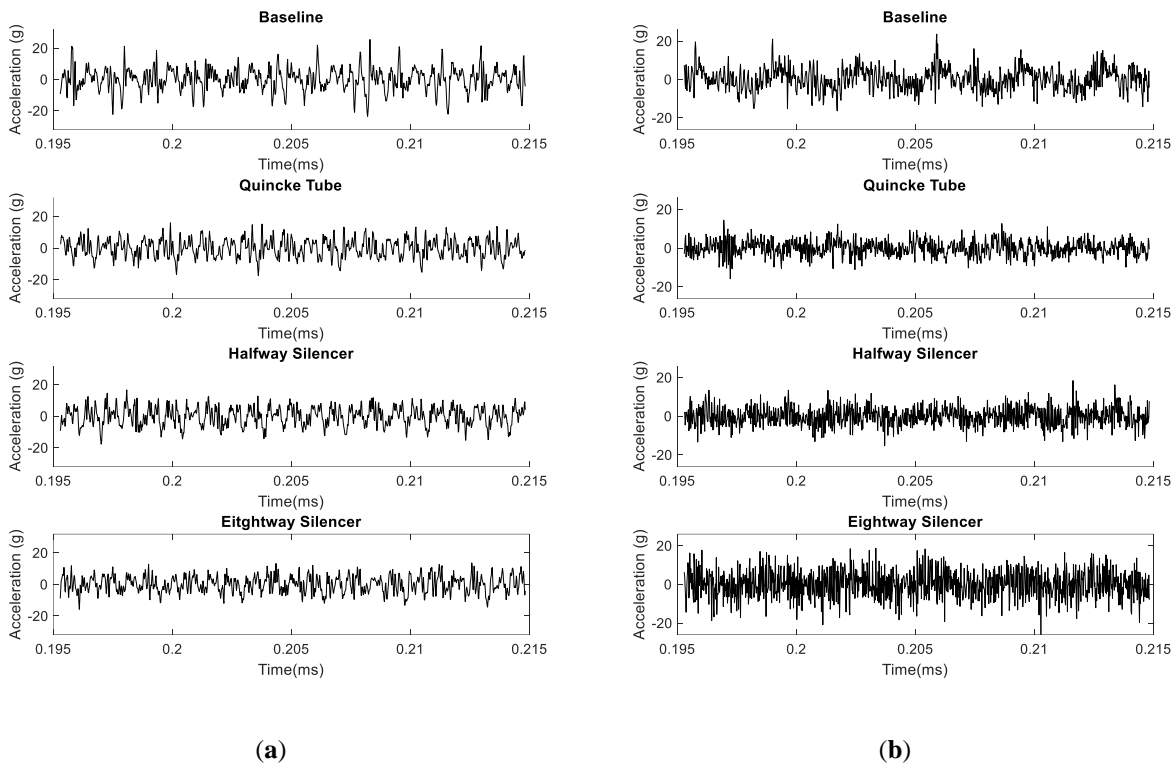


Figure 7.15 Measured accelerations at 1920 rpm 250 bar (a) A_1 (b) A_4

7.2 Tandem unit destructive interference index results

For evaluating the impact of the 20° indexation to achieve odd harmonics destructive interference at the tandem pump the Modification Spectral Power Ratio (*MSPR*) was also used. The case where the tandem unit has 0° indexation between both units rotation kits was used as a baseline and the 20° index case was considered the modified case. Figure 7.16 shows the spectral power ratio in the frequency-domain for the unit running at 1200 rpm. Figure 7.17 displays the spectral power when the units are running at 1660 rpm. The pressure ripple from the branch through the whole line to the end was drastically reduced specifically in the first and third units' fundamental harmonics. At 1200 rpm the first harmonic was reduced by 15.32 dB at p1 and by 16.87 dB at p3. At 1660 rpm the first harmonic was respectively reduced by 17.96dB .87 dB at p1 and p3. Concerning the third harmonic, at 1200 rpm and 1660 rpm respectively, there were attenuations of 10.31 and 9.55 dB at p1 and of 11.63 and 9.3 dB at p3. Reductions on first and third fundamental harmonics could also be observed in the measured accelerations and sound pressure measurements,

however, at a lower rate than it was observed on pressure ripple. Concerning pipe wall vibrations and sound, at 1200 rpm the first and third harmonics respectively were reduced by 0 and 9 dB while at 1660 rpm the first and third harmonics respectively were reduced by 2 and 4.66 dB.

However, it is possible to verify that this noise source reduction was not conserved for all odd harmonics higher than the third harmonic. The indexing strategy resulted in random patterns increasing or decreasing the excitations at higher harmonics.

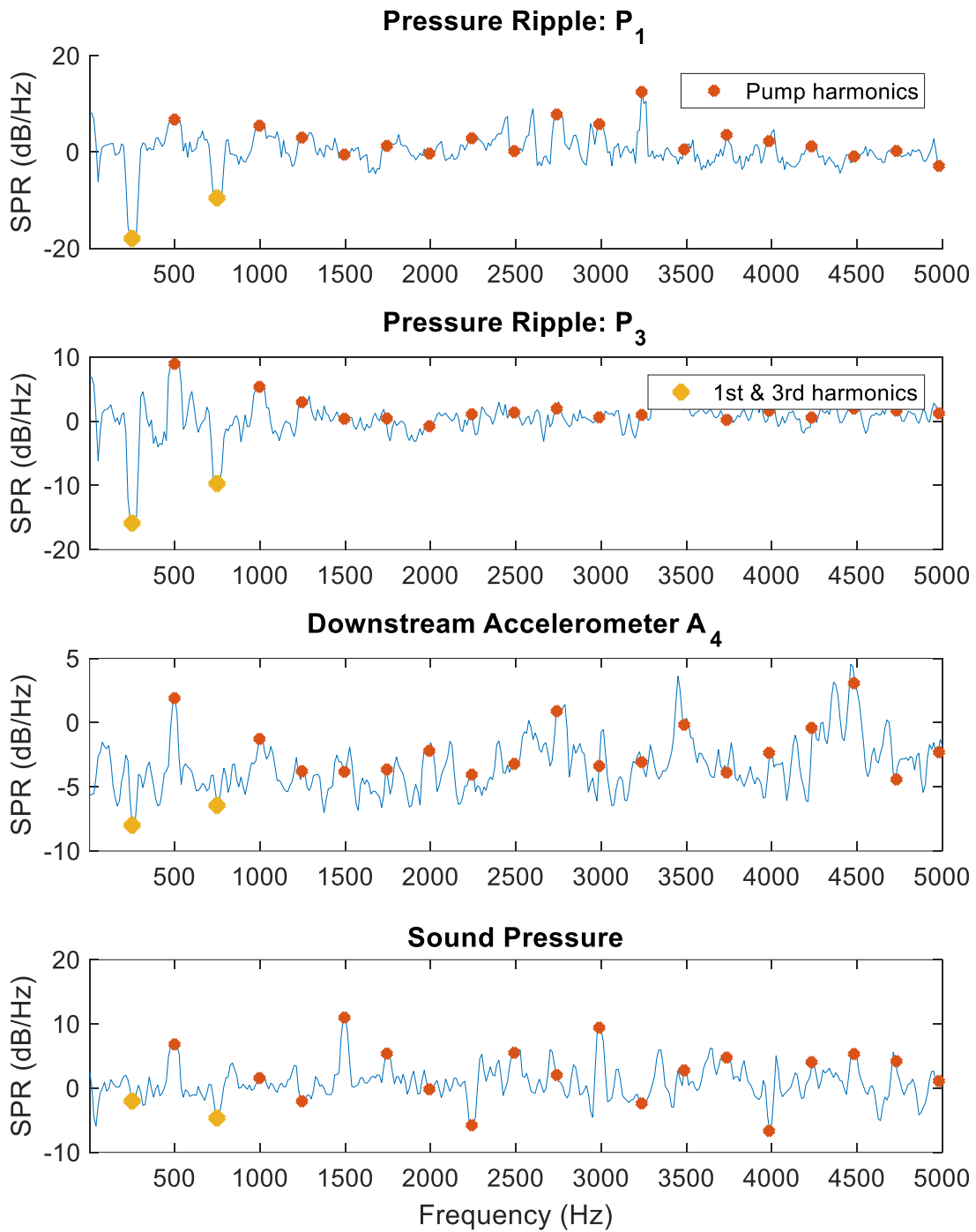


Figure 7.16 MSPR frequency response function: 20° Index normalized over 0° index n=1200 rpm

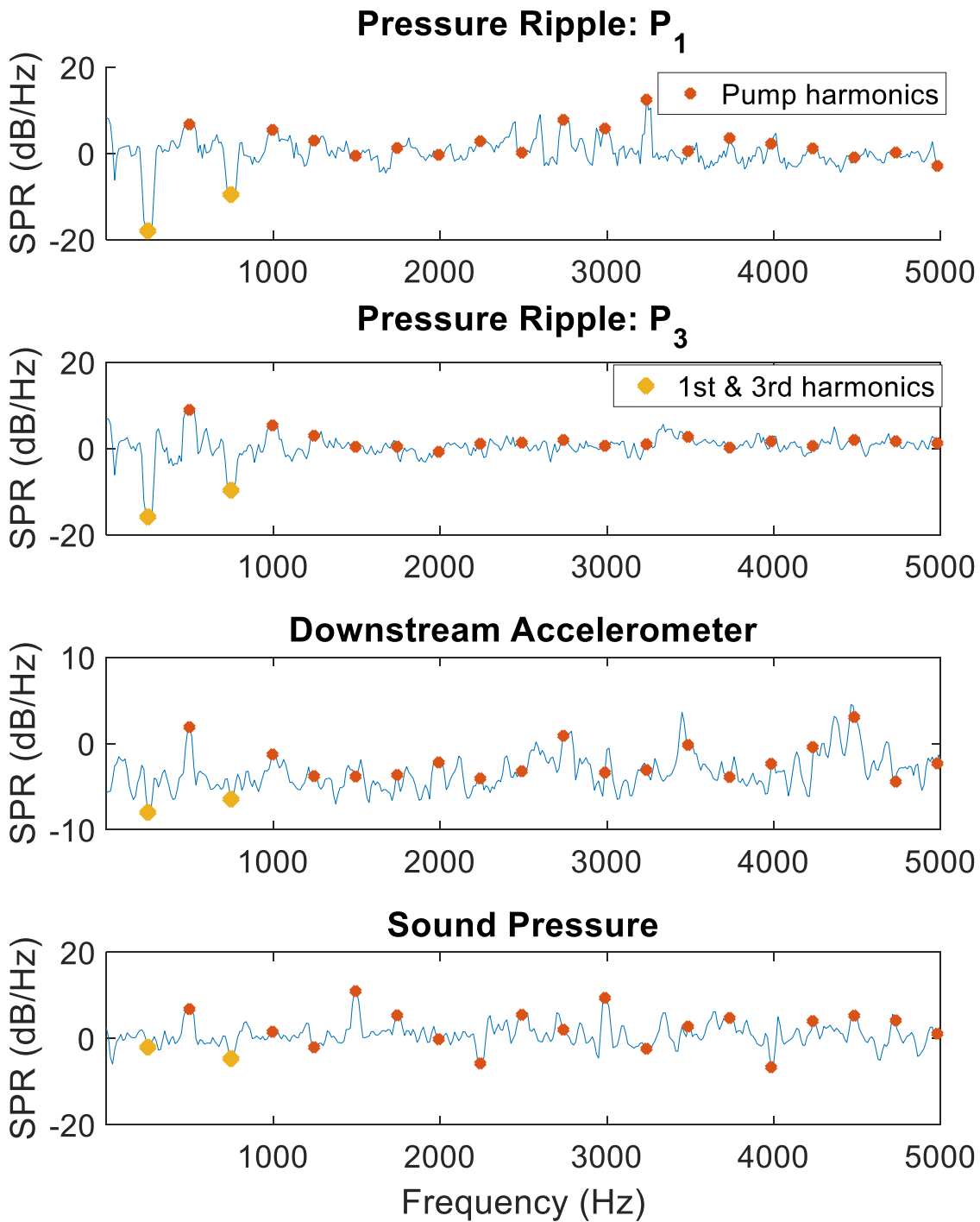


Figure 7.17 MSPR frequency response function: 20° Index normalized over 0° index n=1660 rpm;

In axial piston units, the first two harmonics are very dominant for the time domain response of pressure ripple. The sharp noise source reduction on the first and third harmonics was less than expected by the numerical model, nonetheless, it is still enough to contribute with peak to peak pressure ripple also pipe wall vibrations on most measurements. Figure 7.18 and Figure 7.19 shows pressure ripples p_1 and p_2 while Figure 7.20 displays acceleration A_I .

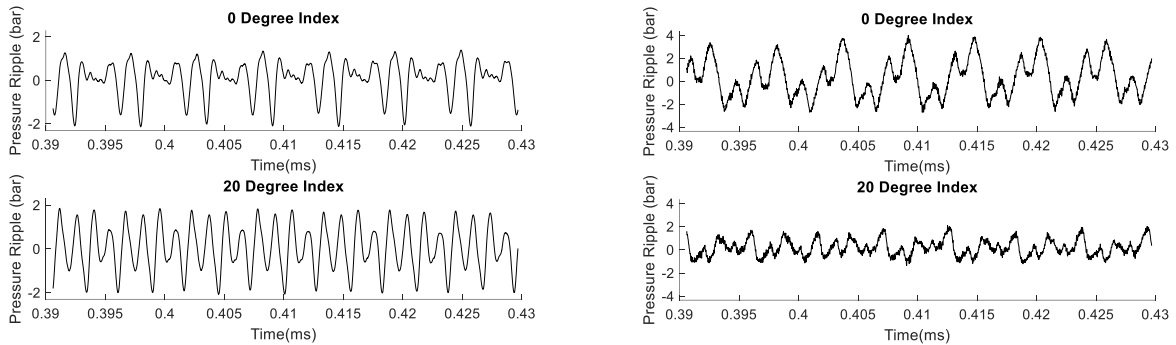


Figure 7.18 Measured pressure ripples at 1200 rpm 250 bar (a) Δp_1 (b) Δp_2

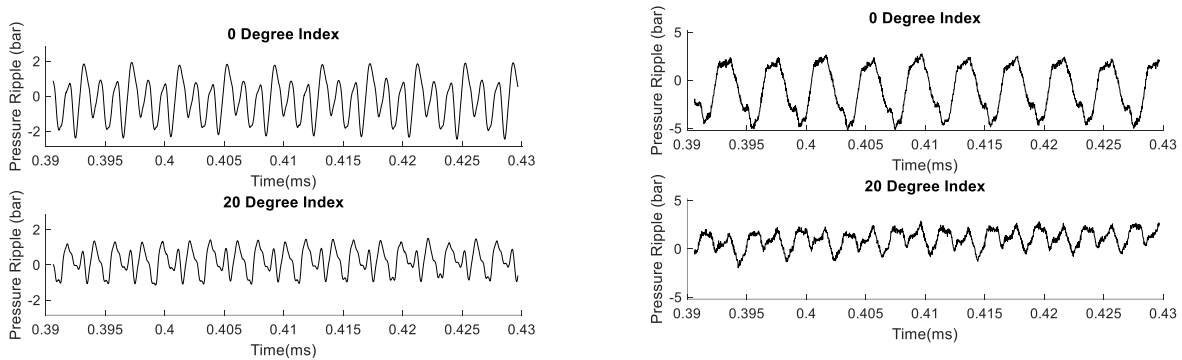


Figure 7.19 Measured pressure ripples at 1660 rpm 250 bar (a) Δp_1 (b) Δp_2

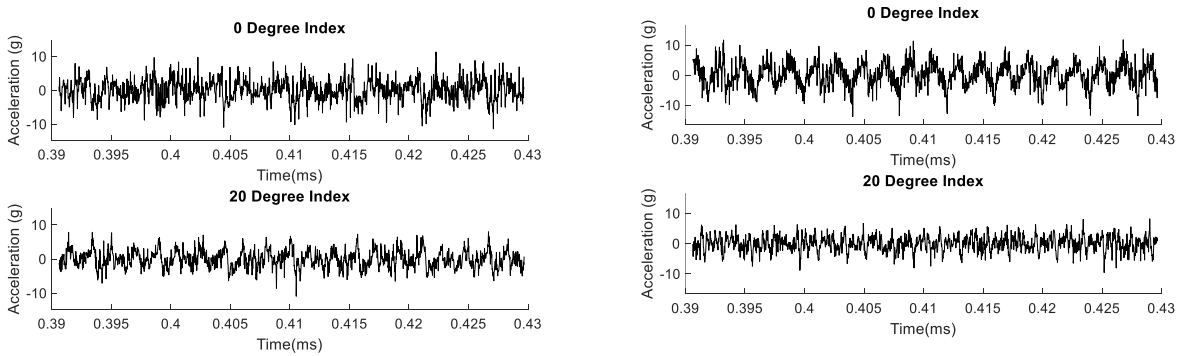


Figure 7.20 Measured Acceleration A_I at 170 bar (a) 1200 rpm (b) 1660rpm

7.3 Sound Pressure Measurements

This section summarizes the sound pressure measurements made by the microphone. A single microphone is not enough to map the acoustic behavior of a hydraulic system, however, it can provide a glance at how the strategies affect audible noise. Since the scope of this thesis is investigatory, a deeper understanding of the sound field with the influence of the passive strategies is left for future work.

Table 7.1 summarizes sound pressure measurements of the passive elements when compared to the baseline. The lowest measured sound pressure is highlighted in blue while the highest one is highlighted in red. Specifically, for this microphone position, the Quincke tube was the element that yielded the highest sound mitigation. However, the two closed-branch silencers also lower noise levels than the baseline.

Table 7.2 summarizes the tandem unit sound pressure measurements for different indexes. Since the strategy is not effective for the whole original projected frequency band and presents compromises at higher frequencies, the 0° index achieves smaller measured sound pressure for the unit running at 1660 rpm regardless of the pressure ripple cancelation in the first and third harmonic.

Table 7.1 Sound pressure measurements: Passive elements vs baseline

Speed		1200 rpm				1920m rpm		
Pressure	100 bar	100 bar	170 bar	250 bar	100 bar	100 bar	170 bar	250 bar
Displacement(%)	50	100			50	100		
Baseline	83.22dB	83.26dB	86.74dB	87.23dB	83.93dB	83.93dB	90.14dB	92.34dB
Quincke T.	80.97dB	80.97dB	84.77dB	87.56dB	82.92dB	82.92dB	87.34dB	91.20dB
Halfway Sil.	81.04dB	81.25dB	84.79dB	87.70dB	83.60dB	83.60dB	88.26dB	92.41dB
Eighthway Sil.	81.96dB	81.91dB	85.39dB	87.97dB	83.01dB	83.01dB	86.92dB	90.44dB

Table 7.2 Sound pressure measurements: 20° Index vs 0° Index

Speed		1200 rpm				1660m rpm		
Pressure	100 bar	100 bar	170 bar	250 bar	100 bar	100 bar	170 bar	250 bar
Displacement(%)	50	100			50	100		
0° Index	83.9dB	86.7dB	92.0dB	94.0dB	85.4dB	84.8dB	89.1 dB	91.8 dB
20° Index	82.9dB	84.3dB	89.4 dB	92.7dB	85.1dB	85.9 dB	90.3dB	93.6 dB

Another factor that can influence why the 20° index provided worst results than the 0° Index case at high speed is the weighted influence of the compromised frequencies at the total sound power summation. Figure 7.17 showed at upstream pressure ripple the 0° Index case had a lower magnitude for several harmonics between 2500Hz and 4000Hz. Figure 7.21 shows the transfer functions where pressure ripple is the input and pipe wall is the output for both the positions where piezoelectrics sensors Δp_1 and Δp_2 are installed. The figure shows a critical frequency band from 2500-4000 Hz where amplifications up to 40 dB higher than the lower frequencies can be spotted. Thus, while the strategy was successful in reducing pressure ripple for most of the 0-5000Hz frequency band, the compromised frequencies dominated the pipe wall behavior resulting in higher vibrations for the 20° Index case.

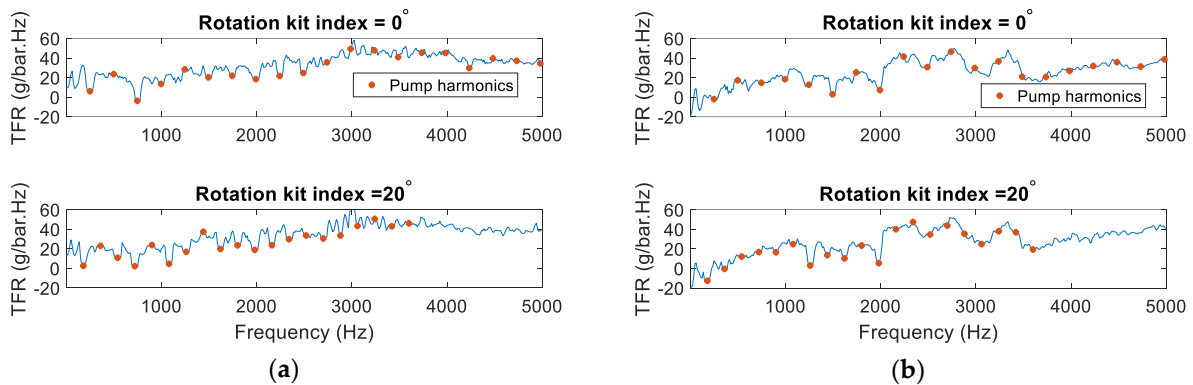


Figure 7.21 Transfer Function Ratio of pressure ripple vs pipe wall acceleration $n=1660$ rpm at
 (a) Branch (b) Pipe Downstream

8. CONCLUSIONS

This thesis covered passive fluid-borne noise source reductions, which are techniques capable of affecting large bands of frequencies and do not require extra energy of the system nor the usage of data feedback. Often these techniques have low implementing costs. A coupled system time-domain modeling approach was developed and then studied to provide a better comprehension of the topic. The time-domain approach was extended to a frequency domain evaluation through a novel proposed approach in which the time domain model is used, but each frequency is isolated and then evaluated in a targeted 0-5000 Hz band.

Using the time-domain model and the frequency-domain approach, effects such as line friction, curvatures, pipe wall material variation, and diameter variation could be evaluated more simply, and passive fluid-borne noise mitigation techniques were computationally investigated. Through simulation study and verification, this thesis presents the development of new ideas to be implemented may be a great contribution to the development of feasible and practical strategies to reduce hydraulic machinery noise and thus meeting regulations standards, achieving better comfort for operators, and reaching novel applications.

To validate the model, experiments with the mode switching hydraulic hybrid circuit were conducted at Maha Fluid Power Research Center on a compact test rig with known line diameter variations, hose segments, and elbows. The main high-pressure line contained three piezoelectric sensors capable of verifying the pressure ripple for a range of operating conditions. Later, for verifying the techniques found with the computational investigation, another experiment was designed to have a hydraulic line that could be modified with ease to isolate the behavior of the proposed solutions.

To find a hydraulic system-oriented fluid-borne noise source reduction technique, a holistic, comprehensive study of mid-size hydraulic applications was conducted. The investigation found three noticeable candidate passive elements, a Quinke tube, and two closed-end branches introduced in different positions. The passive elements sizing and positioning were calibrated through the computational investigation, and only the best solutions for each design were tested experimentally. A flowchart strategy for application-oriented fluid borne noise reduction was

developed. Experiments showed the candidate elements could attenuate pressure ripple and acceleration most of 0 to 5000 Hertz band when compared to a reference line behavior, and sound pressure reduction also was observed most of the time.

Also, source flow ripple reduction techniques were investigated using the developed time-domain model. A tandem-unit interference strategy capable of setting all unit's odd harmonics into destructive interference was found analytically and successfully tested in simulation. This FBNS reduction strategy has shown in simulation the advantage of being effective for multiple operating conditions since it is not dependent on unit speed. Experiments were conducted to show that the technique did indeed reduce the pressure ripple and pipe wall acceleration for the first and third fundamental harmonic of the unit greatly. This behavior was consistent for different speeds. However, since there was an unexpected increase in oscillation for higher harmonics due to phenomena that were not predicted on the original model, the sound pressure was only reduced in the cases where the pump speed was low.

While this research provided good prognostics on the noise sources effects of passive strategies, which elements had sizing and positioning determined numerically, reducing noise sources is still just the first step. Further understanding of the interaction of pressure ripple and vibration and the system, irradiation, and sound field is necessary to create strategies that will be effective in a broader number of operation conditions.

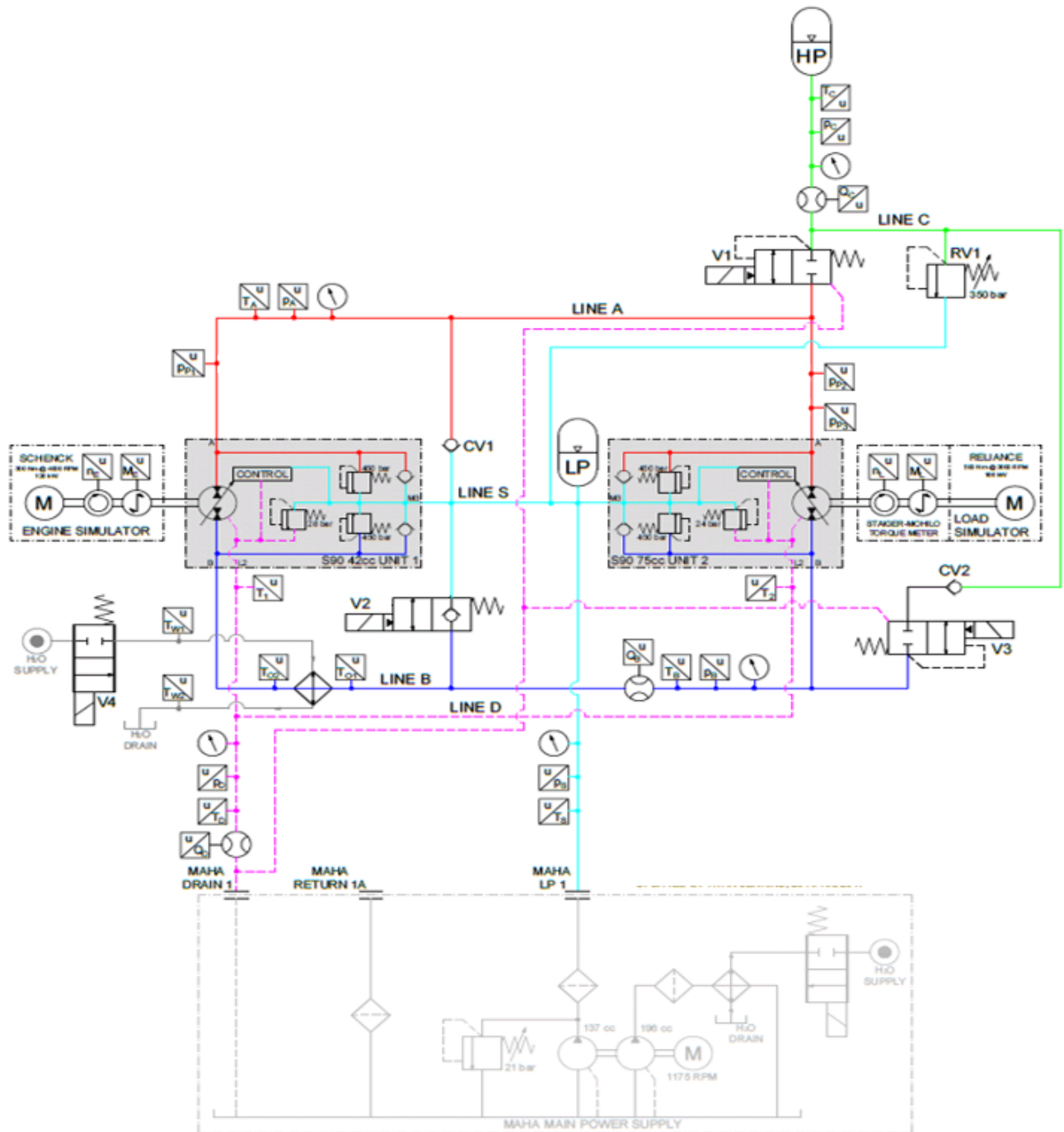
However, the purpose sought by this research, which is to tackle pressure ripple early and target a very broad 0-5000Hz frequency band, proved to be a good heuristic for finding strategies that could reduce noise sources in most cases and audible noise eventually. The numerical studies suggested it was possible to have a considerable downstream reduction on pressure ripple without compromising the upstream pressure ripple as long as the passive elements had good positioning, and the experiments agreed with this result.

In summary, the following original contributions were made:

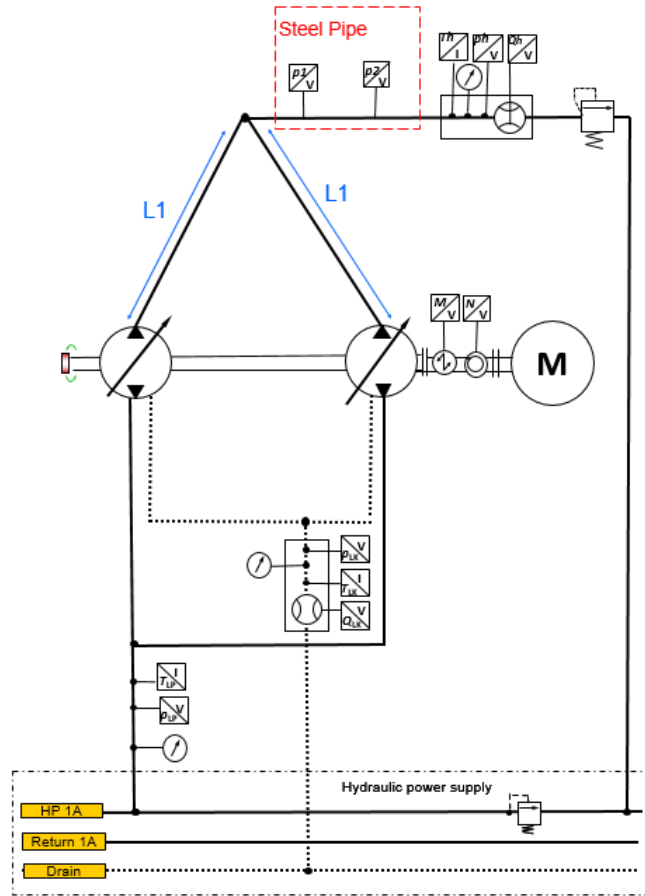
- Development of a block-diagram based coupled hydraulic model for evaluating FBNS generation and propagation

- Discretization of the MOC based line model and inclusion of enhanced friction effect by curvatures among other factors
- Design and execution of an experiment for verifying the effect of passive elements at pressure ripple and vibration
- Developed an axial piston unit FBNS reduction strategy based on coupled units, and designed and performed an experiment to show it effective in the first and third pump harmonics
- Studied passive element placement methodology based on line length ratio placement
- Developed a frequency-domain analysis based on time domain modeling methodology
- Elaboration of a flowchart-based tool for application engineers to use low-cost passive elements in hydraulic systems

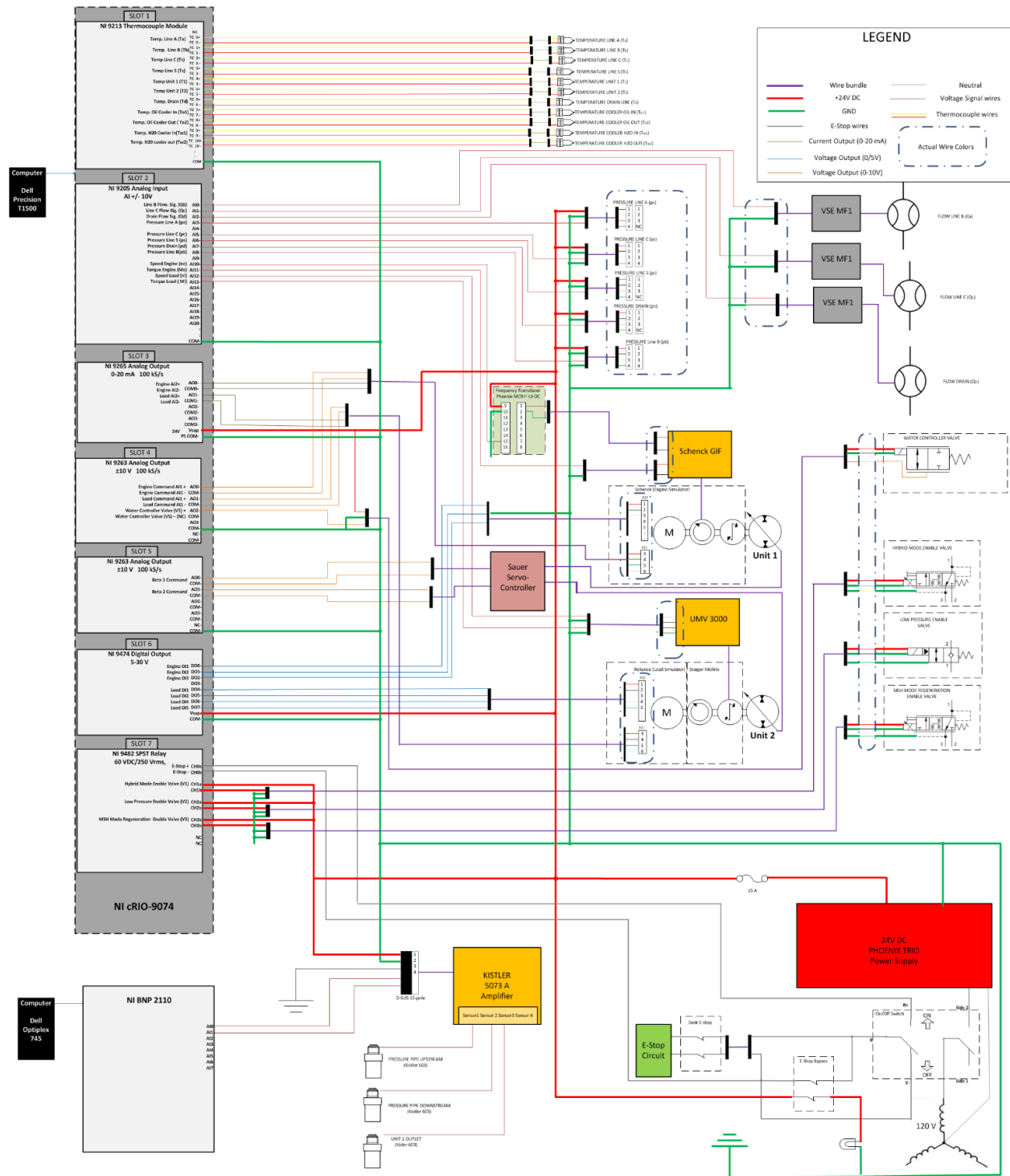
APPENDIX A. HYBRID-IN-THE-LOOP HYDRAULIC SCHEMATICS



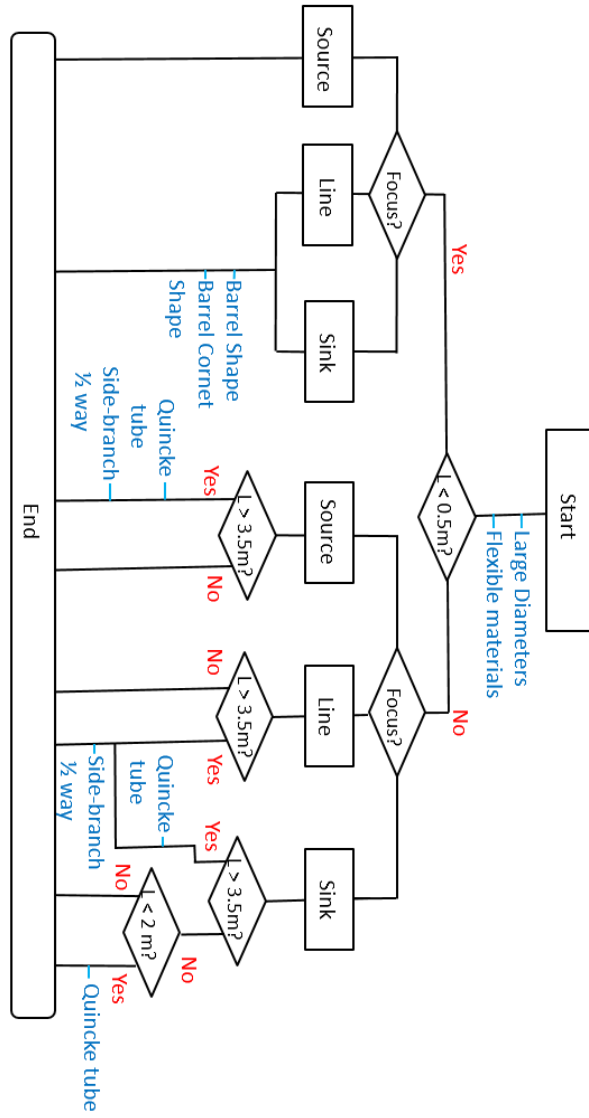
APPENDIX B. COUPLED UNITS HYDRAULIC SKETCH



APPENDIX C. HYBRID-IN-THE-LOOP ELECTRONICS



APPENDIX D. GENERAL TOOL FOR PASSIVE FBNS ATTENUATION



VITA

- Ph.D. Candidate at the Department of Agricultural in Biological Engineering with a Fluid Power Specialization. 2015-2020- Purdue University, West Lafayette, USA
- Masters in mechanical engineering, with specialization in solid mechanics and mechanical project and fluidthermic systems. 2010 – 2012: Unicamp, Campinas , Brazil
- Quality engineering specialization by the PROMIMP program , with attached courser of maintenance and logistics. 2009 : PUC-PR ,Curitiba , Brazil
- Electrical engineering technical institute Trainee 2008: Dresden Technische Universitat Dresden , Germany
- B.Sc. in control and automation engineering by the Campinas state university.2004 – 2008: Unicamp, Campinas , Brazil

Research Interests

- Noise sources in hydraulic systems
- CFD
- Automation in hydraulic systems
- Sensors development for oil engineering

Teaching Experience

- ES663- Industrial Automation Eletronics 2nd semester 2010 – assistent monitor

Computer Languages

- C, C++,Pascal, Assembly

Simulation tools

- Matlab,Labview, Mathematica, MultiSim,Amesim

Engineering Tools

- ProE, Autocad,Ifix,

REFERENCES

- [1] **Achten, P., Schellekens, M., Murrenhoff, H., Deeken, M.** Efficiency and Low Speed Behavior of the Floating Cup Pump. *Journal of Commercial Vehicles, SAE Transactions*, 2004, 113, 366-376.
- [2] **Achten P. and Eggenkamp, S.** Barrel tipping in axial piston pumps and motors. 15th Scandinavian International Conference, SICFP2017 7-9, 2017 , Linköping, Swede
- [3] **Adamkowski, A. and Lewandowski, M.** 2006. Experimental examination of unsteady friction models for transient pipe flow simulation. *Journal of Fluids Engineering ASME*, pp. 1351–1363.
- [4] **Akers A. ,Gassman M. and Smith R.** 2006. *Hydraulic Power System Analysis*. CRC Press
- [5] **Alster M.** 1972. Improved calculation of resonant frequencies of Helmholtz resonators. *Journal of Sound and Vibration*, 24(1), pp.63-85.
- [6] **Becker R.J.** 1970. Quieting hydraulic systems and components. SAE Technical Paper 700711.
- [7] **Bedout J. M. De, Franchek M.A., Bernhardt R.J., Mongeau L.** 1997. Adaptive-passive noise control with self-tuning Helmholtz resonators, *Journal of Sound and Vibration*, 202(1), 109-123
- [8] **Bernhard R. J., Hall H. R. and Jones J. D.** 1992. Adaptive–passive noise control, *Inter-Noise 92*, pp. 427–430.
- [9] **Bodén H, Carlsson U., Glav R., Wallin H. P, and Åbom M.** 1999. *Ljud och vibrationer*. The Royal Institute of Technology, Norstedts Tryckeri AB, 2nd edition, Stockholm, Sweden.
- [10] **Chanaud R.C.** 2014. *Noise ordinances: Tools for Enactment, Modification and Enforcement of a Community Noise Ordinance* , Prescott, Arizona, USA
- [11] **Clark R.L., Saunders W.R., and Gibbs G.P.** 1998. *Adaptive Structures: Dynamics and Control*, volume 28. Wiley New York, USA.
- [12] **Devendran R.S. and Vacca A.** 2013. Optimal design of gear pumps for exhaust gas aftertreatment applications, *Simulation Modelling Practice and Theory* 38 (2013) 1–19
- [13] **Dodson J.M., Dowling D.R. and Grosh K.** 1998. Experimental investigation of quarter wavelength silencers in large scale hydraulic systems. *Noise Control Engineering Journal*, 46(1), pp.15-22.
- [14] **Duan H.F. ,Ghidaoui M.,Lee P. J. and Tung Y.K.** 2010. Unsteady friction and viscoelasticity in pipe fluid transients, *Journal of Hydraulic Research*, 48:3, 354-362, DOI: 10.1080/00221681003726247

- [15] **Edge K. A. and Darling J.** 1986. Cylinder pressure transients in oil hydraulic pumps with sliding plate valves. *Proceedings of the Institution of Mechanical Engineers* ,Vol. 200, No. B1, pp 45-54.
- [16] **Edge, K.A.** 1999. Designing quieter hydraulic systems - some recent developments and contributions. In *Fourth JHPS International Symposium on Fluid Power*. Tokyo, Japan.
- [17] **Elliott. S.** 2000. *Signal Processing for Active Control*. Academic press,
- [18] **Franchek M.A., Ryan M.W. and Bernhard R. J.** 1994, Adaptive–passive vibration control , *Journal of Sound and Vibration* ,189, pp. 565–585.
- [19] **Hara S., Omata T. and Nakano M.** 1985. Synthesis of repetitive control systems and its application. *24th Conference on Decision Control*, pp. 1384–1392.
- [20] **Harrison A.M.** 1997.Reduction of axial piston pump pressure ripple. PhD thesis, University of Bath, United Kingdom.
- [21] **Harrison A.M. and Edge, K.A.** 2000. Reduction of axial piston pump pressure ripple. *Proceedings of the Institution of Mechanical Engineers, Part I: Journal of Systems and Control Engineering*, 214(1), 53–64. <https://doi.org/10.1243/0959651001540519>
- [22] **Harper M. and Leung R.** 1993. Active vibration control in pipes. *Inter-Noise 93*, pp.871-874.
- [23] **Helgestad B O.** 1967. An Investigation of Noise Emission from an Axial Piston Hydraulic Pump. PhD thesis, University of Birmingham, UK.
- [24] **Helgestad B. O., Foster K., and Bannister F. K.** 1973. Noise in an axial piston pump. In *Proc. of the Institution of Mechanical Engineers, Seminar on noise emitted by fluid power equipment - its causes and control*, pp. 51–62.
- [25] **Helgestad B O, Foster K, and Bannister F K.** 1974. Pressure transients in an axial piston hydraulic pump. *Proc. of the Institution of Mechanical Engineers 1847-1996*, 188(17):189–199.
- [26] **Ichiyanagi, T.** 1999. Research on Reducing the Fluid-Borne Noise in Fluid Power Systems. PhD thesis, Department of Mechanical Systems Engineering, National Defense Academy, Japan.
- [27] **Ichiyanagi T., Nishiumi T.,** 2008. Study on the Insertion Loss Characteristics of Side Branch Resonator in Hydraulic Line. *Proceedings of 7th JFPS International Symposium on Fluid Power*, Toyama,Japan
- [28] **Ichiyanagi T.,Kuribayashi T. and Nishiumi T.,** 2013. Design criteria os a Helmholtz silencer with multiple degrees of freedom for hydraulic systems. *Journal of Fluid Science and Technology*, Vol. 8, N° 3, pp. 277-293, DOI: 10.1115/1.4034618
- [29] **Ichiyanagi T.,Kuribayashi T. and Nishiumi T.,** 2017. Investigationon wave propagation of pressure pulsation in a Helmholtz-type hydraulic siliencer with a hemispherical vessel. *Journal of Vibration and Acoustics*, Vol. 139, DOI 10.1299/jfst8.277

- [30] **Ivantysynova M.** 1999. A new approach to the design of sealing and bearing gaps of displacement machines. *Fourth JHPS International Symposium on Fluid Power*, pp. 45-50, Tokyo, Japan.
- [31] **Ivantysyn, J.** and **Ivantysynova, M.** 2001. *Hydrostatic Pumps and Motor, Principles, Designs, Performance, Modeling, Analysis, Control and Testing*. New Delhi, Academic Books International, ISBN-81-85522-16-2.
- [32] **Ivantysynova, M., Grabbel J.** and **Ossyra, J.C.** 2002. Prediction of swash plate moment using the simulation tool CASPAR. *ASME International Mechanical Engineering Congress, IMECE 2002-39322*, New Orleans, USA.
- [33] **Ivantysynova M., Seeniraj G.** and **Huang C.** 2005. Comparison of different valve-plate designs focusing on oscillating forces and flow pulsation. *The Ninth Scandinavian International Conference on Fluid Power, SICFP '05*, Linköping, Sweden.
- [34] **Jiao Z., Chen P., Hua Q.,** and **Wang S.** 2003. Adaptive vibration active control of pressure pulsations. *Proceedings of the Institution of Mechanical Engineers, Part I: Journal of Systems and Control Engineering*, 217(4), pp. 311-318.
- [35] **Johansson, A.** and **Werndin R.** 2001. A general simulation model for axial piston machines based on TLM. Technical Report, IKP-R-100, Linköping University, Sweden.
- [36] **Johansson, A., Anderson, J.** and **Palmberg J.O.** 2002. Optimal design of the cross-angle for pulsation reduction in variable displacement machines. *Proc. Of Power Transmission and Motion Control (PTMC)*, University of Bath, UK.
- [37] **Johansson A.** 2005. Design Principles for Noise Reduction in Hydraulic Piston Pumps - Simulation, Optimization and Experimental Verification. PhD thesis, Linköping University, Sweden.
- [38] **Johnston D.N.** and **Edge K.A.** 1989. Simulation of the pressure ripple characteristics of hydraulic circuits. *Proceedings of Institution of Mechanical Engineers*, 203, pp. 275–282,
- [39] **Johnston, N.** 2012 The transmission line method formodelling laminar flow of liquid in pipelines. *Proceedings of the Institution of Mechanical Engineers, Part I: Journal of Systems and Control Engineering*, 5, 226(5), pp. 586-597.
- [40] **Johnston, N., Pan, M. Kudzma, S.** 2014 An enhanced transmission line method for modelling laminar flow of liquid in pipelines. *Proceedings of the Institution of Mechanical Engineers. Part I: Journal of Systems and Control Engineering*, 228(4), pp. 193-206
- [41] **Kalbfleisch P.** 2015. Computational Valve Plate Design. MS Thesis, Purdue University, USA
- [42] **Karnopp, D.** 1972. Bond graph models for fluid dynamic systems. *ASME Journal of Dynamic Systems Measurements and Control*, pp. 222-229.

- [43] **Kartha, S.C.** 2000. Active, Passive and Active/Passive Control Techniques for Reduction of Vibrational Power Flow in Fluid Filled Pipes. MS Thesis, Virginia Polytechnic Institute and State University, USA.
- [44] **Kassem, S.A.** 1988. Dynamic analysis of hydraulic transmission lines by a lumped model. *Bulletin of Fac. Of Eng., Vol.22, No.2, Mechanical Engineering, Ain Shams University*, pp.1-18.
- [45] **Kela L.** 2010. Attenuating Amplitude of pulsating pressure in a low-pressure hydraulic system by an adaptive Helmholtz resonator; *International Journal of Mechanical, Aerospace, Industrial, Mechatronic and Manufacturing Engineering* Vol:4, No:8, 2010 University of Oulu
- [46] **Kim K.H., Jang J.S., Jung D.S. and Kim H.E.** 2005. Reduction of pressure ripples using a parallel line in hydraulic pipeline. *International Journal of Automotive Technology*, Vol .6, N ,pp. 65-70
- [47] **Kim T., Kalbeisch P., and Ivantysynova M.** 2014. The Effect of Cross Porting on Derived Displacement Volume. *International Journal of Fluid Power*, 15(2):77,85,
- [48] **Kim T.** 2017. Active Vibration/Noise Control of Axial Piston Machine using Swash Plate Control. PhD thesis, Purdue University.
- [49] **Kinsler L.E., Frey A.R., Coppens A.B. and Sanders J.V.** 1982. *Fundamentals of Acoustics*, John Wiley & Sons.
- [50] **Kojima, E. and Shinada, M.** 1986. Characteristics of Fluid-borne Noise Generated by a Fluid Power Pump (4th Report, Pressure Ripple in Hydrostatic Power Transmission). *Bulletin of JSME*, Vol. 29. No. 258, pp. 4147-4155.
- [51] **Kojima E. and Shinada M.** 1991. Development of an active attenuator for pressure pulsation in liquid piping systems: a real time-measuring method of progressive wave in a pipe. *JSME international journal*, 34(4), pp. 466-473.
- [52] **Kojima E., Shinada M. and Yamaoka T.** 1992. Development of an active attenuator for pressure pulsation in liquid piping systems (3rd report, trial construction of the control system and fundamental experiments for wide-band random pressure pulsation). *Transactions of the Japan Society of Mechanical Engineers (B)*, 58(533), pp. 47-54.
- [53] **Kojima, E.** 1992. A new method for the experimental determination of pump fluid borne noise characteristics. *Proceedings of the 5th Bath International Power Workshop*, pp. 111-137, University of Bath, UK.
- [54] **Kojima E. and Ichiyanagi T.** 1998. Development research of new types of multiple volume resonators. Bath Workshop on Power Transmission and Motion Control, Professional Engineering Publishing, pp. 193–206, University of Bath, UK.
- [55] **Kojima E. and Ichiyanagi T.** 2000. Research on Pulsation Attenuation Characteristics of Silencers in Practical Fluid Power Systems, *International Journal of Fluid Power*, 1:2, 29-38, DOI: 10.1080/14399776.2000.10781089

- [56] **Kostek T.M., Franchek M.A., and Bolton J.S.** 1998. Hybrid noise control in ducts. *Noise-Con 98*, pp.277-282.
- [57] **Klop, R. and Ivantysynova, M.** 2008. Influence of Line Length Concerning Noise Source Generating in Hydrostatic Transmissions. SAE International, 08CV-0161
- [58] **Klop, R., Vacca A. and Ivantysynova, M.** 2009. A Method of Characteristics Based Coupled Pump/Line Model to Predict Noise Sources of Hydrostatic Transmissions. *Bath ASME Symposium on Fluid Power and Motion Control*, Hollywood, USA.
- [59] **Klop, R.J.** 2010. Investigation of Hydraulic transmission Noise Sources. PhD thesis, Purdue University, USA.
- [60] **Kuo S.M. and Morgan D.** 1995. *Active Noise Control Systems: Algorithms and DSP Implementations*. John Wiley & Sons, Inc.
- [61] **Larsson P.**, 1989. Fluid Power Attenuators Analysis, Measurements and Performance Optimization, Proceedings of the JFPS International Symposium on Fluid Power, 55-62, November 08, ISSN 2185-6303, <https://doi.org/10.5739/isfp.1989.55>
- [62] **Lueg P.** 1934. Process of silencing sound oscillator. US Patent No. 2 043 416.
- [63] **Maillard J.** 1998. Active control of pressure pulsations in piping systems. Research Report, University of Karlskrona/Ronneby, Ronneby, Sweden.
- [64] **Manring, N. D. and Dong Z.** 2004. The impact of using a secondary swash-plate angle within an axial piston pump. *ASME Journal of Dynamic Systems, Measurement, and Control*. Vol. 126, pp. 65-74.
- [65] **Manhartsgruber, B.** 2019. H2-Optimal Low Order Transmission Line Models. Proceedings of the ASME/BATH 2019 Symposium on Fluid Power and
- [66] **Masuda K. and Ohuchi H.** 1996. Noise reduction of a variable piston pump with even number of cylinders. *Third JHPS International Symposium*, 1996(3), pp. 91-96, Osaka, Japan.
- [67] **Menon E.S.** 2004. *Piping Calculations Manual*, McGraw-Hill Calculations
- [68] **Mikota J.**, 2000. Comparison of various designs of solid body compensators for the filtering of fluid flow pulsations in hydraulic systems. *1st FPNI PhD Symposium*, TU Hamburg, Hamburg, Germany.
- [69] **Mikota J. and Manhartsgruber B.** 2001. Transient response dynamics of dynamic vibration absorbers for the attenuation of fluid-flow pulsations in hydraulic systems. *Bath Workshop on Power Transmission and Motion Control (PTMC'01)*, Bath, UK.
- [70] **Mikota J.** 2001. A novel, compact pulsation compensator to reduce pressure pulsations in hydraulic systems. *Proceedings of ICANOV – International Conference on Noise, Acoustics and Vibration*, Ottawa, Canada

- [71] **Minav T.A., Laurila L.I.E. and Pyrhönen J.J.**, 2011. Axial piston pump flow ripple; Compensation by adjusting the pump speed with an electric drive, Twelfth Scandinavian, International Conference on Fluid Power, May 18-20, Tampere, Finland.
- [72] **Mitome K.**, Seki K., 1983. A New Continuous Contact Low-Noise Gear Pump, ASME J of Mech Design, Vol 105, Dec
- [73] **Nakagawa S., Ichiyanagi T., and Nishiumi T.**, 2015. A consideration on the behavior of hydraulic pressure ripples in relation to hydraulic oil temperature . Proceedings of the ASME/BATH 2015 Symposium on Fluid Power and Motion Control, FPMC 2015, October 12-14, 2015, Chicago, Illinois, USA
- [74] **Negrini S.**, 1996. A gear Pump Designed for Noise abatement and Flow Ripple Reduction, Int. Fluid Power Exposition and Technical conference, 23-25 April
- [75] **Ngah, Z. and Edge, K.A.** 2001. The measurement of positive displacement pump and motor noise using sound intensity techniques. *Off-highway Powerplant Congress and Exposition*, SAE, pp. 1-6, Warrendale, PA, USA.
- [76] **Ohuchi H., Kenji M., and Tasuku O.** 2002. Noise reduction of a variable displacement axial piston pump by compensating the exciting force: Experimental verification of the effect of compensation. *Transactions of the Japan Fluid Power Systems society*, 33(3), pp. 76-81.
- [77] **O'Shea C.** 2016. Hydraulic Flow Ripple Cancellation Using the Primary Flow Source, Proceedings of the BATH/ASME 2016 Symposium on Fluid Power and Motion Control , FPMC2016, September 7-9, 2016, Bath, UK
- [78] **Ortwig H.** 2005, Experimental and analytical vibration analysis in fluid power systems, International Journal of Solids and Structures, Volume 42, Issues 21–22, Pages 5821-5830, ISSN 0020-7683, <https://doi.org/10.1016/j.ijsolstr.2005.03.028>.
- [79] **Lipscombe, B. R.** 1987, The reduction of gear pump pressure ripple by source flow modification. PhD thesis, School of Power Engineering, University of Bath
- [80] **Palmberg, J. O.** 1989. Modelling of flow ripple from fluid power piston pumps. *2nd Bath International Power Workshop*, University of Bath, UK.
- [81] **Pan, M., Johnston, D. N., and Hillis, A. J.**, 2012, “Active Control of Pressure Pulsation in a Switched Inertance Hydraulic System Using a Rectangular-Wave Reference Signal,” Bath/ASME Symposium on Fluid Power and Motion Control, Bath, UK, Sept. 12–14, pp. 165–177.
- [82] **Pan, M., Johnston, D. N., and Hillis, A. J.**, 2013, “Active Control of Pressure Pulsation in a Switched Inertance ,” Proc. Inst. Mech. Eng., Part I, 227(7), pp. 610–620.

- [83] **Platzer T., Van Malsen R.A.H.; Achten, P.A.J.** 2004 Floating Cup - Ein neues Konstruktionsprinzip für hydrostatische Maschinen, *Ölhydraulik und Pneumatik*, (5)
- [84] **Pavic G.** 1992. Vibroacoustical energy flow through straight pipes. *Journal of Sound and Vibration*, 154(3), pp.411-429.
- [85] **Pettersson M., Weddfelt K. and Palmberg J. O.** 1991. Methods of reducing flow ripple from fluid power piston pumps - a theoretical approach. *SAE International Off-highway and Powerplant Congress*, Milwaukee, USA.
- [86] **O. Pingchao, J. Zongxia, L. Hongmei, L. Shuli and L. Yunhua**, 2006 Active Control on Fluid Borne Pulsation Using Piezoelectric Valve as Absorber, *2006 IEEE Conference on Robotics, Automation and Mechatronics*, Bangkok, , pp. 1-5, doi: 10.1109/RAMECH.2006.252607.
- [87] **Rabie, M.G.** 2007. On the application of oleo-pneumatic accumulators for the protection of hydraulic transmission lines against water hammering – a theoretical study. *International Journal of Fluid Power*, Vol. 8, No. 1.
- [88] **Rebel, J.** 1977. Active liquid noise-suppressions in oil hydraulics (in German). *VDI-Z.*, 119, 937–943.
- [89] **Rydberg K.E.** 2001. Hydraulic pulsation dampers, *The HP-Symposium '01*, no. LiTH-IKP-CR0358, pp. 19-21, Oslo, Norway.
- [90] **Schohl, G.A.** 1993.“Improved approximate method for simulating frequency-dependent friction in transient laminar flow. *Journal of Fluids Engineering*, ASME, 115(3), pp. 420-424.
- [91] **Seeniraj, G.K.** 2009. Model based optimization of axial piston machines focusing on noise and efficiency. PhD thesis, Purdue University, USA.
- [92] **Sprengel, M. and Ivantysynova, M.** 2012. Novel Transmission Configuration for Hydraulic Hybrid Vehicles. *Proceedings of the International Sci-Tech Conference “Machine Dynamics and Vibro Acoustics”*. Sept. 5-6, 2012. Samara, Russia.
- [93] **Sprengel, M, Bleazard T.** 2015. Haria H. Ivantysynova,M., Implementation of a Novel Hydraulic Hybrid Powertrain in a Sports Utility Vehicle. *IFAC-PapersOnLine*,4815,pp. 187-194
- [94] **Sprengel, M.** 2015. Influence of architecture design on the performance and fuel efficiency of hydraulic hybrid transmissions. PhD thesis, Purdue University, USA.
- [95] **Vardy A. E. and Hwang K.L.** 1993. A weighting function model of transient turbulent pipe friction, *Journal of Hydraulic Research*, 31:4, 533-548, DOI: 10.1080/00221689309498876
- [96] **Vardy A. E. and Brown J.M.B.** 1995. Transient, turbulent, smooth pipe friction, *Journal of Hydraulic Research*, 33:4, 435-456, DOI: 10.1080/00221689509498654
- [97] **Verheij J.W.** 1980. Cross spectral density methods for measuring structure borne power flow on beams and pipes. *Journal of Sound and Vibration*, 70(1), pp.133-139.

- [98] **Walker, J. S., Phillips, J. W.** 1977. Pulse Propagation in Fluid Filled Tubes," *ASME Journal of Applied Mech.*, pp. 31-35.
- [99] **Wang, L., and Johnston, D. N.**, 2008, "Adaptive Attenuation of Narrow Band Fluid Borne Noise in a Simple Hydraulic System," Bath/ASME Symposium on Fluid Power and Motion Control, University of Bath, Bath, UK, Sept. 10, pp.357–368.
- [100] **Wang, L.** 2008. Active Control of Fluid-Borne Noise. PhD thesis, University of Bath, UK
- [101] **Weddfelt K., Larsson P. and Palmberg J.O.** 1987. Investigation of the performance of expansion chamber attenuators by means of simulations and measurements. *16th EASTED International Conference Identification, Modelling and Simulation*, pp. 22-24, Paris, France.
- [102] **Weiss M., Patel M.K., Junginger M., Perujo A., Bonnel P., van Grootveld G.** , 2012, On the electrification of road transport - Learning rates and price forecasts for hybrid-electric and battery-electric vehicles, *Energy Policy*, Volume 48,Pages 374-393
- [103] **Weiss M., Patel M.K., Dekker P., Moro A. and Scholtz H.**, 2015, On the electrification of road transportation – A review of the environmental, economic, and social performance of electric two-wheelers, *Transportation Research Part D: Transport and Environment*, Volume 41 ,Pages 348-366,ISSN 1361-9209,
- [104] **Wiggert D.C., Otwell R. S. and Hatfield F. J.** 1985. The Effect of Elbow Restraint on Pressure Transients. *ASME J. Fluids Eng*, 107(3), pp. 402-406
- [105] **Wieczorek, U. and Ivantysynova, M.** 2000. Caspar – a computer-aided design tool for axial piston machines. *Proceedings of the Bath Workshop on Power Transmission and Motion Control*, University of Bath, UK, 113-126.
- [106] **Wylie, E. and Streeter, V.** 1978. *Fluid Transients*. McGraw-Hill Inc. ISBN 0-07-072187-4.
- [107] **Yokota S., Somada H. and Yamaguchi H.** 1996. Study on an active accumulator.(active control of high-frequency pulsation of systems). *JSME International Journal Series B Fluids and Thermal Engineering*, 39(1), pp.119-124.
- [108] **Zanetti-Rocha L., Gerges S.N.Y, Johnston D. N. and Arenas J. P.** 2013. Rotating Group; Design for Vane Pump Flow Ripple Reduction, *International Journal of Acoustics and Vibration*, Vol. 18, No. 4, pp. 192-200.
- [109] **Zarzycki, Z.** 2000. On weighting functions for wall shear stress during unsteady turbulent pipe flow." 8th International Conference on Pressure Surges, The Hague.
- [110] **Zarzycki, Z. and Kudzma, S.** 2004. Simulations of transient flow in liquid lines using time-dependent frictional losses. 9th International Conference on Pressure Surges, BHR Group, Chester, UK.
- [111] **Zielke, W.** 1968. Frequency-dependent friction in transient pipe flow. *Journal of Basic Engineering*, ASME, 90 (1), 109-115

PUBLICATIONS

Journal Publications

Danes, L.; Vacca, A. The influence of line and fluid parameters on pressure ripple in hydraulic transmissions. *SN Appl. Sci.* 2,2020 , 1281, <https://doi.org/10.1007/s42452-020-3032-5>

Danes, L.; Vacca, A. A tandem axial-piston unit based strategy for the reduction of noise sources in hydraulic systems *MDPI Energies* 2020, *13*(20), 5377; <https://doi.org/10.3390/en13205377>

Danes, L.; Vacca, A. A frequency-domain-based study for fluid-borne noise reduction in hydraulic system with simple passive elements. *International Journal of Hydromechatronics*, 2020 , UNDER REVIEW